

ARMY RESEARCH LABORATORY



Characterizing the Electromagnetic Environment Produced by the Army's Repetitive Electromagnetic Pulse Simulator (REPS)

by Bruce T. Benwell

ARL-TR-306

October 1994



19950112 024

DTIC QUALITY INSURED &

The findings in this report are not to be construed as an official Department of the Army position unless so designated by other authorized documents.

Citation of manufacturer's or trade names does not constitute an official endorsement or approval of the use thereof.

Destroy this report when it is no longer needed. Do not return it to the originator.

REPORT DOCUMENTATION PAGE

Form Approved
OMB No. 0704-0188

Public reporting burden for this collection of information is estimated to average 1 hour per response, including the time for reviewing instructions, searching existing data sources, gathering and maintaining the data needed, and completing and reviewing the collection of information. Send comments regarding this burden estimate or any other aspect of this collection of information, including suggestions for reducing this burden, to Washington Headquarters Services, Directorate for Information Operations and Reports, 1215 Jefferson Davis Highway, Suite 1204, Arlington, VA 22202-4302, and to the Office of Management and Budget, Paperwork Reduction Project (0704-0188), Washington, DC 20503.

1. AGENCY USE ONLY (Leave blank)		2. REPORT DATE October 1994	3. REPORT TYPE AND DATES COVERED Final, 1-31 August 1988							
4. TITLE AND SUBTITLE Characterizing the Electromagnetic Environment Produced by the Army's Repetitive Electromagnetic Pulse Simulator (REPS)			5. FUNDING NUMBERS PE: 62120							
6. AUTHOR(S) Bruce T. Benwell										
7. PERFORMING ORGANIZATION NAME(S) AND ADDRESS(ES) U.S. Army Research Laboratory Attn: AMSRL-WT-NF 2800 Powder Mill Road Adelphi, MD 20783-1197			8. PERFORMING ORGANIZATION REPORT NUMBER ARL-TR-306							
9. SPONSORING/MONITORING AGENCY NAME(S) AND ADDRESS(ES) U.S. Army Research Laboratory 2800 Powder Mill Road Adelphi, MD 20783-1197			10. SPONSORING/MONITORING AGENCY REPORT NUMBER							
11. SUPPLEMENTARY NOTES AMS code: 612120.H250011 ARL project no.: XE78E5										
12a. DISTRIBUTION/AVAILABILITY STATEMENT Approved for public release; distribution unlimited.			12b. DISTRIBUTION CODE							
13. ABSTRACT (Maximum 200 words) This report characterizes the time-domain electromagnetic field environment generated by the Army's Repetitive Electromagnetic Pulse Simulator (REPS). The REPS system is a free-field radiating 300-m "longwire" dipole antenna that is driven at the center by a 1-MV pulse generator. The RF environment generated by REPS was characterized in terms of two heights (1 and 2 m), field uniformity, symmetry about the antenna, and wavefront planarity. Based on measured data, "usable" and "recommended" test volumes have been defined.										
			<table border="1"> <tr> <td><input checked="" type="checkbox"/></td> <td></td> </tr> <tr> <td><input type="checkbox"/></td> <td></td> </tr> <tr> <td><input type="checkbox"/></td> <td></td> </tr> </table>		<input checked="" type="checkbox"/>		<input type="checkbox"/>		<input type="checkbox"/>	
<input checked="" type="checkbox"/>										
<input type="checkbox"/>										
<input type="checkbox"/>										
			<table border="1"> <tr> <td colspan="2">Codes</td> </tr> <tr> <td>Dist</td> <td>Avail and/or Special</td> </tr> <tr> <td>A-1</td> <td></td> </tr> </table>		Codes		Dist	Avail and/or Special	A-1	
Codes										
Dist	Avail and/or Special									
A-1										
14. SUBJECT TERMS EMP simulator, electromagnetic pulse, EMP, longwire dipole			15. NUMBER OF PAGES 223							
			16. PRICE CODE							
17. SECURITY CLASSIFICATION OF REPORT Unclassified	18. SECURITY CLASSIFICATION OF THIS PAGE Unclassified	19. SECURITY CLASSIFICATION OF ABSTRACT Unclassified	20. LIMITATION OF ABSTRACT UL							

Contents

	Page
1. Introduction	7
2. Simulator	8
2.1 <i>REPS History</i>	8
2.2 <i>REPS Simulator</i>	10
2.2.1 <i>Simulator Description</i>	10
2.2.2 <i>Pulser Output Field Monitoring System</i>	12
3. REPS Test Volume	14
3.1 <i>Field-Mapping Coordinate System</i>	14
3.2 <i>Locating Test Points</i>	15
3.3 <i>Test Volume Topography</i>	15
3.4 <i>Ground Constants</i>	15
3.5 <i>Test Point Determination</i>	17
4. Instrumentation	18
4.1 <i>Field Sensors</i>	18
4.1.1 <i>E-Field Sensors</i>	18
4.1.2 <i>H-Field Sensors</i>	18
4.2 <i>Sensor Calibration</i>	19
4.3 <i>Data Acquisition Instrumentation</i>	19
5. Measured Field Data	22
5.1 <i>Field Components</i>	22
5.2 <i>Symmetry</i>	22
5.3 <i>Data Set Organization</i>	31
5.3.1 <i>Data Collected at Height of 1 m</i>	31
5.3.2 <i>Data Collected at Height of 2 m</i>	34
6. Field Uniformity	48
6.1 <i>Locating Test Points</i>	48
6.2 <i>Planewave Approximation</i>	53
7. Inspection of Data Set	56
7.1 <i>Sensor Bandwidth Limitations</i>	56
7.2 <i>Discontinuity in Pulser Output Waveform</i>	57
8. Conclusions	59
Acknowledgement	59
References	60
Distribution	227

Appendices

A.—Pulser Output Monitoring System	61
B.—Sensor Calibration and Positioning	69
C.—Measured Field Data	83
D.—Pulser Output Waveforms	185

Tables

1. Dielectric constant and conductivity of REPS soil	16
2. Calibration factors for sensors used during test	19

Figures

1. Repetitive Electromagnetic Pulse Simulator (REPS)	8
2. Woodbridge Research Facility (WRF) layout showing current and past locations for REPS	9
3. REPS pulser cross-sectional view	10
4. REPS antenna endome earth ground	11
5. Typical pulser output monitor waveform	13
6. Overlay of three consecutive pulse output waveforms	13
7. Coordinate system for REPS field mapping	14
8. Test point location grid in relation to REPS antenna	15
9. Topological map of REPS test volume	16
10. Test point locations used for symmetrical comparisons	17
11. Typical frequency response for Nanofast optical link	20
12. Block diagram of IVAN's data acquisition process	21
13. Sample hardcopy of typical waveform collected by IVAN	21
14. Field components of expanding wavefront	23
15. Comparison of horizontal component of E-field (E_x) collected at 0/50/1 and 0/-50/1	24
16. Comparison of radial component of H-field (H_y) collected at 0/50/1 and 0/-50/1	24
17. Comparison of vertical component of H-field (H_z) collected at 0/50/1 and 0/-50/1	24
18. Comparison of horizontal component of E-field (E_x) collected at 0/75/1 and 0/-75/1	24
19. Comparison of radial component of H-field (H_y) collected at 0/75/1 and 0/-75/1	25
20. Comparison of horizontal component of E-field (E_x) collected at 50/25/1 and -50/25/1	25
21. Comparison of radial component of E-field (E_y) collected at 50/25/1 and -50/25/1	25
22. Comparison of vertical component of E-field (E_z) collected at 50/25/1 and -50/25/1	25
23. Comparison of horizontal component of H-field (H_x) collected at 50/25/1 and -50/25/1	26
24. Comparison of radial component of H-field (H_y) collected at 50/25/1 and -50/25/1	26
25. Comparison of vertical component of H-field (H_z) collected at 50/25/1 and -50/25/1	26

26.	Comparison of horizontal component of E-field (E_x) collected at 50/50/1 and -50/50/1	26
27.	Comparison of radial component of E-field (E_y) collected at 50/50/1 and -50/50/1	27
28.	Comparison of vertical component of E-field (E_z) collected at 50/50/1 and -50/50/1	27
29.	Comparison of horizontal component of H-field (H_x) collected at 50/50/1 and -50/50/1	27
30.	Comparison of radial component of H-field (H_y) collected at 50/50/1 and -50/50/1	27
31.	Comparison of vertical component of H-field (H_z) collected at 50/50/1 and -50/50/1	28
32.	Comparison of horizontal component of E-field (E_x) collected at 25/50/1 and -25/50/1	28
33.	Comparison of radial component of E-field (E_y) collected at 25/50/1 and -25/50/1	28
34.	Comparison of vertical component of E-field (E_z) collected at 25/50/1 and -25/50/1	28
35.	Comparison of horizontal component of H-field (H_x) collected at 25/50/1 and -25/50/1	29
36.	Comparison of radial component of H-field (H_y) collected at 25/50/1 and -25/50/1	29
37.	Comparison of vertical component of H-field (H_z) collected at 25/50/1 and -25/50/1	29
38.	Comparison of horizontal component of E-field (E_x) collected at 35/35/1 and -35/35/1	29
39.	Comparison of radial component of E-field (E_y) collected at 35/35/1 and -35/35/1	30
40.	Comparison of vertical component of E-field (E_z) collected at 35/35/1 and -35/35/1	30
41.	Comparison of horizontal component of H-field (H_x) collected at 35/35/1 and -35/35/1	30
42.	Comparison of radial component of H-field (H_y) collected at 35/35/1 and -35/35/1	30
43.	Comparison of vertical component of H-field (H_z) collected at 35/35/1 and -35/35/1	31
44.	Field distribution of peak E-field measured at height of 1 m	32
45.	Field distribution of peak H-field measured at height of 1 m	33
46.	Polarity (direction) of E- and H-field components	34
47.	Field distribution of horizontal component of E-field (E_x) measured at 1 m	35
48.	Field distribution of radial component of E-field (E_y) measured at 1 m	37
49.	Field distribution of vertical component of the E-field (E_z) measured at 1 m	39
50.	Field distribution of horizontal component of H-field (H_x) measured at 1 m	41
51.	Field distribution of radial component of H-field (H_y) measured at 1 m	43
52.	Field distribution of vertical component of the H-field (H_z) measured at 1 m	45

53.	Field distribution of peak E-field measured at 2 m	47
54.	Field distribution of peak H-field measured at 2 m	47
55.	Location of test points for investigation of expanding wavefront uniformity	49
56.	Peak amplitude of electric and magnetic fields measured at 1 m on 50- and 85-m arcs	50
57.	Peak amplitudes of electric and magnetic fields measured at 2 m on 50- and 85-m arcs	51
58.	Usable REPS test volume	52
59.	Vector components for incident and reflected magnetic fields	53
60.	Range dependence of incident E-field along centerline	54
61.	Range dependence of horizontal E-field (E_x) measured along centerline	54
62.	Range dependence of radial H-field (H_y) measured along centerline	55
63.	Range dependence of vertical H-field (H_z) measured along centerline	55
64.	Comparison of measured and bandwidth-compensated H-field response	57
65.	Risetime discontinuity in pulser output waveform	58

1. Introduction

The Repetitive Electromagnetic Pulse Simulator (REPS) is a transportable, sub-threat-level, electromagnetic pulse (EMP) simulator. REPS is basically a free-field-radiating, 300-m "longwire" dipole antenna, which is driven in the center by a 1-MV (nominal) pulse generator. REPS was built in 1973 for Harry Diamond Laboratories (HDL)* by the Physics International (PI) company to simulate the electromagnetic (EM) environment produced by an exoatmospheric nuclear burst on ground-based military systems. This report documents the time-domain EM environment that is produced by REPS.

At the time that REPS was developed, it was not feasible to perform an extensive mapping of the REPS EM environment because of the simulator's intensive testing schedule. Early documentation of its performance consisted of selected field measurements intended to verify the design characteristics of the simulator or measurements taken at specific field locations required by the various tests in which the REPS was used.

This report details the most extensive field mapping of the REPS field environment, performed in August 1988 to support the Army's High-Altitude Electromagnetic Pulse (HEMP) Department of Defense (DoD) Standards and Specifications Program (DSSP).

In addition to documenting the time-domain EM environment produced by REPS, this report examines the mechanisms and environment in which the data were collected. An in-depth theoretical description into the waveform structure will not be addressed. However, E. L. Patrick [1] gives a thorough explanation of the waveform structure (inclusive of the complex ground reflections) generated by a horizontally polarized longwire dipole antenna system very similar to that of REPS.

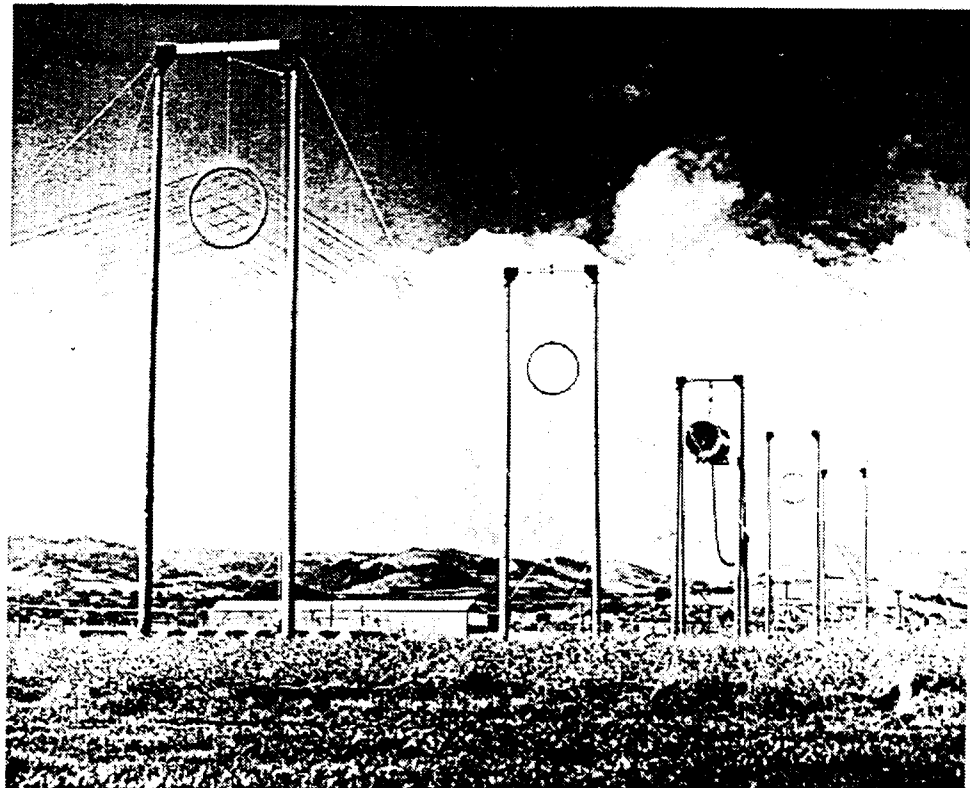
*Now part of the Army Research Laboratory (ARL).

2. Simulator

2.1 REPS History

REPS was constructed by PI in June 1973. A series of acceptance tests were immediately performed at Camp Parker, CA, to verify and optimize the pulser and antenna systems. These tests were completed in February 1974. Figure 1 shows REPS while in operation at Camp Parker. Following these acceptance tests, REPS was transported directly to North Dakota to support the Safeguard anti-ballistic missile system tests. Throughout 1975, REPS was used exclusively for a test at the Safeguard site. When this test was over, REPS was returned to PI for storage. In April 1976, REPS was shipped to the ARL Woodbridge Research Facility (WRF) and set up at the WRF "staging area" (fig. 2). Field mapping measurements [2] were conducted to verify its performance and characteristics and to support its future use on the Defense Nuclear Agency's Program for EMP Testing (PREMPT) test on the ESS-1 Automatic Voice Network (AUTOVON) switch at Pickens, MS. At the completion of these measurements at WRF in July 1976, REPS was used in a test at Pickens, MS, from August through October 1976. At the completion of this test, REPS was returned to PI for extensive refurbishment.

Figure 1. Repetitive Electromagnetic Pulse Simulator (REPS) erected at Camp Parker, CA.



In October 1977, after being refurbished, REPS was returned to WRF, where it was used to support numerous HEMP tests. In May 1980, REPS was set up at its present location at WRF to provide extensive support to the Generic Verification Facility test program.

In August 1988 the REPS was used to support the Army's DSSP. This program required an extensive description of the EM environment produced by REPS for use in later program activities. The field mapping measurements taken for this program are the basis for this report.

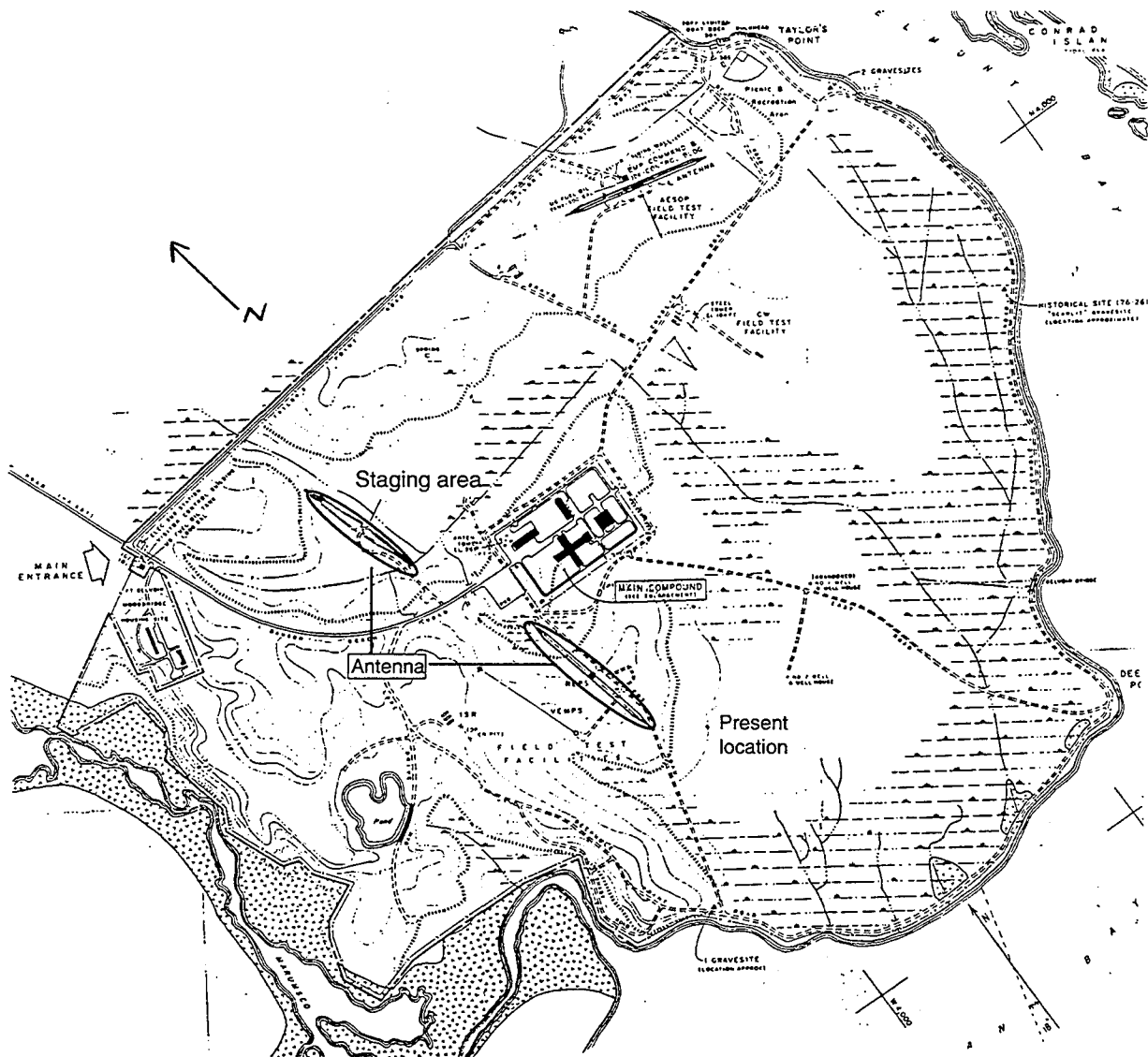


Figure 2. Woodbridge Research Facility (WRF) layout showing current and past locations for REPS.

2.2 REPS Simulator

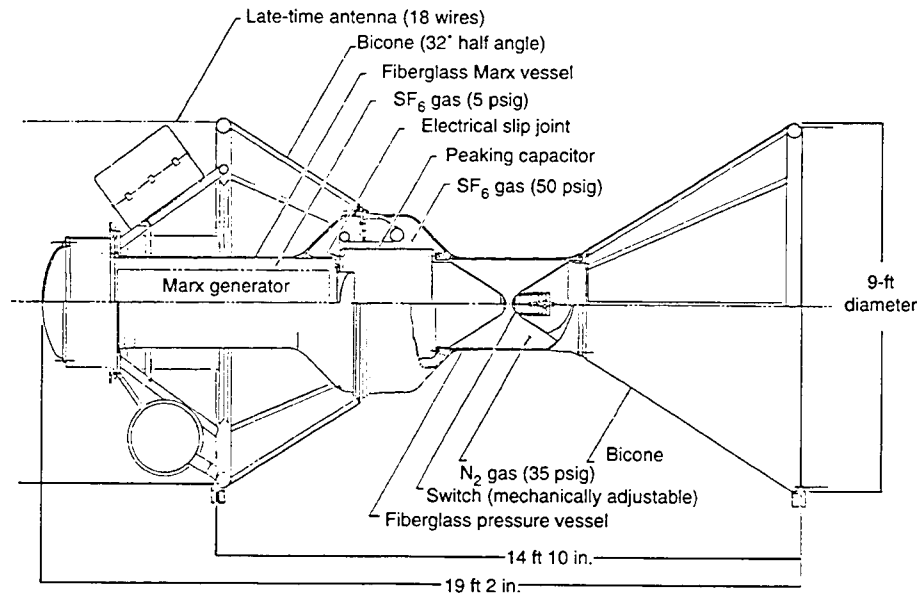
2.2.1 Simulator Description

REPS is basically a free-field-radiating, 300-m longwire dipole antenna, which is driven at the center by a 1-MV (nominal) pulse generator.

The REPS pulse generator (fig. 3) consists of a 16-stage Marx generator, a gas-insulated peaking capacitor (to produce the required fast-rising current that the Marx generator cannot provide because of its large series inductance), and a self-breakdown, single-channel output switch. REPS can launch a single-event pulse on demand or be operated repetitively at a pulse rate of one pulse every 15 seconds [3].

These components are housed within fiberglass vessels contained between two aluminum biconical feed sections. These feed sections allow a smooth electrical transition for the launched high-voltage pulse from the output switch to the late-time antenna cage. Each bicone is 9 ft in diameter at its base, and has a half-angle of 32 deg. The late-time antenna, constructed of 18- $\frac{1}{8}$ -in. steel aircraft cables equally spaced around 9-ft-diameter aluminum hoops, guides the current pulse from the source to the terminations found at each end of the antenna. The overall length of the antenna is 300 m, with the pulser located at the center of the antenna. Normal elevation of the pulser and antenna is 15 m. The last 50 m of each end of the antenna slants downward from the normal 15-m elevation to 1.3 m above ground. The diameter of the antenna is also reduced in this region from its normal 9-ft diameter to an 18-in. diameter at the antenna's

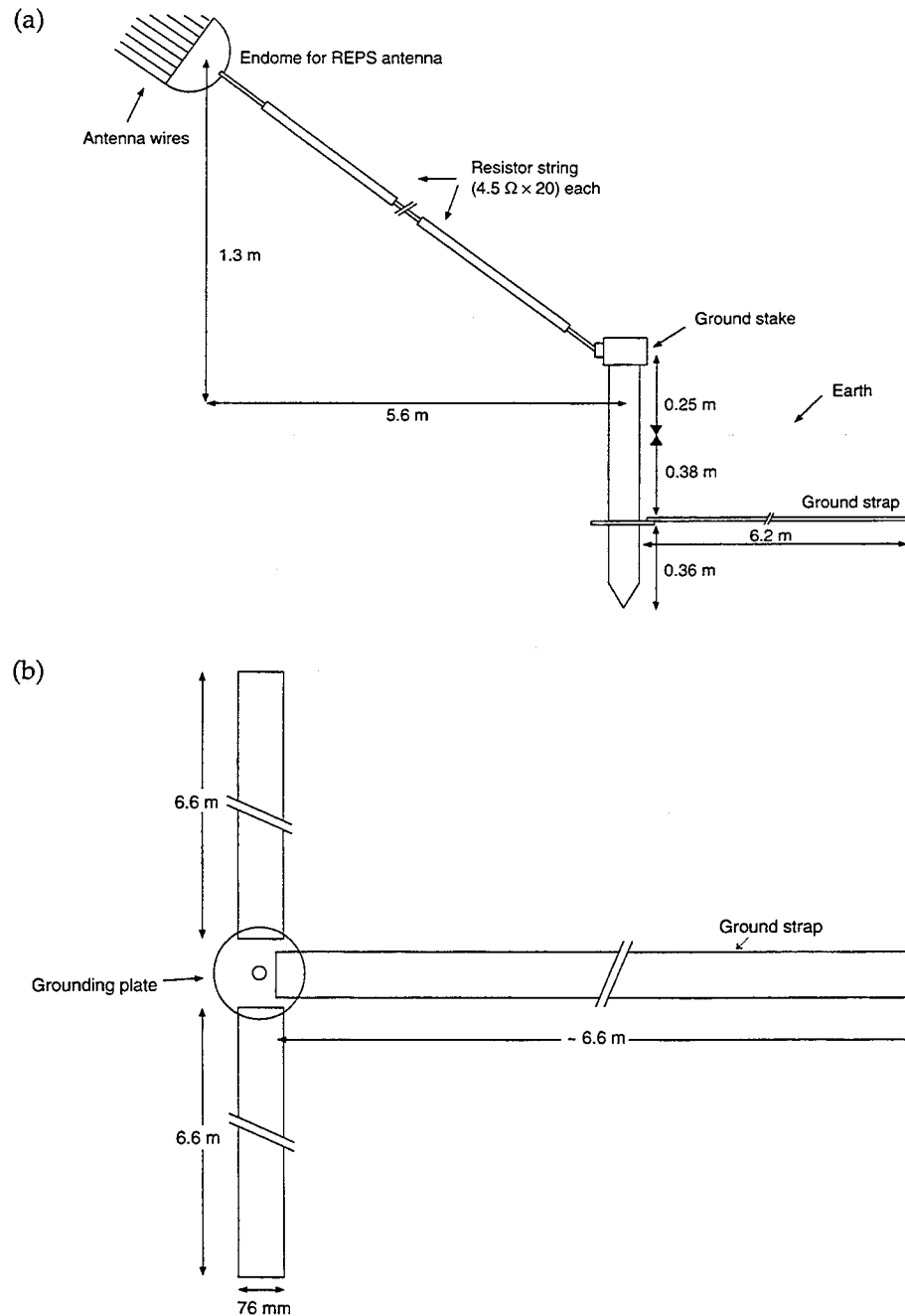
Figure 3. REPS pulser cross-sectional view.



end to keep the impedance of the downward sloping portion of the antenna constant.

Each end of the antenna is terminated to earth ground through a matched resistive load consisting of two series resistor strings whose total resistance is 180Ω (fig. 4(a)). The terminating resistors are attached to a grounding plate that is buried approximately 1 ft below ground. Connected to this plate are three aluminum strips, each 3 in. wide and 20 ft long, which radiate outward horizontally from each plate (fig. 4(b)).

Figure 4. REPS antenna endome earth ground: (a) side view and (b) top view.



The antenna cage and pulser are supported with a system of wood telephone poles and cross beams. All poles are guyed with fiberglass rods that are attached to buried concrete anchor blocks.

All pulser operations are controlled from a command and control (C²) trailer through a set of hydraulic, pneumatic, and optical control lines. Located within the C² trailer are the pulser operating controls and the hydraulic and gas support systems, as well as the output field-level monitoring system.

2.2.2 *Pulser Output Field Monitoring System*

Although the pulser output waveform is generally controlled by the charged Marx voltage, several factors can cause the amplitude of the output pulse to vary or drift. Field variation can be attributed to such factors as jitter in the self-breakdown output switch or drifting gas pressures within the pulser.

To account for any pulse-to-pulse variation, each output pulse is monitored using a permanently mounted reference sensor. The output monitor is an EG&G MGL-2 B-dot sensor located 15 m from the pulser at a height of 3.66 m. The output of the B-dot sensor is electronically integrated to give the incident magnetic field.

It is convenient to convert the magnetic field measured at the B-dot sensor location to the incident E-field at a distance of 50 m from the pulser (since the incident E-field must be well defined within the REPS test volume whenever HEMP testing is performed on military systems). The equations used to reduce the recorded B-dot to the incident E-field at 50 m are given in appendix A. Figure 5 shows a typical B-dot waveform. Each B-dot waveform is recorded with an automated monitoring system comprising a fiber-optic data link, a Tektronix (TEK) 7912 transient digitizer, and a Digital Equipment Corporation (DEC) PDP 11/23 computer, to control the optics and TEK 7912, as well as to process and save the recorded output pulse. A more detailed description of the B-dot monitoring system can also be found in appendix A.

Although the design specifications for the REPS pulser allow a shot-to-shot variability of 10 percent, the actual shot-to-shot variability is much better. Figure 6 shows an overlay of three consecutive B-dot measurements, which vary by approximately 4 percent. Shot-to-shot variations of this order were typical of the entire field-mapping effort.

Figure 5. Typical pulser output monitor waveform.

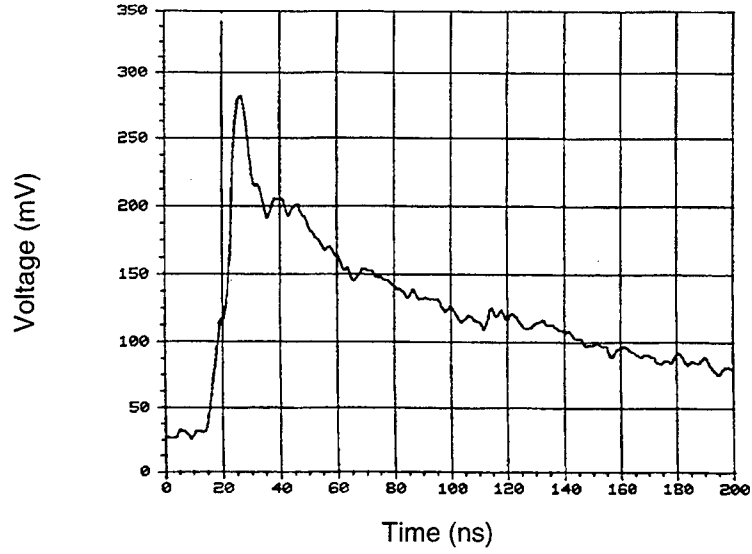
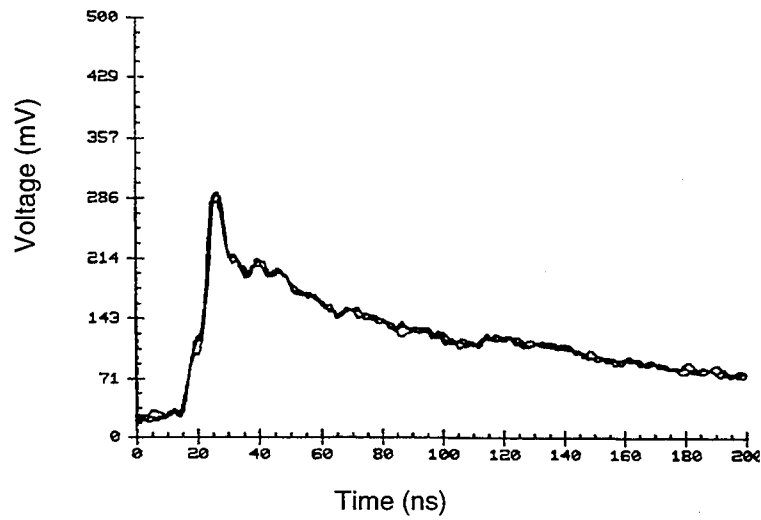


Figure 6. Overlay of three consecutive pulse output waveforms.



3. REPS Test Volume

3.1 Field-Mapping Coordinate System

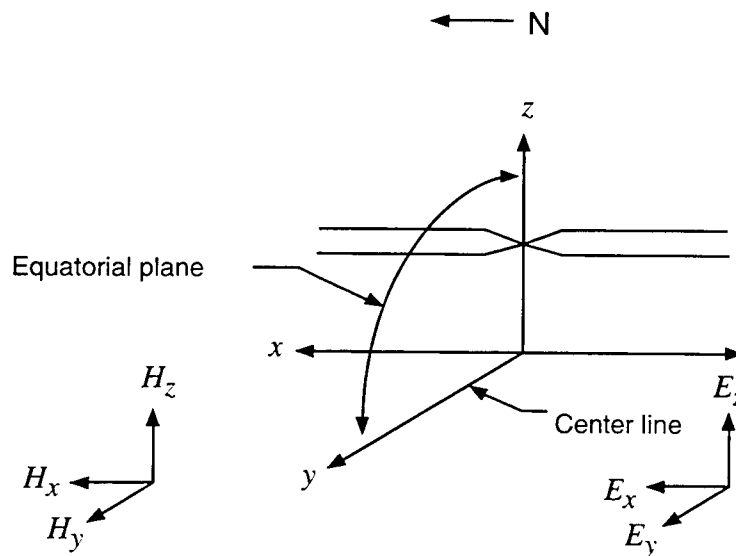
The total electric and magnetic fields generated by REPS are defined in terms of the three Cartesian coordinates centered on the earth directly beneath the REPS pulser.

For REPS, the coordinates (see fig. 7) used to locate a measurement point in the test volume have their origin on the ground at a point directly below the center of the biconical pulse launcher.

The z-axis passes through the center of the bicone and is perpendicular to the ground. The x-axis is parallel to the ground and coplanar with the axis of the antenna structure. The y-axis is parallel to the ground and perpendicular to the antenna axis. The y-axis is referred to as the centerline.

Specific points in this coordinate system are designated by the notation $\pm x/\pm y/z$. For an observer on the west side of the antenna, +x would be to the left (north) as you face the simulator (refer to fig. 7), +y would be along the centerline pointing away from the simulator (west), and z would be straight up.

Figure 7. Coordinate system for REPS field mapping.



3.2 Locating Test Points

Prior to any field mapping, we surveyed the southwestern quadrant of the REPS test volume and placed stakes at 25-m intervals, creating a rectangular grid (fig. 8). The origin of the grid was also the origin of the mapping coordinate system. We also staked two equidistant arcs at 50- and 85-m distances from the grid origin. The entire grid was located using a surveyor's transit.

3.3 Test Volume Topography

Figure 9 shows the test point location grid overlaid on a topographical map of the REPS test volume [4]. As can be seen, much of the southwestern quadrant of the REPS test volume is reasonably flat to an off-axis range of approximately 100 m.

3.4 Ground Constants

The net EM fields measured at a point above ground are the summation of the incident and ground reflected waves. Reflection coefficients (and therefore the reflected waves) are complicated functions of frequency, angle of incidence, and the ground dielectric constant and conductivity. Table 1 lists the values to be expected within the REPS test volume for these variables. They are based on measurements conducted in 1980 by the National Institute for Standards and Technology (NIST) for a previous test [5].

Figure 8. Test point location grid in relation to REPS antenna.

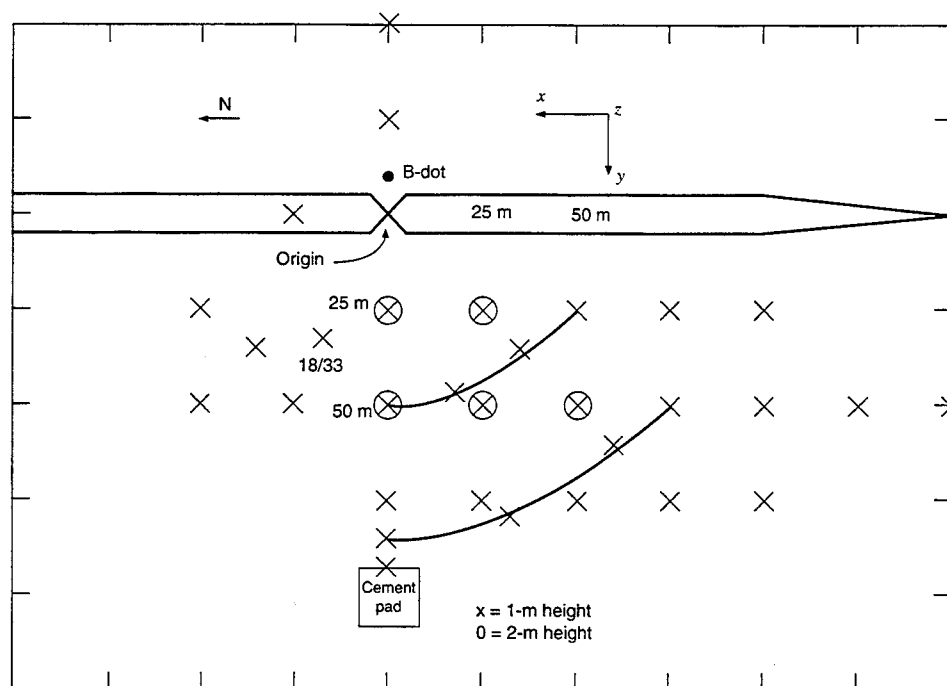


Figure 9. Topological map of REPS test volume.

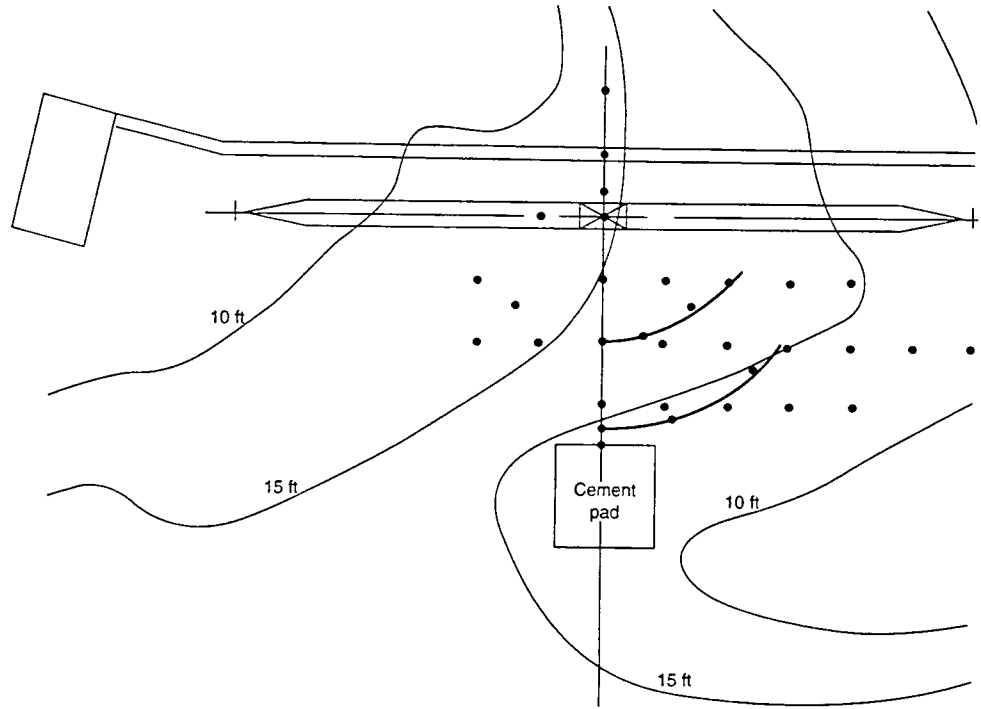


Table 1. Dielectric constant and conductivity of REPS soil.

Frequency (MHz)	Received moisture content (%)	Dielectric constant	Conductivity (mmho/cm)	$\sigma/w\epsilon^*$
6-in. depth				
0.50	7.39	15.9	0.0065	1.47
0.75	7.39	13.3	0.0079	1.42
1.00	7.39	12.4	0.0090	1.31
50.0	7.39	6.15	0.0420	0.246
100.0	7.39	5.77	0.0542	0.169
150.0	7.39	5.55	0.0632	0.137
Surface				
0.50	5.19	18.5	0.0066	1.28
0.75	5.19	15.7	0.0079	1.21
1.00	5.19	13.8	0.0091	1.19
50.0	5.19	5.68	0.0499	0.316
100.0	5.19	5.20	0.0668	0.231
150.0	5.19	4.95	0.0800	0.194

* σ = conductivity
 w = radian frequency
 ϵ = permittivity

3.5 Test Point Determination

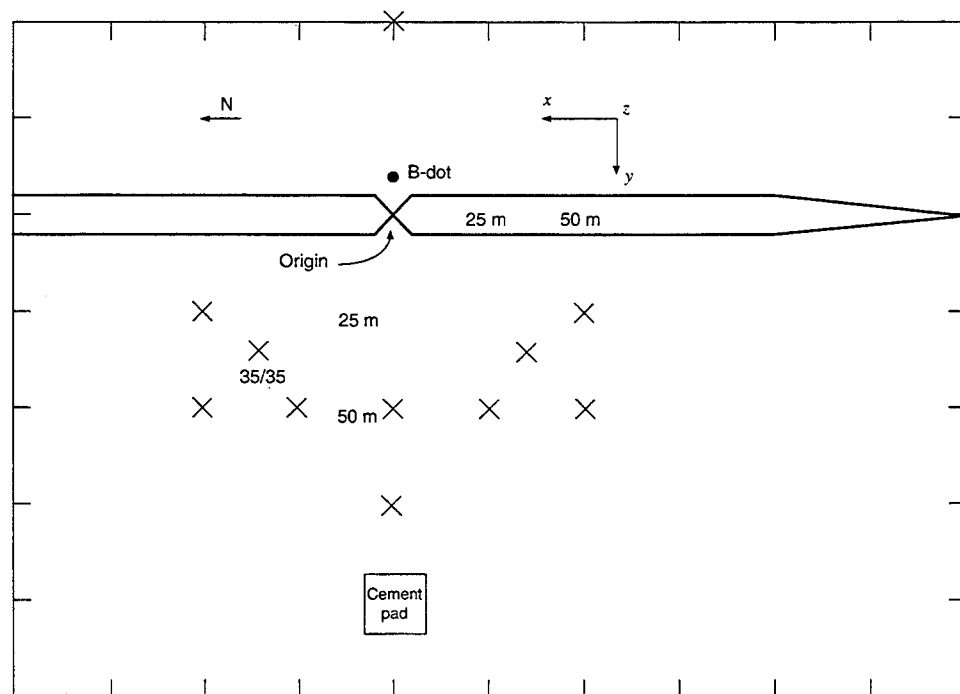
As stated earlier, the 1987 mapping effort was in support of the DSSP program. For this reason, the majority of the test point locations were dictated by the requirements of the DSSP.

The field-mapping objectives for the DSSP can be summarized as follows: (1) characterize a majority of the REPS EM environment at a height of 1 m, (2) characterize that region of the REPS test volume within the bicone angle of the pulser at a height of 2 m, and (3) characterize the uniformity of the expanding wavefront launched from the pulser at two distances.

The specific test points chosen to accomplish these objectives are displayed in figure 8. Specific test points necessary to accomplish the third field-mapping objective will be covered in section 6.1.

The actual number of testpoints used to define the electromagnetic fields produced by REPS was minimized by taking advantage of the expected field symmetry about the centerline, as well as about the simulator's antenna axis. In this way, we could locate the majority of the testpoints in one quadrant. We verified the symmetry by comparing the fields measured at symmetrically located test points about the centerline (e.g., 50/50/1 and -50/50/1), as well as about the antenna axis (0/50/1 and 0/-50/1). Testpoints locations used for symmetry comparisons are shown in figure 10.

Figure 10. Test point locations used for symmetrical comparisons.



4. Instrumentation

4.1 Field Sensors

All of the field data presented in this report were recorded with ground-plane electric and magnetic field sensors built for HDL by the Stanford Research Institute (SRI) [6]. Both the electric and magnetic field sensors are mounted on a 0.218-m circular (8-½-in.) aluminum plate that provides both a finite ground plane and a mounting surface for the sensors. These sensors are then mounted on an aluminum cylinder approximately 0.254 m (10 in.) long with a diameter of 0.167 m (6-½ in.). We chose the dimensions of this cylinder to allow the electric and magnetic field sensors to be mounted on the metallic cylinder without serious sensor modification, and to house and electromagnetically shield the transmitter portion of the fiberoptic data link, small signal amplifiers, power supply, and coaxial cables associated with the collection of field data.

Since this metallic cylinder is now an integral part of the sensor, we had to examine and characterize the effect that the metallic cylinder had on the measurement of EM fields, so that its effect could be removed (see app. B).

4.1.1 *E-Field Sensors*

Four different series of E-field sensors of decreasing sensitivities were used during this effort, to measure the wide range of field strengths found within the REPS test volume. Each sensor is a capacitively loaded monopole, connected to a built-in unity-gain preamplifier that provides an input impedance of 10 M Ω , shunted by a total of 10.5 pF and a low output impedance to drive 50- Ω signal cables. The 3-dB bandwidth for all of the sensors is 0.005 to 160 MHz, which is determined by the preamplifier [7].

4.1.2 *H-Field Sensors*

Only one type of H-field sensor was used to cover the H-field strengths encountered during this mapping effort. This sensor consists of a semicircular, shielded half-loop coaxial cable. The half-loop has an outer diameter of 2.25 in. and is made of UT-141A 50- Ω semi-rigid miniature coaxial cable. Within the sensor, a Tektronix CT-2 current probe was used to measure the short-circuit current induced on the loop's inner conductor. The shield on this cable is connected to the ground plane at one end and gapped at the other to minimize electric field coupling. These H-field sensors have a bandwidth of 90 kHz to 200 MHz [7]. The sensor is protected by a white plastic

cover, which is marked with an arrow indicating the field direction needed for a positive output voltage.

Appendix B describes how each sensor/cylinder was positioned to assure the proper and consistent measurement of each field component.

4.2 Sensor Calibration

All of the sensors used during this effort were calibrated to obtain an accurate measurement of both the magnitude and frequency response of the sensor's transfer function (which is simply defined as the ratio of applied field strength to sensor output voltage). Because all of the mapping data are recorded in the time domain, it is important that these sensors possess a flat frequency response over the frequency spectrum of the EMP pulse so that one scaling factor can be chosen to represent the entire frequency response. In this way, the pulsed data could be scaled by a single number instead of a frequency-dependent function. The scaling factors for each sensor (including metallic cylinder effect) are summarized in table 2. The frequency response for each of the sensors used for this mapping effort, together with a general description of the sensor calibration procedure, can be found in appendix B.

4.3 Data Acquisition Instrumentation

A SMART IVAN (System for Monitoring and Recording Transients Instrumentation Van) was used to acquire all field response data. SMART IVAN is a portable shielded trailer that contains all of the instrumentation necessary to properly record transient signals. The heart of SMART IVAN is the Tektronix R7912 transient digitizer.

This digitizer uses a scan-conversion technique to sample a transient signal and perform the analog-to-digital conversion of transient signals at an effective sampling rate up to 100 GHz. The analog "single-shot" bandwidth of this digitizer is 500 MHz, with nine bits of vertical resolution.

Table 2. Calibration factors for sensors used during test.

Sensor	Scaling factor ¹
H104-C	43 A/m/V
E102-C	237 V/m/V
E201-C	2567
E303-C	25669
E304-C	24233
E403-C	133169.0

¹Magnitude chosen at 50 MHz, effect of metallic cylinder included.

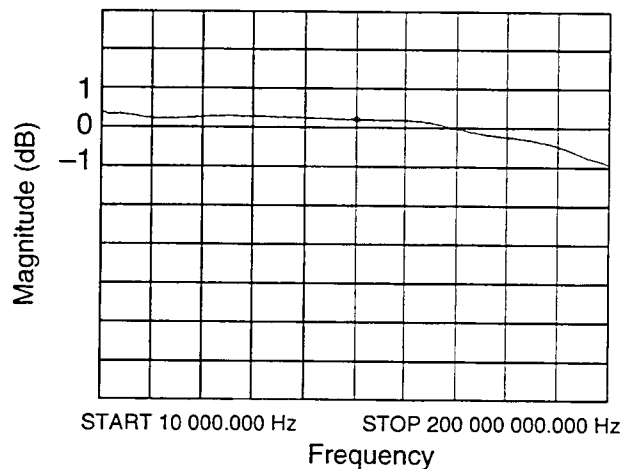
A DEC PDP 11/34 acts as the controller/processor to control most onboard functions, such as reading the gathered data from the R7912 digitizer's internal memory, remotely controlling the optical links, and performing all data processing through the execution of a series of predeveloped programs. The display terminal controls program sequencing, enters test parameters, and plots data for evaluation. A TEK 4685 hard-copy unit produces 8- × 11-in. (22- × 28-cm) copies of the information presented on the display terminal.

A wideband Nanofast fiber-optic link was used to transmit the output of a sensor to the IVAN. The Nanofast OP300-2A fiber-optic data link consisted of a transmitter, fiber-optic cables, and a receiver. The sensor output was connected to the fiber-optic transmitter's input. The fiber-optic system's (OP300-2A) risetime (10 to 90 percent) is 1.5 ns with a 1-dB upper bandwidth of 200 MHz. The lower 3-dB point is 160 Hz. Figure 11 shows a typical frequency response for the Nanofast links. The root mean square (RMS) signal-to-noise ratio is higher than 40 dB and the harmonic distortion is less than 36 dB [8].

The SMART IVAN contains three independent data acquisition "channels" used to digitize transient data. Each channel consists of a fiber-optic data link and two R7912 digitizers remotely controlled with the DEC PDP 11/34. Each digitizer is set to a different sweep speed to optimize the measurement of the wideband signals typically produced by REPS. Figure 12 shows a block diagram of SMART IVAN's data acquisition process.

The first digitizer of each channel is set at a fast sweep speed to capture the high-frequency, fast-rising portion of the waveform, while the second digitizer is set to a slower sweep speed to capture low-frequency information. Through the simultaneous use of two digitizers for each data channel, an entire pulse can typically be defined

Figure 11. Typical frequency response for Nanofast optical link.



using one simulator pulse. A sample hardcopy of a typical waveform collected using SMART IVAN is shown in figure 13.

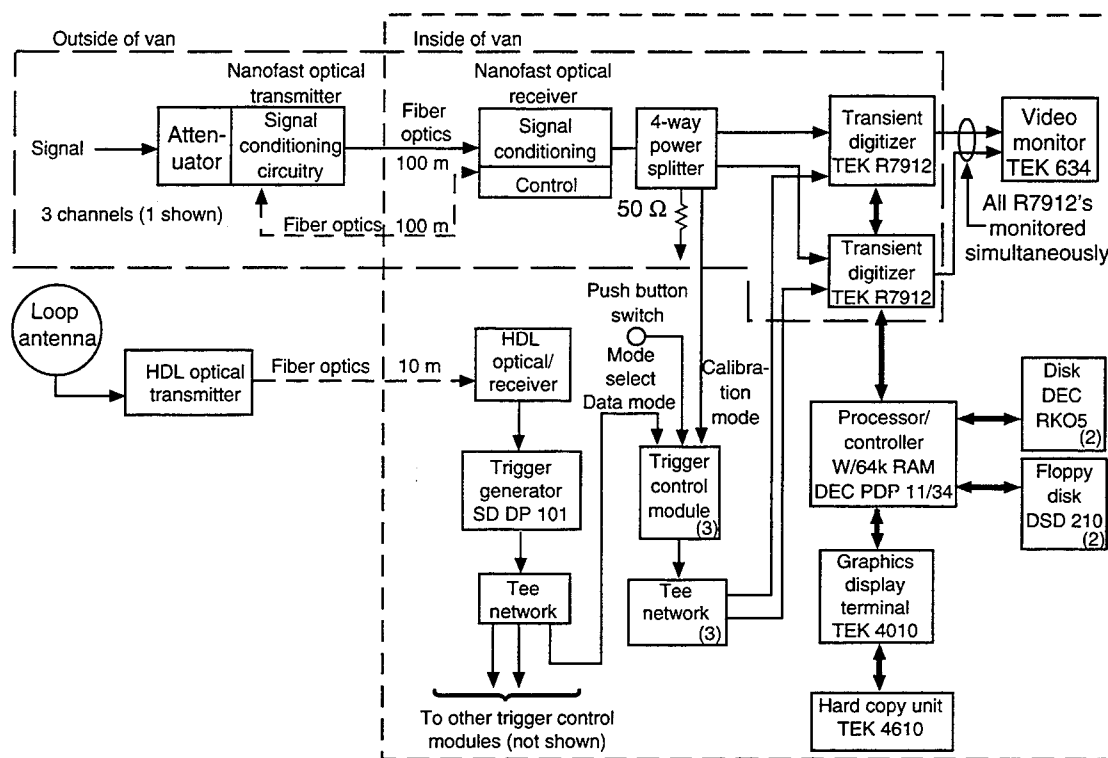
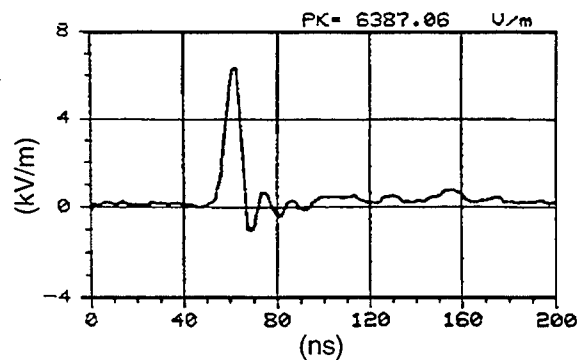


Figure 12. Block diagram of IVAN's data acquisition process.

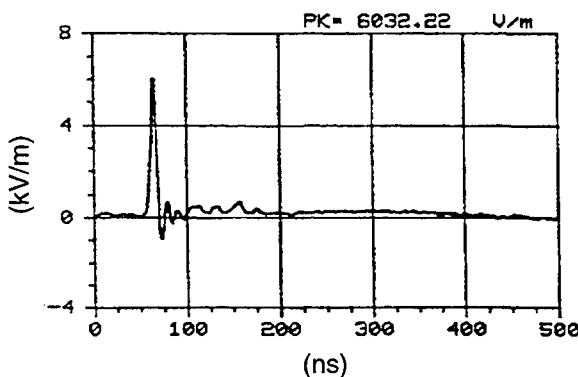
Figure 13. Sample hardcopy of typical waveform collected by IVAN.



Test information
Name: REPS mapping
Object location: 0/25/2
TP code: EX

Simulator information
Simulator: REPS
B-dot: 286 mV
Shot number: 46

Output level
at 50 m: 6.1 kV/m



Channel information
FOL cal gain: 12.23 dB
FOL attenuation: 6 dB
Other attenuation: 0 dB

Probe information
Type: E300 series
Serial number: E304-C
Cal factor: 24233

5. Measured Field Data

Before starting the mapping effort, we decided that the best way to optimize the collection of field data was to define a minimal set of digitizer sweep speeds that would provide the best representation of all of the collected data [9]. This would not only aid in the processing and presentation of the collected data, but would also optimize the measurement of the sheer volume of data that needed to be recorded. To adequately represent the waveform, the rule of thumb employed was to maintain a sweep-speed separation factor of five between the fast and slow digitizer sweep speeds used in SMART IVAN. In this way, the waveforms have been adequately sampled to allow the early- and late-time waveforms to be "time-tied" together for processing (e.g., Fourier transforms). The typical sweep speeds used to best represent the measured data were a 200-ns total window fast sweep speed and a 1- μ s total window for the slow sweep speed. For waveforms whose late-time energy could not be defined in 1 μ s, an additional 200-ns/5- μ s total window sweep speed combination was taken.

5.1 Field Components

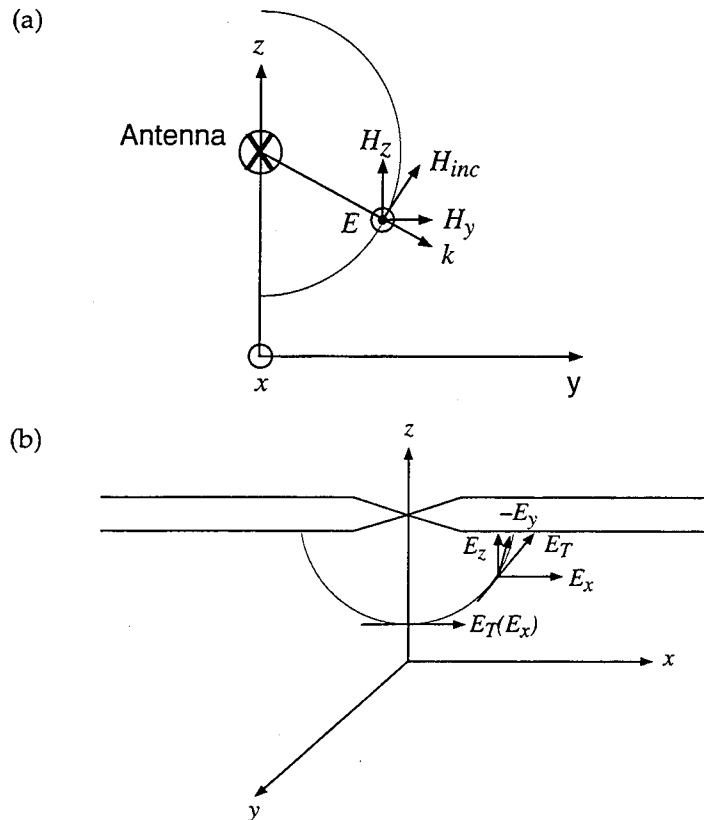
As with any finite length antenna, REPS radiates a spherically expanding wavefront. For an observer on the centerline, the wavefront can be represented by the "major" field components E_x , H_y , and H_z (see fig. 14(a)). In reality, "minor" components (E_y , E_z , and H_x) can also be measured on the centerline and are caused by a combination of imprecise recording of the field on the "true" electrical centerline, a non-symmetrical pulser antenna, or dissimilar antenna terminations. The amplitude of the minor components on the centerline were typically less than 10 percent of the peak of the major components. As would be expected from a spherical wavefront, as you move off the centerline, the amplitudes of the minor components increase as the field lines terminate back onto the antenna (see fig. 14(b)).

5.2 Symmetry

To simplify the location of testpoints and minimize the amount of data to be collected, we assumed that field symmetry existed on each side of the centerline, as well as on either side of the simulator antenna. If symmetry exists for these two cases, then all of the field mapping data could be located within one quadrant.

To determine if symmetry exists on either side of the simulator, the dominant field components (E_x , H_y , and H_z) were measured at ranges of 50 and 75 m along the centerline on both sides of the an-

Figure 14. Field components of expanding wavefront: (a) major field components on centerline and (b) off-axis field components.



tenna axis. Figures 15 to 17 compare E_x , H_y , and H_z components measured at $0/50/1$ and $0/-50/1$. Figures 18 and 19 compare E_x and H_y field components measured at $0/75/1$ and $0/-75/1$. Data at both locations compare remarkably well, showing excellent symmetry. Slight variations in peak amplitude can be attributed to a slightly inadequate sweep speed used to capture the early-time waveform.

To examine symmetry about the centerline, all six field components (E_x , E_y , E_z , H_x , H_y , and H_z) were measured at four locations on either side of the centerline. Figures 20 to 25 compare the components measured at $50/25/1$ and $-50/25/1$. Figures 26 to 31 compare the components measured at $50/50/1$ and $-50/50/1$. Figures 32 to 37 compare the components measured at $25/50/1$ and $-25/50/1$. Figures 38 to 43 compare the components measured at $35/35/1$ and $-35/35/1$. For all locations, symmetrical major components compared well, showing that REPS is indeed symmetrical about the centerline and antenna axis. All of the E_z components (see fig. 22, 28, 34, and 40) diverge at times past $1 \mu\text{s}$, suggesting that each end of the antenna may be terminated in different impedances. Again, variations in peak amplitude can be attributed to a slightly inadequate sweep speed used to capture the early-time waveform.

Figure 15. Comparison of horizontal component of E-field (E_x) collected at 0/50/1 and 0/-50/1 (dotted line).

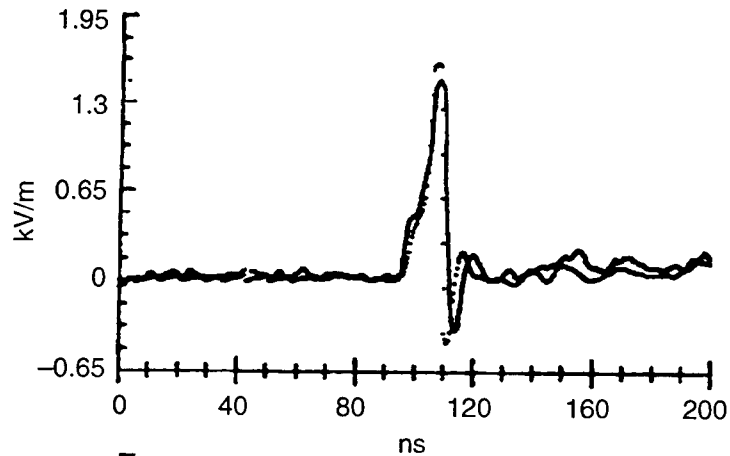


Figure 16. Comparison of radial component of H-field (H_y) collected at 0/50/1 and 0/-50/1 (dotted line).

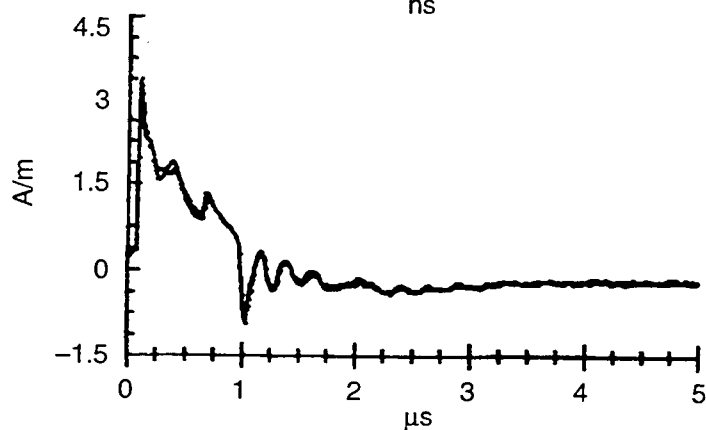


Figure 17. Comparison of vertical component of H-field (H_z) collected at 0/50/1 and 0/-50/1 (dotted line).

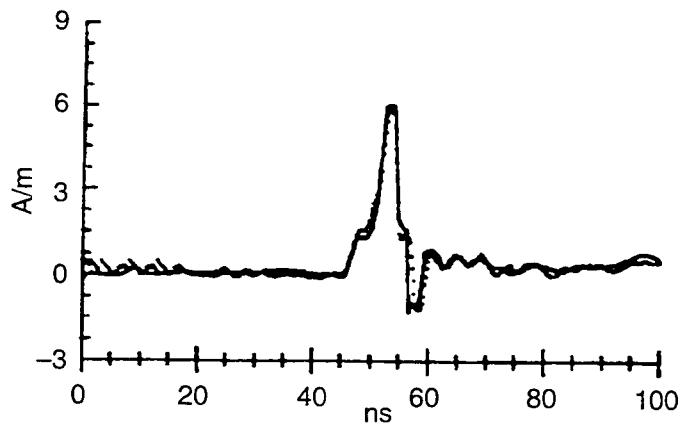


Figure 18. Comparison of horizontal component of E-field (E_x) collected at 0/75/1 and 0/-75/1 (dotted line).

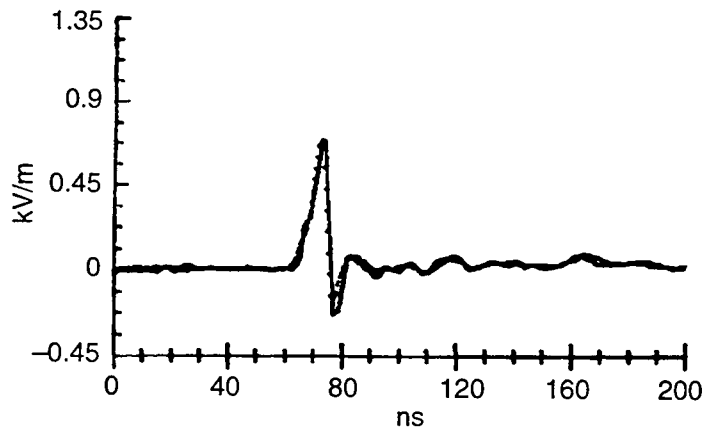


Figure 19. Comparison of radial component of H-field (H_y) collected at 0/75/1 and 0/-75/1 (dotted line).

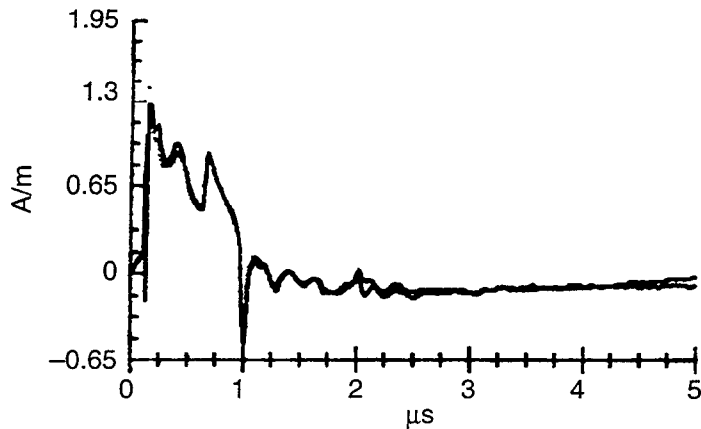


Figure 20. Comparison of horizontal component of E-field (E_x) collected at 50/25/1 and -50/25/1 (dotted line).

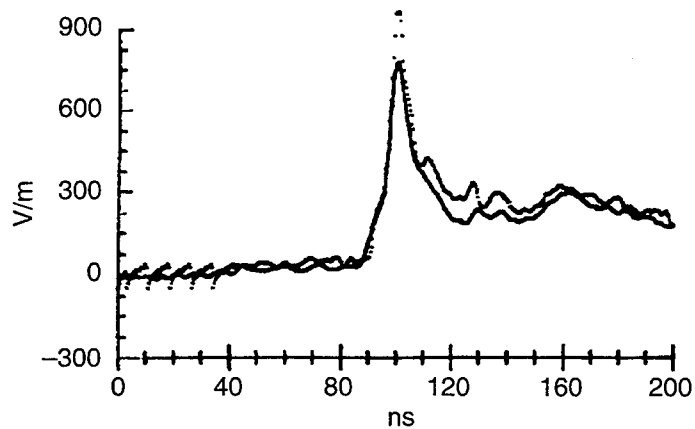


Figure 21. Comparison of radial component of E-field (E_y) collected at 50/25/1 and -50/25/1 (solid line).

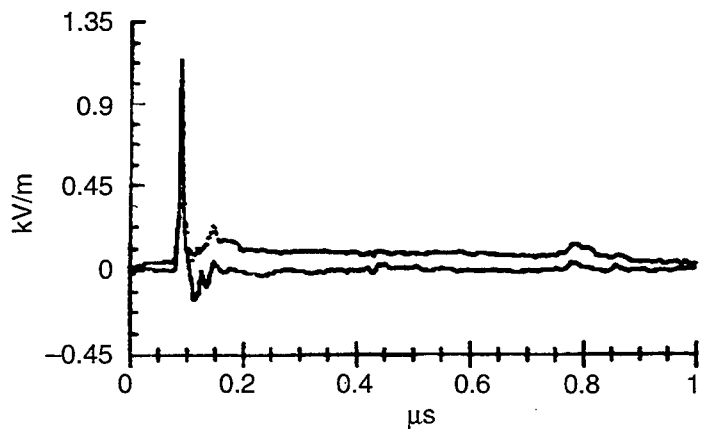


Figure 22. Comparison of vertical component of E-field (E_z) collected at 50/25/1 and -50/25/1 (dotted line).

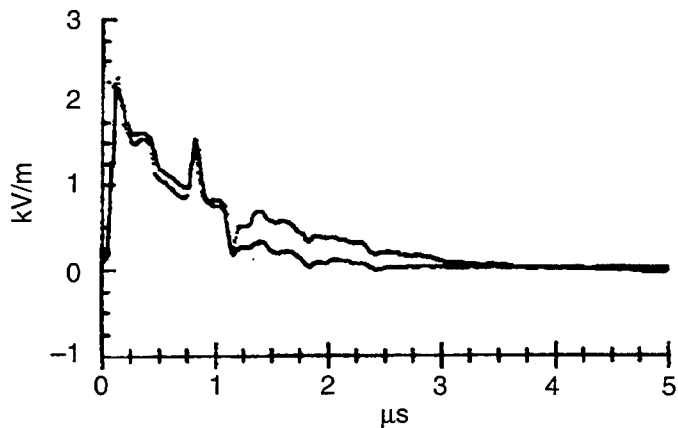


Figure 23. Comparison of horizontal component of H-field (H_x) collected at 50/25/1 and -50/25/1 (dotted line).

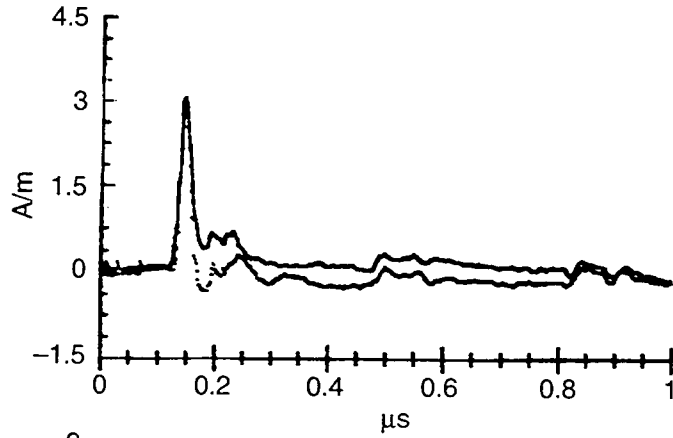


Figure 24. Comparison of radial component of H-field (H_y) collected at 50/25/1 and -50/25/1 (dotted line).

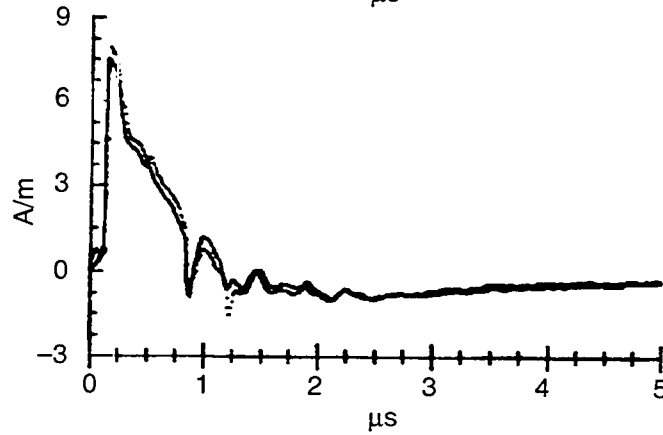


Figure 25. Comparison of vertical component of H-field (H_z) collected at 50/25/1 and -50/25/1 (dotted line).

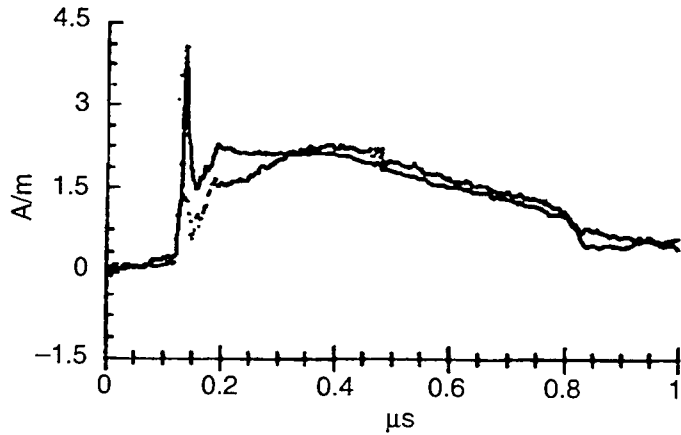


Figure 26. Comparison of horizontal component of E-field (E_x) collected at 50/50/1 and -50/50/1 (dotted line).

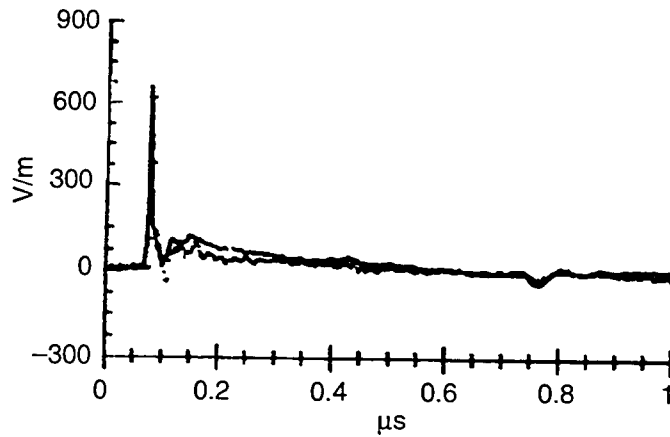


Figure 27. Comparison of radial component of E-field (E_y) collected at 50/50/1 and -50/50/1 (dotted line).

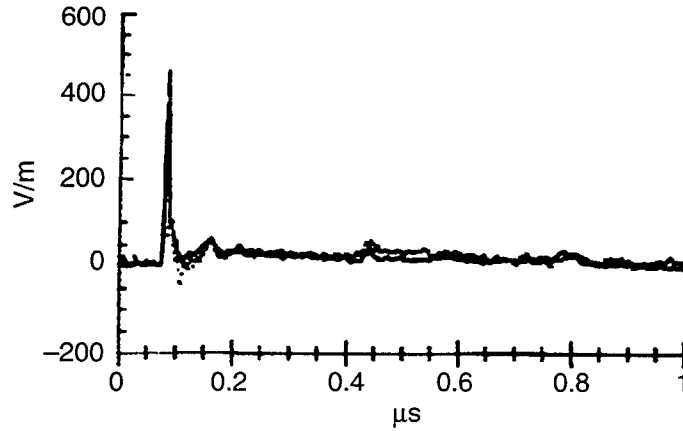


Figure 28. Comparison of vertical component of E-field (E_z) collected at 50/50/1 and -50/50/1 (solid line).

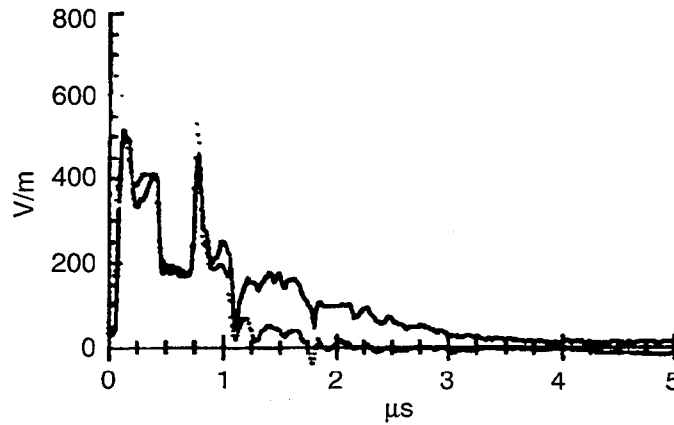


Figure 29. Comparison of horizontal component of H-field (H_x) collected at 50/50/1 and -50/50/1 (solid line).

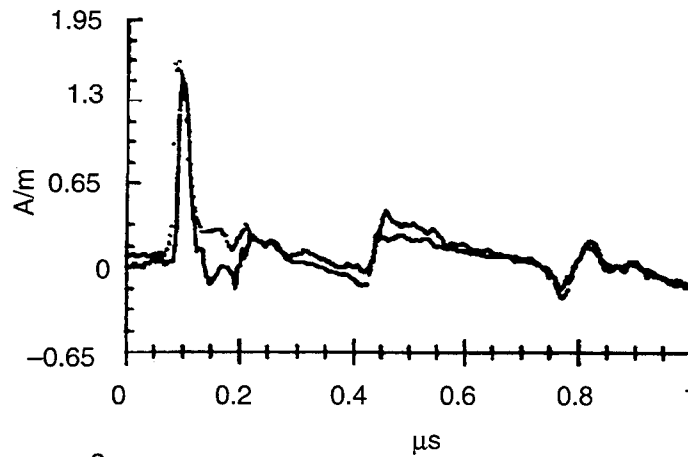


Figure 30. Comparison of radial component of H-field (H_y) collected at 50/50/1 and -50/50/1 (dotted line).

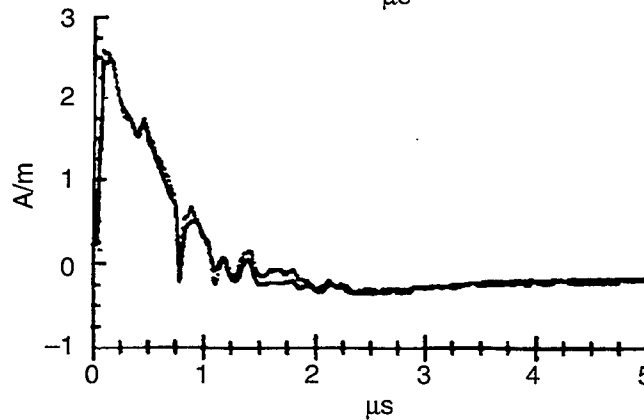


Figure 31. Comparison of vertical component of H-field (H_z) collected at 50/50/1 and -50/50/1 (solid line).

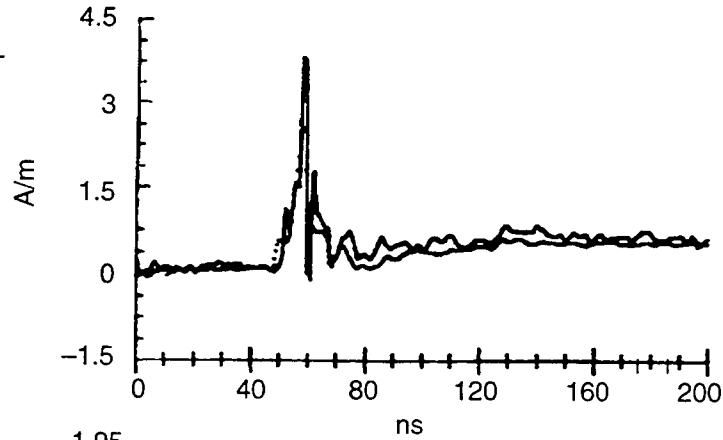


Figure 32. Comparison of horizontal component of E-field (E_x) collected at 25/50/1 and -25/50/1 (dotted line).

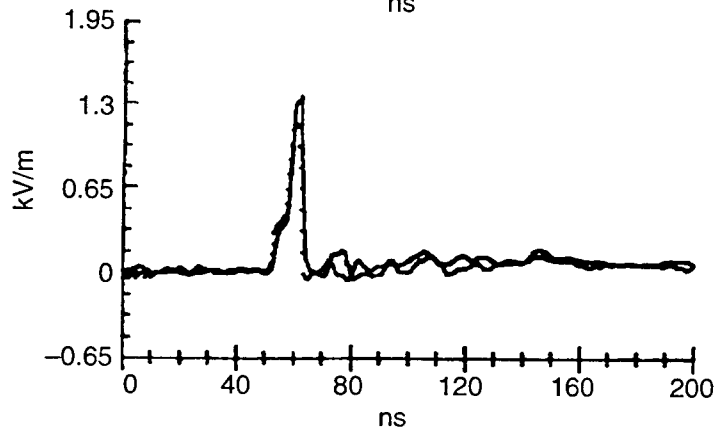


Figure 33. Comparison of radial component of E-field (E_y) collected at 25/50/1 and -25/50/1 (solid line).

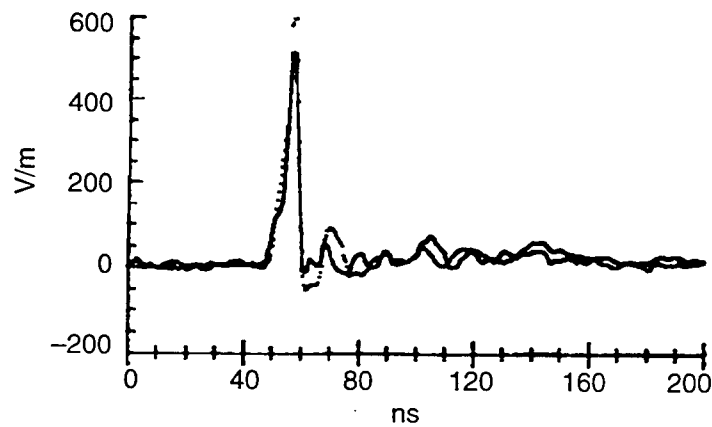


Figure 34. Comparison of vertical component of E-field (E_z) collected at 25/50/1 and -25/50/1 (dotted line).

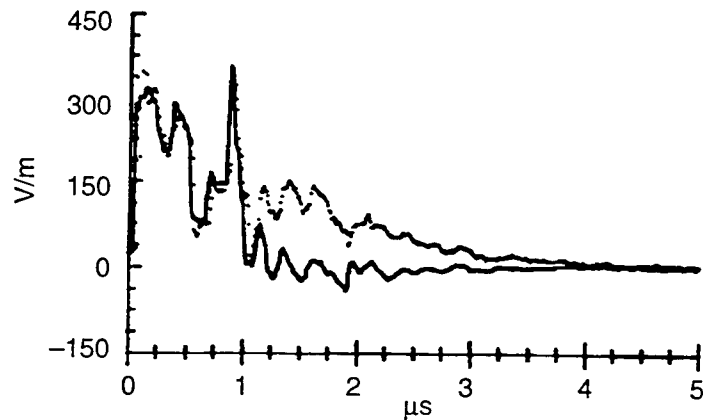


Figure 35. Comparison of horizontal component of H-field (H_x) collected at 25/50/1 and -25/50/1 (solid line).

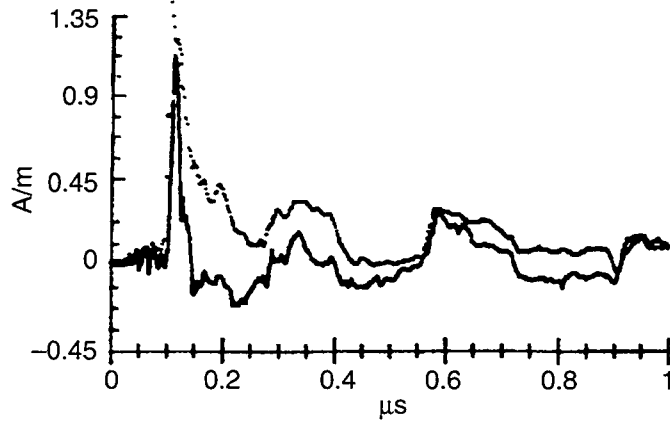


Figure 36. Comparison of radial component of H-field (H_y) collected at 25/50/1 and -25/50/1 (solid line).

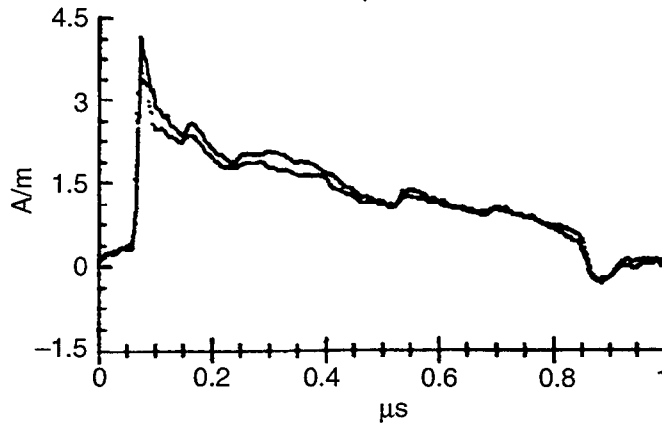


Figure 37. Comparison of vertical component of H-field (H_z) collected at 25/50/1 and -25/50/1 (solid line).

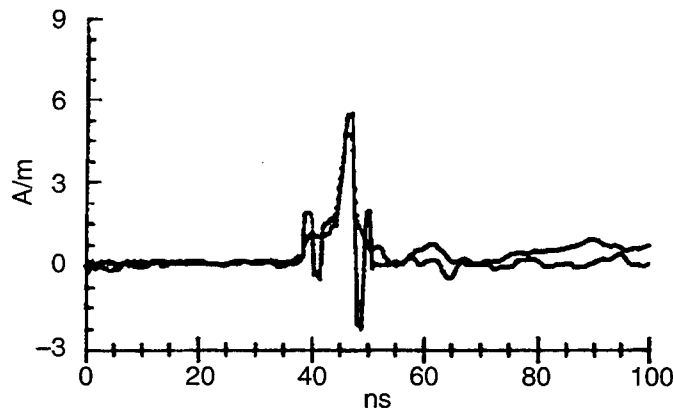


Figure 38. Comparison of horizontal component of E-field (E_x) collected at 35/35/1 and -35/35/1 (solid line).

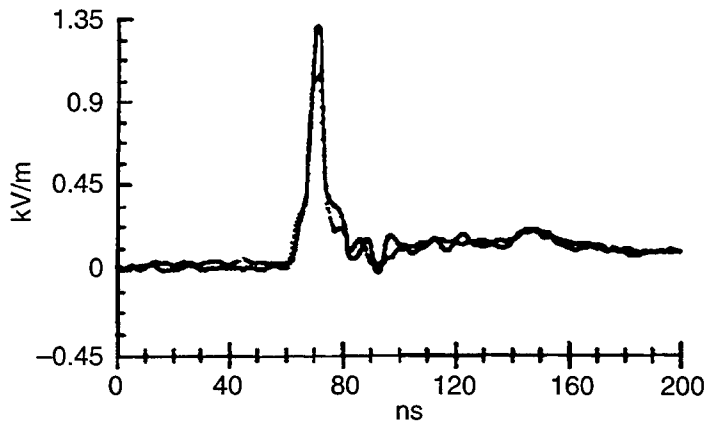


Figure 39. Comparison of radial component of E-field (E_y) collected at 35/35/1 and -35/35/1 (dotted line).

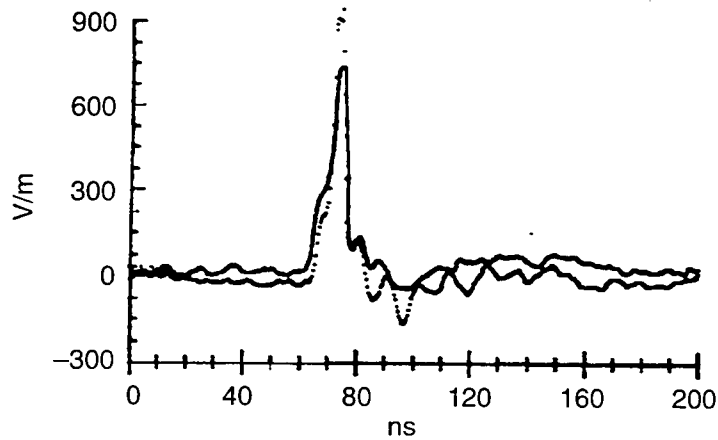


Figure 40. Comparison of vertical component of E-field (E_z) collected at 35/35/1 and -35/35/1 (dotted line).

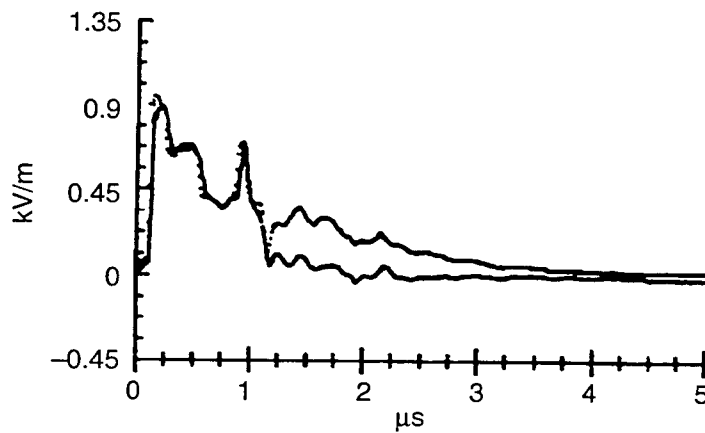


Figure 41. Comparison of horizontal component of H-field (H_x) collected at 35/35/1 and -35/35/1 (solid line).

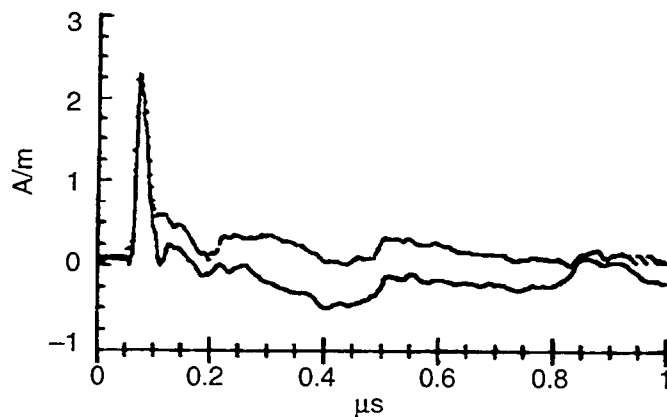


Figure 42. Comparison of radial component of H-field (H_y) collected at 35/35/1 and -35/35/1 (dotted line).

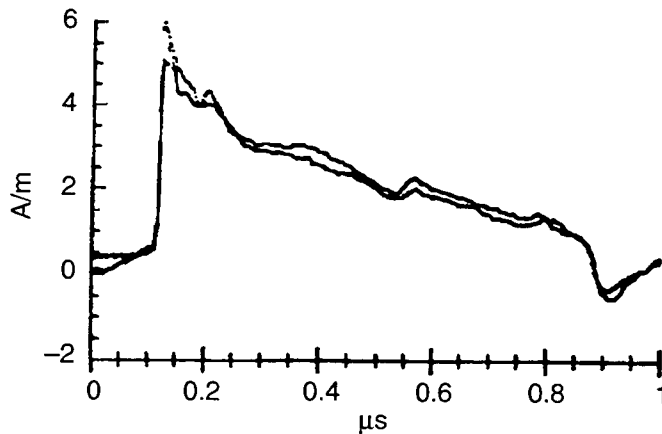
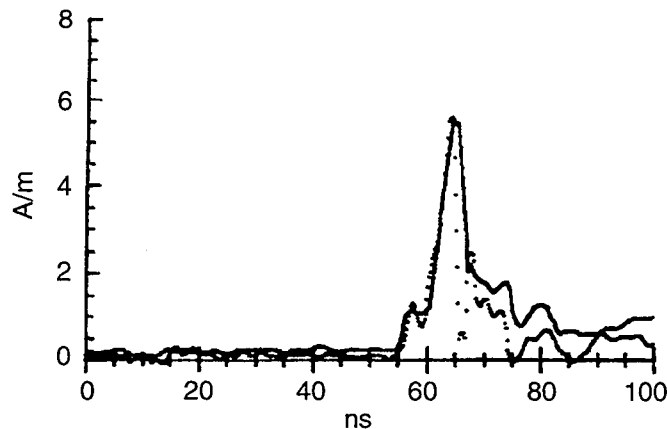


Figure 43. Comparison of vertical component of H-field (H_z) collected at 35/35/1 and -35/35/1 (dotted line).



5.3 Data Set Organization

To allow easier interpretation of the measured data, the data set was organized and broken into three groups: data collected at a height of 1 m, data collected at a height of 2 m, and data collected to examine the field contour of the expanding pulse wavefront. For comparison purposes, all of the data presented in these three groups have been normalized to a common incident E-field strength of 6.5 kV/m at a range of 50 m from the REPS pulser. The original IVAN data sets for all of the measured data are presented in appendix C.

5.3.1 Data Collected at Height of 1 m

Figure 44 gives the electric field distributions, at a height of 1 m across the REPS test volume based on the peak amplitude of each of the electric field components (E_x , E_y , and E_z). Figure 45 displays the peak amplitude of the magnetic field components (H_x , H_y , and H_z) measured at a height of 1 m across the REPS test volume. Figure 46 summarizes the polarity (direction) of each of the field vectors within the test volume.

The pulse waveshape for each of the electric and magnetic field components, measured at a height of 1 m over the test volume, are displayed in figures 47 through 52. These figures should only be used to monitor the overall pulse waveshape of each component. The slower digitizer sweep speeds, necessary to capture the entire waveform, cannot properly capture the high-frequency risetime and amplitude of many of the components. Appendix C should be referred to if a more accurate measurement of the pulse's early-time waveshape is required.

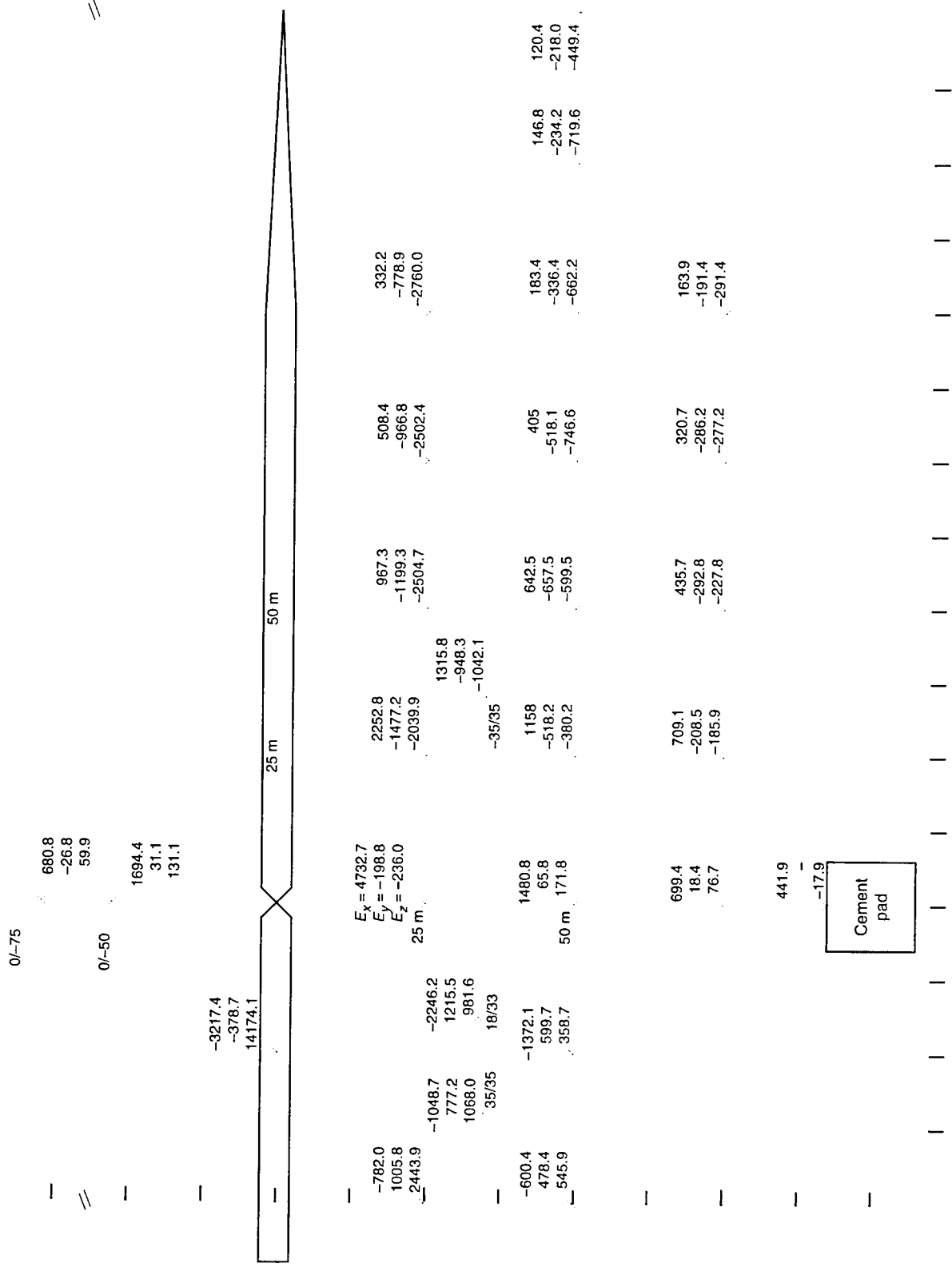


Figure 44. Field distribution of peak E-field measured at 1 m (normalized to 6.5 kV/m at 50 m).

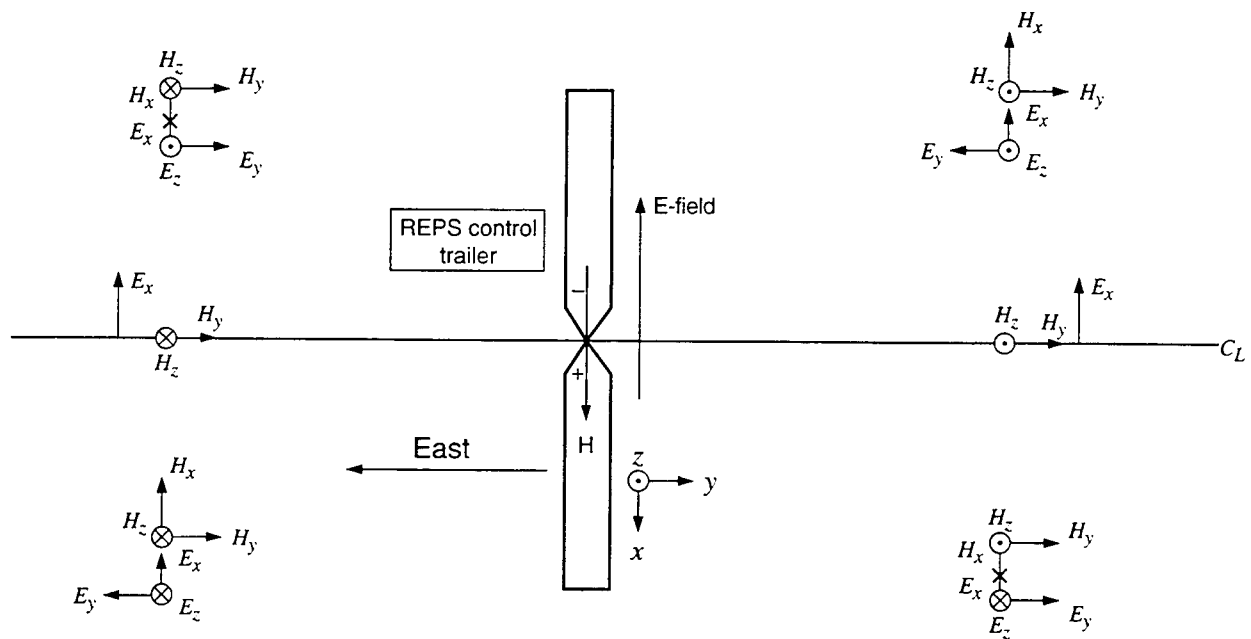


Figure 46. Polarity (direction) of E- and H-field components.

5.3.2 Data Collected at Height of 2 m

The data collected at a height of 2 m are presented in the same manner as the 1-m data. Figures 53 and 54 show the field distribution of the electric and magnetic fields in terms of peak amplitude. The entire pulse waveshape for each of the field components is displayed in appendix C.

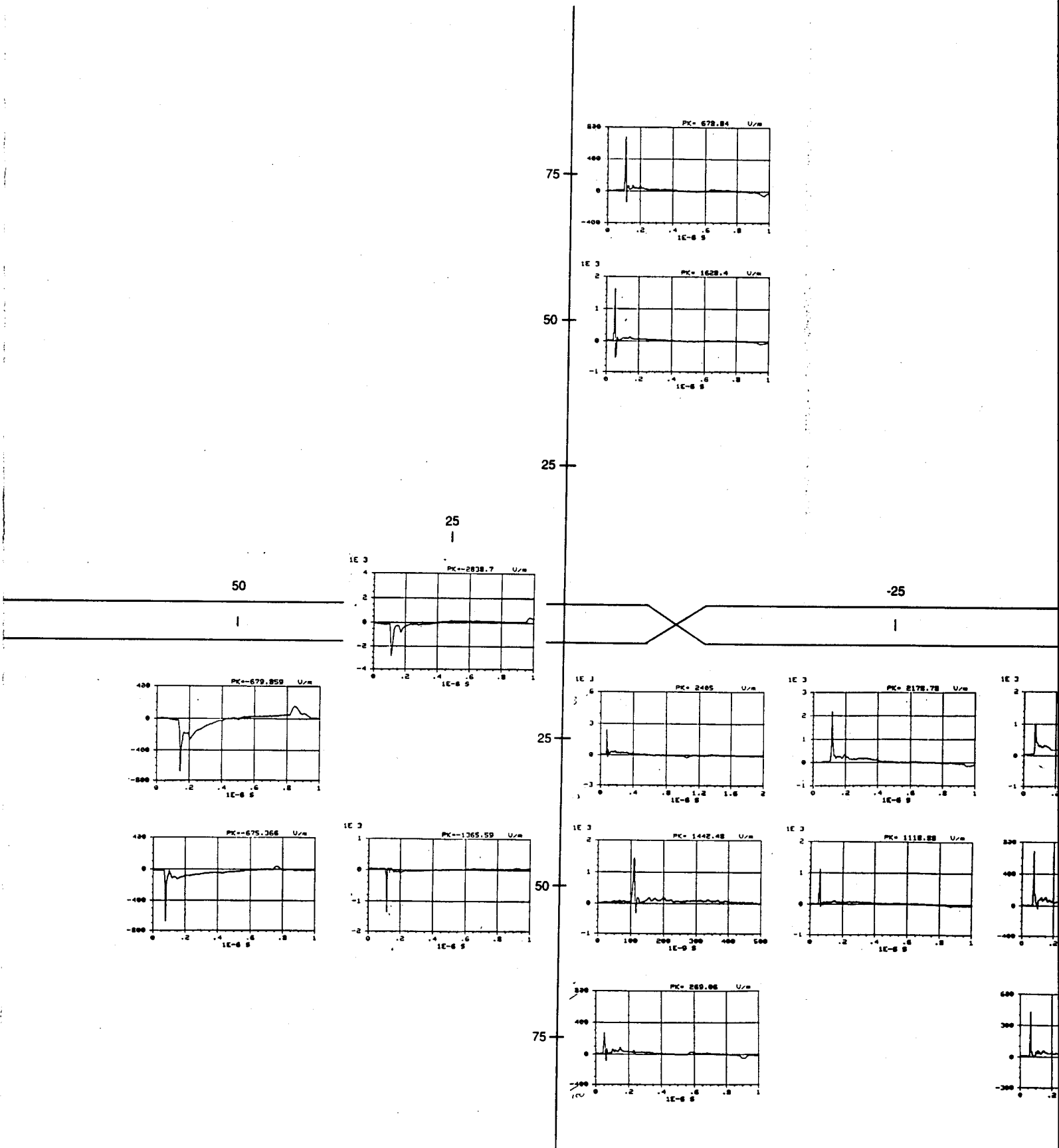


Figure 47. Field distribution of horizontal component of E-field (E_x) measured at 1 m (normalized to 6.5 kV/m at 50 m).

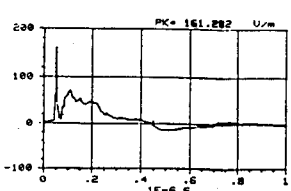
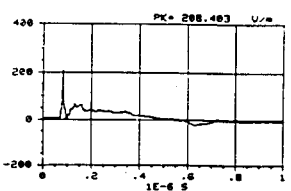
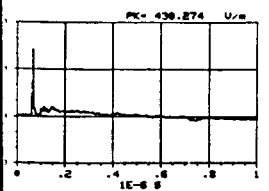
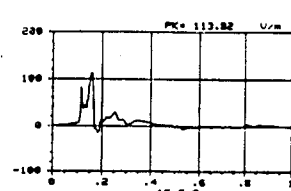
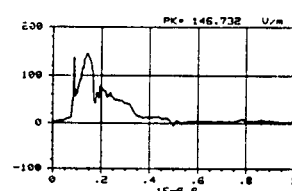
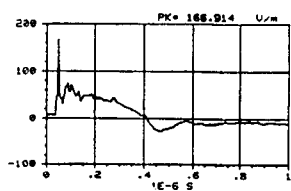
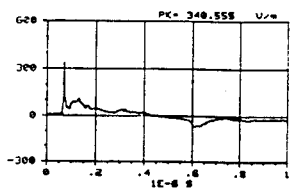
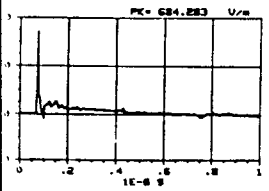
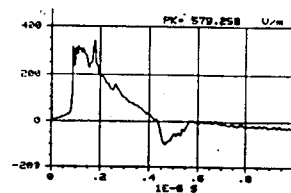
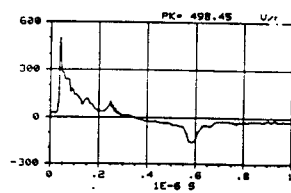
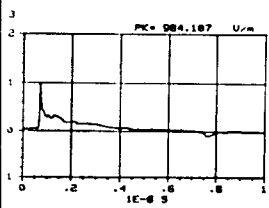
-50

-75

-100

-125

-150



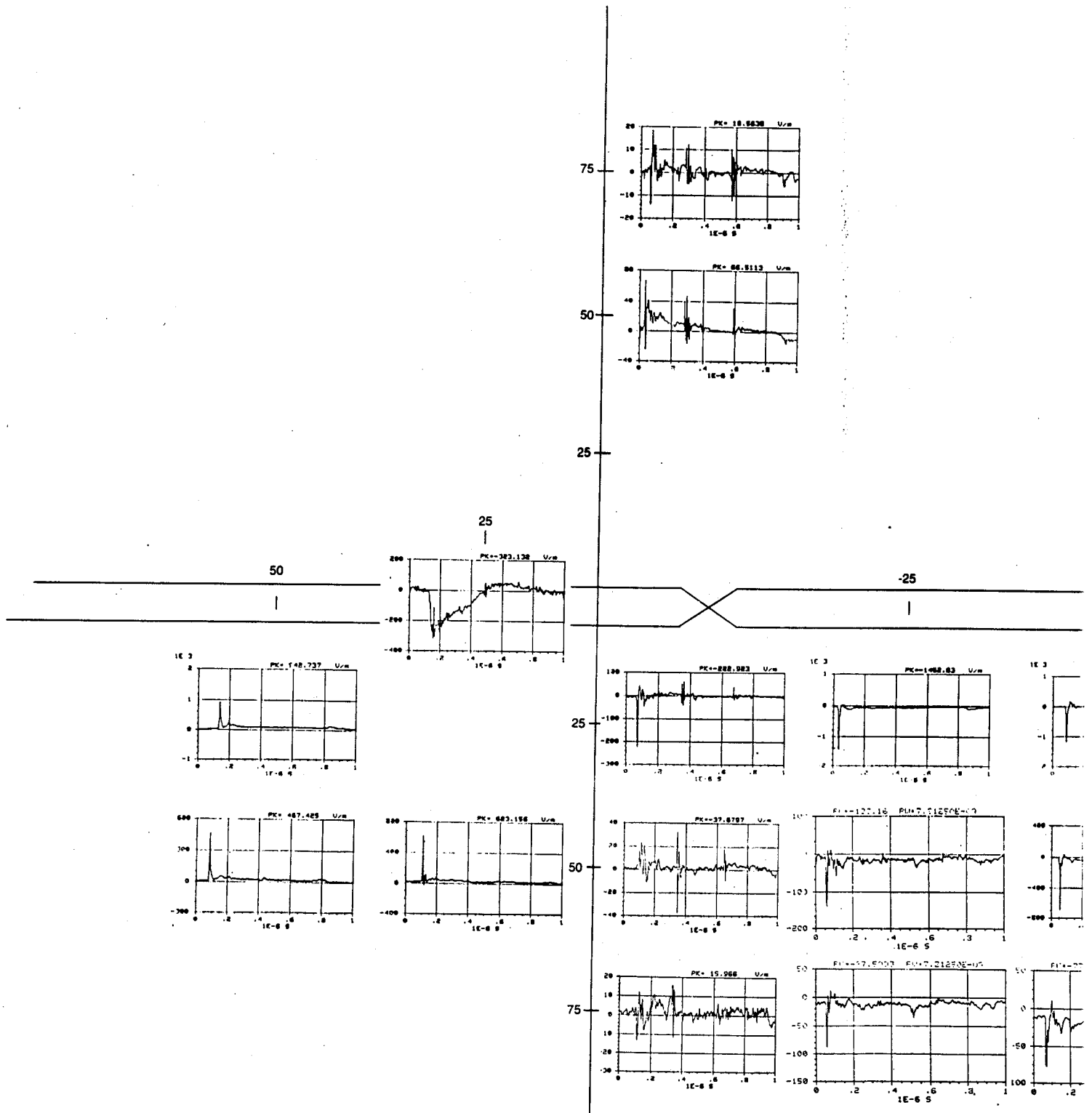


Figure 48. Field distribution of radial component of E-field (E_r) measured at 1 m (normalized to 6.5 kV/m at 50 m).

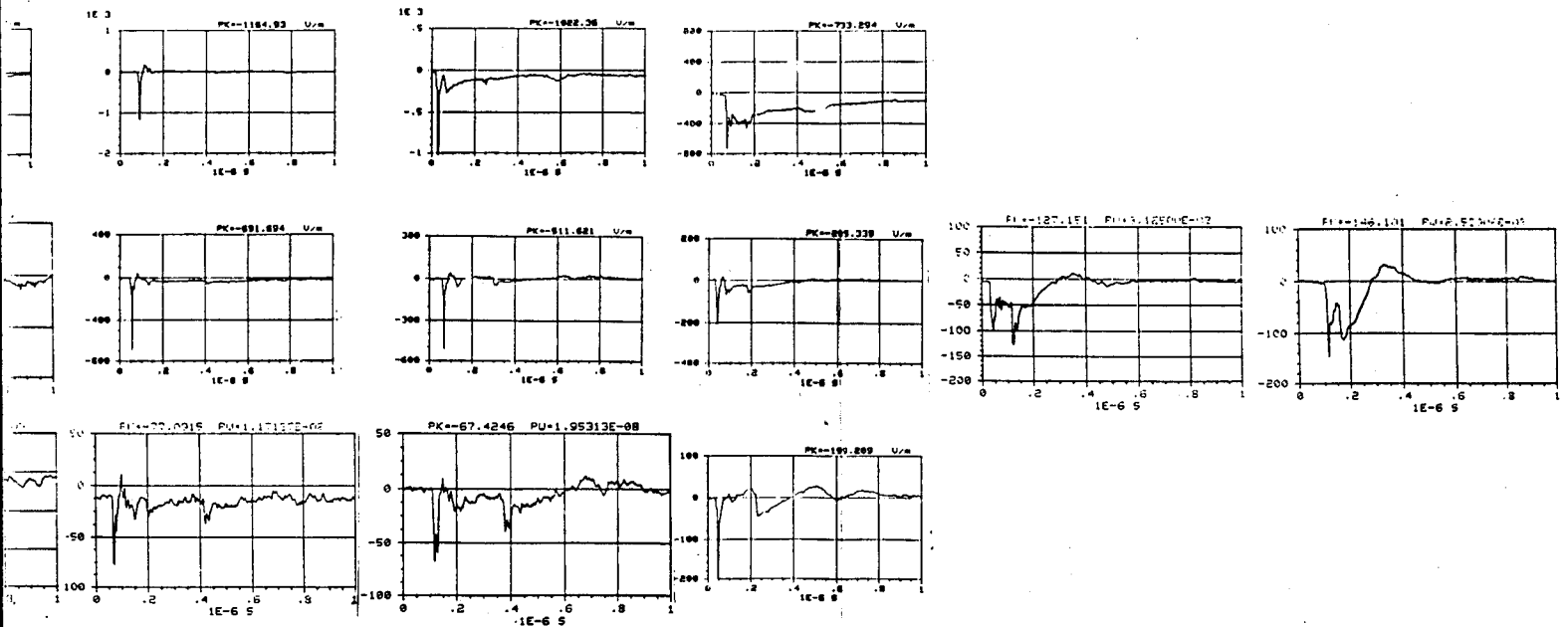
-50

-75

-100

-125

-150



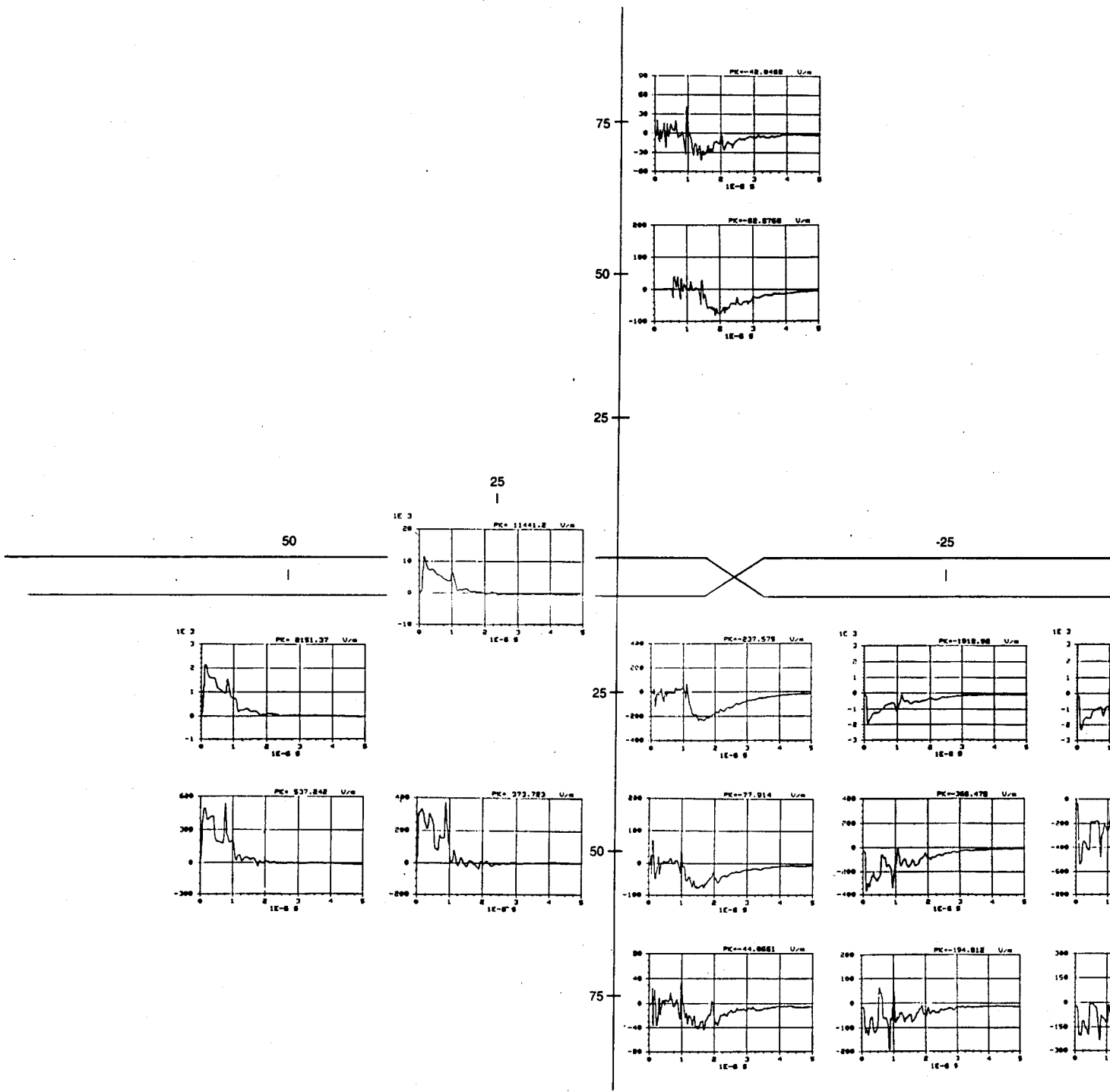


Figure 49. Field distribution of vertical component of E-field (E_z) measured at 1 m (normalized to 6.5 kV/m at 50 m).

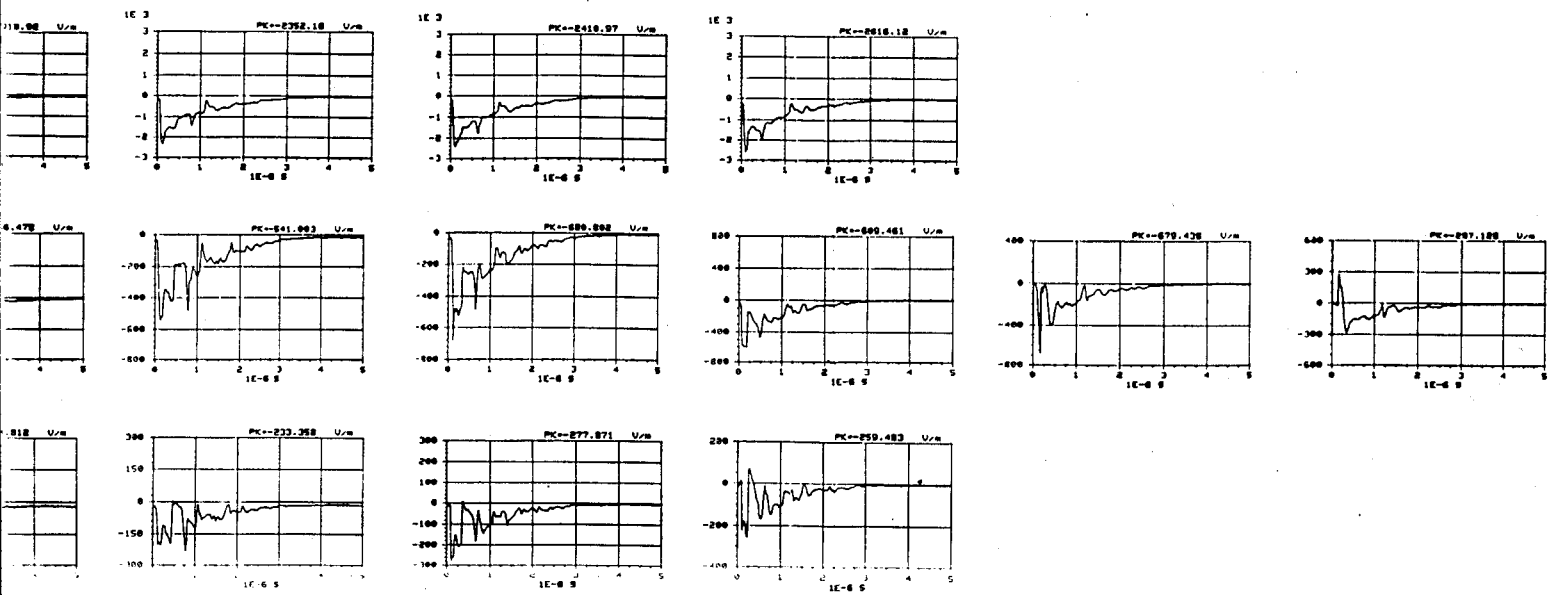
-50

-75

-100

-125

-150



(V/m at 50 m).

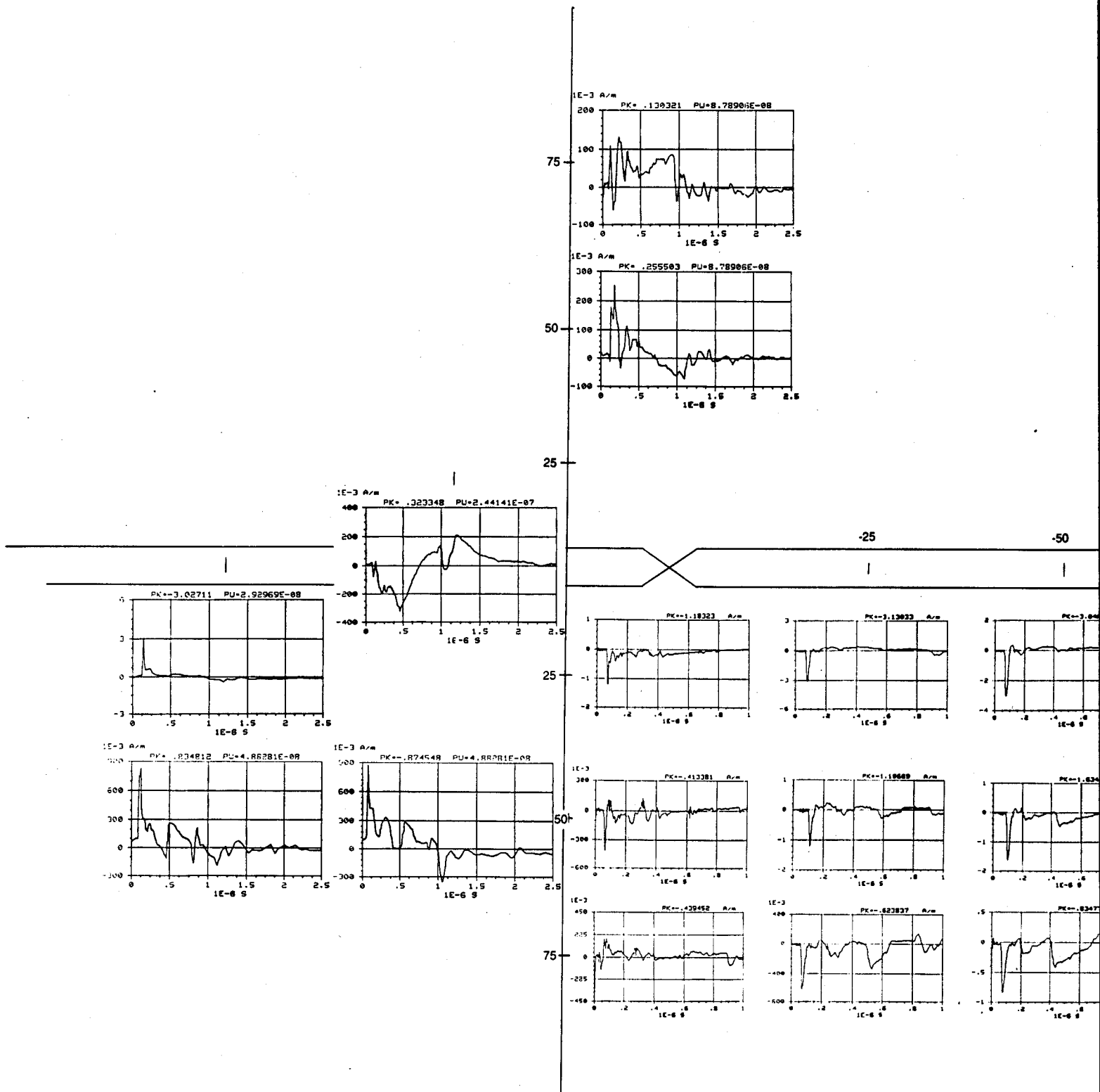


Figure 50. Field distribution of horizontal component of H-field (H_x) measured at 1 m (normalized to 6.5 kV/m at 50 m).

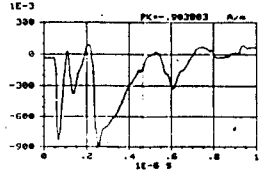
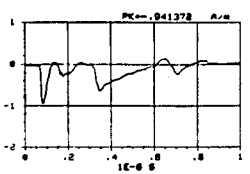
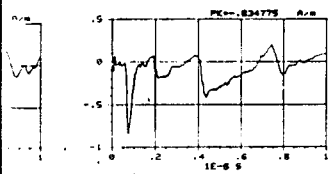
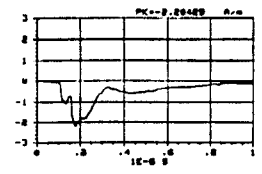
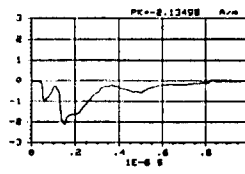
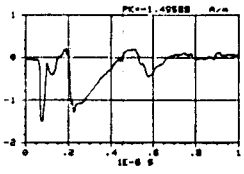
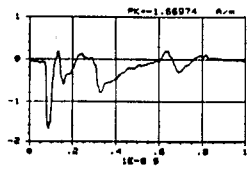
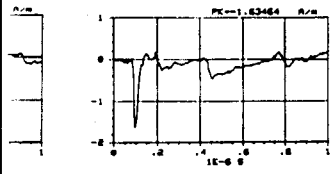
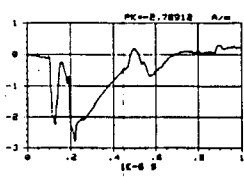
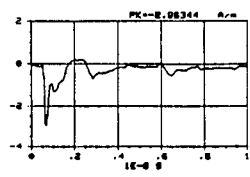
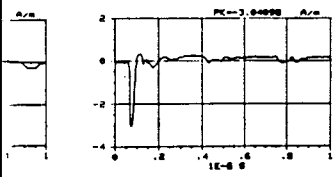
-50

-75

-100

-125

-150



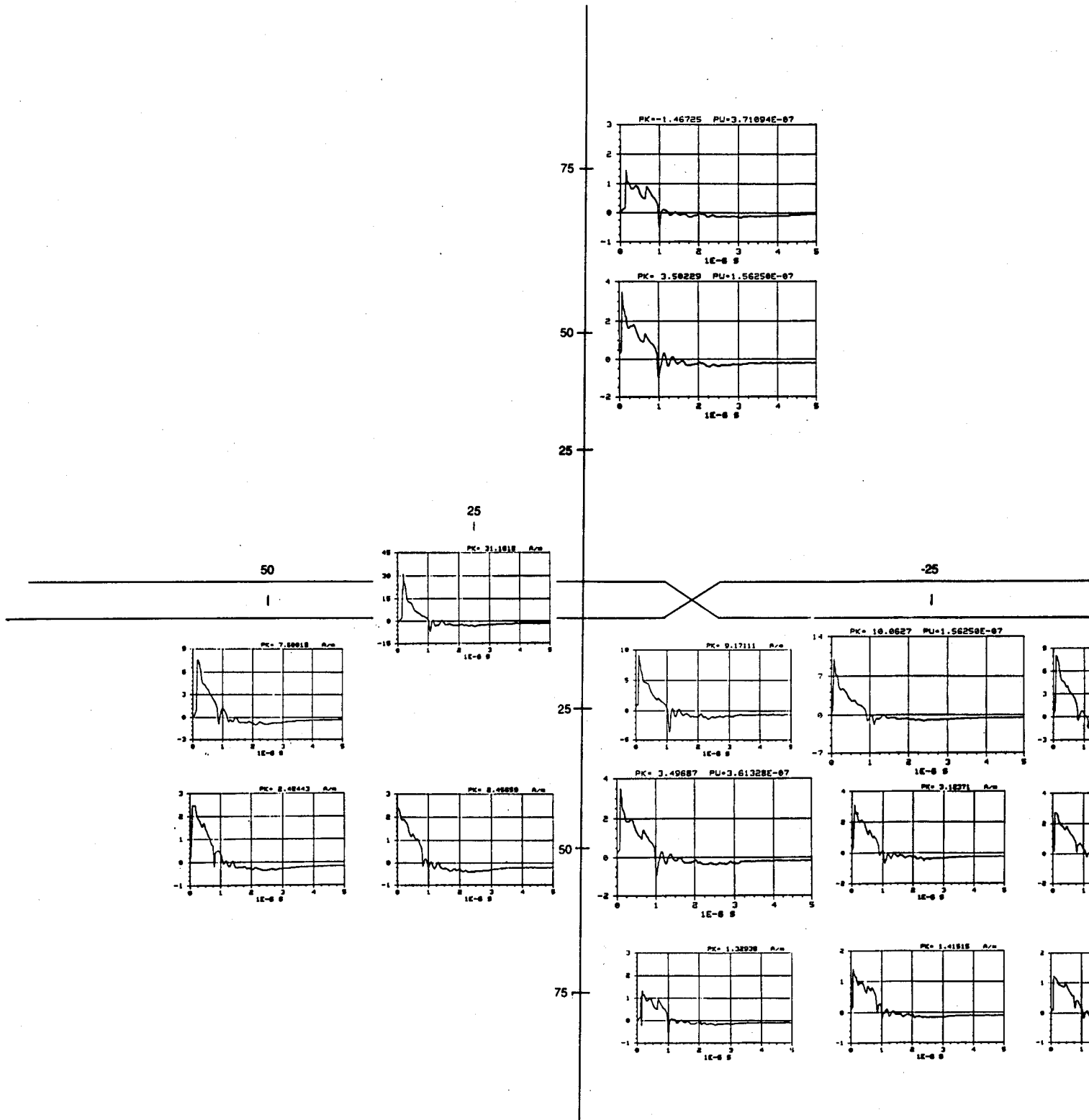


Figure 51. Field distribution of radial component of H-field (H_y) measured at 1 m (normalized to 6.5 kV/m at 50 m).

25

-50

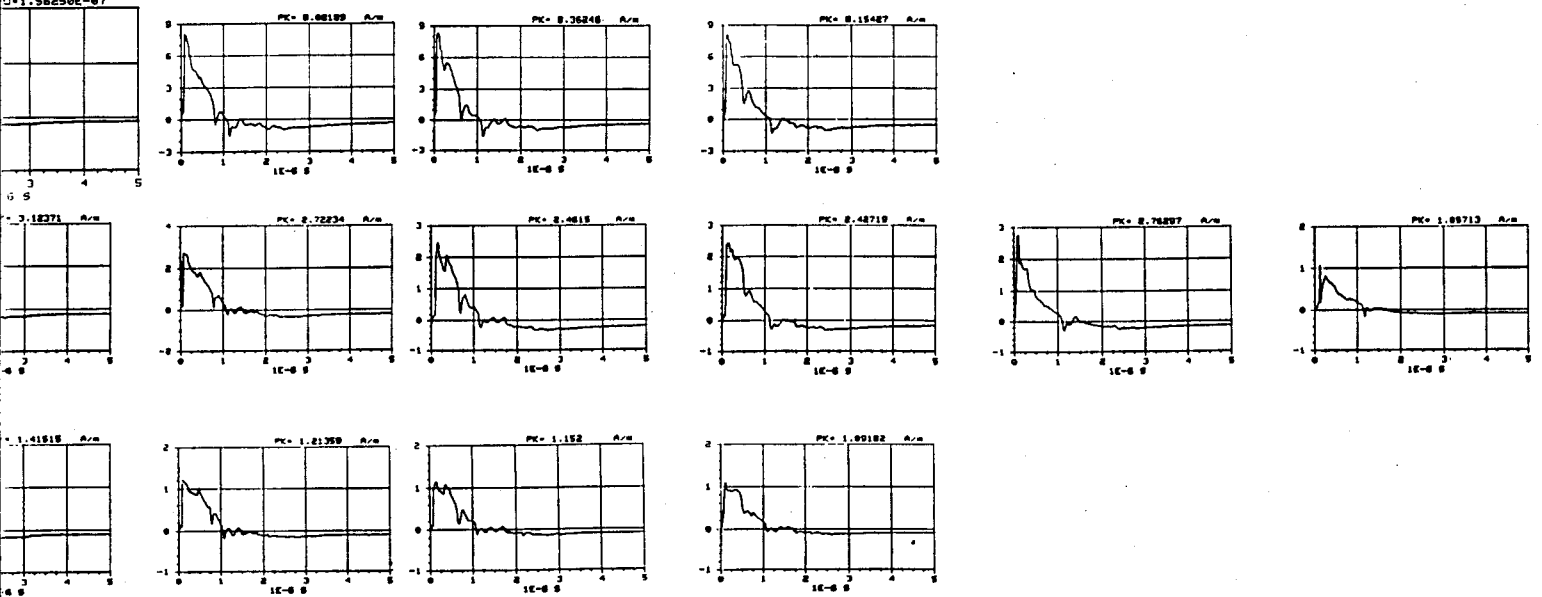
-75

-100

-125

-150

U=1.56250E-07



m at 50 m).

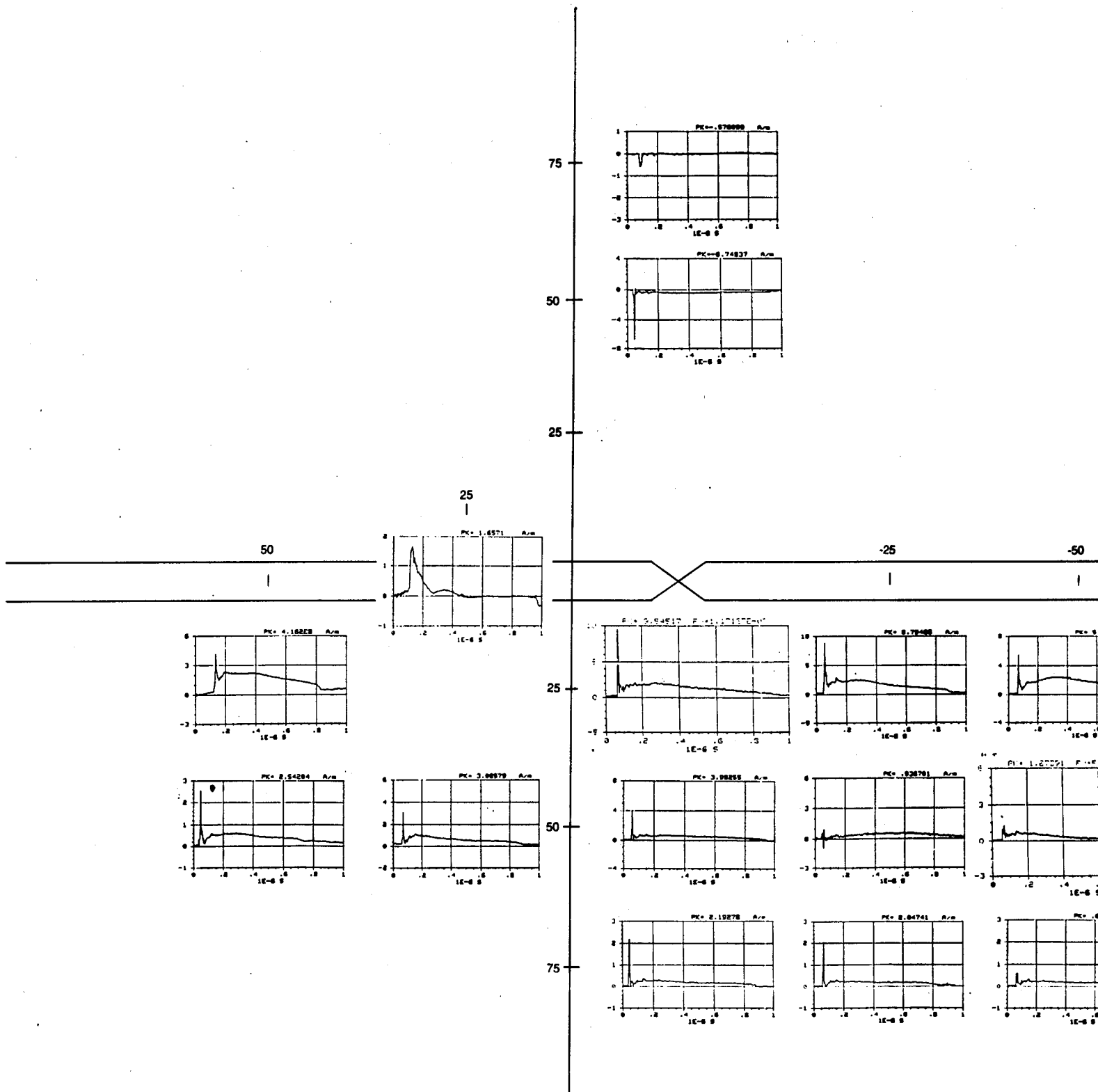


Figure 52. Field distribution of vertical component of H-field (H_z) measured at 1 m (normalized to 6.5 kV/m at 50 m).

-50

-75

-100

-125

-150

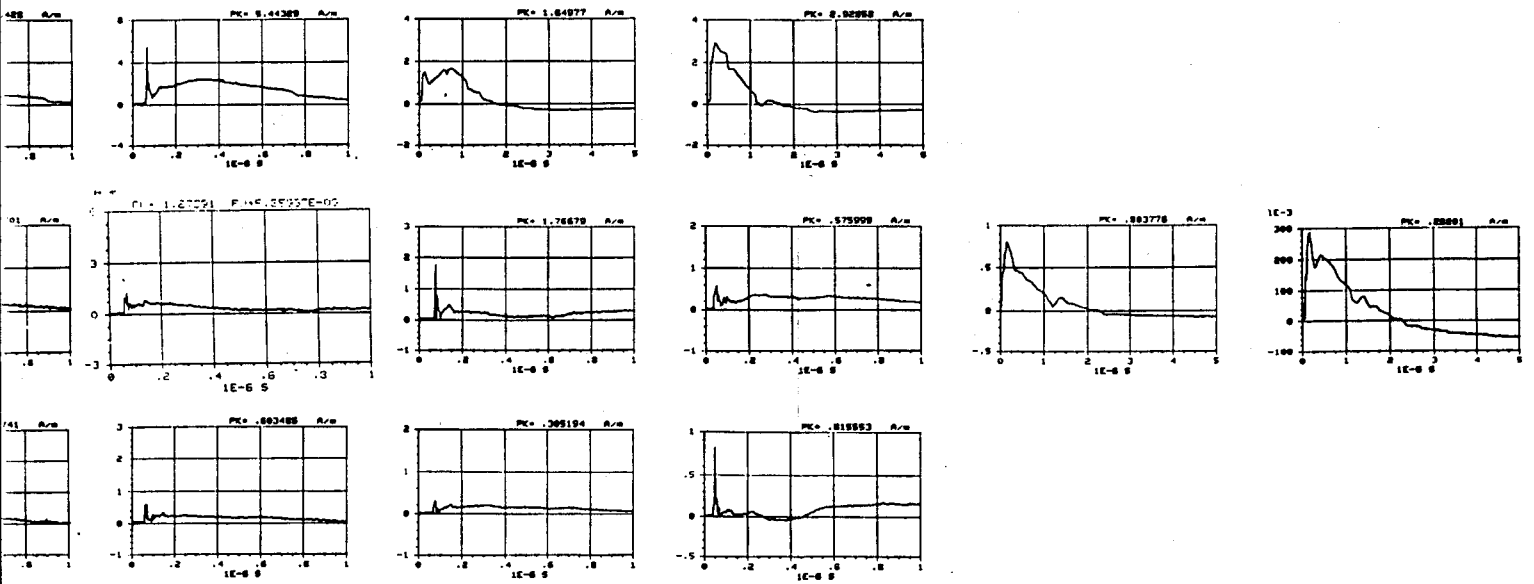


Figure 53. Field distribution of peak E-field measured at 2 m (normalized to 6.5 kV/m at 50 m).

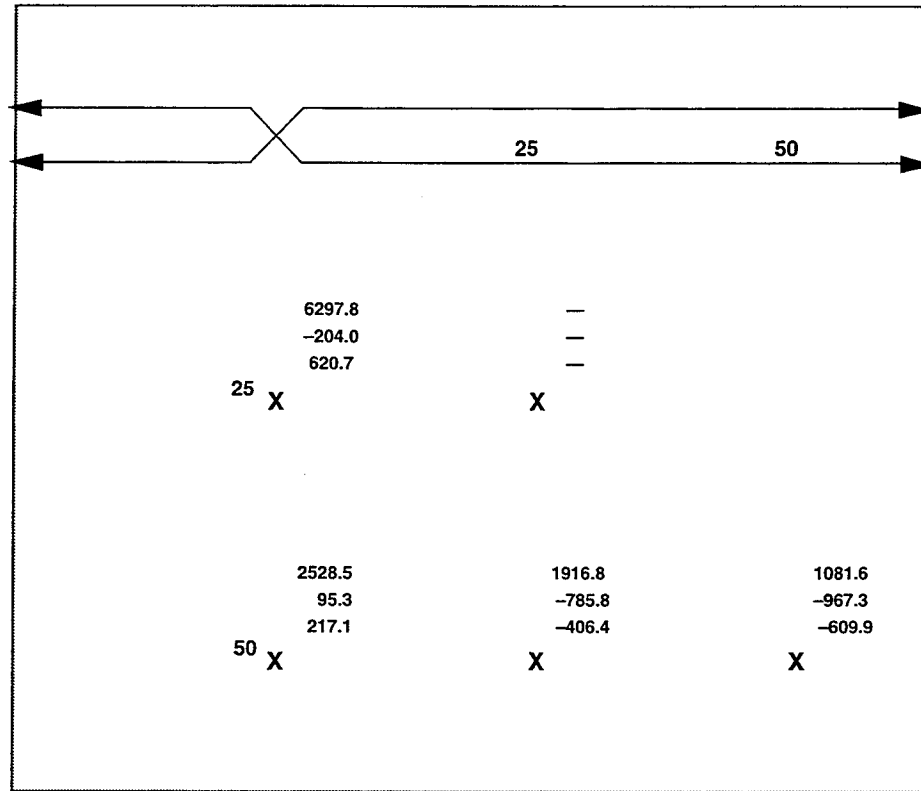
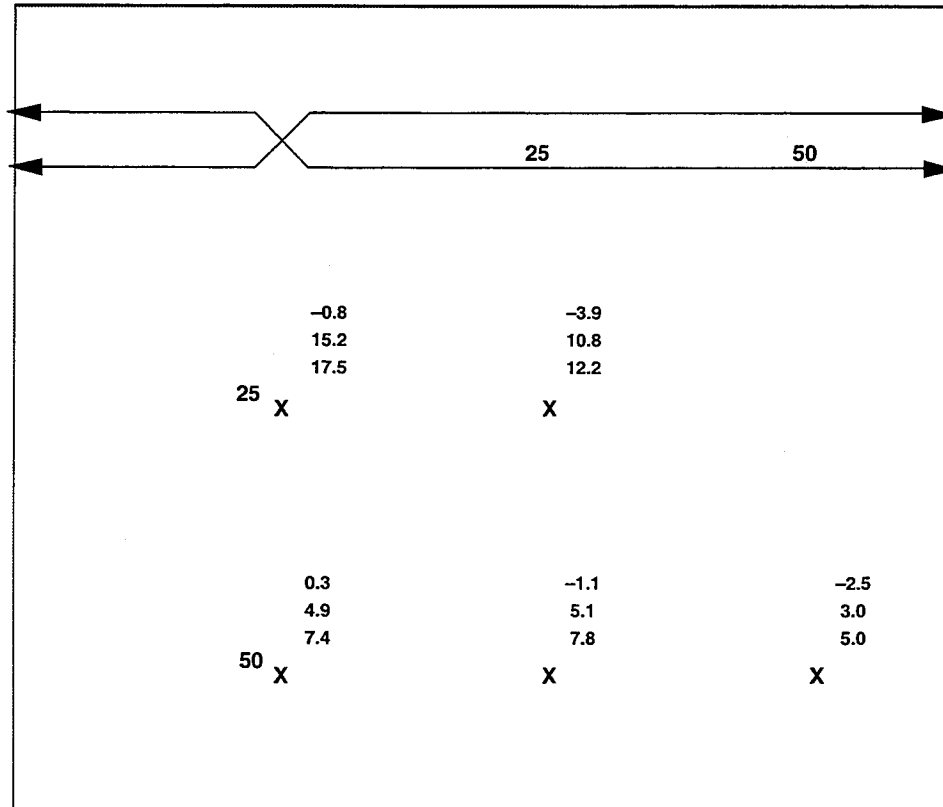


Figure 54. Field distribution of peak H-field measured at 2 m (normalized to 6.5 kV/m at 50 m).



6. Field Uniformity

To properly characterize the fields launched from the REPS pulser, it is important to examine the uniformity of the expanding wavefront. Up to this point, the total E- and H-field reported in this document have been measured and described in terms of six Cartesian components. One disadvantage to measuring fields through individual components is that it is much harder to characterize the uniformity of the expanding wavefront because of its spherical nature. A more direct method of examining wavefront uniformity would be to position the sensors to measure the transverse electric and magnetic fields directly. Because it is difficult to place the sensors at the angles required to measure these vectors, and since a majority of military systems to be tested at REPS will have cables oriented parallel to the earth, we decided that only the vector of the tangential E-field (E_t) parallel to the ground (E_x on the centerline) and the radial vector of the incident H-field (H_r) parallel to the ground (H_y on the centerline) would be measured. These two components would provide the most coupling to ground-deployed cables.

6.1 Locating Test Points

To examine the expanding wavefront, we placed two arcs inside the REPS test volume, one at a 50-m ground range and another at an 85-m range. The measurement points to be examined on these two arcs were surveyed and staked in the same manner as the rectangular grid mentioned in section 3.2. The test point locations for these two arcs are shown in figure 55.

Figures 56 and 57 show the peak amplitudes of the tangential electric field and the radial magnetic field measured at each test point at heights of 1 and 2 m. The entire waveform for all the data measured at these locations is found in appendix C. As expected, figures 56 and 57 show that the wavefront is indeed uniform within the measured region of the REPS test volume. Slight variations in peak amplitude can be attributed to digitizer error and measurement uncertainty created by having to place the sensors at difficult angles.

Figure 56 shows that at 50 m from the antenna, the peak amplitude of the expanding wavefront varies by no more than approximately 10 percent out to an angle of 45 degrees from the centerline. At 85 m from the antenna, field uniformity is better than 5 percent out to 45 degrees. This angle therefore provides a useful bound for the "usable REPS test volume" (see fig. 58).

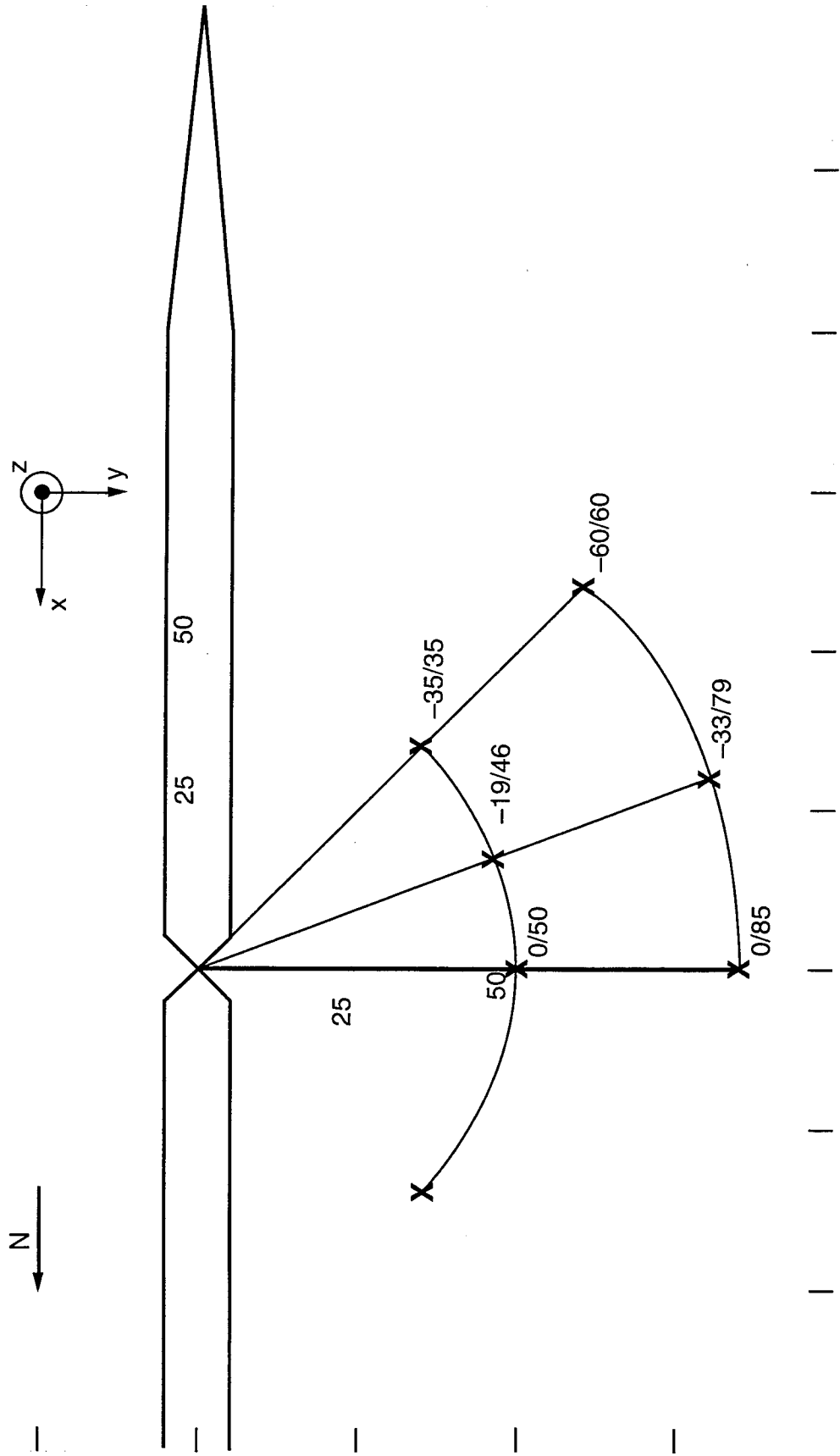


Figure 55. Location of test points for investigation of expanding wavefront uniformity.

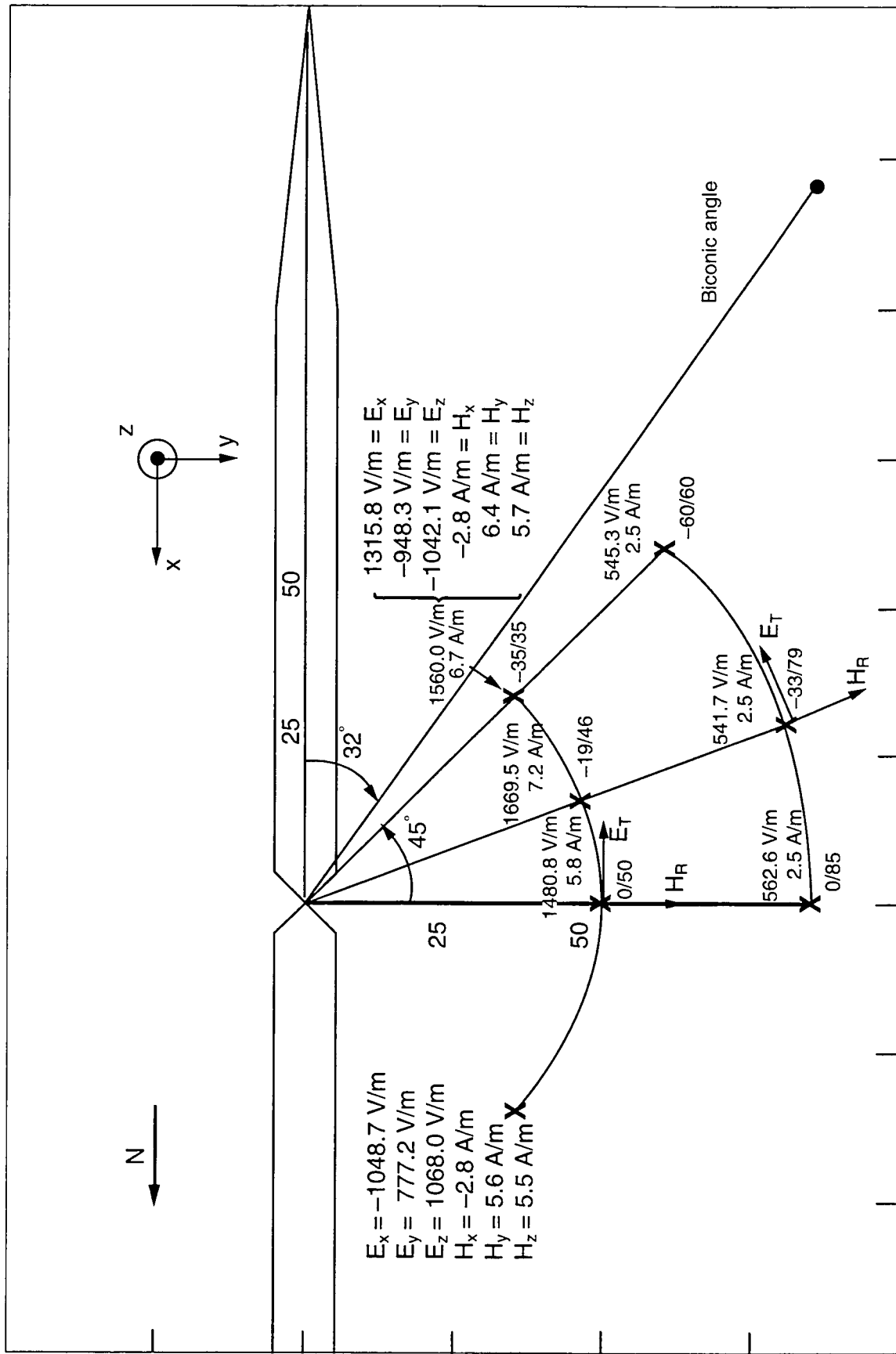


Figure 56. Peak amplitude of tangential electric and radial magnetic fields measured at 1 m on 50- and 85-m arcs (normalized to 6.5 kV/m at 50 m).

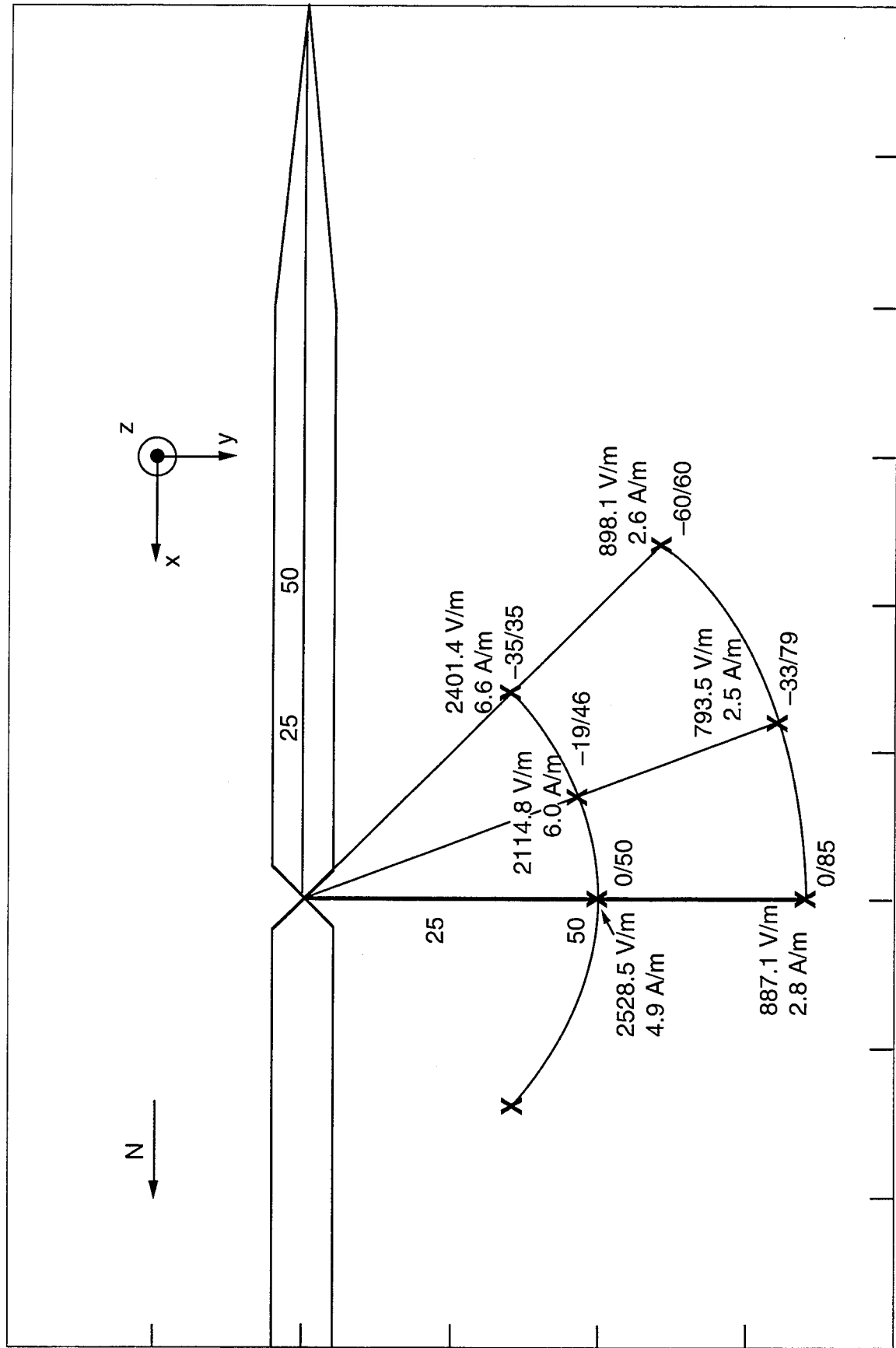


Figure 57. Peak amplitudes of electric and magnetic fields measured at 2 m on 50- and 85-m arcs (normalized to 6.5 kV/m at 50 m).

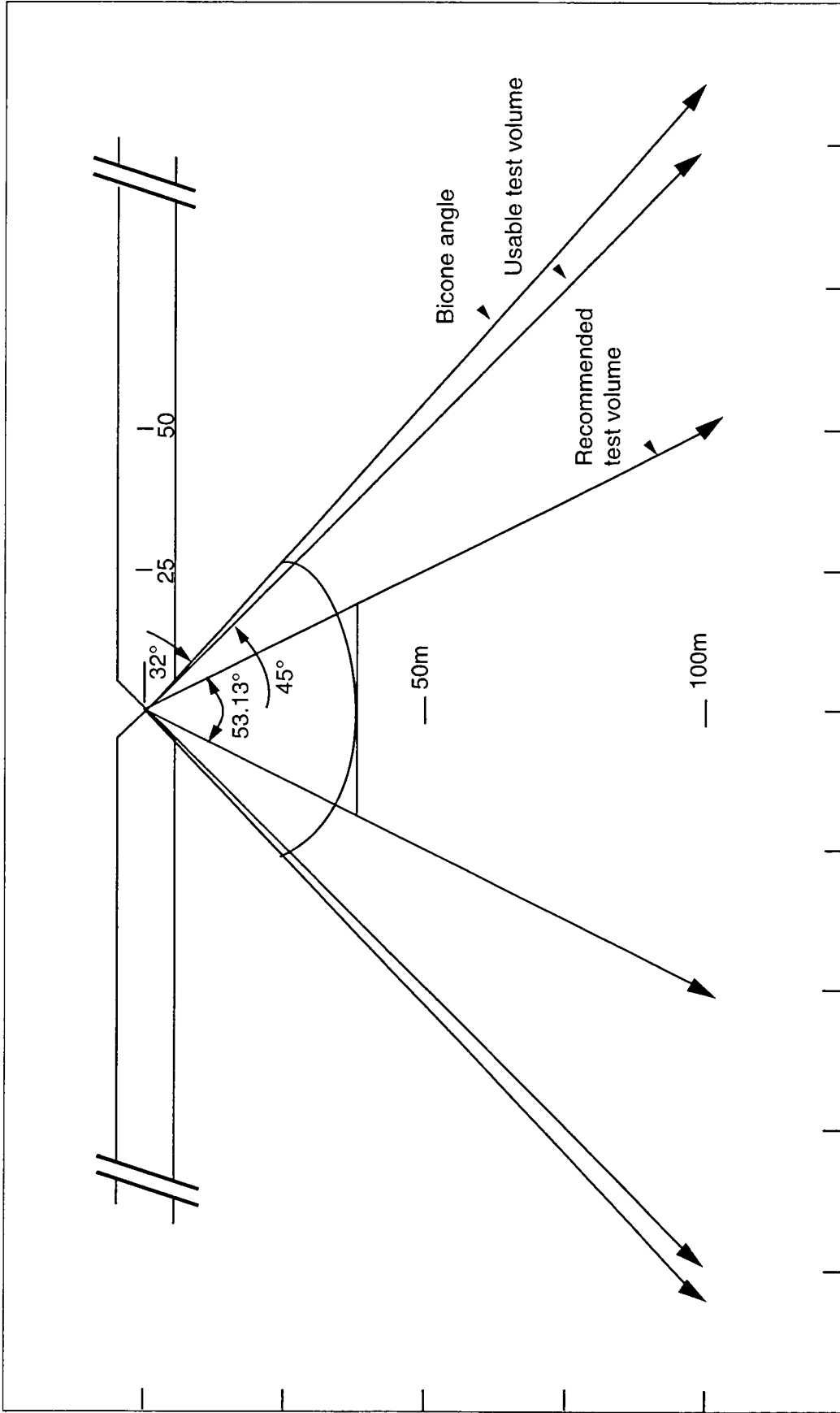


Figure 58. Usable REPS test volume.

6.2 Planewave Approximation

To determine if the wavefront launched from REPS approximated a planewave, we calculated the peak amplitude of the incident E-field at increasing ranges from the pulser and compared this amplitude to the expected $1/R$ field rolloff dependence.

To recreate the incident pulse from measured ground interacted magnetic field components measured during this test, we used the following derivation. Using figure 59, one can trigonometrically determine the y -component of the magnetic field (H_y) and the z -component of the magnetic field (H_z) from the incident (H_i) and reflected (H_r) H-field as follows.

$$H_y = H_i \sin \alpha + H_r \sin \beta ; \quad (1)$$

$$H_z = H_i \cos \alpha - H_r \cos \beta . \quad (2)$$

Solving for H_i and H_r ,

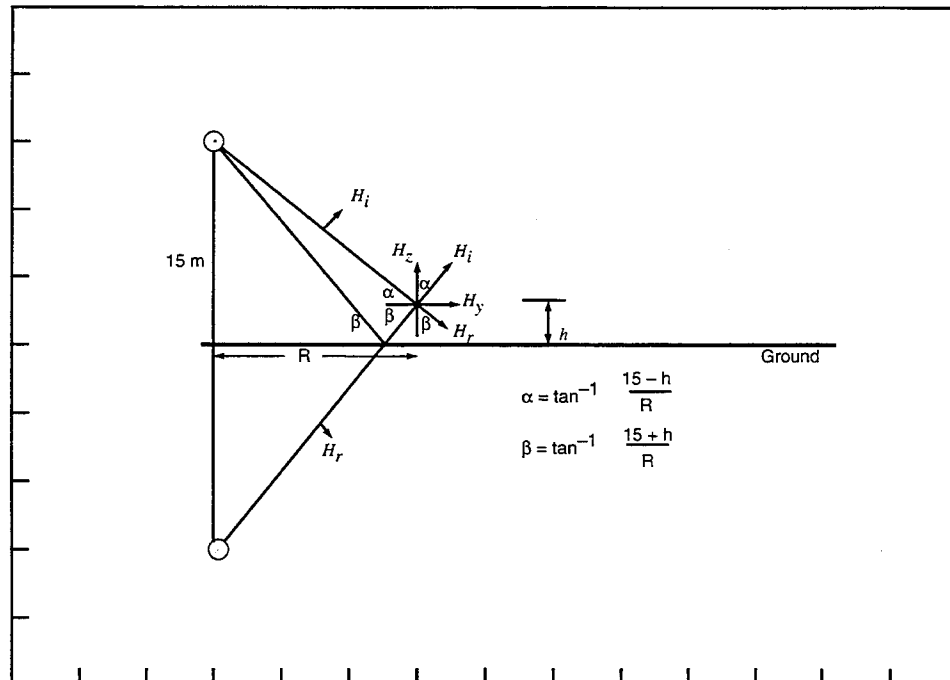
$$H_i = (H_y - H_r \sin \beta) / \sin \alpha ; \quad (3)$$

$$H_r = (H_i \cos \alpha - H_z) / \cos \beta . \quad (4)$$

Combining equations (3) and (4),

$$H_i = (H_y - (H_i \cos \alpha - H_z / \cos \beta) \sin \beta) / \sin \alpha . \quad (5)$$

Figure 59. Vector components for incident and reflected magnetic fields.



Solving for H_i ,

$$H_i = (H_y \cos \beta + H_z \sin \beta) / (\sin \alpha \cos \beta + \cos \alpha \sin \beta), \quad (6)$$

using the algebraic identity $\sin(\alpha + \beta) = \sin \alpha \cos \beta + \cos \alpha \sin \beta$,

$$H_i \text{ (A/m)} = (H_y \cos \beta + H_z \sin \beta) / \sin(\alpha + \beta). \quad (7)$$

Figure 60 shows a plot of the calculated range dependence (using eq (7)) for the incident field launched from REPS based on measured H_y and H_z components. A statistical power regression of these data shows a range dependence of $1/R^{0.97}$, which agrees with the theoretical planewave range dependence of $1/R$. This implies that based on peak amplitudes, the wavefront launched from REPS does approximate a planewave.

The range dependence of the dominant ground-interacted components along the centerline (E_x , H_y , and H_z) have also been determined, as shown in figures 61 to 63. Figures 60 to 63 can be used to infer the EM environment produced by REPS at ranges beyond the typical test volume.

Figure 60. Range dependence of incident E-field along centerline.

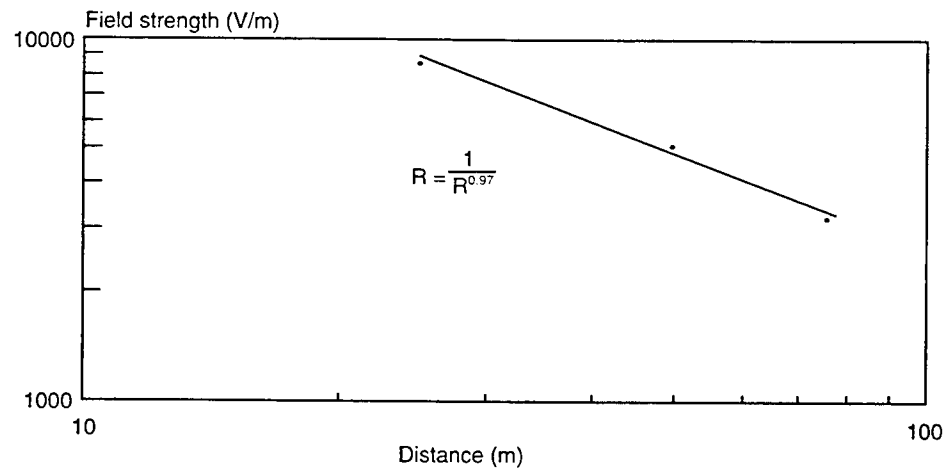


Figure 61. Range dependence of horizontal E-field (E_x) measured along centerline.

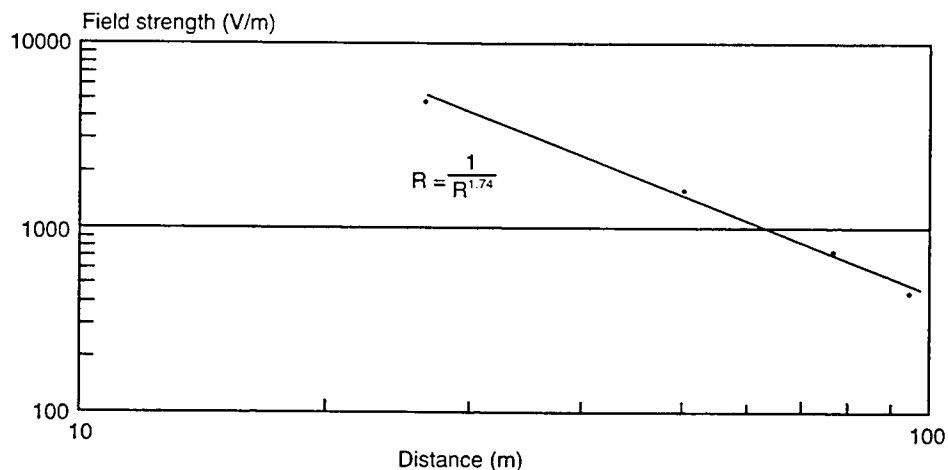


Figure 62. Range dependence of radial H-field (H_y) measured along centerline.

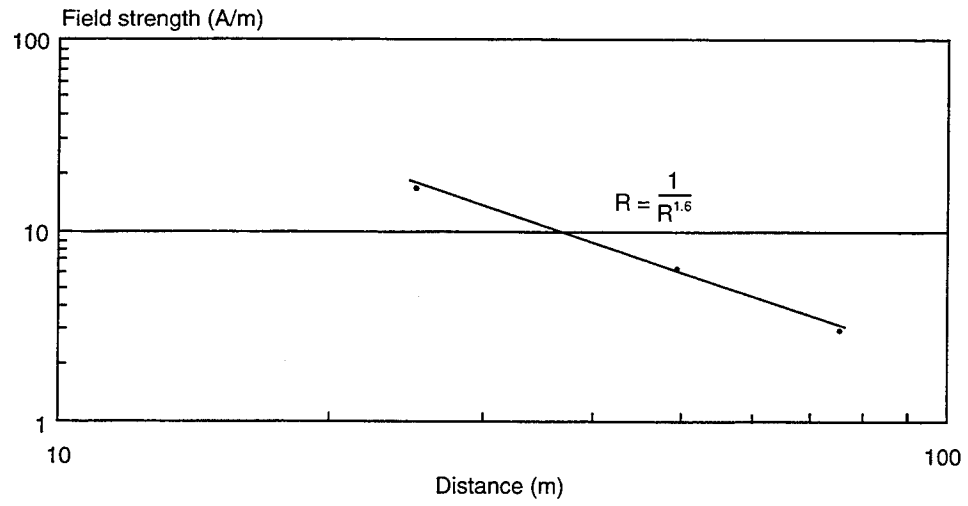
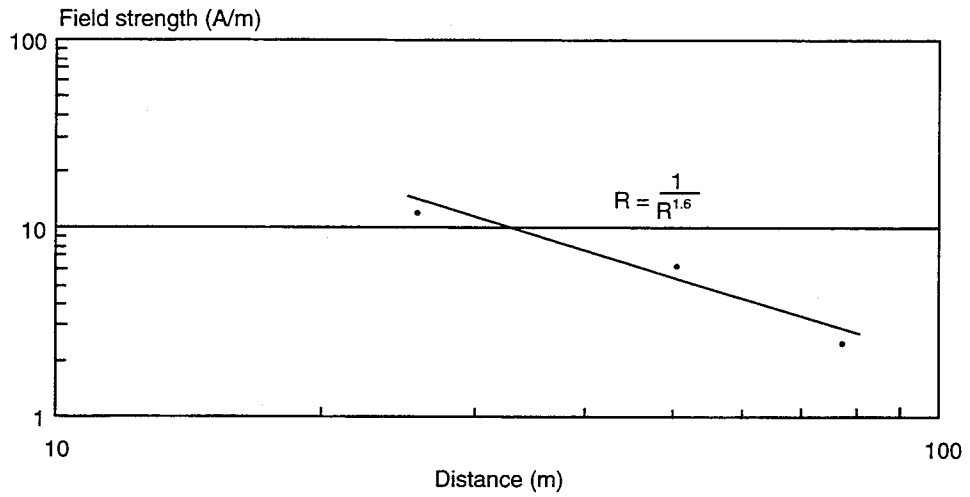


Figure 63. Range dependence of vertical H-field (H_z) measured along centerline.



7. Inspection of Data Set

7.1 Sensor Bandwidth Limitations

When examining the magnetic field waveforms, one must realize that the lower 3-dB bandwidth of the magnetic field sensors used to record the data is approximately 100 kHz (see fig. B-13). For magnetic fields with significant energy below 100 kHz, the late time response (lower frequencies) will be attenuated by the rolloff of the sensor's transfer function.

To properly correct for the sensors response, one must Fourier transform the data, correct for the sensors response, and then inverse Fourier transform this product.

Because the bandwidth limitation of this sensor affects only the late time of the pulse (it does not affect the peak), and because of our concern about introducing processing errors, we decided that this effect did not warrant the correction of the entire data set in appendix C.

To gain insight into the effect that the bandwidth-limited response of the sensor introduces, the following time-domain correction technique was performed on sample waveforms.

The corrected time-domain response is related to the measured field by [10]

$$H_c(t) = H_m(t) + (1/\tau) \int H_m(\phi) d\phi, \quad (8)$$

where $H_c(t)$ = corrected H-field

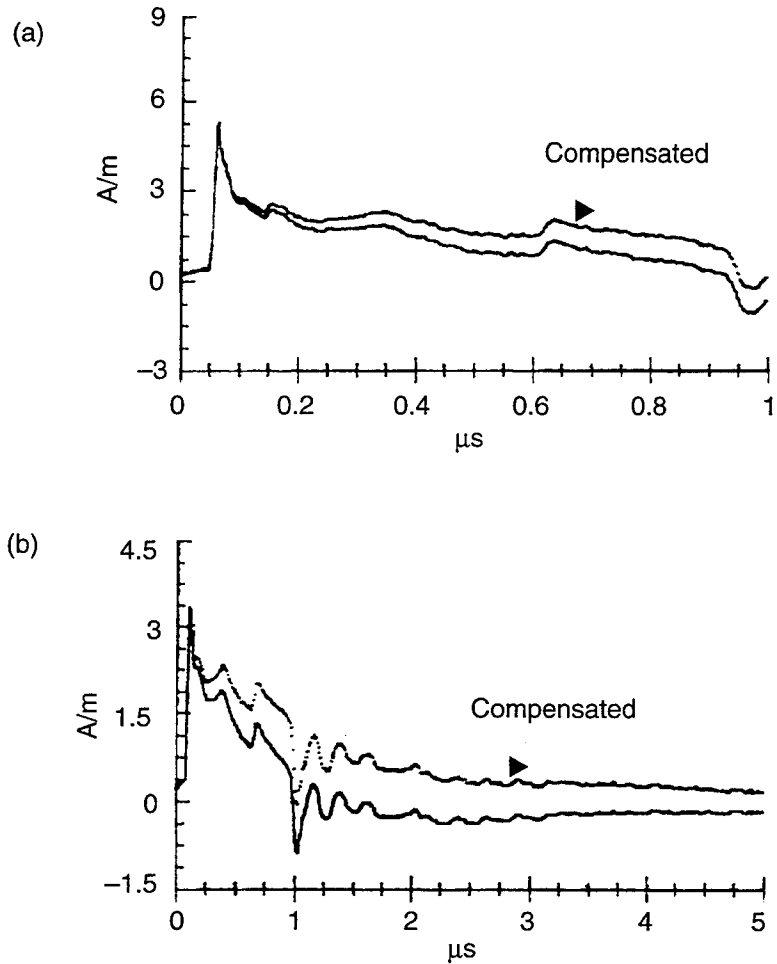
$H_m(\phi)$ = measured H-field

τ = time constant of H-field sensor (measured to be 1.51 μ s for H104-C).

Figure 64 shows overlays of the measured and corrected magnetic field. It is important to state that equation (8) is only an approximation, and a deconvolution technique should be used for a more accurate analysis. As figure 64 shows, the bandwidth limited sensor only introduced a late time effect. There is no effect on the peak, and less than 10 percent of an effect for approximately the first 200 ns of each time history.

Measured E-field data do not need to be corrected since the E-field sensors used during this effort have a flat frequency response to \approx 5 kHz.

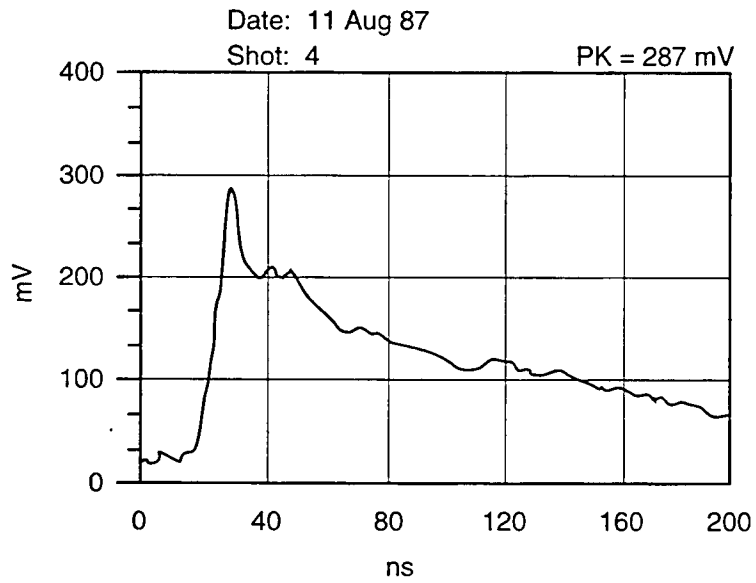
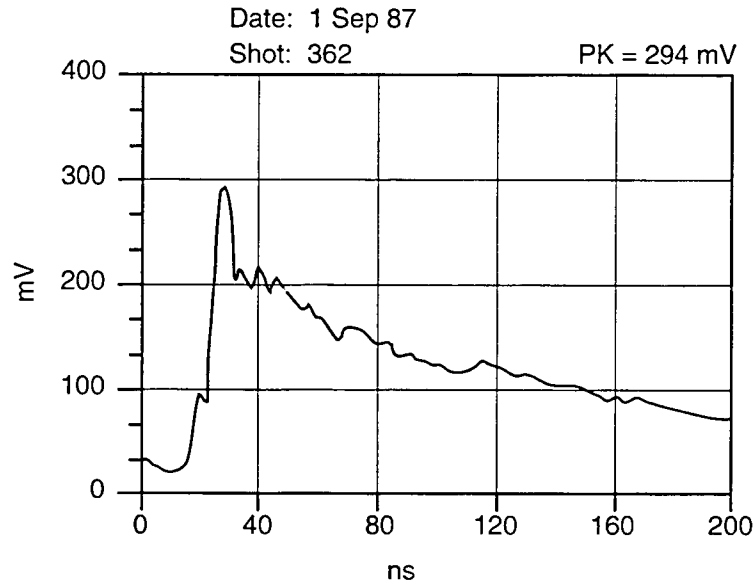
Figure 64. Comparison of measured and bandwidth-compensated H-field response to (a) 1 μs and (b) 5 μs .



7.2 Discontinuity in Pulser Output Waveform

Although the peak and overall waveshape of the B-dot pulser output monitor are reasonably stable, there was an intermittent discontinuity in the pulse risetime. Figure 65 shows this discontinuity. Although this discontinuity may not appear to be significant, under proper circumstances its effect can become exaggerated once the incident and ground reflected waves interact within the test volume. Since the discontinuity is intermittent, it is important when analyzing the field component data to refer to the B-dot monitor waveshape if the component risetime is in question. For comparison, appendix D contains all of the B-dots recorded with the field components within the test volume listed consecutively by pulser firing number. The B-dot that corresponds to each of the measured field components is listed with each waveform in appendix C.

Figure 65. Risetime discontinuity in pulser output waveform.



8. Conclusions

The biconical launching section and longwire antenna structure used in the REPS provides a realistic HEMP simulation technique for illuminating large ground-based systems to an approximated uniform EM planewave environment.

This report documents an extensive field characterization of the Army's REPS. Field mapping of the REPS consisted of recording the total EM environment at 41 locations surrounding the REPS antenna. Through this effort, the EM environment from REPS has been characterized in terms of height (1 and 2 m), field uniformity, symmetry about the antenna, and wavefront planarity. Throughout this effort, the conditions under which the data were measured were carefully documented, including instrumentation, sensors, pulser parameters, sensor placement, test point location, and waveform correctness.

As expected with any finite length antenna, REPS launches a spherically expanding waveform. By bounding the width of the test volume and maximizing the range of the test object from the antenna, REPS will accurately approximate a uniform planewave over large test areas.

The incident E-field (based on measured H-field components) demonstrates a $1/R^{0.97}$ range dependence. This, together with the observation that the individual major components (E_x , H_y , and H_z) vary less than 10 percent within an angle of 26.7 degrees from the centerline, defines a "recommended test volume" in which the wavefront can be thought of as planar. The "usable test volume" can also be defined based on the observation that the tangential E-field (E_t) and the radial magnetic field (H_r) of the expanding wavefront varies less than 10 percent out to an angle of 45 degrees (relative to the centerline). Figure 58 shows the "usable test volume" as well as the "recommended test volume."

Acknowledgement

I would like to express my appreciation to David Frohnapfel, John Stewart, Larry Tranthem, and James Kirkhoff for their invaluable support in setting up and carrying out this test. I would also like to thank Eugene Patrick for his technical critique and advice, and Lillian Wilson for her assistance in preparing this report.

References

- [1] E. L. Patrick and S. L. SooHoo, *Transportable Electromagnetic Pulse Simulator (TEMPS) Field Mapping Report*, Harry Diamond Laboratories, HDL-TR-1743 (September 1976).
- [2] E. L. Patrick and W. D. Fowler, *Repetitive Electromagnetic Pulse Simulator (REPS) Field Mapping Report*, Harry Diamond Laboratories, unpublished (March 1978).
- [3] *Repetitive Electromagnetic Pulse Simulator (REPS)*, Physics International Company, PIMM-563 (August 1974).
- [4] *General Site Map—Woodbridge Research Facility*, Department of the Army Baltimore District, Corps of Engineers, Baltimore, Maryland, drawing 18-02-35 (30 July 1980).
- [5] A. A. Cuneo, Jr., and J. J. Loftus, *Scale Modeling for the Patriot Electromagnetic Pulse Test*, Harry Diamond Laboratories, HDL-TM-81-16 (May 1981).
- [6] Bruce C. Tupper, Roy H. Stehle, Russel T. Wolfram, and V. Donald Cone, *EMP Instrumentation Development*, Stanford Research Institute (June 1972).
- [7] Y. M. Lee and B. T. Benwell, *Calibration Techniques and Procedures for Ground-Plane-Version Electric and Magnetic Field Sensors*, Harry Diamond Laboratories, HDL-TR-2159 (July 1989).
- [8] Nanofast specification sheet for the OP300-2A optical link.
- [9] Memorandum from Larry Rose of Mission Research Corporation, Colorado Springs, CO, to Harry Diamond Laboratories (HDL) Department of Defense (DoD) Standards and Specifications Program (DSSP) TPAC (August 1987).
- [10] P. M. McKenna and R. A. Perala, *Numerical Analysis of the Response of an S280C Shelter to a Simulated NEMP Environment and the Effects of Nearby Ground Planes on Electromagnetic Sensor Enhancement Factors*, Electromagnetic Applications, Inc., EMA-85-R-17, under contract to Harry Diamond Laboratories (December 1984).

Appendix A.—Pulser Output Monitoring System

Contents

	Page
A-1. System Description	63
A-2. B-Dot Calibration.....	64

Figures

A-1. Geometry of pulser monitoring system	63
A-2. Pulser monitoring system	64
A-3. Frequency response of balun and cable loss	66

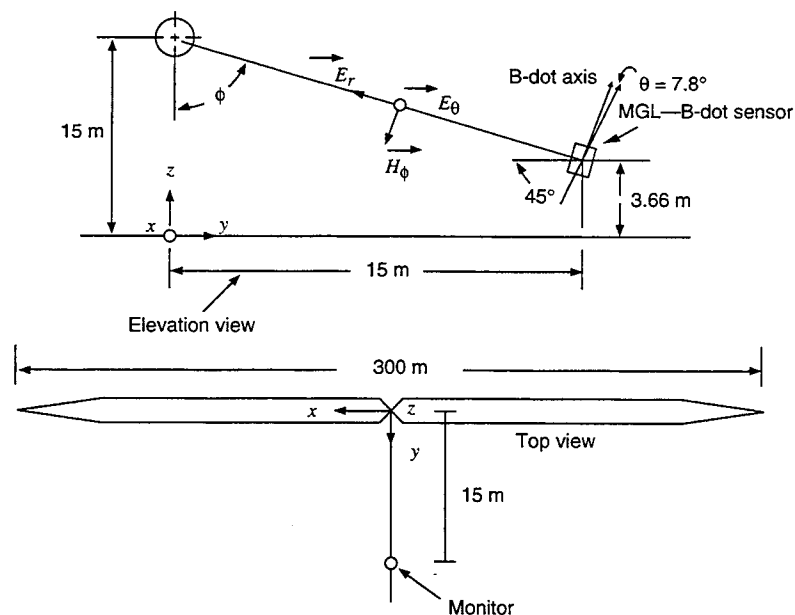
A-1. System Description

As mentioned in section 2.2.1 of the main report, we monitored the output of the Repetitive Electromagnetic Pulse Simulator (REPS) pulser during each pulse with an EG&G MGL-2 B-dot sensor. The B-dot sensor was located on the centerline, 15 m from the pulser at a height of 3.66 m. Figure A-1 shows the B-dot sensor geometry and its relation to REPS.

The MGL-2 measured the time rate of change of the magnetic flux (dB/dt). The output of the MGL-2 was then integrated so that the magnetic flux (B) could be measured directly. The integrator we used was internal to the optical data link, which transmitted the output voltage of the MGL-2 to an automated B-dot monitoring system.

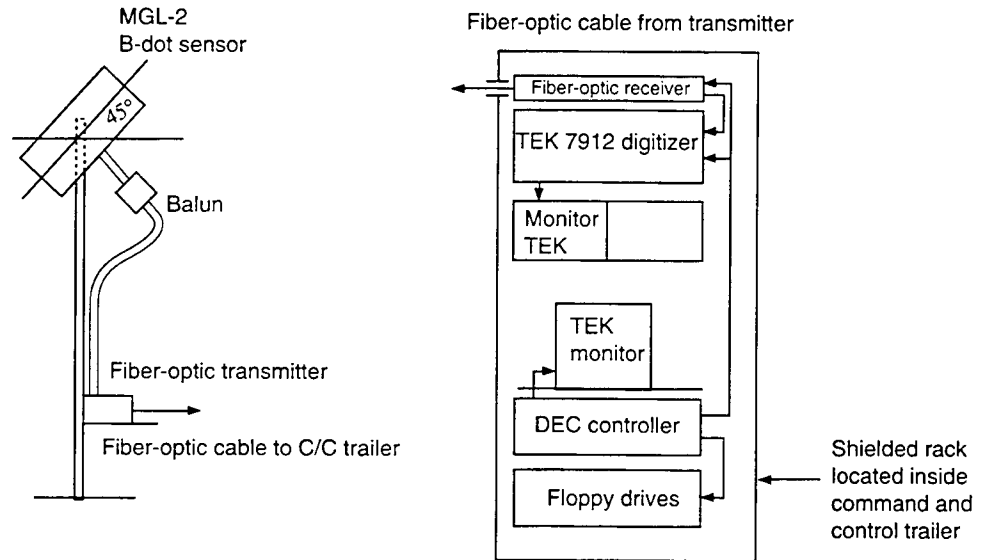
The automated B-dot monitoring system consists of a Nanofast optical data link, Tektronix 7912 AD transient digitizer, and Digital Equipment Corporation (DEC) 11/23 processor. The 11/23 remotely controls the optical link and transient digitizer, as well as processes and saves each pulse on floppy disk. Figure A-2 is a diagram of the B-dot monitor. The optical data link receiver, transient digitizer, and 11/23 processor are all contained within a TEMPEST-shielded rack located within the REPS command and control trailer. The bandwidth of the Nanofast optical link is 160 Hz to >200 MHz. The dynamic range of this link is approximately 40 dB. The single-slot "transient" bandwidth of the 7912 is approximately 200 MHz. The bandwidth of the MGL-2 and balun is also >200 MHz.

Figure A-1. Geometry of pulser monitoring system.



Appendix A

Figure A-2. Pulser monitoring system.



A-2. B-Dot Calibration

It is convenient to monitor the output of the pulser in terms of the incident electric field it produces at some reference point located within the test volume. We chose this point to be located at a slant range of 50 m from the pulser. The incident electric field 50 m from the REPS pulser can be derived from the recorded B-dot as follows.

The output of the MGL-2 can be expressed as

$$V_o(t) = \left(\frac{A_{eq} \times \cos \theta}{BL} \right) \left(\frac{dB}{dt} \right), \quad (\text{A-1})$$

where $V_o(t)$ = output voltage,

A_{eq} = equivalent area of the MGL-2 ($1 \times 10^{-2} \text{ m}^2$),¹

θ = angle between the sensor axis and the incident field vector,

dB/dt = time rate of change of the magnetic flux density vector, and

BL = balun loss factor (includes loss of cable from balun to fiber-optic transmitter).

Rearranging equation (A-1),

$$\frac{dB}{dt} = \frac{BL}{A_{eq} \times \cos \theta} V_o(t). \quad (\text{A-2})$$

¹EG&G Standard EMP and Lightning Instrumentation Catalog, data sheet 1100 (September 1980).

Appendix A

Since an integrator within the fiber-optic transmitter was used, equation (A-1) becomes

$$\int \frac{dB}{dt} \approx \frac{BL}{A_{eq} \times \cos \theta} (\tau) \int V_i(t), \quad (A-3)$$

$$B \approx \frac{BL \times \tau}{A_{eq} \times \cos \theta} V_i(t), \quad (A-4)$$

where τ = time constant of the integrator (seconds) and

$V_i(t)$ = output of integrator (in volts) (or output of fiber-optic link).

With $B = \mu_o H$, the magnetic field at the B-dot sensor location then becomes

$$H(t) \approx \frac{BL \times \tau}{A_{eq} \times \cos \theta \times \mu_o} V_i(t), \quad (A-5)$$

where μ_o = permeability of free space = $4\pi \times 10^{-7}$ and

$H(t)$ = magnetic field at sensor location.

Equation (A-5) is then scaled to a slant range of 50 m by

$$E_{50} \approx \left(\frac{R_1}{R_2}\right) \left(\frac{BL \times \tau \times N_o}{A_{eq} \times \cos \theta \times \mu_o}\right) V_i(t), \quad (A-6)$$

where N_o = permittivity of free space = 120π ,

R_1 = slant range to B-dot sensor, and

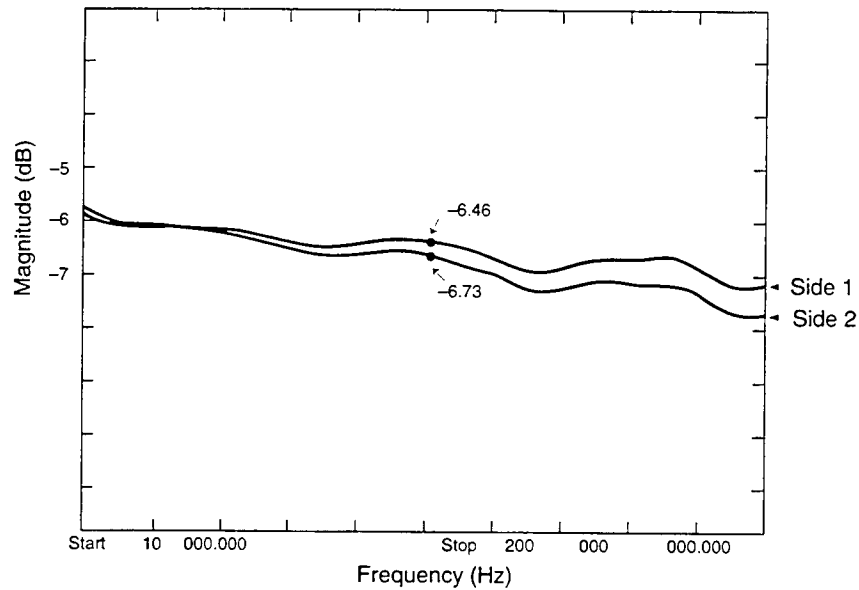
R_2 = slant range to point in test volume (50 m).

The values for R_1 and θ are derived from the geometry of the B-dot sensor shown in figure A-1.

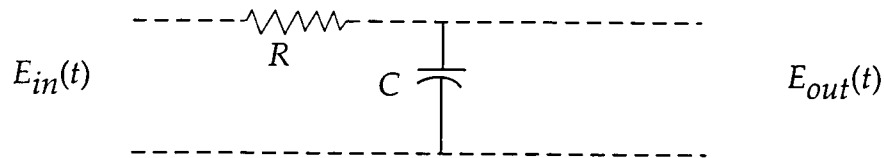
The value for BF (the loss associated with the balun and coaxial cable from the balun to the fiber-optic link) was determined using a Hewlett Packard (HP) 3577 network analyzer. Figure A-3 shows the result of this measurement. BL was chosen to be the average value of the loss in each leg of the balun at 50 MHz. This value is 6.6 dB.

Appendix A

Figure A-3.
Frequency response
of balun and cable
loss.



The integrator time constant was determined using the following derivation:²



In the integrator circuit above, the complex input-to-output relationship would be

$$\frac{E_{out}(t)}{E_{in}(t)} = \frac{1}{1 + j\omega RC} \quad (\text{A-7})$$

The magnitude of equation (A-7) is derived by multiplication with its complex conjugate:

$$\left| \frac{E_{out}(t)}{E_{in}(t)} \right|^2 = \frac{1}{1 + (\omega RC)^2} \quad (\text{A-8})$$

Defining the time constant of the integrator to be $\tau = RC$ and solving for RC ,

$$\tau = \frac{1}{2\pi f} \left[\left(\frac{E_{in}}{E_{out}} \right)^2 - 1 \right]^{1/2} \quad (\text{A-9})$$

²Letter from D. L. Trone, EG&G, Inc., Albuquerque, NM, to J. Stewart, Harry Diamond Laboratories (December 1974).

Appendix A

The response of the integrator was swept with an HP 3577 network analyzer to determine the ratio of E_{in}/E_{out} versus frequency.

The value of τ to be used in equation (A-6) was determined by averaging the value of τ recorded using the HP 3577 at several discrete frequencies over the entire region. τ was calculated to be 0.95 μ s.

The values used in equation (A-6) are summarized in table A-1.

Table A-1. Values assigned to variables in equation (A-6).

Variable	Value
N_o	377
μ_o	$4\pi \times 10^{-7}$
R_1	18.8 m
R_2	50 m
τ	0.95 μ s
BF	6.6 dB
A_{eq}	$1 \times 10^{-2} \text{ m}^2$
θ	7.9°

Equation (A-6) now becomes:

$$E_{50} = \frac{18.8 \times 377 (0.95 \times 10^{-6}) 2.14}{50 (1 \times 10^{-2}) 0.99 (4\pi \times 10^{-7})} V_i(t) \text{ (in V/m)}. \quad (\text{A-10})$$

$$E_{50} = 23.3 \times V_i(t) \text{ kV/m}. \quad (\text{A-11})$$

Appendix B.—Sensor Calibration

Contents

	Page
B-1. Sensor Background	71
B-2. Calibration Procedure	72
B-3. Sensor/Cylinder Positioning	79
B-3.1 Electric-Field Sensor/Cylinder Positioning	79
B-3.2 Magnetic-Field Sensor/Cylinder Positioning	81

Table

B-1. Scalar correction factors	79
--------------------------------------	----

Figures

B-1. Equipment setup for sensor calibration	71
B-2. Equipment setup to remove response of probes and cables	72
B-3. Frequency response of sensor E102 from 10 kHz to 10 MHz	73
B-4. Frequency response of sensor E102 from 10 MHz to 200 MHz	73
B-5. Frequency response of sensor E201 from 10 kHz to 10 MHz	74
B-6. Frequency response of sensor E201 from 10 MHz to 200 MHz	74
B-7. Frequency response of sensor E303 from 10 MHz to 200 MHz	75
B-8. Frequency response of sensor E303 from 10 kHz to 10 MHz	75
B-9. Frequency response of sensor E304 from 10 kHz to 10 MHz	76
B-10. Frequency response of sensor E304 from 10 MHz to 200 MHz	76
B-11. Frequency response of sensor E403 from 10 MHz to 200 MHz	77
B-12. Frequency response of sensor E403 from 10 kHz to 10 MHz	77
B-13. Frequency response of sensor H104 from 10 kHz to 10 MHz	78
B-14. Frequency response of sensor H104 from 10 MHz to 200 MHz	78
B-15. Magnetic field sensor supported by dielectric sensor stand	80

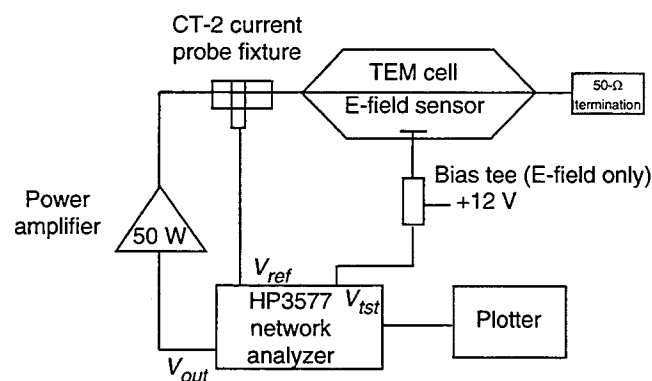
B-1. Sensor Background

Each of the field sensors used during this test was calibrated immediately before and after the test, to verify the scaling factor used to represent the sensor's transfer function (ratio of applied field strength to sensor output voltage) and to assure that the frequency response of the sensor was flat over its intended operating range. Because all of the mapping data are recorded in the time domain, it is important that these sensors possess a flat frequency response over the frequency spectrum of the electromagnetic pulse (EMP) so that one scaling factor can be chosen to represent the entire frequency response. In this way, the pulsed data could be scaled by a single number instead of a frequency-dependent function.

The procedure we used to calibrate each sensor was based upon the procedure typically used by Army Research Laboratory (ARL) to calibrate ground plane E- and H-field sensors.¹ With this procedure, we used a Hewlett-Packard (HP) 8407A network analyzer to generate an accurate signal source, as well as to provide an accurate signal receiver. An IFI model 102 transverse electromagnetic (TEM) cell was used in conjunction with the network analyzer to generate a well-defined uniform field strength for each sensor. We also used a high-power amplifier to bring the field strength generated within the TEM cell to within the operating range of each sensor.

For this effort, we improved upon the calibration procedure in reference 1 by using an HP3577 network analyzer and ENI model 5100L and 2100L power amplifiers, and then referencing the sensor output voltage to the voltage driving the TEM cell. Using this equipment, in conjunction with a modified calibration procedure, we could measure the sensor calibration factor from 10 kHz to 200 MHz, void of any influence from the amplifier, sources, or cables. Figure B-1 shows the equipment setup used to calibrate the E- and H-field sensors.

Figure B-1.
Equipment setup for
sensor calibration.



¹Y. M. Lee and B. T. Benwell, *Calibration Techniques and Procedures for Ground-Plane-Version Electric and Magnetic Field Sensors*, Harry Diamond Laboratories, HDL-TR-2159 (July 1989).

Appendix B

B-2. Calibration Procedure

Before we calibrated the sensor, we configured the CT-1 current probe fixture (used to monitor the voltage driving the TEM) and all relevant cables as in figure B-2. The responses of these components were stored in memory for later use. By dividing the measured response of each sensor (configured as in fig. B-1) by the response of the CT-1 reference fixture, the measured response reduces to

$$\frac{V_{sensor}}{V_{ref}} = G_{TEM} - CF_{sensor}(-51.53)^* \quad , \quad (B-1)$$

where $\frac{V_{sensor}}{V_{ref}}$ = voltage ratio measured by network analyzer,

V_{sensor} = sensor output voltage in volts,

V_{ref} = reference probe output voltage in volts,

G_{TEM} = gain of TEM cell (2.63 1/m for sensor mounted to ground plane of IFI model 102, TEM cell),

CF_{sensor} = calibration factor of sensor, and

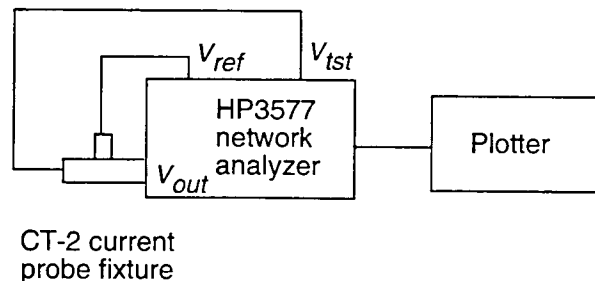
(-51.53) = impedance of free space (377).

The values for G_{TEM} and the impedance of free space were added to data registers within the network analyzer and subtracted directly from the measurement.

Figures B-3 through B-14 show the response of each of the sensors used for this effort. Each response has been corrected for the gain of the TEM cell and impedance of free space (for magnetic fields).

The calibration factor measured in this fashion will give a calibration factor for the sensor only. However, in reality, each sensor is mounted to a metallic cylinder that houses the fiber-optic transmitter necessary to isolate the sensors output signal from the ambient

Figure B-2.
Equipment setup to
remove response of
probes and cables.



*Include for H-field sensors only

EM environment. Since this metallic cylinder is now an integral part of the sensor, it was important that we examine and characterize the effect the metallic cylinder had on the measurement of EM fields, so that its effect could be removed. Through previous efforts, we determined that the close proximity of this metallic cylinder to the sensor causes a linear E-field enhancement over the frequency range of interest.² The E-field enhancement factor is 1.87. There is no field enhancement for magnetic fields.

Figure B-3.
Frequency response
of sensor E102 from
10 kHz to 10 MHz.

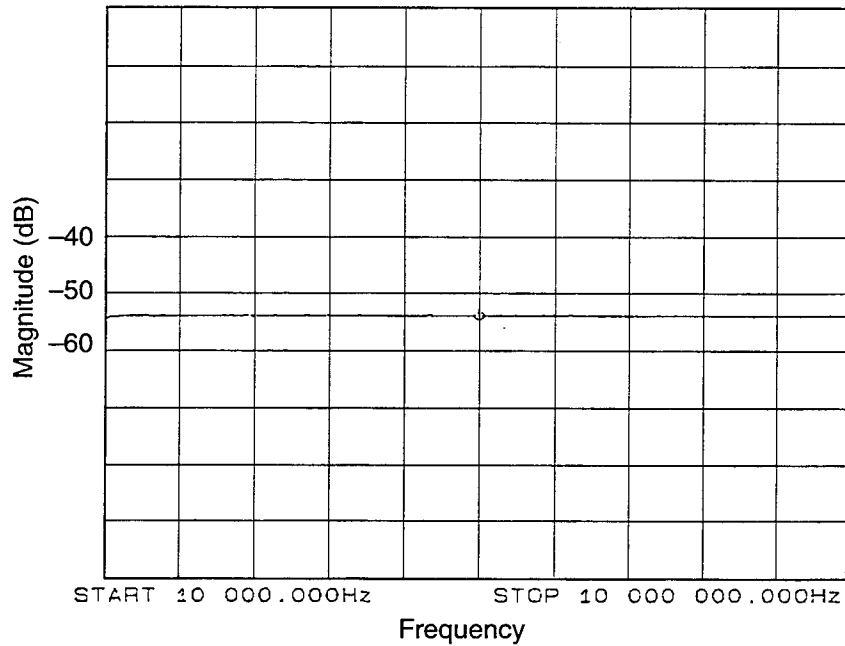
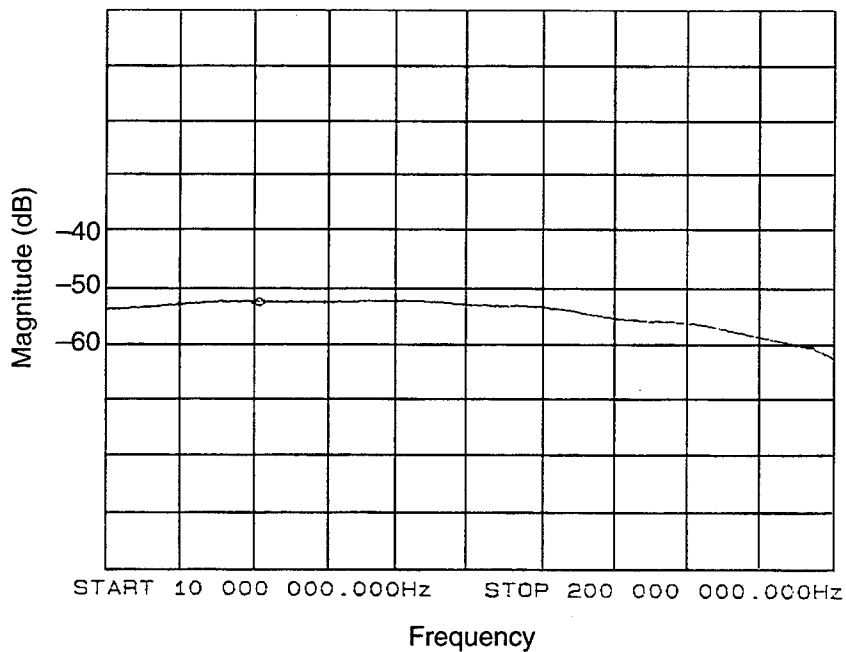


Figure B-4.
Frequency response
of sensor E102 from
10 MHz to 200 MHz.



²B. T. Benwell and Y. M. Lee, *The Effects of Mounting a Metallic Cylinder Behind a Ground-Plane-Version Electromagnetic Field Sensor*, Harry Diamond Laboratories, HDL-TR-2153 (January 1989).

Appendix B

Figure B-5. Frequency response of sensor E201 from 10 kHz to 10 MHz.

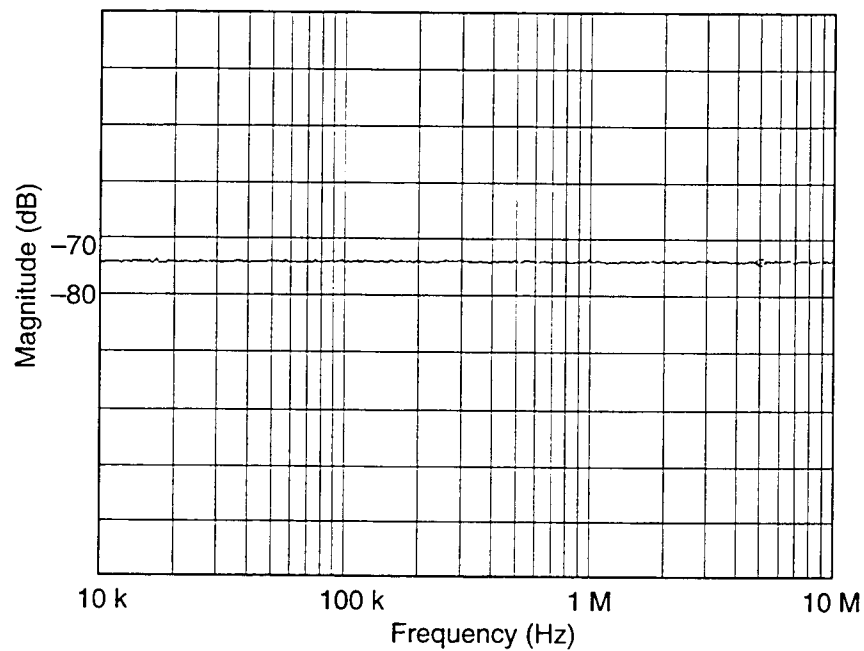


Figure B-6. Frequency response of sensor E201 from 10 MHz to 200 MHz.

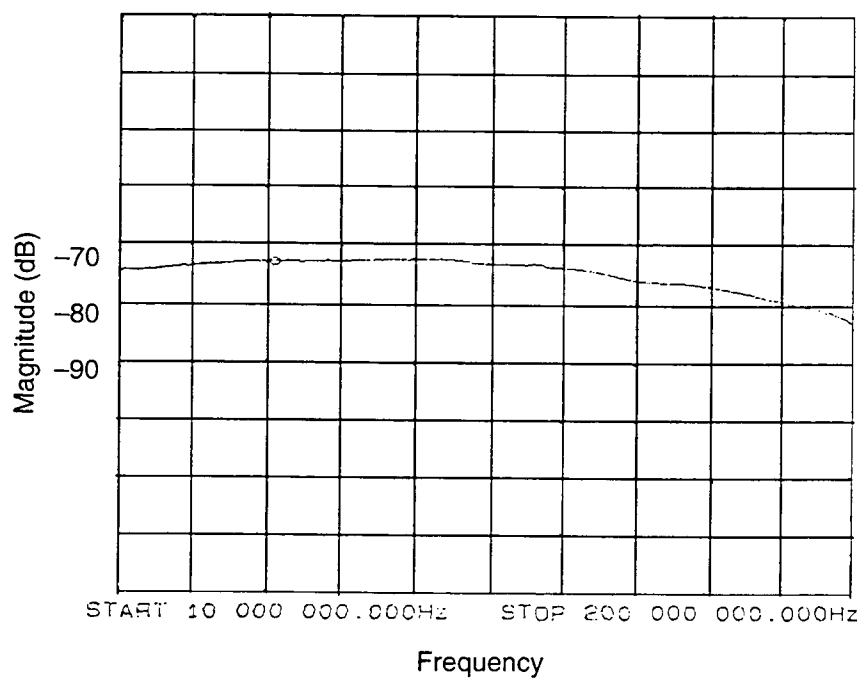


Figure B-7.
Frequency response
of sensor E303 from
10 MHz to 200 MHz.

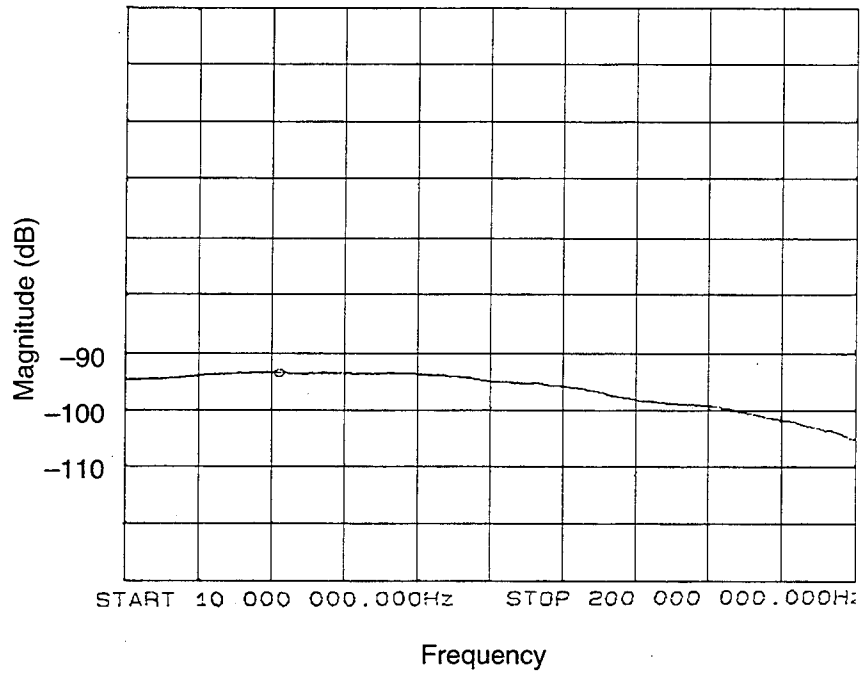
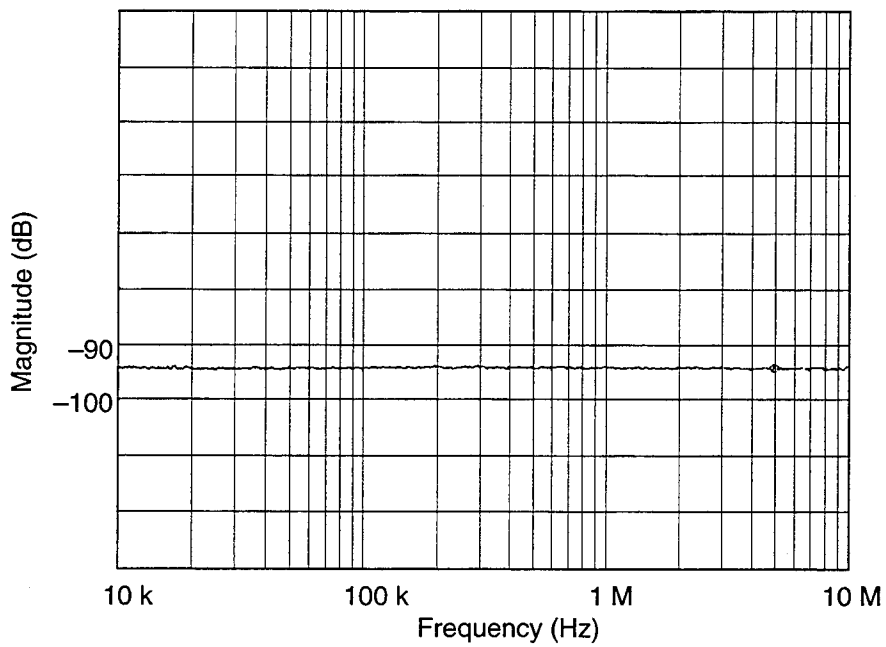


Figure B-8.
Frequency response
of sensor E303 from
10 kHz to 10 MHz.



Appendix B

Figure B-9.
Frequency response
of sensor E304 from
10 kHz to 10 MHz.

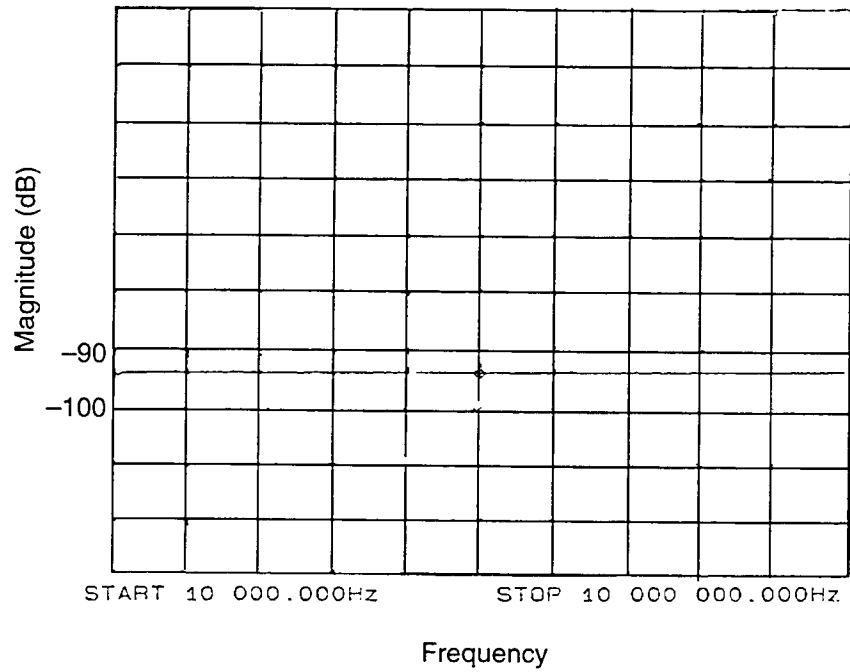


Figure B-10.
Frequency response
of sensor E304 from
10 MHz to 200 MHz.

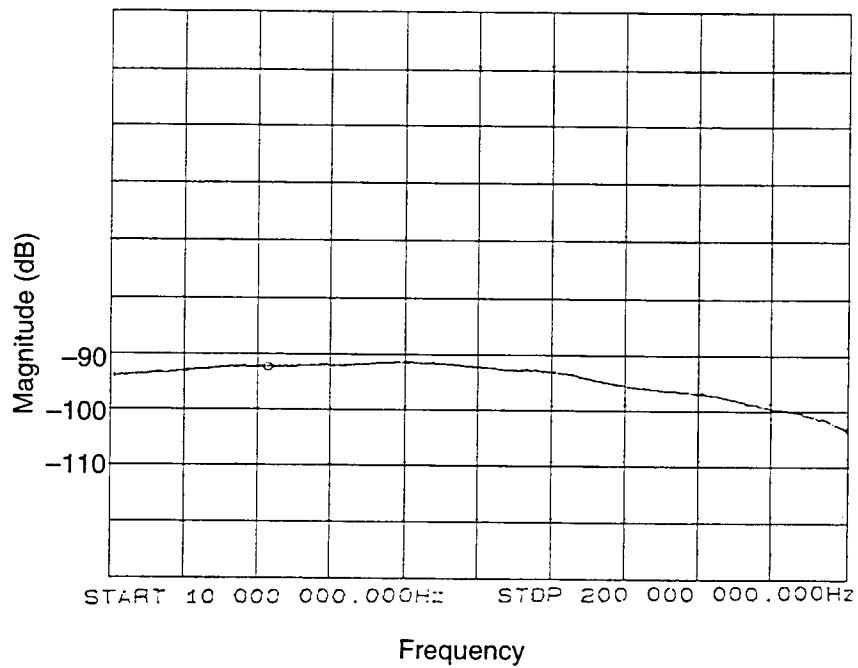


Figure B-11.
Frequency response
of sensor E403 from
10 MHz to 200 MHz.

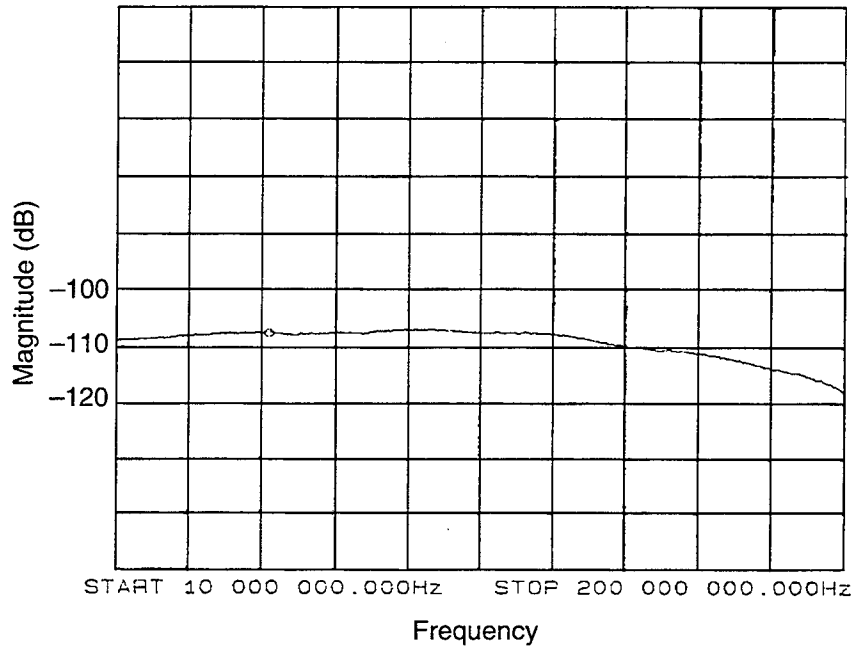
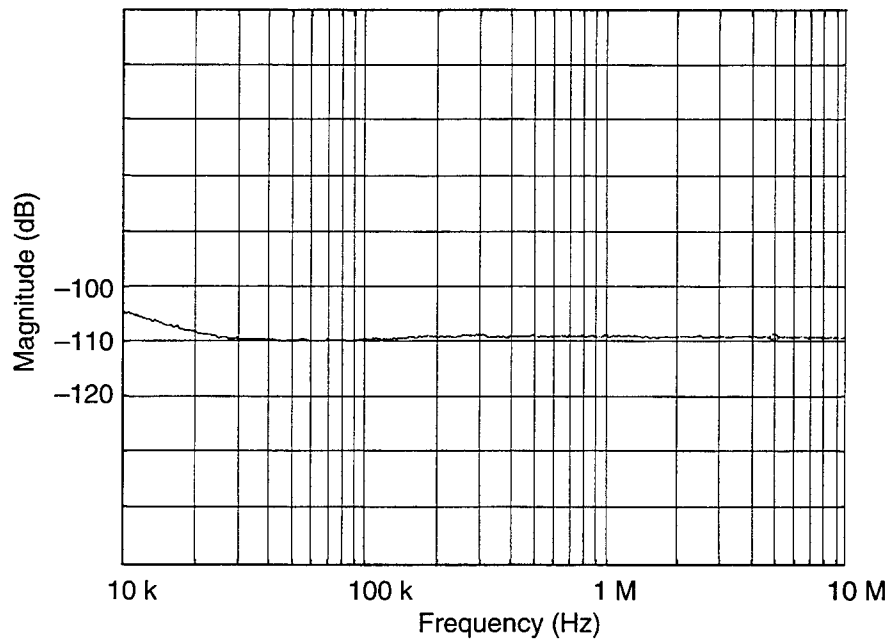


Figure B-12.
Frequency response
of sensor E403 from
10 kHz to 10 MHz.



Appendix B

Figure B-13.
Frequency response
of sensor H104 from
10 kHz to 10 MHz.

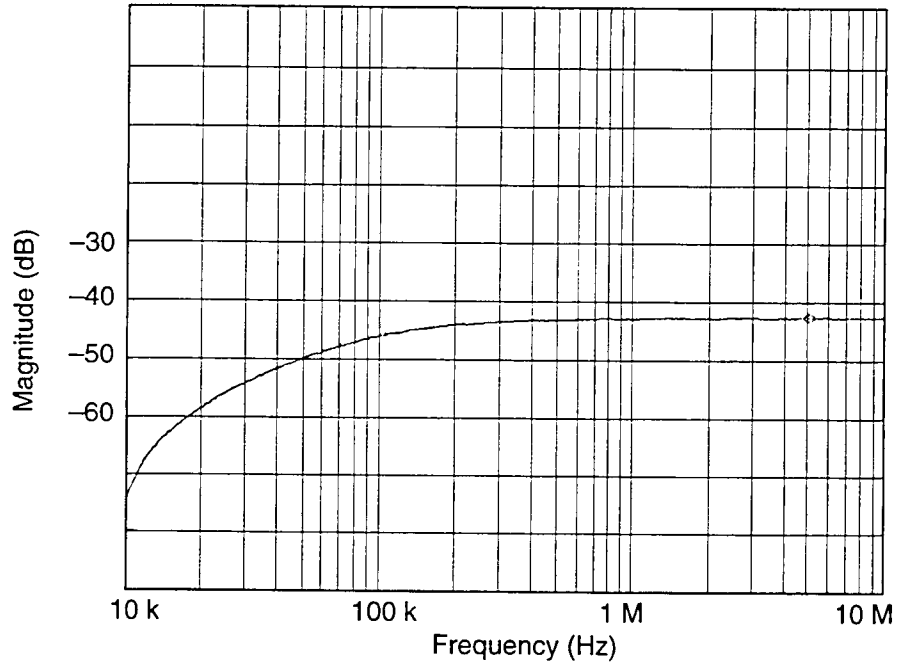
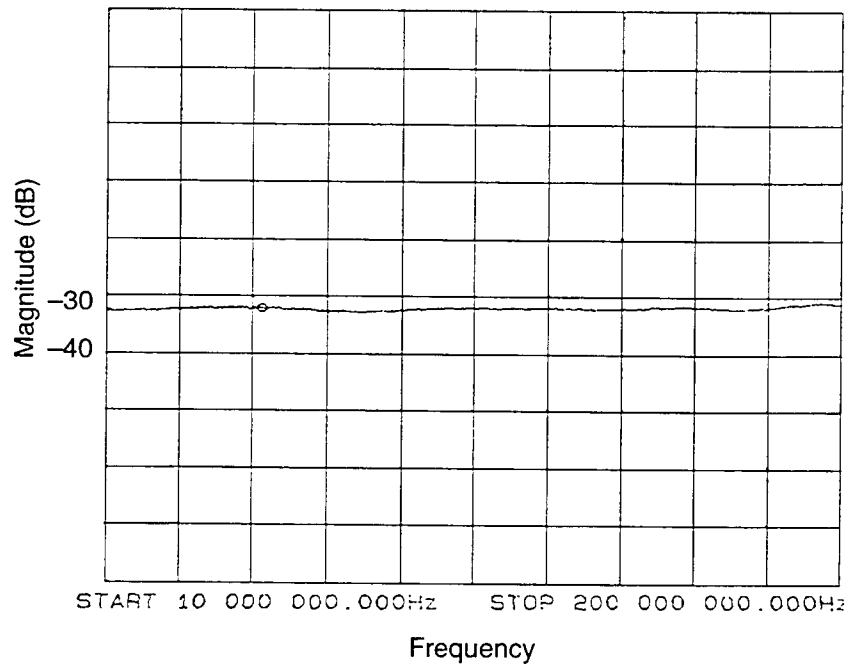


Figure B-14.
Frequency response
of sensor H104 from
10 MHz to 200 MHz.



Since the response of each sensor is flat over the frequency range of interest, we corrected the measured data using only a scalar correction factor for each sensor. Table B-1 shows the calibration factor used for each sensor. These numbers include the presence of the metallic cylinder.

Table B-1. Scalar correction factors.

Sensor	Calibration factor*
H104-C	43 A/m/V
E102-C	237 V/m/V
E201-C	2567
E303-C	25669
E304-C	24233
E403-C	133169.0

*Magnitude chosen at 50 MHz, effect of metallic cylinder included.

B-3. Sensor/Cylinder Positioning

During field mapping, the sensor/cylinder was positioned with a dielectric stand. This stand allowed us to position the sensor/cylinder through a full 360 degrees in any direction. The height of the sensor/cylinder is also adjustable between 1 and 10 ft. Figure B-15 shows a magnetic field sensor attached to the cylinder being supported by the dielectric stand.

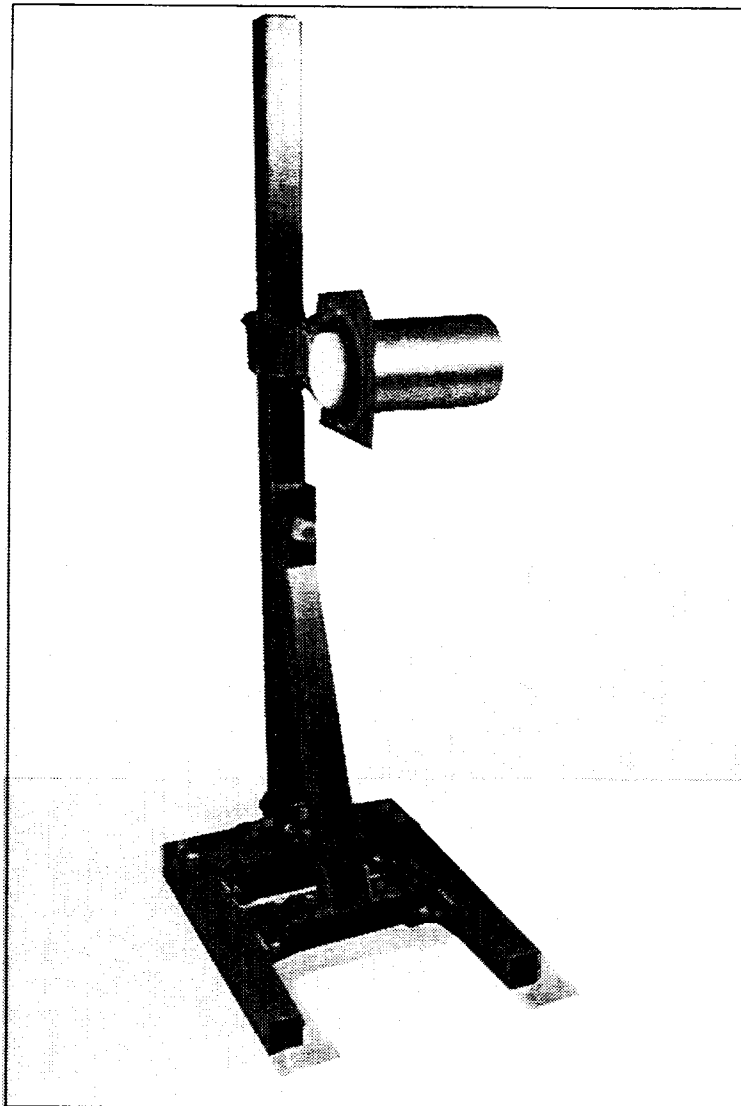
At each measurement location within the surveyed grid of the REPS test volume, we measured the total electric and magnetic field in terms of its three Cartesian components (vectors). To assure the proper measurement of these components, we had to define the proper orientation of the sensor/cylinder.

B-3.1 Electric-Field Sensor/Cylinder Positioning

All of the electric-field sensors must be positioned with the face of the sensor perpendicular to the component of the field to be measured. To achieve this, the axis of the sensor/cylinder must always be parallel to the component that is being measured. Since the sensor is mounted on one end of the cylinder, the sensor face is automatically set perpendicular to the component to be measured when the cylinder axis is parallel to that component. When the output of the electric field sensor is positive, the electric field vector is pointing toward the sensor face. When we used the sensor/cylinder for any

Appendix B

Figure B-15. Magnetic field sensor (attached to metallic cylinder housing fiber-optic transmitter) supported by dielectric sensor stand.



electric field mapping on the west side of the simulator, the following conventions were used.

X-component.—For (a) centerline measurements, the sensor was pointed in the positive X-direction (north), parallel with the antenna; and for (b) off-centerline measurements, the sensor was pointed in the direction of the Y-axis centerline.

Y-component.—The sensor was pointed at the simulator and parallel with the Y-axis centerline.

Z-component.—The sensor was pointed up, perpendicular with the X-Y plane.

B-3.2 Magnetic-Field Sensor/Cylinder Positioning

When the sensor/cylinder was used for any magnetic field mapping on the west side of the simulator, the following conventions were used. These positions were used on and off the centerline.

X-component.—The cylinder was parallel with the Y-axis (centerline); the arrow on the sensor pointed in the positive X-direction axis of the antenna (north).

Y-component.—The cylinder pointed up (parallel with the Z-axis); the arrow on the sensor was parallel with the Y-axis (centerline), pointing away from the simulator (west).

Z-component.—The cylinder was placed parallel with the Y-axis (centerline); the arrow on the sensor pointed up (positive Z-direction), with the sensor facing the simulator.

For measurements made on the east side of the simulator, the Y-component was recorded with the cylinder pointing up and the sensor arrow facing the simulator (west).

Appendix C.—Measured Field Data

Contents

	Page
C-1. Data Collection	103
C-2. Data Organization	103

Figures

Location 0/25/1

C-1. X component of the electric field measured at location 0/25/1 using sensor E304-C. REPS pulse 45 generating 6.3 kV/m at 50 m	105
C-2. -Y component of the electric field measured at location 0/25/1 using sensor E201-C. REPS pulse 39 generating 6.1 kV/m at 50 m	105
C-3. Z component of the electric field measured at location 0/25/1 using sensor E201-C. REPS pulse 36 generating 6.1 kV/m at 50 m	105
C-4. Z component of the electric field measured at location 0/25/1 using sensor E201-C. REPS pulse 38 generating 6 kV/m at 50 m	105
C-5. X component of the magnetic field measured at location 0/25/1 using sensor H104-C. REPS pulse 6 generating 6.3 kV/m at 50 m	106
C-6. Y component of the magnetic field measured at location 0/25/1 using sensor H104-C. REPS pulse 2 generating 6.4 kV/m at 50 m	106
C-7. Y component of the magnetic field measured at location 0/25/1 using sensor H104-C. REPS pulse 3 generating 6.4 kV/m at 50 m	106
C-8. Z component of the magnetic field measured at location 0/25/1 using sensor H104-C. REPS pulse 4 generating 6.1 kV/m at 50 m	106

Location -25/25/1

C-9. X component of the electric field measured at location -25/25/1 using sensor E304-C. REPS pulse 266 generating 6.2 kV/m at 50 m	107
C-10. -Y component of the electric field measured at location -25/25/1 using sensor E304-C. REPS pulse 267 generating 6 kV/m at 50 m	107
C-11. Z component of the electric field measured at location -25/25/1 using sensor E304-C. REPS pulse 264 generating 6 kV/m at 50 m	107
C-12. Z component of the electric field measured at location -25/25/1 using sensor E304-C. REPS pulse 265 generating 6.1 kV/m at 50 m	107

Appendix C

- C-13. X component of the magnetic field measured at location -25/25/1 using sensor H104-C. REPS pulse 245 generating 6.5 kV/m at 50 m 108
- C-14. Y component of the magnetic field measured at location -25/25/1 using sensor H104-C. REPS pulse 246 generating 6.4 kV/m at 50 m 108
- C-15. Y component of the magnetic field measured at location -25/25/1 using sensor H104-C. REPS pulse 247 generating 6.3 kV/m at 50 m 108
- C-16. Z component of the magnetic field measured at location -25/25/1 using sensor H104-C. REPS pulse 241 generating 6.4 kV/m at 50 m 108

Location -50/25/1

- C-17. X component of the electric field measured at location -50/25/1 using sensor E304-C. REPS pulse 232 generating 6.2 kV/m at 50 m 109
- C-18. -Y component of the electric field measured at location -50/25/1 using sensor E304-C. REPS pulse 235 generating 6.1 kV/m at 50 m 109
- C-19. Z component of the electric field measured at location -50/25/1 using sensor E304-C. REPS pulse 233 generating 6.1 kV/m at 50 m 109
- C-20. Z component of the electric field measured at location -50/25/1 using sensor E304-C. REPS pulse 234 generating 6.1 kV/m at 50 m 109
- C-21. X component of the magnetic field measured at location -50/25/1 using sensor H104-C. REPS pulse 238 generating 6.4 kV/m at 50 m 110
- C-22. Y component of the magnetic field measured at location -50/25/1 using sensor H104-C. REPS pulse 236 generating 6.5 kV/m at 50 m 110
- C-23. Y component of the magnetic field measured at location -50/25/1 using sensor H104-C. REPS pulse 237 generating 6.1 kV/m at 50 m 110
- C-24. Z component of the magnetic field measured at location -50/25/1 using sensor H104-C. REPS pulse 239 generating 6.3 kV/m at 50 m 110
- C-25. Z component of the magnetic field measured at location -50/25/1 using sensor H104-C. REPS pulse 240 generating 6.3 kV/m at 50 m 111

Location -75/25/1

- C-26. X component of the electric field measured at location -75/25/1 using sensor E304-C. REPS pulse 226 generating 6.2 kV/m at 50 m 111
- C-27. -Y component of the electric field measured at location -75/25/1 using sensor E304-C. REPS pulse 230 generating 6.3 kV/m at 50 m 111
- C-28. -Y component of the electric field measured at location -75/25/1 using sensor E304-C. REPS pulse 231 generating 6 kV/m at 50 m 111
- C-29. Z component of the electric field measured at location -75/25/1 using sensor E304-C. REPS pulse 227 generating 6.4 kV/m at 50 m 112

C-30.	Z component of the electric field measured at location -75/25/1 using sensor E304-C. REPS pulse 228 generating 6.3 kV/m at 50 m	112
C-31.	X component of the magnetic field measured at location -75/25/1 using sensor H104-C. REPS pulse 221 generating 6.3 kV/m at 50 m	112
C-32.	X component of the magnetic field measured at location -75/25/1 using sensor H104-C. REPS pulse 222 generating 6.5 kV/m at 50 m	112
C-33.	Y component of the magnetic field measured at location -75/25/1 using sensor H104-C. REPS pulse 216 generating 6.3 kV/m at 50 m	113
C-34.	Y component of the magnetic field measured at location -75/25/1 using sensor H104-C. REPS pulse 217 generating 6.5 kV/m at 50 m	113
C-35.	Z component of the magnetic field measured at location -75/25/1 using sensor H104-C. REPS pulse 223 generating 6.3 kV/m at 50 m	113
C-36.	Z component of the magnetic field measured at location -75/25/1 using sensor H104-C. REPS pulse 224 generating 6.3 kV/m at 50 m	113

Location -100/25/1

C-37.	X component of the electric field measured at location -100/25/1 using sensor E201-C. REPS pulse 192 generating 6.5 kV/m at 50 m	114
C-38.	-Y component of the electric field measured at location -100/25/1 using sensor E201-C. REPS pulse 194 generating 6.4 kV/m at 50 m	114
C-39.	-Y component of the electric field measured at location -100/25/1 using sensor E201-C. REPS pulse 195 generating 6.4 kV/m at 50 m	114
C-40.	Z component of the electric field measured at location -100/25/1 using sensor E303-C. REPS pulse 202 generating 6.2 kV/m at 50 m	114
C-41.	Z component of the electric field measured at location -100/25/1 using sensor E303-C. REPS pulse 203 generating 6.3 kV/m at 50 m	115
C-42.	X component of the magnetic field measured at location -100/25/1 using sensor H104-C. REPS pulse 196 generating 6.5 kV/m at 50 m	115
C-43.	X component of the magnetic field measured at location -100/25/1 using sensor H104-C. REPS pulse 197 generating 6.2 kV/m at 50 m	115
C-44.	Y component of the magnetic field measured at location -100/25/1 using sensor H104-C. REPS pulse 200 generating 6.4 kV/m at 50 m	115
C-45.	Y component of the magnetic field measured at location -100/25/1 using sensor H104-C. REPS pulse 201 generating 6.3 kV/m at 50 m	116
C-46.	Z component of the magnetic field measured at location -100/25/1 using sensor H104-C. REPS pulse 198 generating 6.3 kV/m at 50 m	116

Appendix C

- C-47. Z component of the magnetic field measured at location -100/25/1 using sensor H104-C. REPS pulse 199 generating 6.4 kV/m at 50 m 116

Location 0/50/1

- C-48. X component of the electric field measured at location 0/50/1 using sensor E304-C. REPS pulse 47 generating 6.1 kV/m at 50 m 116
- C-49. -Y component of the electric field measured at location 0/50/1 using sensor E201-C. REPS pulse 49 generating 6.3 kV/m at 50 m 117
- C-50. -Y component of the electric field measured at location 0/50/1 using sensor E201-C. REPS pulse 52 generating 6 kV/m at 50 m 117
- C-51. Z component of the electric field measured at location 0/50/1 using sensor E201-C. REPS pulse 53 generating 6.1 kV/m at 50 m 117
- C-52. Z component of the electric field measured at location 0/50/1 using sensor E201-C. REPS pulse 54 generating 6.4 kV/m at 50 m 117
- C-53. X component of the magnetic field measured at location 0/50/1 using sensor H104-C. REPS pulse 17 generating 6.6 kV/m at 50 m 118
- C-54. Y component of the magnetic field measured at location 0/50/1 using sensor H104-C. REPS pulse 13 generating 6.3 kV/m at 50 m 118
- C-55. Y component of the magnetic field measured at location 0/50/1 using sensor H104-C. REPS pulse 15 generating 6.3 kV/m at 50 m 118
- C-56. Z component of the magnetic field measured at location 0/50/1 using sensor H104-C. REPS pulse 16 generating 6.6 kV/m at 50 m 118

Location -25/50/1

- C-57. X component of the electric field measured at location -25/50/1 using sensor E304-C. REPS pulse 83 generating 6.1 kV/m at 50 m 119
- C-58. -Y component of the electric field measured at location -25/50/1 using sensor E304-C. REPS pulse 86 generating 6.3 kV/m at 50 m 119
- C-59. Z component of the electric field measured at location -25/50/1 using sensor E304-C. REPS pulse 84 generating 6.2 kV/m at 50 m 119
- C-60. Z component of the electric field measured at location -25/50/1 using sensor E304-C. REPS pulse 85 generating 6.3 kV/m at 50 m 119
- C-61. X component of the magnetic field measured at location -25/50/1 using sensor H104-C. REPS pulse 76 generating 6.3 kV/m at 50 m 120
- C-62. X component of the magnetic field measured at location -25/50/1 using sensor H104-C. REPS pulse 75 generating 6.3 kV/m at 50 m 120
- C-63. Y component of the magnetic field measured at location -25/50/1 using sensor H104-C. REPS pulse 73 generating 6.3 kV/m at 50 m 120

C-64.	Y component of the magnetic field measured at location -25/50/1 using sensor H104-C. REPS pulse 74 generating 6.3 kV/m at 50 m	120
C-65.	Z component of the magnetic field measured at location -25/50/1 using sensor H104-C. REPS pulse 77 generating 6.2 kV/m at 50 m	121
Location -50/50/1		
C-66.	X component of the electric field measured at location -50/50/1 using sensor E304-C. REPS pulse 92 generating 6.6 kV/m at 50 m	121
C-67.	-Y component of the electric field measured at location -50/50/1 using sensor E304-C. REPS pulse 95 generating 6.5 kV/m at 50 m	121
C-68.	Z component of the electric field measured at location -50/50/1 using sensor E304-C. REPS pulse 93 generating 6.3 kV/m at 50 m	121
C-69.	Z component of the electric field measured at location -50/50/1 using sensor E304-C. REPS pulse 94 generating 6.3 kV/m at 50 m	122
C-70.	X component of the magnetic field measured at location -50/50/1 using sensor H104-C. REPS pulse 104 generating 6.5 kV/m at 50 m	122
C-71.	X component of the magnetic field measured at location -50/50/1 using sensor H104-C. REPS pulse 105 generating 6.5 kV/m at 50 m	122
C-72.	Y component of the magnetic field measured at location -50/50/1 using sensor H104-C. REPS pulse 101 generating 6.4 kV/m at 50 m	122
C-73.	Y component of the magnetic field measured at location -50/50/1 using sensor H104-C. REPS pulse 103 generating 6.3 kV/m at 50 m	123
C-74.	Z component of the magnetic field measured at location -50/50/1 using sensor H104-C. REPS pulse 106 generating 6.2 kV/m at 50 m	123
Location -75/50/1		
C-75.	X component of the electric field measured at location -75/50/1 using sensor E201-C. REPS pulse 161 generating 6.1 kV/m at 50 m	123
C-76.	-Y component of the electric field measured at location -75/50/1 using sensor E201-C. REPS pulse 164 generating 6 kV/m at 50 m	123
C-77.	Z component of the electric field measured at location -75/50/1 using sensor E201-C. REPS pulse 162 generating 6 kV/m at 50 m	124
C-78.	Z component of the electric field measured at location -75/50/1 using sensor E201-C. REPS pulse 163 generating 6.1 kV/m at 50 m	124
C-79.	X component of the magnetic field measured at location -75/50/1 using sensor H104-C. REPS pulse 159 generating 6.4 kV/m at 50 m	124
C-80.	Y component of the magnetic field measured at location -75/50/1 using sensor H104-C. REPS pulse 155 generating 6.4 kV/m at 50 m	124

Appendix C

- C-81. Y component of the magnetic field measured at location -75/50/1 using sensor H104-C. REPS pulse 156 generating 6.3 kV/m at 50 m 125
- C-82. Z component of the magnetic field measured at location -75/50/1 using sensor H104-C. REPS pulse 158 generating 6.3 kV/m at 50 m 125

Location -100/50/1

- C-83. X component of the electric field measured at location -100/50/1 using sensor E201-C. REPS pulse 185 generating 6.5 kV/m at 50 m 125
- C-84. -Y component of the electric field measured at location -100/50/1 using sensor E201-C. REPS pulse 190 generating 6.3 kV/m at 50 m 125
- C-85. Z component of the electric field measured at location -100/50/1 using sensor E201-C. REPS pulse 186 generating 6.3 kV/m at 50 m 126
- C-86. Z component of the electric field measured at location -100/50/1 using sensor E201-C. REPS pulse 187 generating 6.1 kV/m at 50 m 126
- C-87. X component of the magnetic field measured at location -100/50/1 using sensor H104-C. REPS pulse 181 generating 6.2 kV/m at 50 m 126
- C-88. X component of the magnetic field measured at location -100/50/1 using sensor H104-C. REPS pulse 182 generating 6.3 kV/m at 50 m 126
- C-89. Y component of the magnetic field measured at location -100/50/1 using sensor H104-C. REPS pulse 179 generating 6.2 kV/m at 50 m 127
- C-90. Y component of the magnetic field measured at location -100/50/1 using sensor H104-C. REPS pulse 180 generating 6.2 kV/m at 50 m 127
- C-91. Z component of the magnetic field measured at location -100/50/1 using sensor H104-C. REPS pulse 183 generating 6.1 kV/m at 50 m 127
- C-92. Z component of the magnetic field measured at location -100/50/1 using sensor H104-C. REPS pulse 184 generating 6.1 kV/m at 50 m 127

Location -125/50/1

- C-93. X component of the electric field measured at location -125/50/1 using sensor E201-C. REPS pulse 204 generating 6.5 kV/m at 50 m 128
- C-94. -Y component of the electric field measured at location -125/50/1 using sensor E201-C. REPS pulse 205 generating 6.4 kV/m at 50 m 128
- C-95. Z component of the electric field measured at location -125/50/1 using sensor E201-C. REPS pulse 206 generating 6.4 kV/m at 50 m 128
- C-96. Z component of the electric field measured at location -125/50/1 using sensor E201-C. REPS pulse 208 generating 6.3 kV/m at 50 m 128
- C-97. X component of the magnetic field measured at location -125/50/1 using sensor H104-C. REPS pulse 209 generating 6.6 kV/m at 50 m 129

C-98.	X component of the magnetic field measured at location -125/50/1 using sensor H104-C. REPS pulse 210 generating 6.4 kV/m at 50 m	129
C-99.	Y component of the magnetic field measured at location -125/50/1 using sensor H104-C. REPS pulse 214 generating 6.5 kV/m at 50 m	129
C-100.	Y component of the magnetic field measured at location -125/50/1 using sensor H104-C. REPS pulse 215 generating 6.4 kV/m at 50 m	129
C-101.	Z component of the magnetic field measured at location -125/50/1 using sensor H104-C. REPS pulse 212 generating 6.4 kV/m at 50 m	130
C-102.	Z component of the magnetic field measured at location -125/50/1 using sensor H104-C. REPS pulse 213 generating 6.2 kV/m at 50 m	130

Location -150/50/1

C-103.	X component of the electric field measured at location -150/50/1 using sensor E201-C. REPS pulse 340 generating 6.4 kV/m at 50 m	130
C-104.	-Y component of the electric field measured at location -150/50/1 using sensor E201-C. REPS pulse 343 generating 6.2 kV/m at 50 m	130
C-105.	Z component of the electric field measured at location -150/50/1 using sensor E201-C. REPS pulse 341 generating 6.4 kV/m at 50 m	131
C-106.	Z component of the electric field measured at location -150/50/1 using sensor E201-C. REPS pulse 342 generating 6.2 kV/m at 50 m	131
C-107.	X component of the magnetic field measured at location -150/50/1 using sensor H104-C. REPS pulse 344 generating 6.3 kV/m at 50 m	131
C-108.	X component of the magnetic field measured at location -150/50/1 using sensor H104-C. REPS pulse 345 generating 6.1 kV/m at 50 m	131
C-109.	Y component of the magnetic field measured at location -150/50/1 using sensor H104-C. REPS pulse 346 generating 6.1 kV/m at 50 m	132
C-110.	Y component of the magnetic field measured at location -150/50/1 using sensor H104-C. REPS pulse 347 generating 6.1 kV/m at 50 m	132
C-111.	Z component of the magnetic field measured at location -150/50/1 using sensor H104-C. REPS pulse 350 generating 6.3 kV/m at 50 m	132
C-112.	Z component of the magnetic field measured at location -150/50/1 using sensor H104-C. REPS pulse 351 generating 6.2 kV/m at 50 m	132

Location 0/75/1

C-113.	X component of the electric field measured at location 0/75/1 using sensor E201-C. REPS pulse 141 generating 6.4 kV/m at 50 m	133
C-114.	X component of the electric field measured at location 0/75/1 using sensor E201-C. REPS pulse 142 generating 6.4 kV/m at 50 m	133

Appendix C

- C-115. -Y component of the electric field measured at location 0/75/1 using sensor E201-C. REPS pulse 140 generating 6.3 kV/m at 50 m 133
- C-116. Z component of the electric field measured at location 0/75/1 using sensor E201-C. REPS pulse 137 generating 6.3 kV/m at 50 m 133
- C-117. Z component of the electric field measured at location 0/75/1 using sensor E201-C. REPS pulse 138 generating 6.3 kV/m at 50 m 134
- C-118. X component of the magnetic field measured at location 0/75/1 using sensor H104-C. REPS pulse 135 generating 6.2 kV/m at 50 m 134
- C-119. Y component of the magnetic field measured at location 0/75/1 using sensor H104-C. REPS pulse 131 generating 6.3 kV/m at 50 m 134
- C-120. Y component of the magnetic field measured at location 0/75/1 using sensor H104-C. REPS pulse 133 generating 6.2 kV/m at 50 m 134
- C-121. Z component of the magnetic field measured at location 0/75/1 using sensor H104-C. REPS pulse 136 generating 6.2 kV/m at 50 m 135

Location -25/75/1

- C-122. X component of the electric field measured at location -25/75/1 using sensor E201-C. REPS pulse 124 generating 6.6 kV/m at 50 m 135
- C-123. -Y component of the electric field measured at location -25/75/1 using sensor E201-C. REPS pulse 121 generating 6.3 kV/m at 50 m 135
- C-124. Z component of the electric field measured at location -25/75/1 using sensor E201-C. REPS pulse 122 generating 6.3 kV/m at 50 m 135
- C-125. Z component of the electric field measured at location -25/75/1 using sensor E201-C. REPS pulse 123 generating 6.4 kV/m at 50 m 136
- C-126. X component of the magnetic field measured at location -25/75/1 using sensor H104-C. REPS pulse 128 generating 6.3 kV/m at 50 m 136
- C-127. X component of the magnetic field measured at location -25/75/1 using sensor H104-C. REPS pulse 129 generating 6.4 kV/m at 50 m 136
- C-128. Y component of the magnetic field measured at location -25/75/1 using sensor H104-C. REPS pulse 126 generating 6.3 kV/m at 50 m 136
- C-129. Y component of the magnetic field measured at location -25/75/1 using sensor H104-C. REPS pulse 127 generating 6.2 kV/m at 50 m 137
- C-130. Z component of the magnetic field measured at location -25/75/1 using sensor H104-C. REPS pulse 130 generating 6 kV/m at 50 m 137

Location -50/75/1

- C-131. X component of the electric field measured at location -50/75/1 using sensor E201-C. REPS pulse 117 generating 6.3 kV/m at 50 m 137

C-132.	-Y component of the electric field measured at location -50/75/1 using sensor E201-C. REPS pulse 120 generating 6.5 kV/m at 50 m	137
C-133.	Z component of the electric field measured at location -50/75/1 using sensor E201-C. REPS pulse 118 generating 6.3 kV/m at 50 m	138
C-134.	Z component of the electric field measured at location -50/75/1 using sensor E201-C. REPS pulse 119 generating 6.3 kV/m at 50 m	138
C-135.	X component of the magnetic field measured at location -50/75/1 using sensor H104-C. REPS pulse 114 generating 6.2 kV/m at 50 m	138
C-136.	X component of the magnetic field measured at location -50/75/1 using sensor H104-C. REPS pulse 115 generating 6.5 kV/m at 50 m	138
C-137.	Y component of the magnetic field measured at location -50/75/1 using sensor H104-C. REPS pulse 112 generating 6.4 kV/m at 50 m	139
C-138.	Y component of the magnetic field measured at location -50/75/1 using sensor H104-C. REPS pulse 113 generating 6.5 kV/m at 50 m	139
C-139.	Z component of the magnetic field measured at location -50/75/1 using sensor H104-C. REPS pulse 116 generating 6.4 kV/m at 50 m	139

Location -75/75/1

C-140.	X component of the electric field measured at location -75/75/1 using sensor E201-C. REPS pulse 143 generating 6.4 kV/m at 50 m	139
C-141.	-Y component of the electric field measured at location -75/75/1 using sensor E201-C. REPS pulse 146 generating 6.5 kV/m at 50 m	140
C-142.	Z component of the electric field measured at location -75/75/1 using sensor E201-C. REPS pulse 144 generating 6.2 kV/m at 50 m	140
C-143.	Z component of the electric field measured at location -75/75/1 using sensor E201-C. REPS pulse 145 generating 6.3 kV/m at 50 m	140
C-144.	X component of the magnetic field measured at location -75/75/1 using sensor H104-C. REPS pulse 149 generating 6.3 kV/m at 50 m	140
C-145.	X component of the magnetic field measured at location -75/75/1 using sensor H104-C. REPS pulse 150 generating 6.3 kV/m at 50 m	141
C-146.	Y component of the magnetic field measured at location -75/75/1 using sensor H104-C. REPS pulse 147 generating 6.3 kV/m at 50 m	141
C-147.	Y component of the magnetic field measured at location -75/75/1 using sensor H104-C. REPS pulse 148 generating 6.4 kV/m at 50 m	141
C-148.	Z component of the magnetic field measured at location -75/75/1 using sensor H104-C. REPS pulse 151 generating 6.5 kV/m at 50 m	141

Appendix C

- C-149. Z component of the magnetic field measured at location -75/75/1 using sensor H104-C. REPS pulse 152 generating 6.5 kV/m at 50 m 142

Location -100/75/1

- C-150. X component of the electric field measured at location -100/75/1 using sensor E201-C. REPS pulse 165 generating 6.2 kV/m at 50 m 142
- C-151. -Y component of the electric field measured at location -100/75/1 using sensor E201-C. REPS pulse 169 generating 6.2 kV/m at 50 m 142
- C-152. Z component of the electric field measured at location -100/75/1 using sensor E201-C. REPS pulse 167 generating 6.3 kV/m at 50 m 142
- C-153. Z component of the electric field measured at location -100/75/1 using sensor E201-C. REPS pulse 168 generating 6.3 kV/m at 50 m 143
- C-154. X component of the magnetic field measured at location -100/75/1 using sensor H104-C. REPS pulse 173 generating 6.1 kV/m at 50 m 143
- C-155. X component of the magnetic field measured at location -100/75/1 using sensor H104-C. REPS pulse 174 generating 6.3 kV/m at 50 m 143
- C-156. Y component of the magnetic field measured at location -100/75/1 using sensor H104-C. REPS pulse 171 generating 6.2 kV/m at 50 m 143
- C-157. Y component of the magnetic field measured at location -100/75/1 using sensor H104-C. REPS pulse 175 generating 6.6 kV/m at 50 m 144
- C-158. Z component of the magnetic field measured at location -100/75/1 using sensor H104-C. REPS pulse 178 generating 6.3 kV/m at 50 m 144
- C-159. Z component of the magnetic field measured at location -100/75/1 using sensor H104-C. REPS pulse 176 generating 6.2 kV/m at 50 m 144
- C-160. Z component of the magnetic field measured at location -100/75/1 using sensor H104-C. REPS pulse 177 generating 6.2 kV/m at 50 m 144

Location 0/92/1

- C-161. X component of the electric field measured at location 0/92/1 using sensor E102-C. REPS pulse 281 generating 6.1 kV/m at 50 m 145
- C-162. Z component of the electric field measured at location 0/92/1 using sensor E102-C. REPS pulse 283 generating 6.2 kV/m at 50 m 145
- C-163. Z component of the electric field measured at location 0/92/1 using sensor E102-C. REPS pulse 284 generating 6 kV/m at 50 m 145
- C-164. Y component of the magnetic field measured at location 0/92/1 using sensor H104-C. REPS pulse 279 generating 6.2 kV/m at 50 m 145
- C-165. Y component of the magnetic field measured at location 0/92/1 using sensor H104-C. REPS pulse 280 generating 6.3 kV/m at 50 m 146

Location 0/25/2

- C-166. X component of the electric field measured at location 0/25/2 using sensor E304-C. REPS pulse 46 generating 6.1 kV/m at 50 m 146
- C-167. -Y component of the electric field measured at location 0/25/2 using sensor E201-C. REPS pulse 40 generating 6.1 kV/m at 50 m 146
- C-168. Z component of the electric field measured at location 0/25/2 using sensor E201-C. REPS pulse 43 generating 6.3 kV/m at 50 m 146
- C-169. Z component of the electric field measured at location 0/25/2 using sensor E201-C. REPS pulse 44 generating 6.2 kV/m at 50 m 147
- C-170. X component of the magnetic field measured at location 0/25/2 using sensor H104-C. REPS pulse 7 generating 6.5 kV/m at 50 m 147
- C-171. Y component of the magnetic field measured at location 0/25/2 using sensor H104-C. REPS pulse 8 generating 6.4 kV/m at 50 m 147
- C-172. Y component of the magnetic field measured at location 0/25/2 using sensor H104-C. REPS pulse 9 generating 6.3 kV/m at 50 m 147
- C-173. Z component of the magnetic field measured at location 0/25/2 using sensor H104-C. REPS pulse 10 generating 6.3 kV/m at 50 m 148
- C-174. Z component of the magnetic field measured at location 0/25/2 using sensor H104-C. REPS pulse 11 generating 6.4 kV/m at 50 m 148

Location -25/25/2

- C-175. X component of the magnetic field measured at location -25/25/2 using sensor H104-C. REPS pulse 6 generating 6.9 kV/m at 50 m 148
- C-176. Y component of the magnetic field measured at location -25/25/2 using sensor H104-C. REPS pulse 2 generating 6.9 kV/m at 50 m 148
- C-177. Y component of the magnetic field measured at location -25/25/2 using sensor H104-C. REPS pulse 3 generating 7 kV/m at 50 m 149
- C-178. Z component of the magnetic field measured at location -25/25/2 using sensor H104-C. REPS pulse 45 generating 6.9 kV/m at 50 m 149

Location 0/50/2

- C-179. X component of the electric field measured at location 0/50/2 using sensor E201-C. REPS pulse 39 generating 6.68 kV/m at 50 m 149
- C-180. -Y component of the electric field measured at location 0/50/2 using sensor E201-C. REPS pulse 36 generating 6.65 kV/m at 50 m 149
- C-181. -Y component of the electric field measured at location 0/50/2 using sensor E201-C. REPS pulse 61 generating 6.1 kV/m at 50 m 150

Appendix C

C-182.	Z component of the electric field measured at location 0/50/2 using sensor E201-C. REPS pulse 56 generating 6 kV/m at 50 m	150
C-183.	X component of the magnetic field measured at location 0/50/2 using sensor H104-C. REPS pulse 18 generating 6.4 kV/m at 50 m	150
C-184.	Y component of the magnetic field measured at location 0/50/2 using sensor H104-C. REPS pulse 19 generating 6.3 kV/m at 50 m	150
C-185.	Y component of the magnetic field measured at location 0/50/2 using sensor H104-C. REPS pulse 20 generating 6.3 kV/m at 50 m	151
C-186.	Z component of the magnetic field measured at location 0/50/2 using sensor H104-C. REPS pulse 21 generating 6.1 kV/m at 50 m	151

Location -25/50/2

C-187.	X component of the electric field measured at location -25/50/2 using sensor E304-C. REPS pulse 91 generating 6.3 kV/m at 50 m	151
C-188.	-Y component of the electric field measured at location -25/50/2 using sensor E304-C. REPS pulse 87 generating 6.3 kV/m at 50 m	151
C-189.	Z component of the electric field measured at location -25/50/2 using sensor E304-C. REPS pulse 88 generating 6.4 kV/m at 50 m	152
C-190.	Z component of the electric field measured at location -25/50/2 using sensor E304-C. REPS pulse 90 generating 6.2 kV/m at 50 m	152
C-191.	X component of the magnetic field measured at location -25/50/2 using sensor H104-C. REPS pulse 81 generating 6.3 kV/m at 50 m	152
C-192.	X component of the magnetic field measured at location -25/50/2 using sensor H104-C. REPS pulse 82 generating 6.5 kV/m at 50 m	152
C-193.	Y component of the magnetic field measured at location -25/50/2 using sensor H104-C. REPS pulse 79 generating 6.2 kV/m at 50 m	153
C-194.	Y component of the magnetic field measured at location -25/50/2 using sensor H104-C. REPS pulse 80 generating 6.2 kV/m at 50 m	153
C-195.	Z component of the magnetic field measured at location -25/50/2 using sensor H104-C. REPS pulse 78 generating 6.3 kV/m at 50 m	153

Location -50/50/2

C-196.	X component of the electric field measured at location -50/50/2 using sensor E304-C. REPS pulse 99 generating 6.4 kV/m at 50 m	153
C-197.	-Y component of the electric field measured at location -50/50/2 using sensor E304-C. REPS pulse 96 generating 6.3 kV/m at 50 m	154
C-198.	Z component of the electric field measured at location -50/50/2 using sensor E304-C. REPS pulse 97 generating 6.2 kV/m at 50 m	154

C-199.	Z component of the electric field measured at location -50/50/2 using sensor E304-C. REPS pulse 98 generating 6.5 kV/m at 50 m	154
C-200.	X component of the magnetic field measured at location -50/50/2 using sensor H104-C. REPS pulse 108 generating 6.2 kV/m at 50 m	154
C-201.	X component of the magnetic field measured at location -50/50/2 using sensor H104-C. REPS pulse 109 generating 6.3 kV/m at 50 m	155
C-202.	Y component of the magnetic field measured at location -50/50/2 using sensor H104-C. REPS pulse 110 generating 6.5 kV/m at 50 m	155
C-203.	Y component of the magnetic field measured at location -50/50/2 using sensor H104-C. REPS pulse 111 generating 6.3 kV/m at 50 m	155
C-204.	Z component of the magnetic field measured at location -50/50/2 using sensor H104-C. REPS pulse 107 generating 6.3 kV/m at 50 m	155
Location 50/25/1		
C-205.	-X component of the electric field measured at location 50/25/1 using sensor E304-C. REPS pulse 361 generating 6 kV/m at 50 m	156
C-206.	-Y component of the electric field measured at location 50/25/1 using sensor E304-C. REPS pulse 364 generating 6.1 kV/m at 50 m	156
C-207.	-Y component of the electric field measured at location 50/25/1 using sensor E304-C. REPS pulse 365 generating 6.2 kV/m at 50 m	156
C-208.	Z component of the electric field measured at location 50/25/1 using sensor E304-C. REPS pulse 362 generating 6.3 kV/m at 50 m	156
C-209.	Z component of the electric field measured at location 50/25/1 using sensor E304-C. REPS pulse 363 generating 5.9 kV/m at 50 m	157
C-210.	-X component of the magnetic field measured at location 50/25/1 using sensor H104-C. REPS pulse 366 generating 6.2 kV/m at 50 m	157
C-211.	-X component of the magnetic field measured at location 50/25/1 using sensor H104-C. REPS pulse 367 generating 6.1 kV/m at 50 m	157
C-212.	Y component of the magnetic field measured at location 50/25/1 using sensor H104-C. REPS pulse 370 generating 6.1 kV/m at 50 m	157
C-213.	Y component of the magnetic field measured at location 50/25/1 using sensor H104-C. REPS pulse 371 generating 6.1 kV/m at 50 m	158
C-214.	Z component of the magnetic field measured at location 50/25/1 using sensor H104-C. REPS pulse 368 generating 6.1 kV/m at 50 m	158
C-215.	Z component of the magnetic field measured at location 50/25/1 using sensor H104-C. REPS pulse 369 generating 6 kV/m at 50 m	158

Appendix C

Location 25/50/1

C-216.	-X component of the electric field measured at location 25/50/1 using sensor E201-C. REPS pulse 339 generating 6.3 kV/m at 50 m	158
C-217.	-X component of the electric field measured at location 25/50/1 using sensor E201-C. REPS pulse 338 generating 6.1 kV/m at 50 m	159
C-218.	-Y component of the electric field measured at location 25/50/1 using sensor E201-C. REPS pulse 337 generating 6.4 kV/m at 50 m	159
C-219.	Z component of the electric field measured at location 25/50/1 using sensor E201-C. REPS pulse 335 generating 6 kV/m at 50 m	159
C-220.	Z component of the electric field measured at location 25/50/1 using sensor E201-C. REPS pulse 336 generating 6.3 kV/m at 50 m	159
C-221.	-X component of the magnetic field measured at location 25/50/1 using sensor H104-C. REPS pulse 331 generating 6.4 kV/m at 50 m.	160
C-222.	-X component of the magnetic field measured at location 25/50/1 using sensor H104-C. REPS pulse 332 generating 6.2 kV/m at 50 m	160
C-223.	Y component of the magnetic field measured at location 25/50/1 using sensor H104-C. REPS pulse 329 generating 6.3 kV/m at 50 m	160
C-224.	Y component of the magnetic field measured at location 25/50/1 using sensor H104-C. REPS pulse 330 generating 6.3 kV/m at 50 m	160
C-225.	Z component of the magnetic field measured at location 25/50/1 using sensor H104-C. REPS pulse 334 generating 6.2 kV/m at 50 m	161

Location 50/50/1

C-226.	-X component of the electric field measured at location 50/50/1 using sensor E304-C. REPS pulse 263 generating 6.1 kV/m at 50 m	161
C-227.	-Y component of the electric field measured at location 50/50/1 using sensor E304-C. REPS pulse 262 generating 6.1 kV/m at 50 m	161
C-228.	Z component of the electric field measured at location 50/50/1 using sensor E304-C. REPS pulse 260 generating 6.1 kV/m at 50 m	161
C-229.	Z component of the electric field measured at location 50/50/1 using sensor E304-C. REPS pulse 261 generating 6 kV/m at 50 m	162
C-230.	X component of the magnetic field measured at location 50/50/1 using sensor H104-C. REPS pulse 254 generating 6.1 kV/m at 50 m	162
C-231.	X component of the magnetic field measured at location 50/50/1 using sensor H104-C. REPS pulse 255 generating 6 kV/m at 50 m	162
C-232.	Y component of the magnetic field measured at location 50/50/1 using sensor H104-C. REPS pulse 256 generating 6.3 kV/m at 50 m	162

- C-233. Y component of the magnetic field measured at location 50/50/1 using sensor H104-C. REPS pulse 257 generating 6 kV/m at 50 m 163
- C-234. Z component of the magnetic field measured at location 50/50/1 using sensor H104-C. REPS pulse 259 generating 6.2 kV/m at 50 m 163

Location 25/0/1

- C-235. -X component of the electric field measured at location 25/0/1 using sensor E403-C. REPS pulse 403 generating 6.2 kV/m at 50 m 163
- C-236. -X component of the electric field measured at location 25/0/1 using sensor E403-C. REPS pulse 404 generating 6 kV/m at 50 m 163
- C-237. -Y component of the electric field measured at location 25/0/1 using sensor E403-C. REPS pulse 407 generating 6.2 kV/m at 50 m 164
- C-238. -Y component of the electric field measured at location 25/0/1 using sensor E403-C. REPS pulse 408 generating 6.3 kV/m at 50 m 164
- C-239. Z component of the electric field measured at location 25/0/1 using sensor E403-C. REPS pulse 405 generating 6.3 kV/m at 50 m 164
- C-240. Z component of the electric field measured at location 25/0/1 using sensor E403-C. REPS pulse 406 generating 6.2 kV/m at 50 m 164
- C-241. -X component of the magnetic field measured at location 25/0/1 using sensor H104-C. REPS pulse 398 generating 6.2 kV/m at 50 m 165
- C-242. -X component of the magnetic field measured at location 25/0/1 using sensor H104-C. REPS pulse 399 generating 6.2 kV/m at 50 m 165
- C-243. Y component of the magnetic field measured at location 25/0/1 using sensor H104-C. REPS pulse 401 generating 6.2 kV/m at 50 m 165
- C-244. Y component of the magnetic field measured at location 25/0/1 using sensor H104-C. REPS pulse 402 generating 6.2 kV/m at 50 m 165
- C-245. Z component of the magnetic field measured at location 25/0/1 using sensor H104-C. REPS pulse 396 generating 6.2 kV/m at 50 m 166
- C-246. Z component of the magnetic field measured at location 25/0/1 using sensor H104-C. REPS pulse 397 generating 6.2 kV/m at 50 m 166

Location 18/33/1

- C-247. -X component of the electric field measured at location 18/33/1 using sensor E304-C. REPS pulse 357 generating 6.2 kV/m at 50 m 166
- C-248. -Y component of the electric field measured at location 18/33/1 using sensor E304-C. REPS pulse 360 generating 6.2 kV/m at 50 m 166
- C-249. Z component of the electric field measured at location 18/33/1 using sensor E304-C. REPS pulse 358 generating 6.1 kV/m at 50 m 167

Appendix C

- C-250. Z component of the electric field measured at location 18/33/1 using sensor E304-C. REPS pulse 359 generating 6.1 kV/m at 50 m 167
- C-251. X component of the magnetic field measured at location 18/33/1 using sensor H104-C. REPS pulse 353 generating 6.2 kV/m at 50 m 167
- C-252. Y component of the magnetic field measured at location 18/33/1 using sensor H104-C. REPS pulse 355 generating 6.3 kV/m at 50 m 167
- C-253. Y component of the magnetic field measured at location 18/33/1 using sensor H104-C. REPS pulse 356 generating 6.3 kV/m at 50 m 168
- C-254. Z component of the magnetic field measured at location 18/33/1 using sensor H104-C. REPS pulse 354 generating 6.1 kV/m at 50 m 168

Location 35/35/1

- C-255. -X component of the electric field measured at location 35/35/1 using sensor E304-C. REPS pulse 378 generating 6.3 kV/m at 50 m 168
- C-256. -Y component of the electric field measured at location 35/35/1 using sensor E304-C. REPS pulse 385 generating 6.1 kV/m at 50 m 168
- C-257. -Y component of the electric field measured at location 35/35/1 using sensor E304-C. REPS pulse 384 generating 6.2 kV/m at 50 m 169
- C-258. Z component of the electric field measured at location 35/35/1 using sensor E304-C. REPS pulse 380 generating 6.1 kV/m at 50 m 169
- C-259. Z component of the electric field measured at location 35/35/1 using sensor E304-C. REPS pulse 383 generating 6.2 kV/m at 50 m 169
- C-260. -X component of the magnetic field measured at location 35/35/1 using sensor H104-C. REPS pulse 372 generating 6.3 kV/m at 50 m 169
- C-261. -X component of the magnetic field measured at location 35/35/1 using sensor H104-C. REPS pulse 373 generating 6.2 kV/m at 50 m 170
- C-262. Y component of the magnetic field measured at location 35/35/1 using sensor H104-C. REPS pulse 276 generating 6.3 kV/m at 50 m 170
- C-263. Y component of the magnetic field measured at location 35/35/1 using sensor H104-C. REPS pulse 377 generating 6.2 kV/m at 50 m 170
- C-264. Z component of the magnetic field measured at location 35/35/1 using sensor H104-C. REPS pulse 374 generating 6.2 kV/m at 50 m 170
- C-265. Z component of the magnetic field measured at location 35/35/1 using sensor H104-C. REPS pulse 375 generating 6 kV/m at 50 m 171

Location 0/-50/1

- C-266. X component of the electric field measured at location 0/-50/1 using sensor E304-C. REPS pulse 270 generating 6.3 kV/m at 50 m 171

C-267.	Y component of the electric field measured at location 0/-50/1 using sensor E304-C. REPS pulse 273 generating 6.2 kV/m at 50 m	171
C-268.	Z component of the electric field measured at location 0/-50/1 using sensor E304-C. REPS pulse 271 generating 6.3 kV/m at 50 m	171
C-269.	Z component of the electric field measured at location 0/-50/1 using sensor E304-C. REPS pulse 272 generating 6.2 kV/m at 50 m	172
C-270.	X component of the magnetic field measured at location 0/-50/1 using sensor H104-C. REPS pulse 274 generating 6.4 kV/m at 50 m.	172
C-271.	X component of the magnetic field measured at location 0/-50/1 using sensor H104-C. REPS pulse 275 generating 6.3 kV/m at 50 m	172
C-272.	Y component of the magnetic field measured at location 0/-50/1 using sensor H104-C. REPS pulse 276 generating 6.3 kV/m at 50 m	172
C-273.	Y component of the magnetic field measured at location 0/-50/1 using sensor H104-C. REPS pulse 277 generating 6.2 kV/m at 50 m	173
C-274.	Z component of the magnetic field measured at location 0/-50/1 using sensor H104-C. REPS pulse 278 generating 6.2 kV/m at 50 m	173

Location 0/-75/1

C-275.	X component of the electric field measured at location 0/-75/1 using sensor E304-C. REPS pulse 387 generating 6.3 kV/m at 50 m	173
C-276.	Y component of the electric field measured at location 0/-75/1 using sensor E304-C. REPS pulse 390 generating 6.2 kV/m at 50 m	173
C-277.	Z component of the electric field measured at location 0/-75/1 using sensor E304-C. REPS pulse 388 generating 6.4 kV/m at 50 m	174
C-278.	Z component of the electric field measured at location 0/-75/1 using sensor E304-C. REPS pulse 389 generating 6.3 kV/m at 50 m	174
C-279.	-X component of the magnetic field measured at location 0/-75/1 using sensor H104-C. REPS pulse 392 generating 6.3 kV/m at 50 m	174
C-280.	-X component of the magnetic field measured at location 0/-75/1 using sensor H104-C. REPS pulse 393 generating 6.1 kV/m at 50 m	174
C-281.	-Y component of the magnetic field measured at location 0/-75/1 using sensor H104-C. REPS pulse 394 generating 6.3 kV/m at 50 m	175
C-282.	-Y component of the magnetic field measured at location 0/-75/1 using sensor H104-C. REPS pulse 395 generating 6.2 kV/m at 50 m	175
C-283.	Z component of the magnetic field measured at location 0/-75/1 using sensor H104-C. REPS pulse 391 generating 6.1 kV/m at 50 m	175

Appendix C

Location 0/50/1

- C-284. X component of the electric field measured at location 0/50/1 using sensor E304-C. REPS pulse 47 generating 6.1 kV/m at 50 m 176
- C-285. Y component of the magnetic field measured at location 0/50/1 using sensor H104-C. REPS pulse 13 generating 6.3 kV/m at 50 m 176

Location -19/46/1

- C-286. T component of the electric field measured at location -19/46/1 using sensor E304-C. REPS pulse 309 generating 6.2 kV/m at 50 m 176
- C-287. R component of the magnetic field measured at location -19/46/1 using sensor H104-C. REPS pulse 305 generating 6.1 kV/m at 50 m 176

Location -35/35/1

- C-288. T component of the electric field measured at location -35/35/1 using sensor E304-C. REPS pulse 293 generating 6.2 kV/m at 50 m 177
- C-289. R component of the magnetic field measured at location -35/35/1 using sensor H104-C. REPS pulse 298 generating 6.4 kV/m at 50 m 177
- C-290. X component of the electric field measured at location -35/35/1 using sensor E304-C. REPS pulse 287 generating 6.3 kV/m at 50 m 177
- C-291. -Y component of the electric field measured at location -35/35/1 using sensor E304-C. REPS pulse 292 generating 6.5 kV/m at 50 m 177
- C-292. Z component of the electric field measured at location -35/35/1 using sensor E304-C. REPS pulse 288 generating 6.3 kV/m at 50 m 178
- C-293. Z component of the electric field measured at location -35/35/1 using sensor E304-C. REPS pulse 289 generating 6.3 kV/m at 50 m 178
- C-294. X component of the magnetic field measured at location -35/35/1 using sensor H104-C. REPS pulse 300 generating 6.2 kV/m at 50 m 178
- C-295. X component of the magnetic field measured at location -35/35/1 using sensor H104-C. REPS pulse 301 generating 6.2 kV/m at 50 m 178
- C-296. Y component of the magnetic field measured at location -35/35/1 using sensor H104-C. REPS pulse 303 generating 6.4 kV/m at 50 m 179
- C-297. Y component of the magnetic field measured at location -35/35/1 using sensor H104-C. REPS pulse 304 generating 6.2 kV/m at 50 m 179
- C-298. Z component of the magnetic field measured at location -35/35/1 using sensor H104-C. REPS pulse 302 generating 6.3 kV/m at 50 m 179

Location 0/85/1

- C-299. X component of the electric field measured at location 0/85/1 using sensor E201-C. REPS pulse 324 generating 6.1 kV/m at 50 m 179
- C-300. Y component of the magnetic field measured at location 0/85/1 using sensor H104-C. REPS pulse 326 generating 6.2 kV/m at 50 m 180

Location -33/79/1

- C-301. T component of the electric field measured at location -33/79/1 using sensor E304-C. REPS pulse 314 generating 6.2 kV/m at 50 m 180
- C-302. R component of the magnetic field measured at location -33/79/1 using sensor H104-C. REPS pulse 316 generating 6.1 kV/m at 50 m 180

Location -60/60/1

- C-303. T component of the electric field measured at location -60/60/1 using sensor E201-C. REPS pulse 320 generating 6 kV/m at 50 m 180
- C-304. R component of the magnetic field measured at location -60/60/1 using sensor H104-C. REPS pulse 318 generating 6.3 kV/m at 50 m 181

Location 0/50/2

- C-305. X component of the electric field measured at location 0/50/2 using sensor E304-C. REPS pulse 48 generating 6.2 kV/m at 50 m 181
- C-306. Y component of the magnetic field measured at location 0/50/2 using sensor H104-C. REPS pulse 19 generating 6.3 kV/m at 50 m 181

Location -19/46/2

- C-307. T component of the electric field measured at location -19/46/2 using sensor E304-C. REPS pulse 313 generating 6.2 kV/m at 50 m 181
- C-308. R component of the magnetic field measured at location -19/46/2 using sensor H104-C. REPS pulse 306 generating 6.2 kV/m at 50 m 182

Location -35/35/1

- C-309. T component of the electric field measured at location -35/35/1 using sensor E304-C. REPS pulse 295 generating 6.3 kV/m at 50 m 182
- C-310. R component of the magnetic field measured at location -35/35/1 using sensor H104-C. REPS pulse 299 generating 6.3 kV/m at 50 m 182

Location 0/85/2

- C-311. X component of the electric field measured at location 0/85/2 using sensor E201-C. REPS pulse 325 generating 6.3 kV/m at 50 m 182
- C-312. Y component of the magnetic field measured at location 0/85/2 using sensor H104-C. REPS pulse 328 generating 6.3 kV/m at 50 m 183

Appendix C

Location -33/79/2

- C-313. *T* component of the electric field measured at location -33/79/2 using sensor E304-C. REPS pulse 315 generating 6.1 kV/m at 50 m 183
- C-314. *R* component of the magnetic field measured at location -33/79/2 using sensor H104-C. REPS pulse 317 generating 6.2 kV/m at 50 m 183

Location -60/60/2

- C-315. *T* component of the electric field measured at location -60/60/2 using sensor E201-C. REPS pulse 322 generating 6.2 kV/m at 50 m 183
- C-316. *R* component of the magnetic field measured at location -60/60/2 using sensor H104-C. REPS pulse 319 generating 6.2 kV/m at 50 m 184

C-1. Data Collection

This appendix contains the complete time history for each field component measured during this effort.

As mentioned in section 4.3, *Data Acquisition Instrumentation*, all the data during this effort were collected using SMART IVAN I. The IVAN uses two digitizers per test point to define the entire pulse. One digitizer is set at a fast sampling rate to capture the high-frequency, fast-rising portion of the waveform, while the second digitizer is set to a slower sampling rate to capture mid- and low-frequency information. All of the data have been scalar corrected to include the effects of the fiber-optic link, sensor/cylinder, and any attenuation used during the measurement.

C-2. Data Organization

We organized the data first by test objective: 1-m height, 2-m height, symmetry data, and arc data. Within each of these sections, the data are further broken down by location (i.e., X/25/X, X/50/X, X/75/X). Within each location the data are then organized by component (i.e., E_x , E_y , E_z , H_x , H_y , H_z).

The data are outlined as follows:

I. 1-m data

- A. Location X/25/1 ($X = 0, -25, -50, -75, -100$)

component E_x , E_y , E_z , H_x , H_y , H_z

- B. Location X/50/1 ($X = 0, -25, -50, -75, -100, -125, -150$)

component E_x , E_y , E_z , H_x , H_y , H_z

- C. Location X/75/1 ($X = 0, -25, -50, -75, -100$)

component E_x , E_y , E_z , H_x , H_y , H_z

- D. Location 0/92/1

component E_x , E_z , H_y

Appendix C

II. 2-m height

A. Location X/25/2 ($X = 0, -25$)

component $E_x, E_y, E_z, H_x, H_y, H_z$

B. Location X/50/2 ($X = 0, -25, -50$)

component $E_x, E_y, E_z, H_x, H_y, H_z$

III. Symmetry data

A. 50/25/1

component $E_x, E_y, E_z, H_x, H_y, H_z$

B. X/50/1 ($X = 25, 50$)

component $E_x, E_y, E_z, H_x, H_y, H_z$

C. 25/0/1

component $E_x, E_y, E_z, H_x, H_y, H_z$

D. 18/33/1

component $E_x, E_y, E_z, H_x, H_y, H_z$

E. 35/35/1

component $E_x, E_y, E_z, H_x, H_y, H_z$

F. 0/-50/1

component $E_x, E_y, E_z, H_x, H_y, H_z$

G. 0/-75/1

component $E_x, E_y, E_z, H_x, H_y, H_z$

IV. Arc data

A. 50-m arc

component E_t, H_r

B. 85-m arc

component E_t, H_r

Appendix C, 1-m data

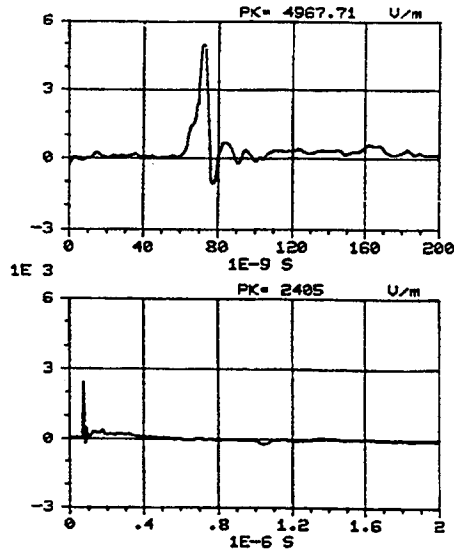


Figure C-1. X component of the electric field measured at location 0/25/1 using sensor E304-C. REPS pulse 45 generating 6.3 kV/m at 50 m.

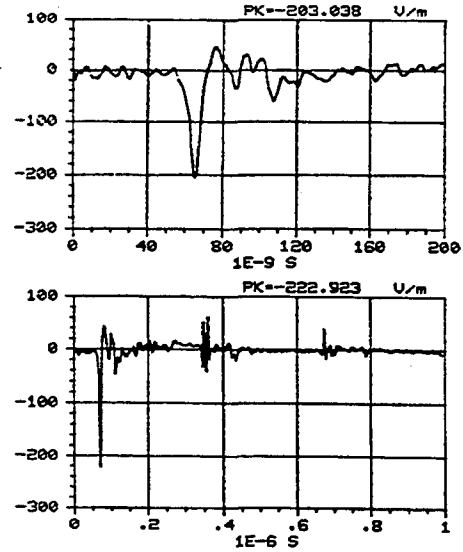


Figure C-2. -Y component of the electric field measured at location 0/25/1 using sensor E201-C. REPS pulse 39 generating 6.1 kV/m at 50 m.

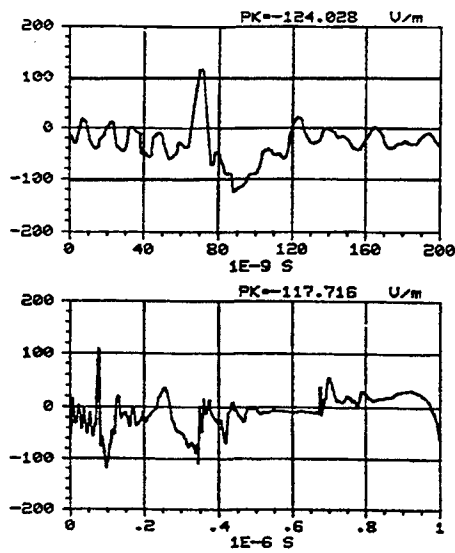


Figure C-3. Z component of the electric field measured at location 0/25/1 using sensor E201-C. REPS pulse 36 generating 6.1 kV/m at 50 m.

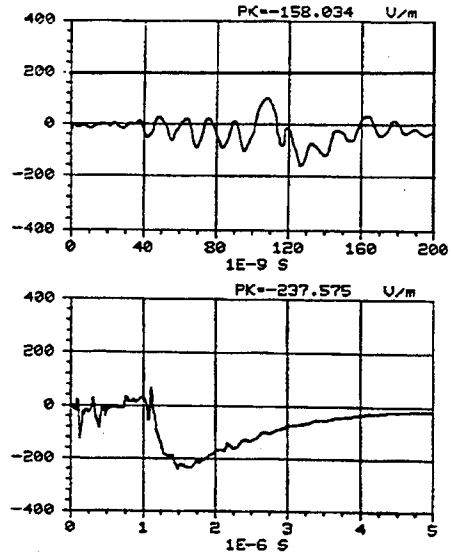


Figure C-4. Z component of the electric field measured at location 0/25/1 using sensor E201-C. REPS pulse 38 generating 6 kV/m at 50 m.

Appendix C, 1-m data

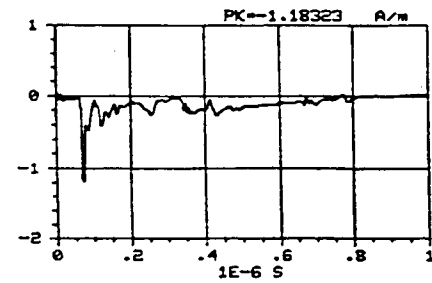
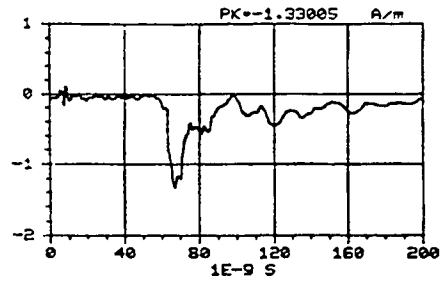


Figure C-5. X component of the magnetic field measured at location 0/25/1 using sensor H104-C. REPS pulse 6 generating 6.3 kV/m at 50 m.

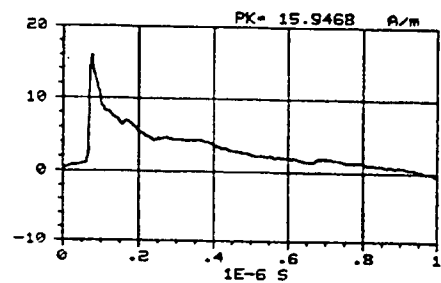
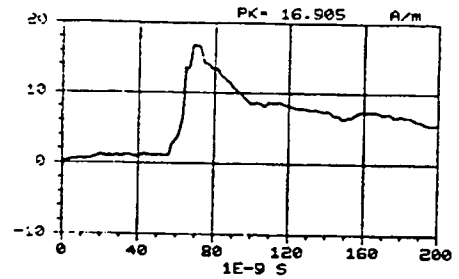


Figure C-6. Y component of the magnetic field measured at location 0/25/1 using sensor H104-C. REPS pulse 2 generating 6.4 kV/m at 50 m.

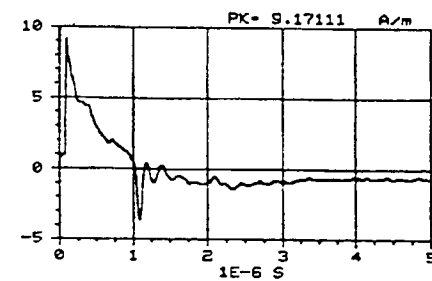
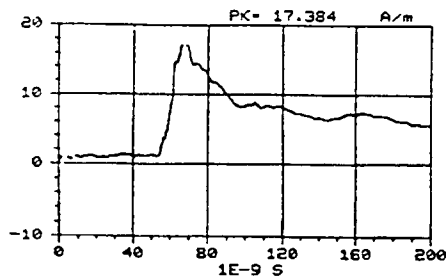


Figure C-7. Y component of the magnetic field measured at location 0/25/1 using sensor H104-C. REPS pulse 3 generating 6.4 kV/m at 50 m.

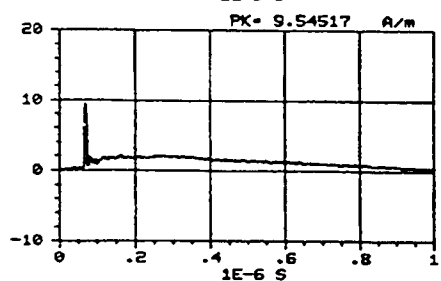
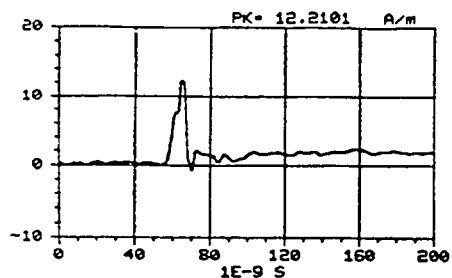


Figure C-8. Z component of the magnetic field measured at location 0/25/1 using sensor H104-C. REPS pulse 4 generating 6.1 kV/m at 50 m.

Appendix C, 1-m data

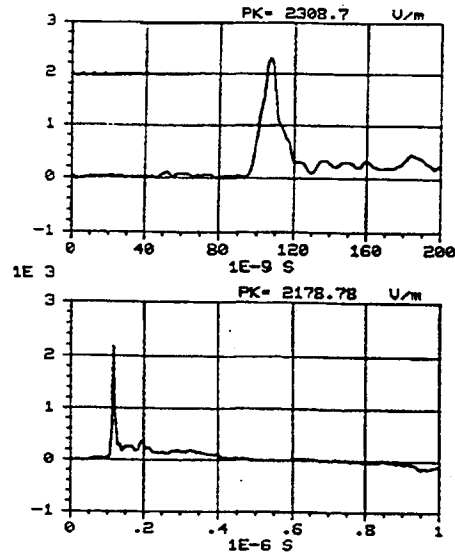


Figure C-9. X component of the electric field measured at location -25/25/1 using sensor E304-C. REPS pulse 266 generating 6.2 kV/m at 50 m.

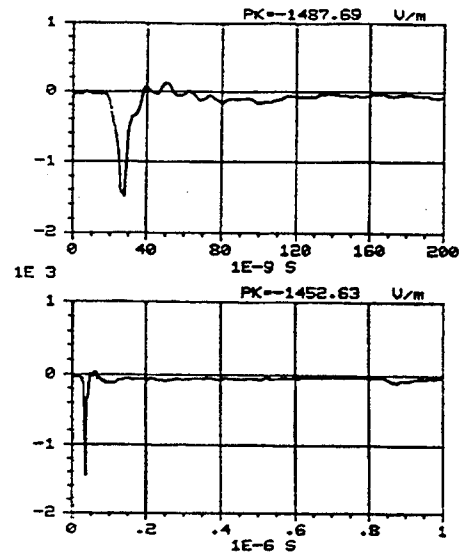


Figure C-10. -Y component of the electric field measured at location -25/25/1 using sensor E304-C. REPS pulse 267 generating 6 kV/m at 50 m.

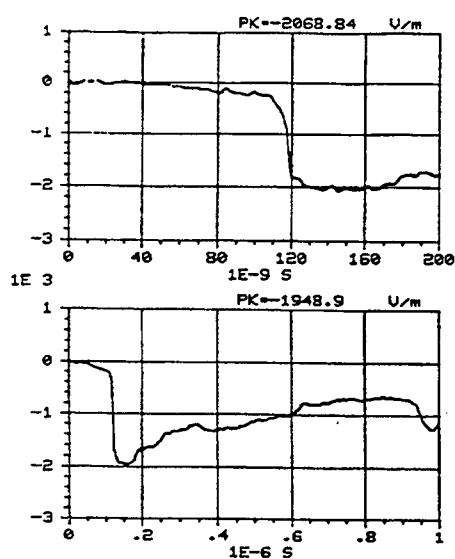


Figure C-11. Z component of the electric field measured at location -25/25/1 using sensor E304-C. REPS pulse 264 generating 6 kV/m at 50 m.

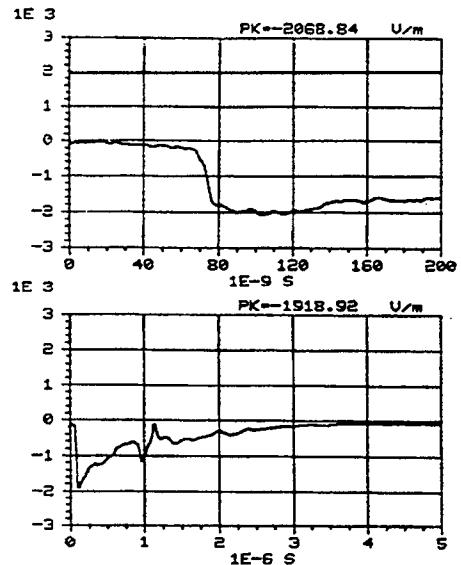


Figure C-12. Z component of the electric field measured at location -25/25/1 using sensor E304-C. REPS pulse 265 generating 6.1 kV/m at 50 m.

Appendix C, 1-m data

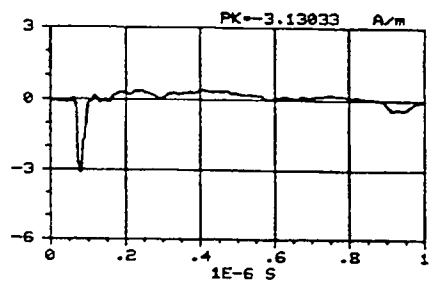
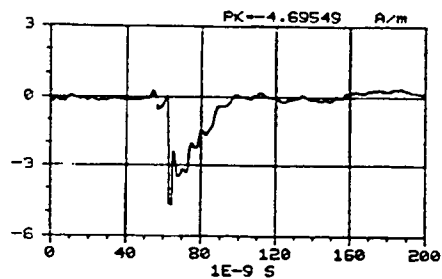


Figure C-13. X component of the magnetic field measured at location -25/25/1 using sensor H104-C. REPS pulse 245 generating 6.5 kV/m at 50 m.

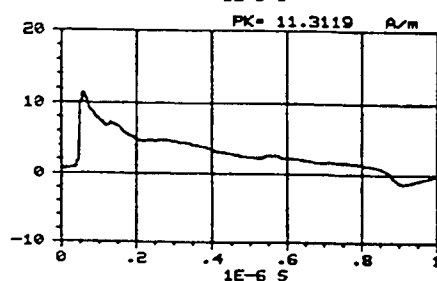
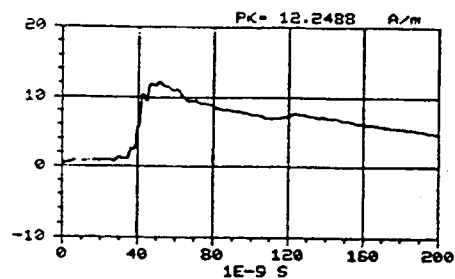


Figure C-14. Y component of the magnetic field measured at location -25/25/1 using sensor H104-C. REPS pulse 246 generating 6.4 kV/m at 50 m.

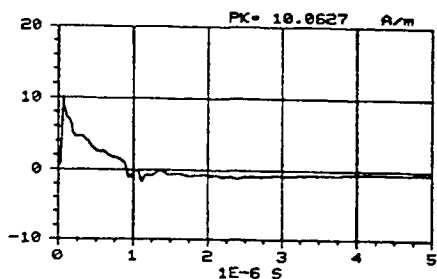
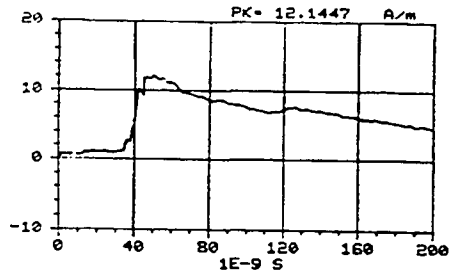


Figure C-15. Y component of the magnetic field measured at location -25/25/1 using sensor H104-C. REPS pulse 247 generating 6.3 kV/m at 50 m.

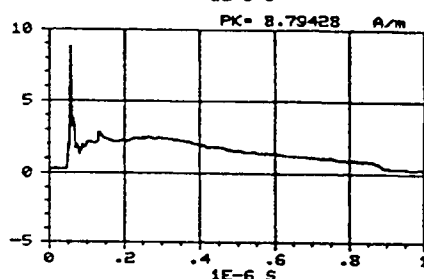
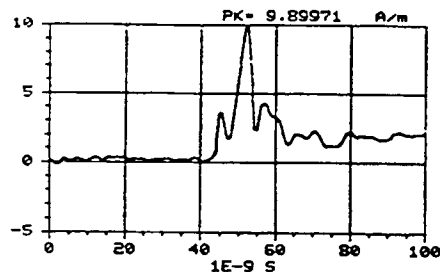


Figure C-16. Z component of the magnetic field measured at location -25/25/1 using sensor H104-C. REPS pulse 241 generating 6.4 kV/m at 50 m.

Appendix C, 1-m data

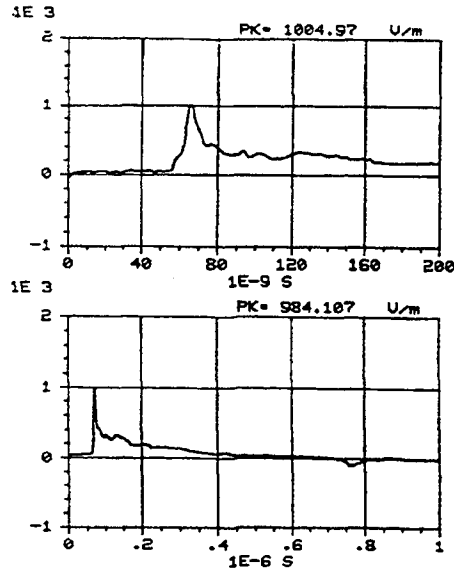


Figure C-17. X component of the electric field measured at location -50/25/1 using sensor E304-C. REPS pulse 232 generating 6.2 kV/m at 50 m.

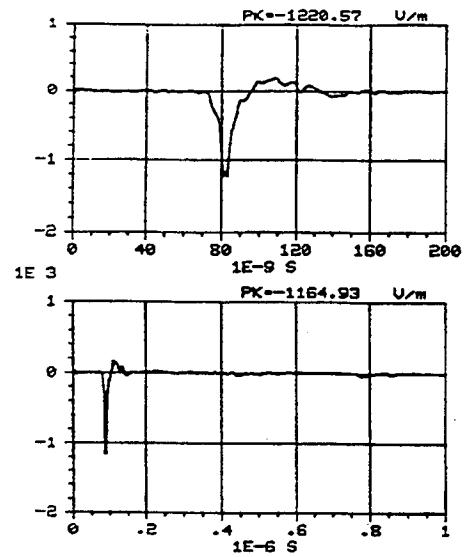


Figure C-18. -Y component of the electric field measured at location -50/25/1 using sensor E304-C. REPS pulse 235 generating 6.1 kV/m at 50 m.

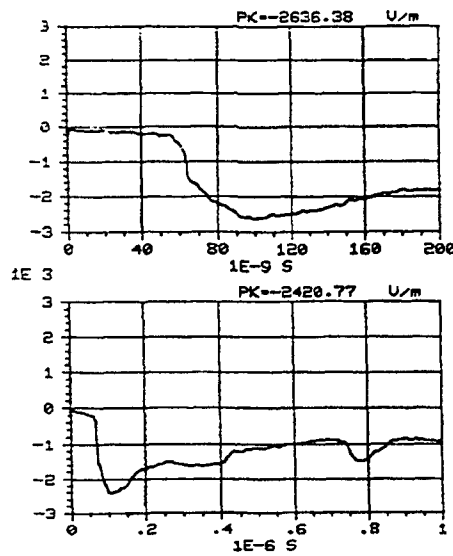


Figure C-19. Z component of the electric field measured at location -50/25/1 using sensor E304-C. REPS pulse 233 generating 6.1 kV/m at 50 m.

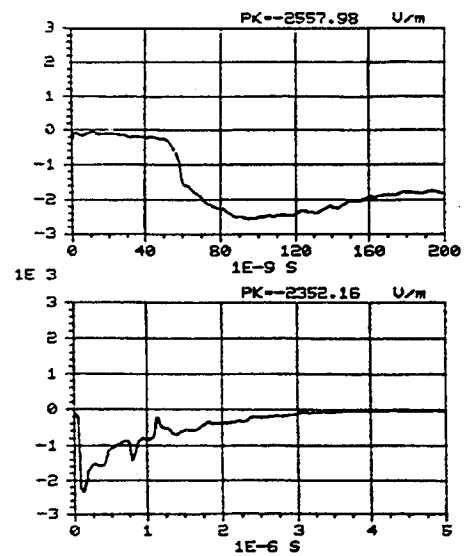


Figure C-20. Z component of the electric field measured at location -50/25/1 using sensor E304-C. REPS pulse 234 generating 6.1 kV/m at 50 m.

Appendix C, 1-m data

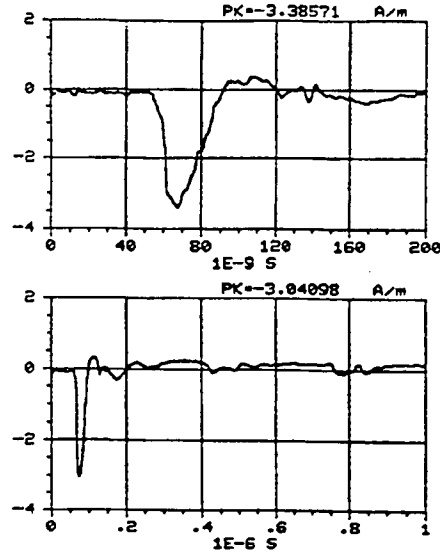


Figure C-21. X component of the magnetic field measured at location -50/25/1 using sensor H104-C. REPS pulse 238 generating 6.4 kV/m at 50 m.

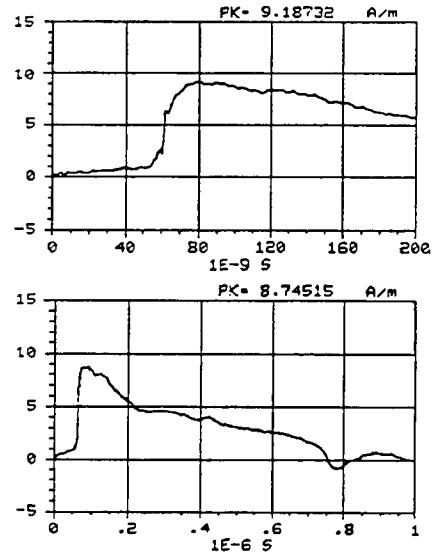


Figure C-22. Y component of the magnetic field measured at location -50/25/1 using sensor H104-C. REPS pulse 236 generating 6.5 kV/m at 50 m.

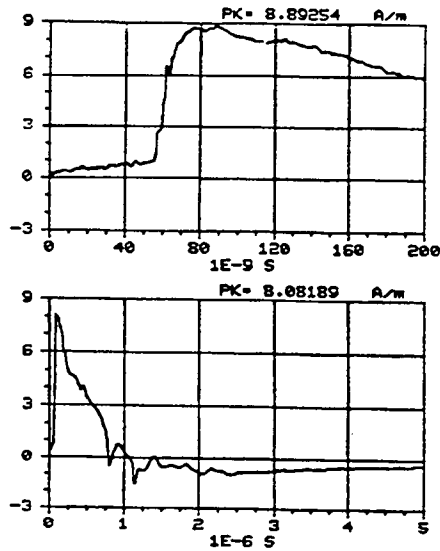


Figure C-23. Y component of the magnetic field measured at location -50/25/1 using sensor H104-C. REPS pulse 237 generating 6.1 kV/m at 50 m.

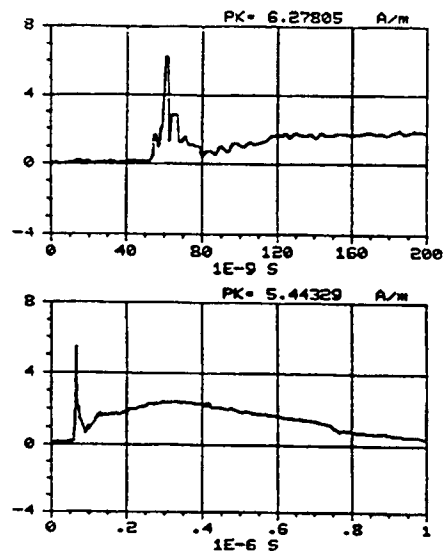


Figure C-24. Z component of the magnetic field measured at location -50/25/1 using sensor H104-C. REPS pulse 239 generating 6.3 kV/m at 50 m.

Appendix C, 1-m data

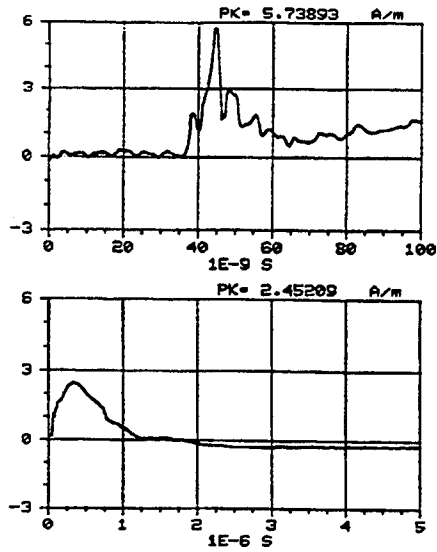


Figure C-25. Z component of the magnetic field measured at location -50/25/1 using sensor H104-C. REPS pulse 240 generating 6.3 kV/m at 50 m.

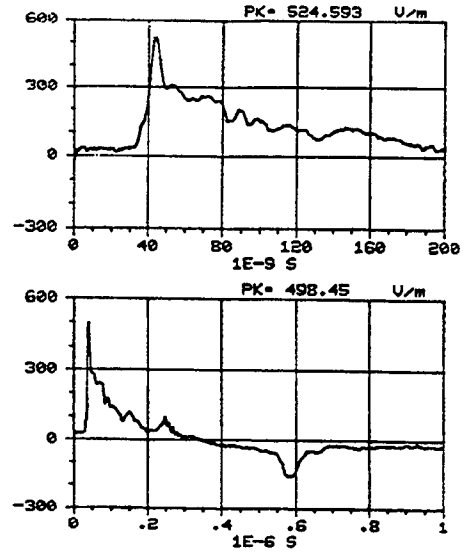


Figure C-26. X component of the electric field measured at location -75/25/1 using sensor E304-C. REPS pulse 226 generating 6.2 kV/m at 50 m.

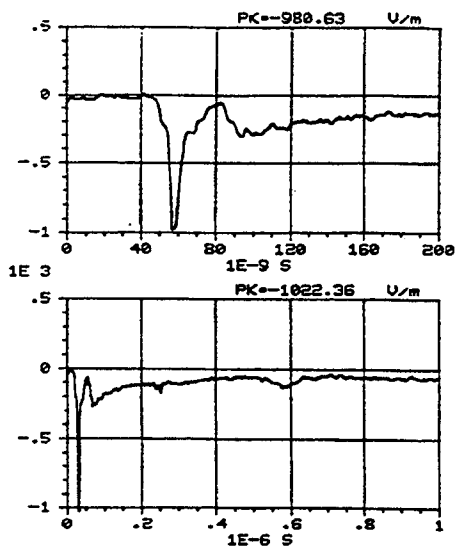


Figure C-27. -Y component of the electric field measured at location -75/25/1 using sensor E304-C. REPS pulse 230 generating 6.3 kV/m at 50 m.

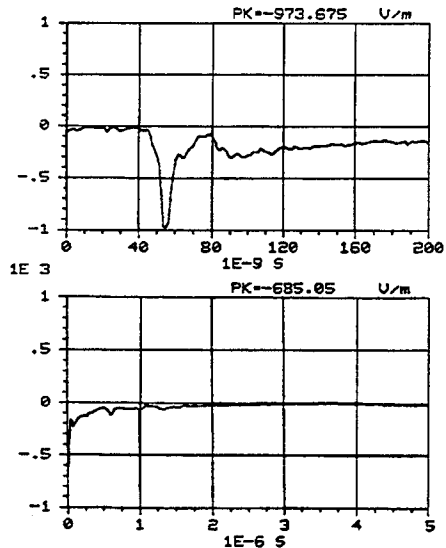


Figure C-28. -Y component of the electric field measured at location -75/25/1 using sensor E304-C. REPS pulse 231 generating 6 kV/m at 50 m.

Appendix C, 1-m data

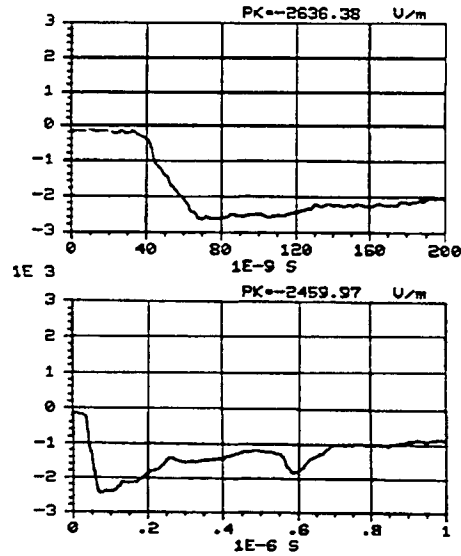


Figure C-29. Z component of the electric field measured at location -75/25/1 using sensor E304-C. REPS pulse 227 generating 6.4 kV/m at 50 m.

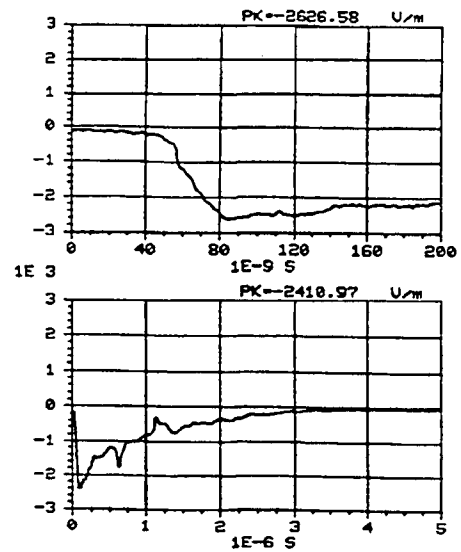


Figure C-30. Z component of the electric field measured at location -75/25/1 using sensor E304-C. REPS pulse 228 generating 6.3 kV/m at 50 m.

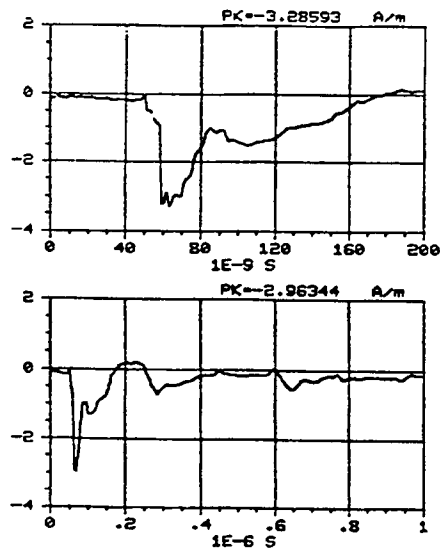


Figure C-31. X component of the magnetic field measured at location -75/25/1 using sensor H104-C. REPS pulse 221 generating 6.3 kV/m at 50 m.

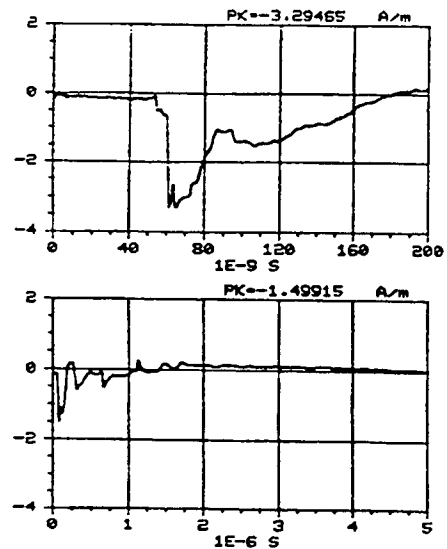


Figure C-32. X component of the magnetic field measured at location -75/25/1 using sensor H104-C. REPS pulse 222 generating 6.5 kV/m at 50 m.

Appendix C, 1-m data

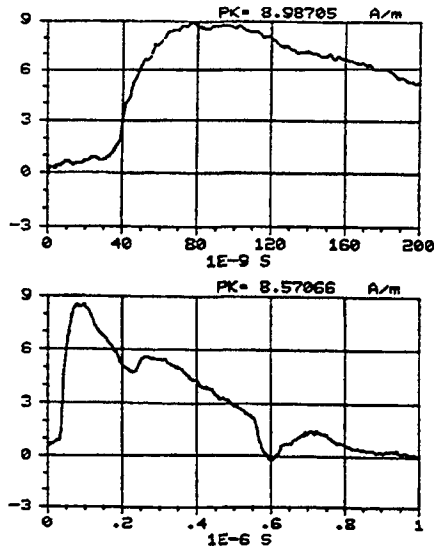


Figure C-33. Y component of the magnetic field measured at location -75/25/1 using sensor H104-C. REPS pulse 216 generating 6.3 kV/m at 50 m.

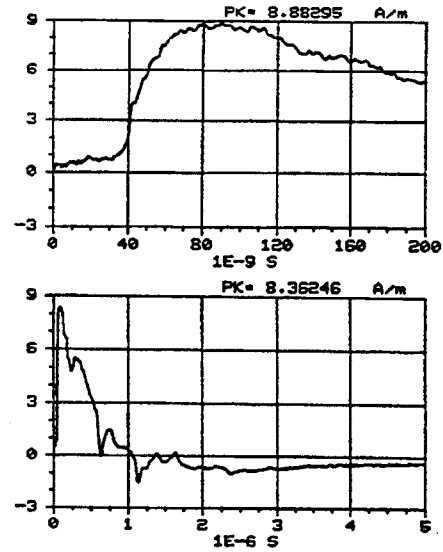


Figure C-34. Y component of the magnetic field measured at location -75/25/1 using sensor H104-C. REPS pulse 217 generating 6.5 kV/m at 50 m.

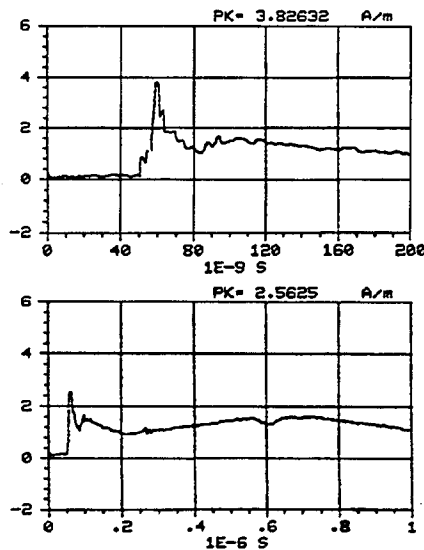


Figure C-35. Z component of the magnetic field measured at location -75/25/1 using sensor H104-C. REPS pulse 223 generating 6.3 kV/m at 50 m.

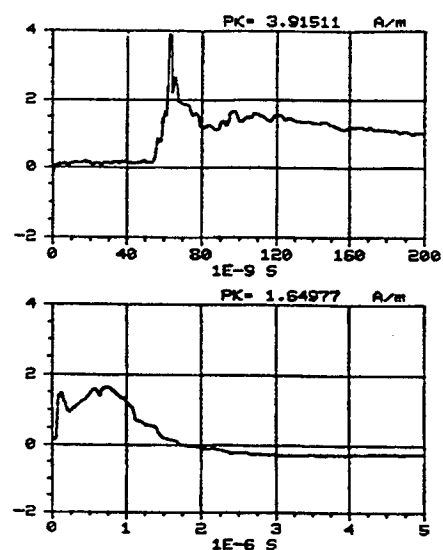


Figure C-36. Z component of the magnetic field measured at location -75/25/1 using sensor H104-C. REPS pulse 224 generating 6.3 kV/m at 50 m.

Appendix C, 1-m data

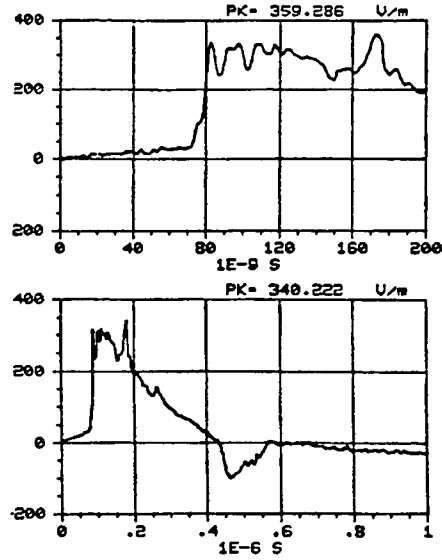


Figure C-37. X component of the electric field measured at location -100/25/1 using sensor E201-C. REPS pulse 192 generating 6.5 kV/m at 50 m.

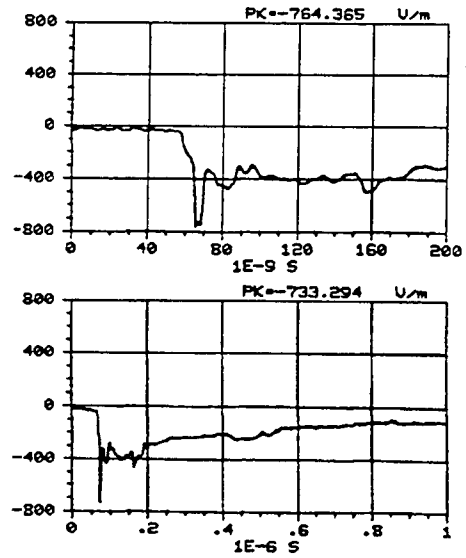


Figure C-38. -Y component of the electric field measured at location -100/25/1 using sensor E201-C. REPS pulse 194 generating 6.4 kV/m at 50 m.

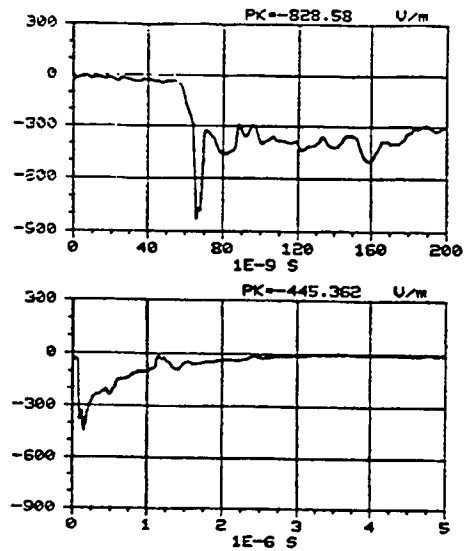


Figure C-39. -Y component of the electric field measured at location -100/25/1 using sensor E201-C. REPS pulse 195 generating 6.4 kV/m at 50 m.

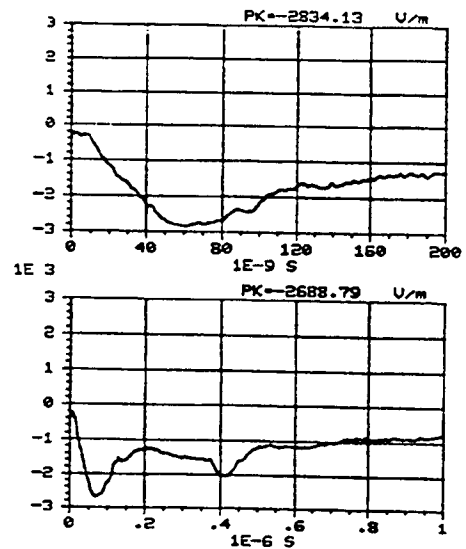


Figure C-40. Z component of the electric field measured at location -100/25/1 using sensor E303-C. REPS pulse 202 generating 6.2 kV/m at 50 m.

Appendix C, 1-m data

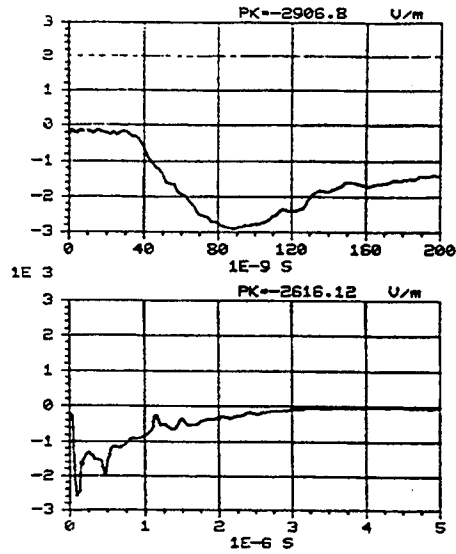


Figure C-41. Z component of the electric field measured at location -100/25/1 using sensor E303-C. REPS pulse 203 generating 6.3 kV/m at 50 m.

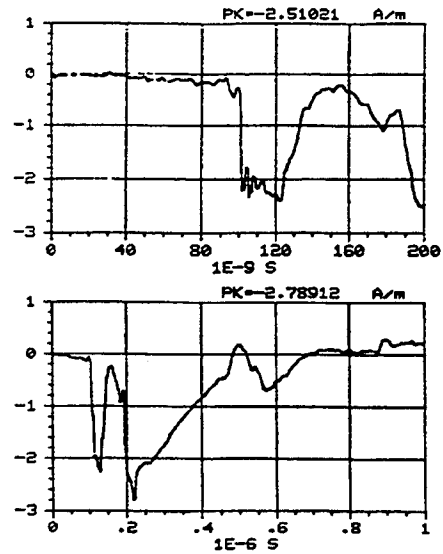


Figure C-42. X component of the magnetic field measured at location -100/25/1 using sensor H104-C. REPS pulse 196 generating 6.5 kV/m at 50 m.

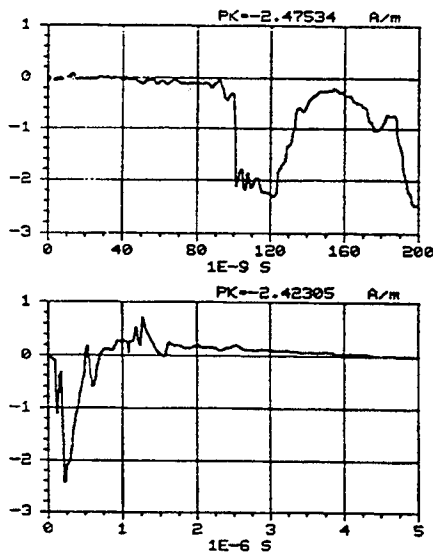


Figure C-43. X component of the magnetic field measured at location -100/25/1 using sensor H104-C. REPS pulse 197 generating 6.2 kV/m at 50 m.

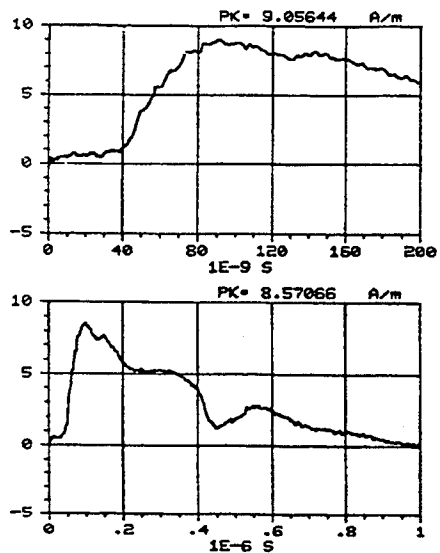


Figure C-44. Y component of the magnetic field measured at location -100/25/1 using sensor H104-C. REPS pulse 200 generating 6.4 kV/m at 50 m.

Appendix C, 1-m data

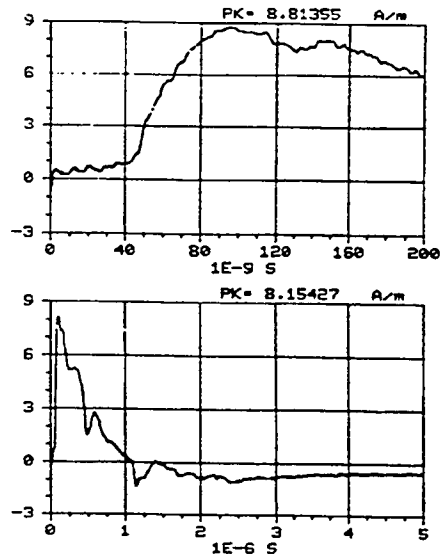


Figure C-45. Y component of the magnetic field measured at location -100/25/1 using sensor H104-C. REPS pulse 201 generating 6.3 kV/m at 50 m.

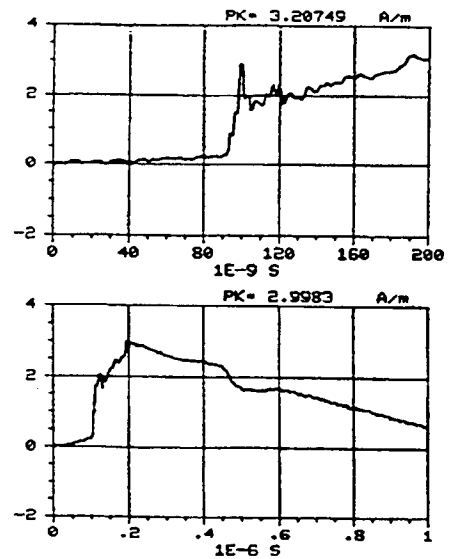


Figure C-46. Z component of the magnetic field measured at location -100/25/1 using sensor H104-C. REPS pulse 198 generating 6.3 kV/m at 50 m.

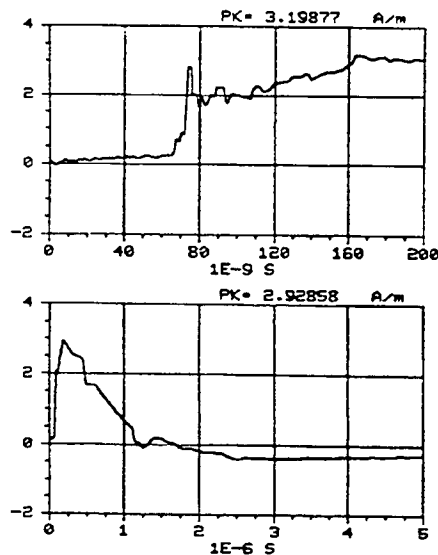


Figure C-47. Z component of the magnetic field measured at location -100/25/1 using sensor H104-C. REPS pulse 199 generating 6.4 kV/m at 50 m.

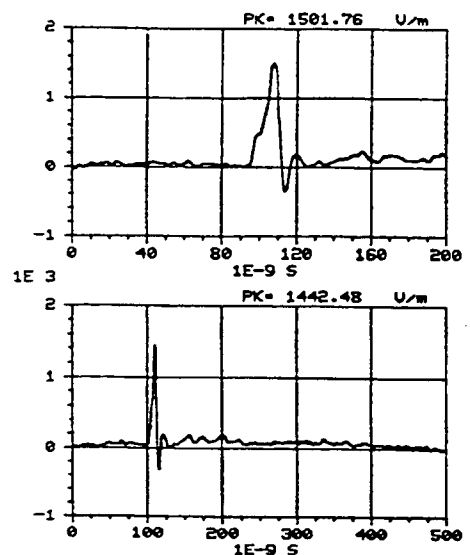


Figure C-48. X component of the electric field measured at location 0/50/1 using sensor E304-C. REPS pulse 47 generating 6.1 kV/m at 50 m.

Appendix C, 1-m data

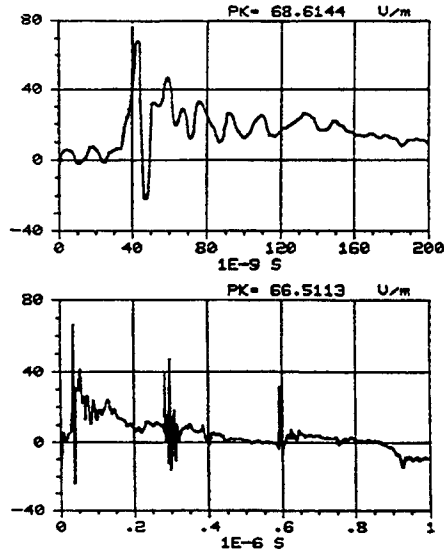


Figure C-49. -Y component of the electric field measured at location 0/50/1 using sensor E201-C. REPS pulse 49 generating 6.3 kV/m at 50 m.

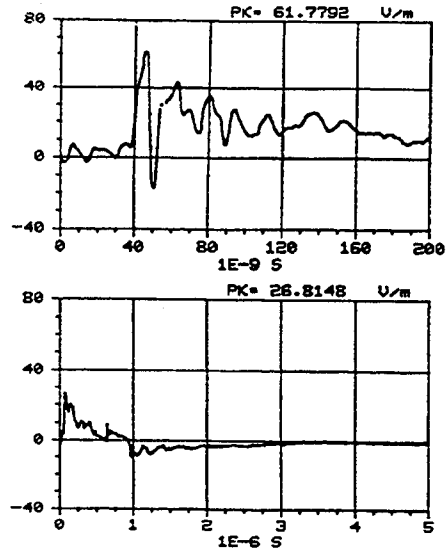


Figure C-50. -Y component of the electric field measured at location 0/50/1 using sensor E201-C. REPS pulse 52 generating 6 kV/m at 50 m.

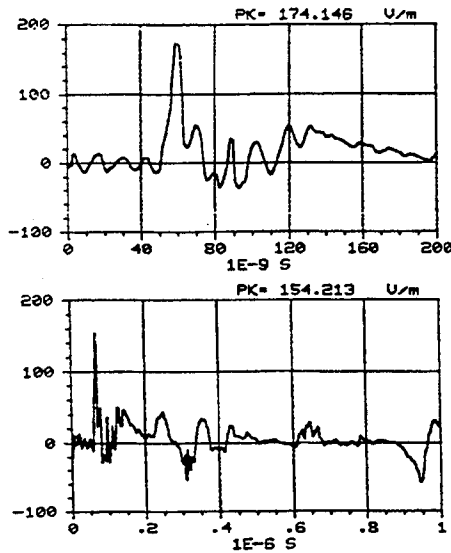


Figure C-51. Z component of the electric field measured at location 0/50/1 using sensor E201-C. REPS pulse 53 generating 6.1 kV/m at 50 m.

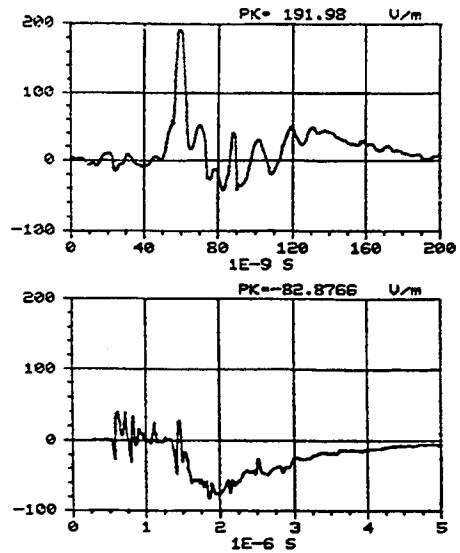


Figure C-52. Z component of the electric field measured at location 0/50/1 using sensor E201-C. REPS pulse 54 generating 6.4 kV/m at 50 m.

Appendix C, 1-m data

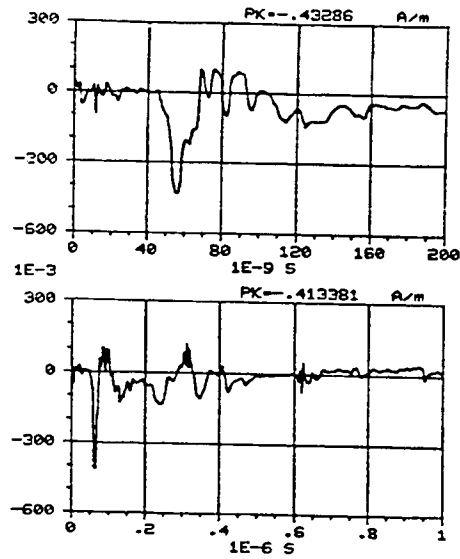


Figure C-53. X component of the magnetic field measured at location 0/50/1 using sensor H104-C. REPS pulse 17 generating 6.6 kV/m at 50 m.

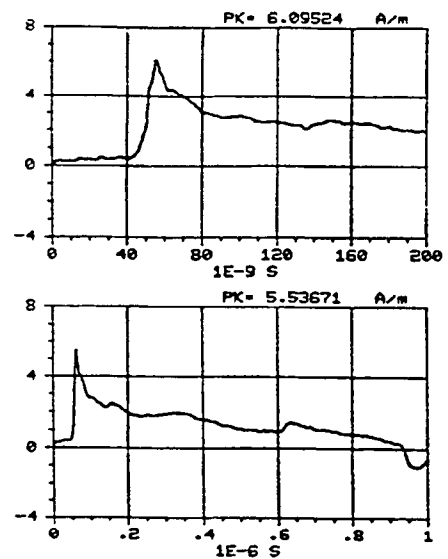


Figure C-54. Y component of the magnetic field measured at location 0/50/1 using sensor H104-C. REPS pulse 13 generating 6.3 kV/m at 50 m.

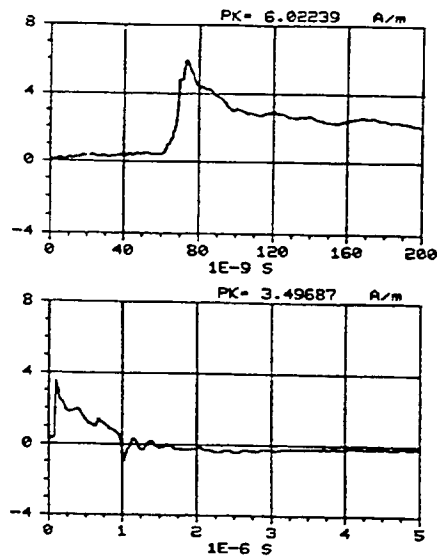


Figure C-55. Y component of the magnetic field measured at location 0/50/1 using sensor H104-C. REPS pulse 15 generating 6.3 kV/m at 50 m.

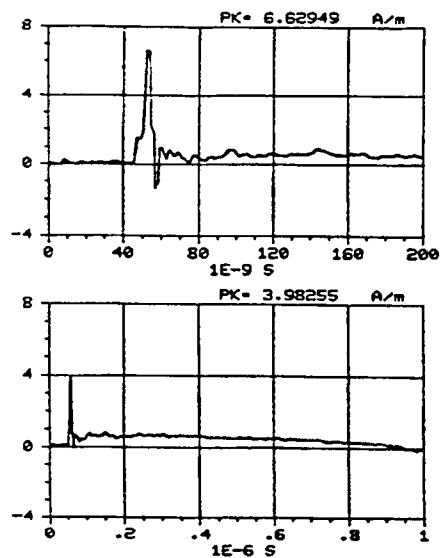


Figure C-56. Z component of the magnetic field measured at location 0/50/1 using sensor H104-C. REPS pulse 16 generating 6.6 kV/m at 50 m.

Appendix C, 1-m data

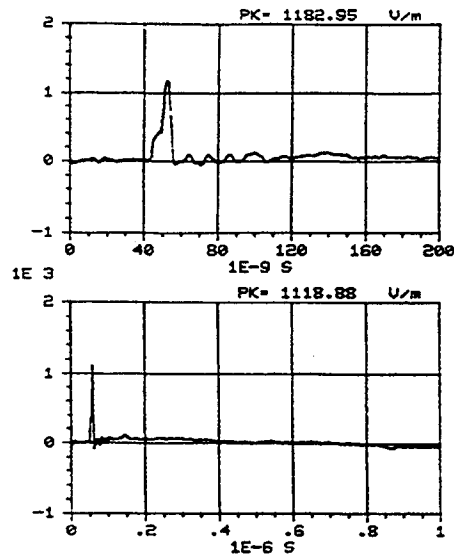


Figure C-57. X component of the electric field measured at location -25/50/1 using sensor E304-C. REPS pulse 83 generating 6.1 kV/m at 50 m.

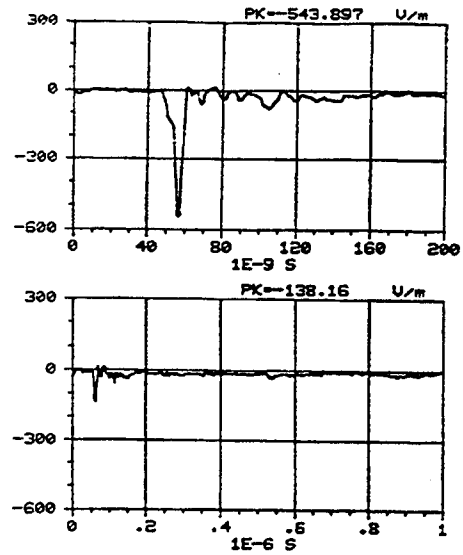


Figure C-58. -Y component of the electric field measured at location -25/50/1 using sensor E304-C. REPS pulse 86 generating 6.3 kV/m at 50 m.

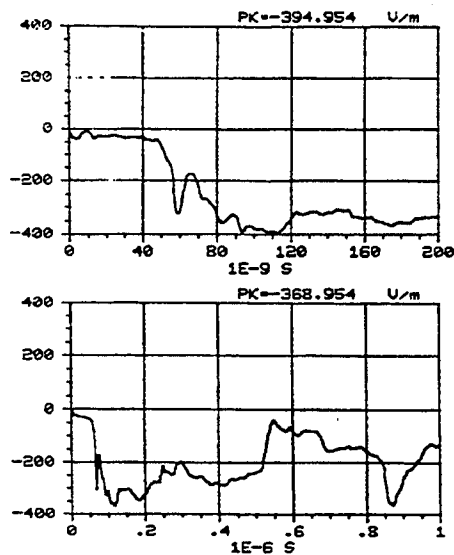


Figure C-59. Z component of the electric field measured at location -25/50/1 using sensor E304-C. REPS pulse 84 generating 6.2 kV/m at 50 m.

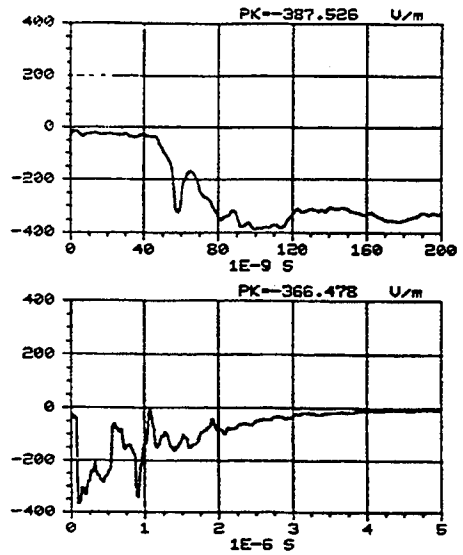


Figure C-60. Z component of the electric field measured at location -25/50/1 using sensor E304-C. REPS pulse 85 generating 6.3 kV/m at 50 m.

Appendix C, 1-m data

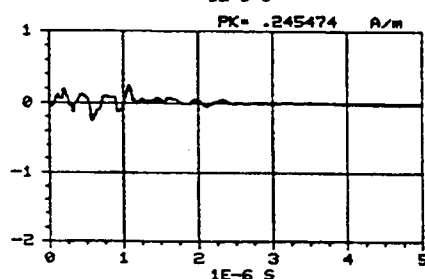
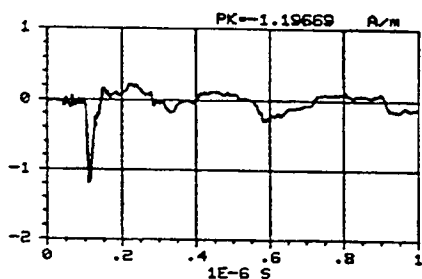
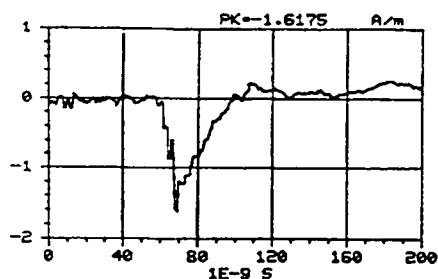
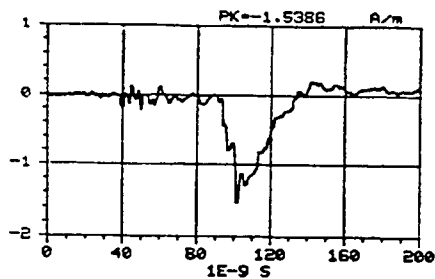


Figure C-61. X component of the magnetic field measured at location -25/50/1 using sensor H104-C. REPS pulse 76 generating 6.3 kV/m at 50 m.

Figure C-62. X component of the magnetic field measured at location -25/50/1 using sensor H104-C. REPS pulse 75 generating 6.3 kV/m at 50 m.

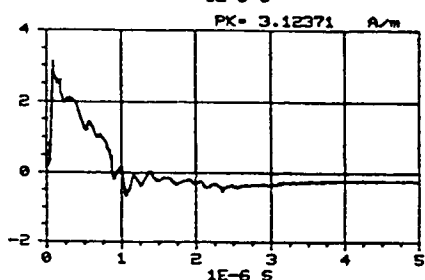
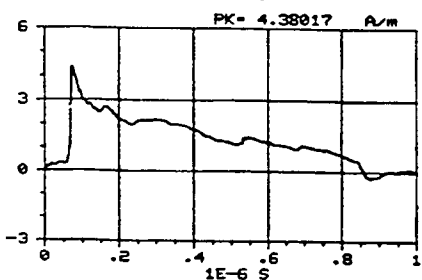
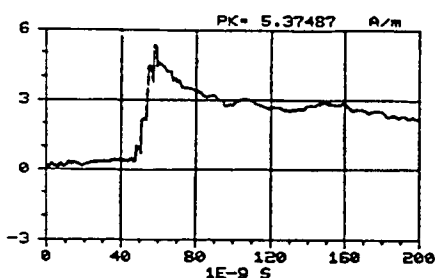
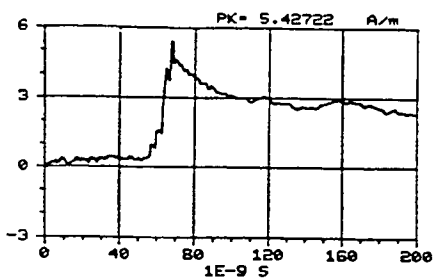


Figure C-63. Y component of the magnetic field measured at location -25/50/1 using sensor H104-C. REPS pulse 73 generating 6.3 kV/m at 50 m.

Figure C-64. Y component of the magnetic field measured at location -25/50/1 using sensor H104-C. REPS pulse 74 generating 6.3 kV/m at 50 m.

Appendix C, 1-m data

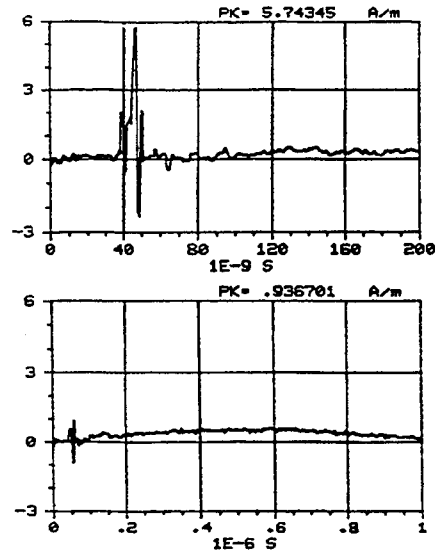


Figure C-65. Z component of the magnetic field measured at location -25/50/1 using sensor H104-C. REPS pulse 77 generating 6.2 kV/m at 50 m.

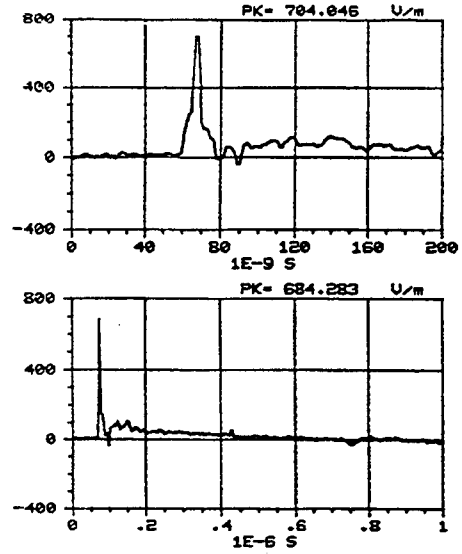


Figure C-66. X component of the electric field measured at location -50/50/1 using sensor E304-C. REPS pulse 92 generating 6.6 kV/m at 50 m.

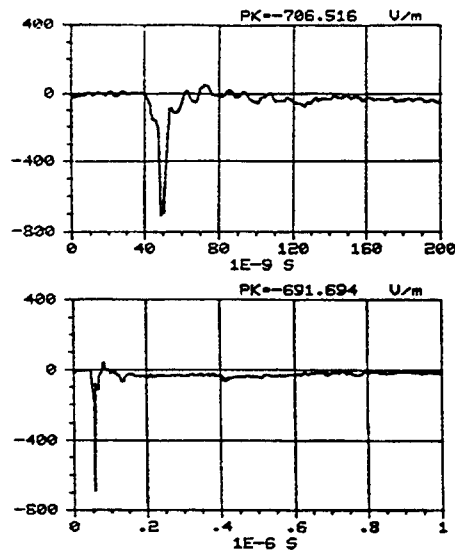


Figure C-67. -Y component of the electric field measured at location -50/50/1 using sensor E304-C. REPS pulse 95 generating 6.5 kV/m at 50 m.

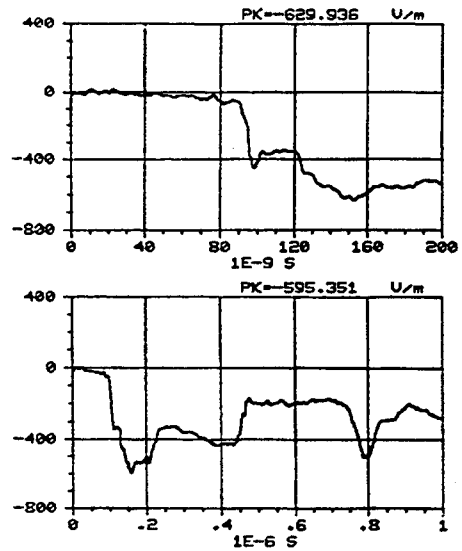


Figure C-68. Z component of the electric field measured at location -50/50/1 using sensor E304-C. REPS pulse 93 generating 6.3 kV/m at 50 m.

Appendix C, 1-m data

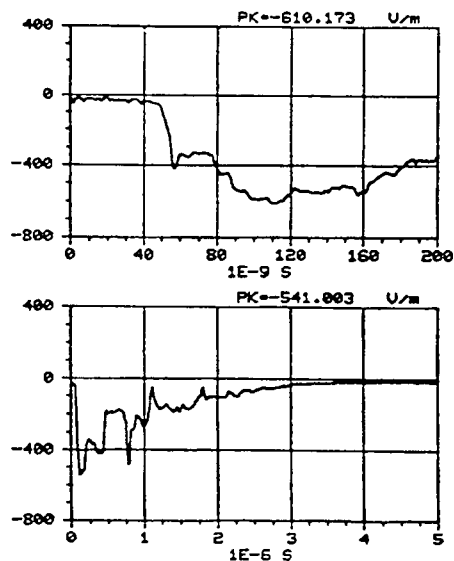


Figure C-69. Z component of the electric field measured at location -50/50/1 using sensor E304-C. REPS pulse 94 generating 6.3 kV/m at 50 m.

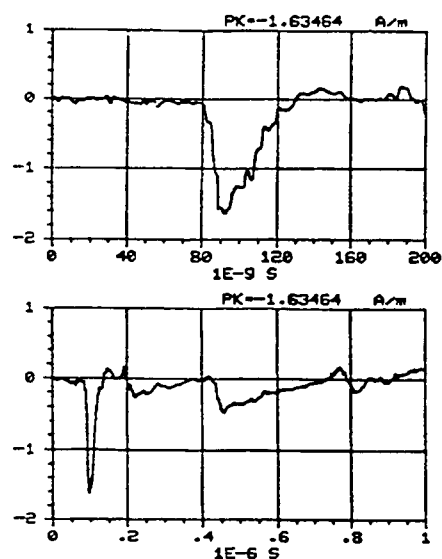


Figure C-70. X component of the magnetic field measured at location -50/50/1 using sensor H104-C. REPS pulse 104 generating 6.5 kV/m at 50 m.

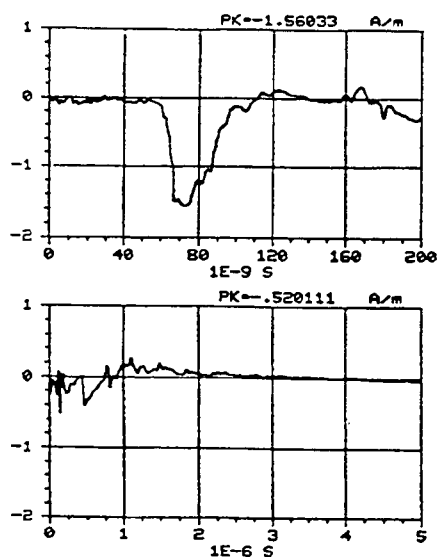


Figure C-71. X component of the magnetic field measured at location -50/50/1 using sensor H104-C. REPS pulse 105 generating 6.5 kV/m at 50 m.

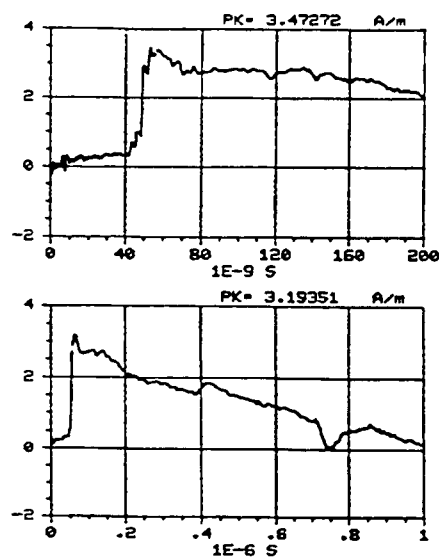


Figure C-72. Y component of the magnetic field measured at location -50/50/1 using sensor H104-C. REPS pulse 101 generating 6.4 kV/m at 50 m.

Appendix C, 1-m data

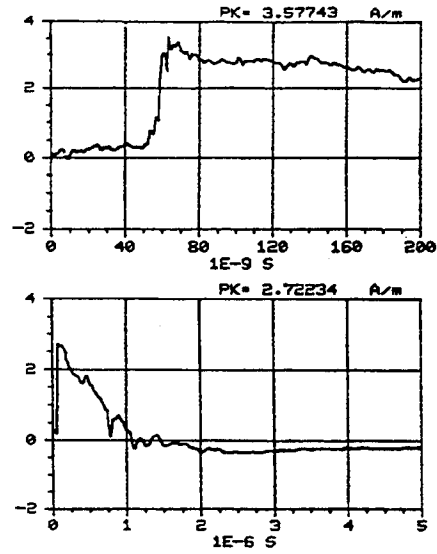


Figure C-73. Y component of the magnetic field measured at location -50/50/1 using sensor H104-C. REPS pulse 103 generating 6.3 kV/m at 50 m.

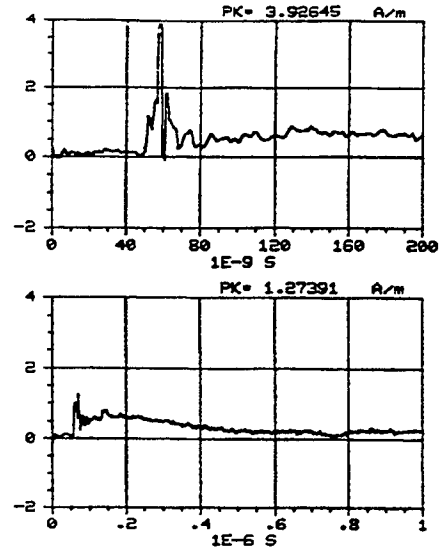


Figure C-74. Z component of the magnetic field measured at location -50/50/1 using sensor H104-C. REPS pulse 106 generating 6.2 kV/m at 50 m.

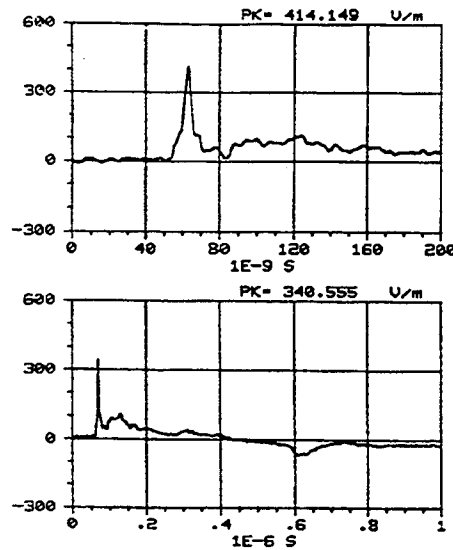


Figure C-75. X component of the electric field measured at location -75/50/1 using sensor E201-C. REPS pulse 161 generating 6.1 kV/m at 50 m.

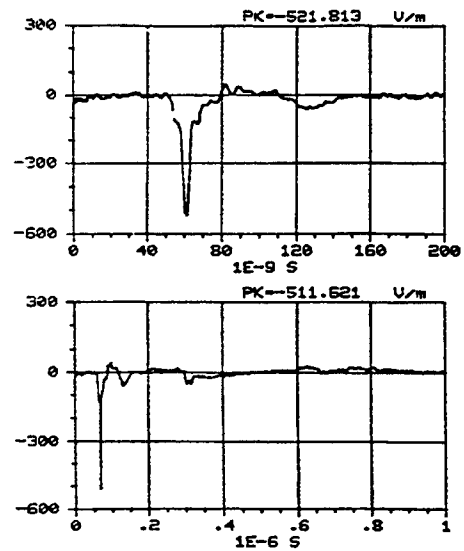


Figure C-76. -Y component of the electric field measured at location -75/50/1 using sensor E201-C. REPS pulse 164 generating 6 kV/m at 50 m.

Appendix C, 1-m data

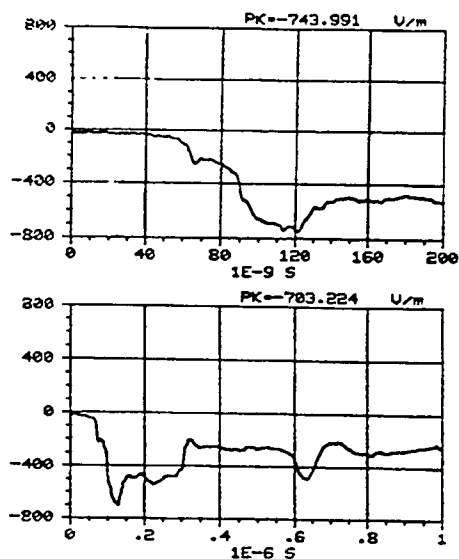


Figure C-77. Z component of the electric field measured at location -75/50/1 using sensor E201-C. REPS pulse 162 generating 6 kV/m at 50 m.

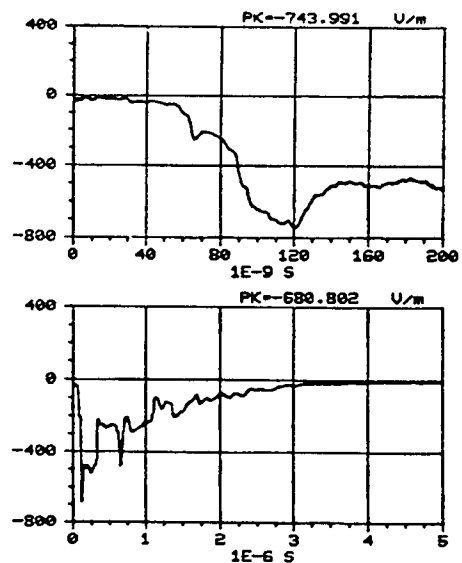


Figure C-78. Z component of the electric field measured at location -75/50/1 using sensor E201-C. REPS pulse 163 generating 6.1 kV/m at 50 m.

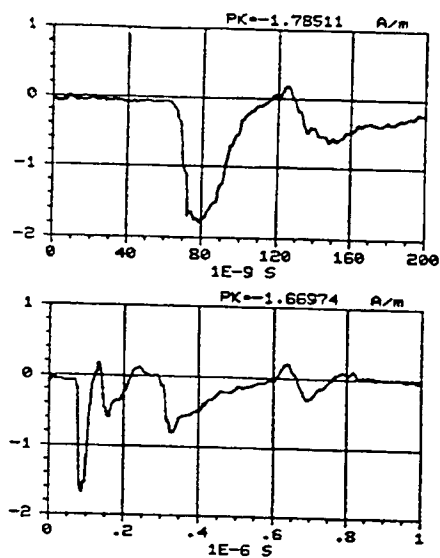


Figure C-79. X component of the magnetic field measured at location -75/50/1 using sensor H104-C. REPS pulse 159 generating 6.4 kV/m at 50 m.

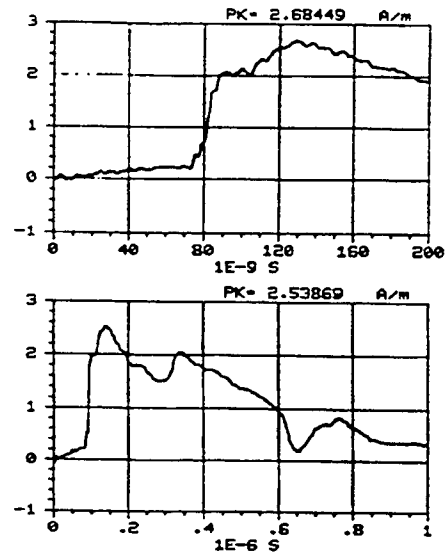


Figure C-80. Y component of the magnetic field measured at location -75/50/1 using sensor H104-C. REPS pulse 155 generating 6.4 kV/m at 50 m.

Appendix C, 1-m data

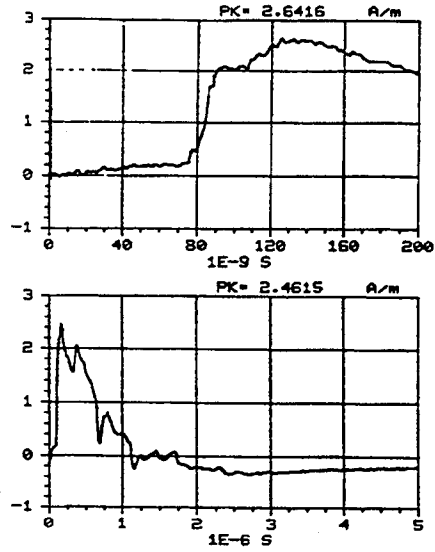


Figure C-81. Y component of the magnetic field measured at location -75/50/1 using sensor H104-C. REPS pulse 156 generating 6.3 kV/m at 50 m.

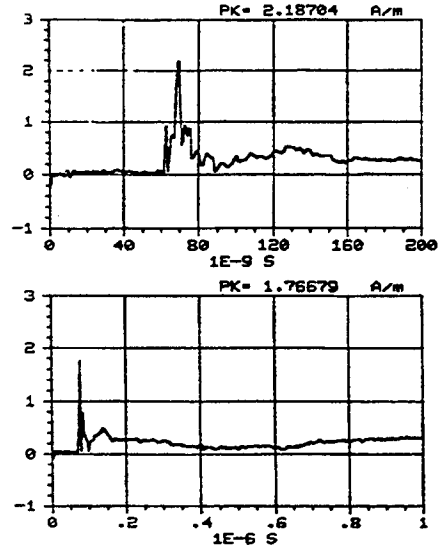


Figure C-82. Z component of the magnetic field measured at location -75/50/1 using sensor H104-C. REPS pulse 158 generating 6.3 kV/m at 50 m.

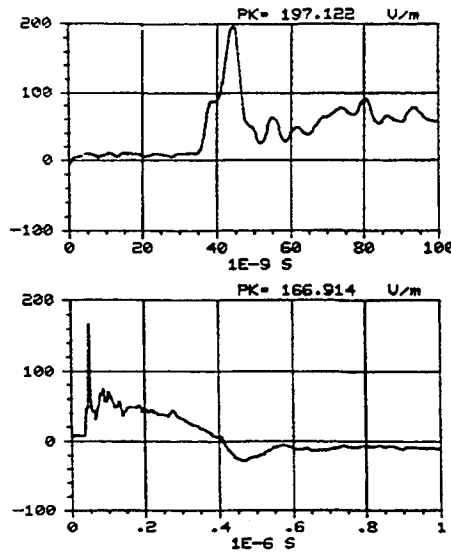


Figure C-83. X component of the electric field measured at location -100/50/1 using sensor E201-C. REPS pulse 185 generating 6.5 kV/m at 50 m.

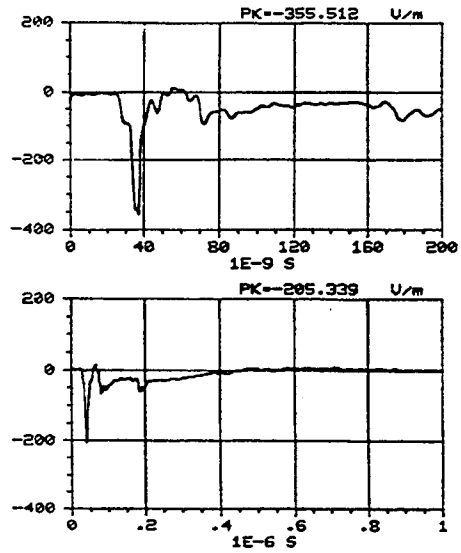


Figure C-84. -Y component of the electric field measured at location -100/50/1 using sensor E201-C. REPS pulse 190 generating 6.3 kV/m at 50 m.

Appendix C, 1-m data

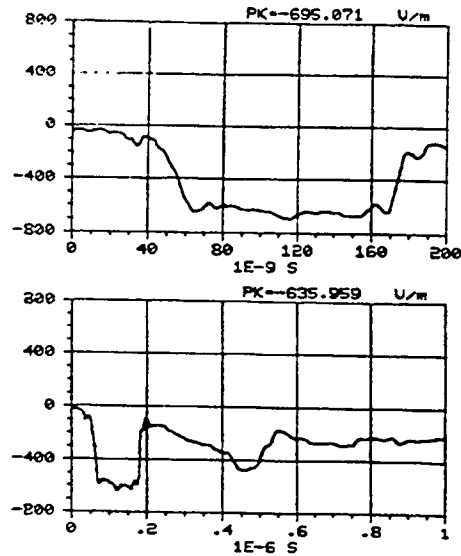


Figure C-85. Z component of the electric field measured at location -100/50/1 using sensor E201-C. REPS pulse 186 generating 6.3 kV/m at 50 m.

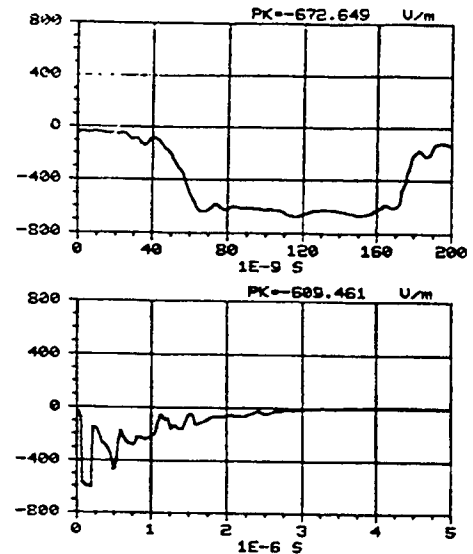


Figure C-86. Z component of the electric field measured at location -100/50/1 using sensor E201-C. REPS pulse 187 generating 6.1 kV/m at 50 m.

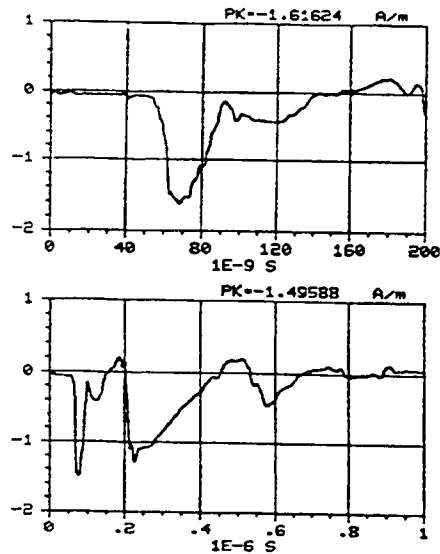


Figure C-87. X component of the magnetic field measured at location -100/50/1 using sensor H104-C. REPS pulse 181 generating 6.2 kV/m at 50 m.

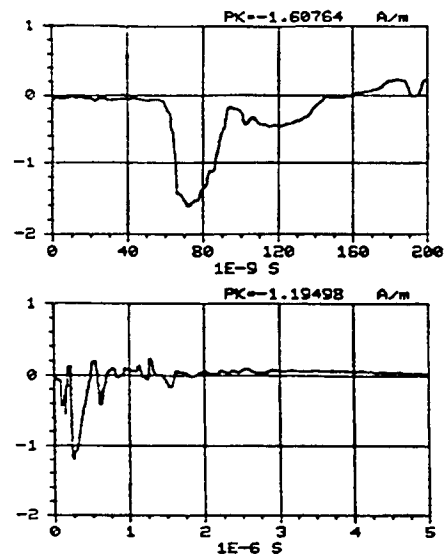


Figure C-88. X component of the magnetic field measured at location -100/50/1 using sensor H104-C. REPS pulse 182 generating 6.3 kV/m at 50 m.

Appendix C, 1-m data

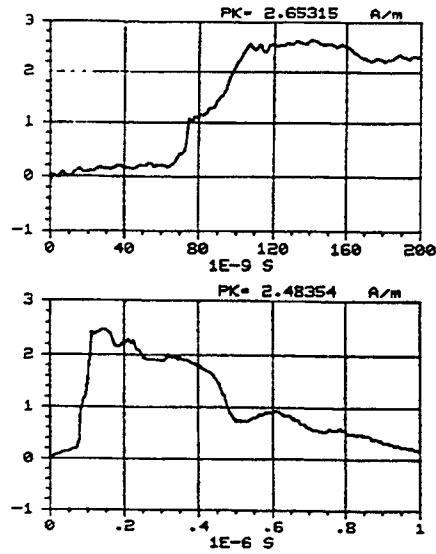


Figure C-89. Y component of the magnetic field measured at location -100/50/1 using sensor H104-C. REPS pulse 179 generating 6.2 kV/m at 50 m.

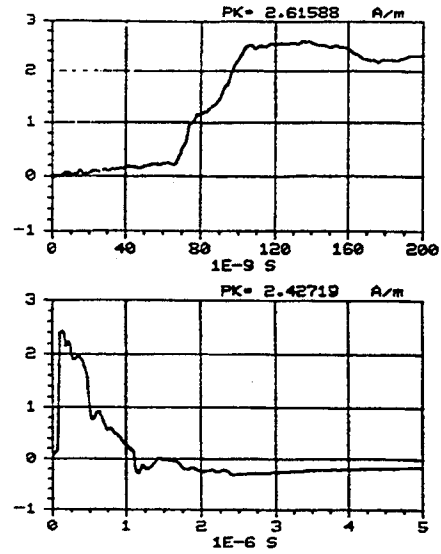


Figure C-90. Y component of the magnetic field measured at location -100/50/1 using sensor H104-C. REPS pulse 180 generating 6.2 kV/m at 50 m.

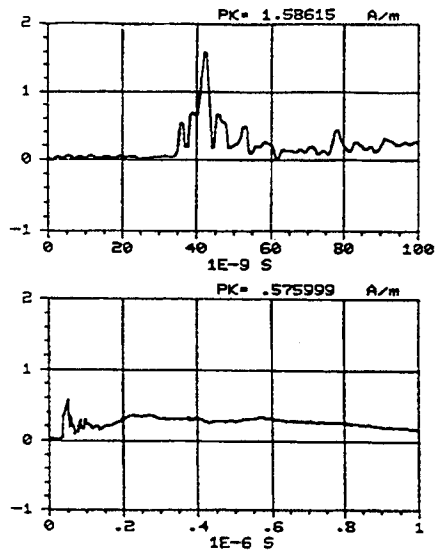


Figure C-91. Z component of the magnetic field measured at location -100/50/1 using sensor H104-C. REPS pulse 183 generating 6.1 kV/m at 50 m.

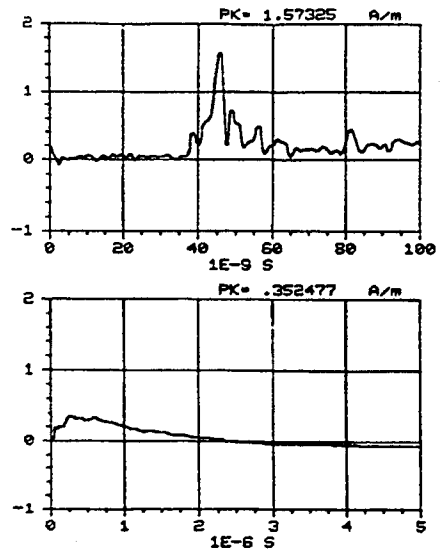


Figure C-92. Z component of the magnetic field measured at location -100/50/1 using sensor H104-C. REPS pulse 184 generating 6.1 kV/m at 50 m.

Appendix C, 1-m data

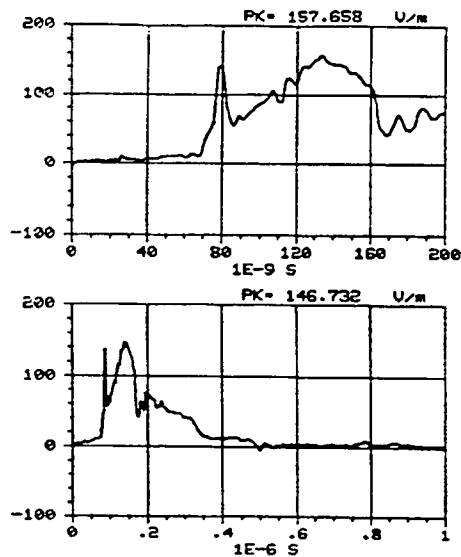


Figure C-93. X component of the electric field measured at location -125/50/1 using sensor E201-C. REPS pulse 204 generating 6.5 kV/m at 50 m.

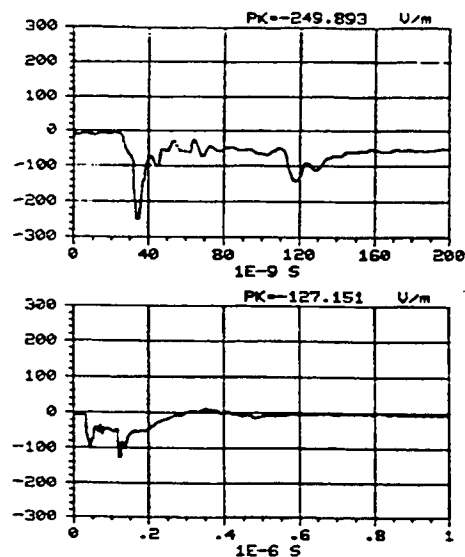


Figure C-94. -Y component of the electric field measured at location -125/50/1 using sensor E201-C. REPS pulse 205 generating 6.4 kV/m at 50 m.

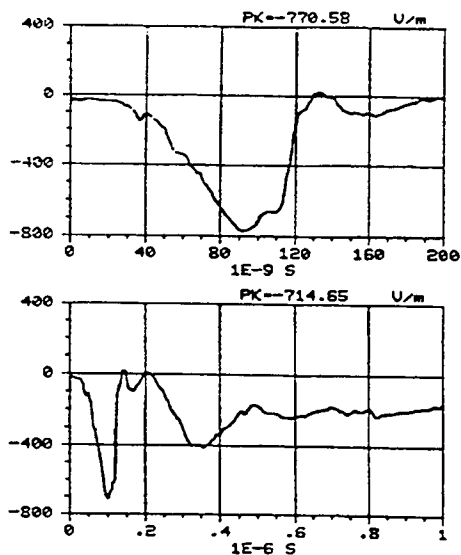


Figure C-95. Z component of the electric field measured at location -125/50/1 using sensor E201-C. REPS pulse 206 generating 6.4 kV/m at 50 m.

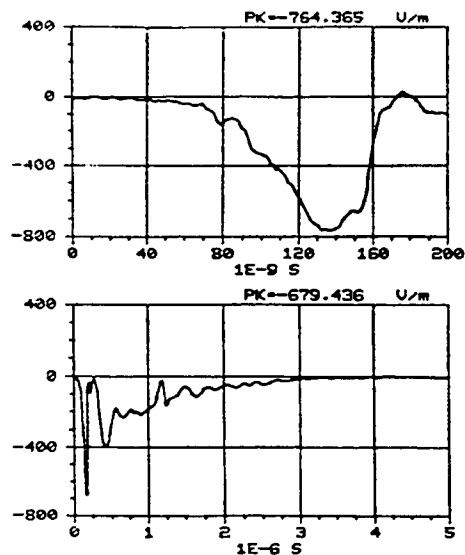


Figure C-96. Z component of the electric field measured at location -125/50/1 using sensor E201-C. REPS pulse 208 generating 6.3 kV/m at 50 m.

Appendix C, 1-m data

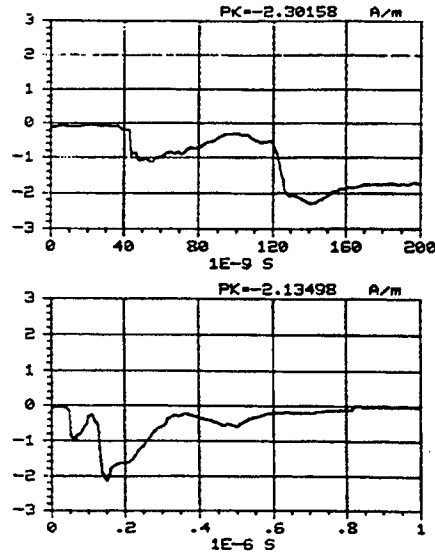


Figure C-97. X component of the magnetic field measured at location -125/50/1 using sensor H104-C. REPS pulse 209 generating 6.6 kV/m at 50 m.

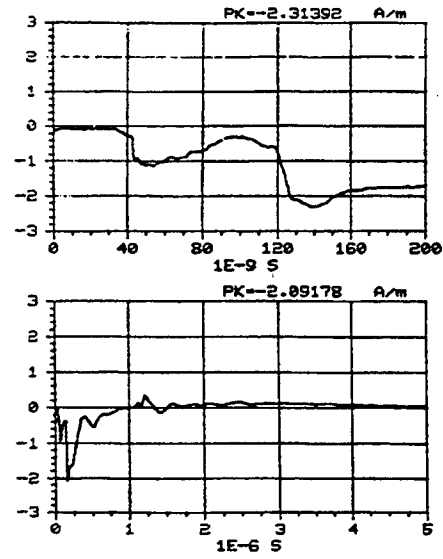


Figure C-98. X component of the magnetic field measured at location -125/50/1 using sensor H104-C. REPS pulse 210 generating 6.4 kV/m at 50 m.

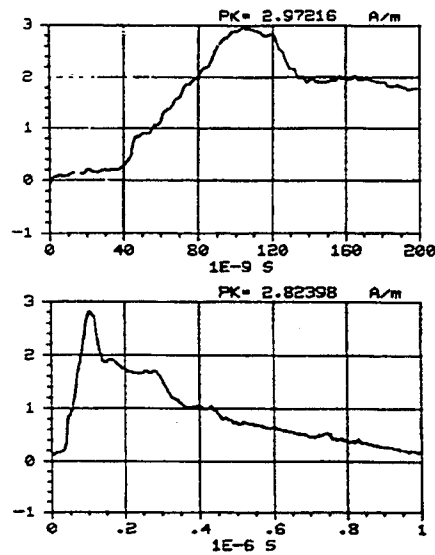


Figure C-99. Y component of the magnetic field measured at location -125/50/1 using sensor H104-C. REPS pulse 214 generating 6.5 kV/m at 50 m.

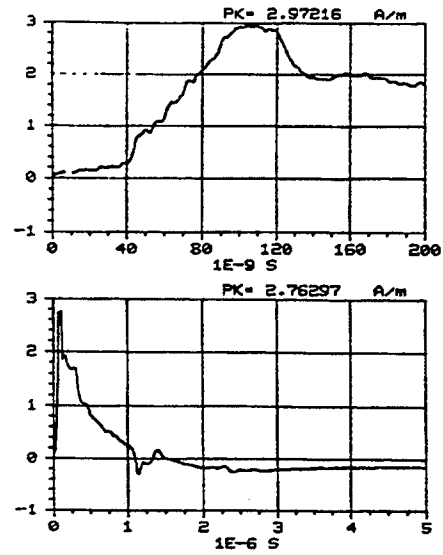


Figure C-100. Y component of the magnetic field measured at location -125/50/1 using sensor H104-C. REPS pulse 215 generating 6.4 kV/m at 50 m.

Appendix C, 1-m data

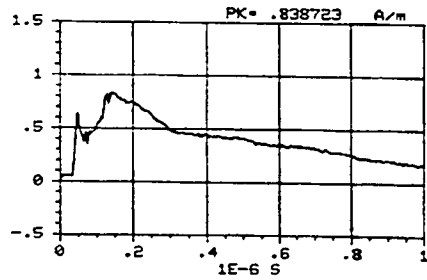
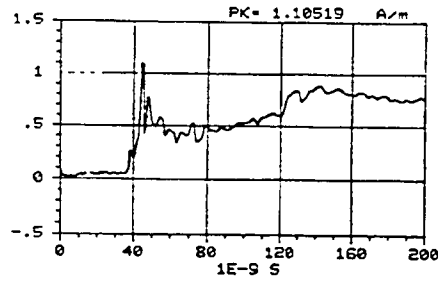


Figure C-101. Z component of the magnetic field measured at location -125/50/1 using sensor H104-C. REPS pulse 212 generating 6.4 kV/m at 50 m.

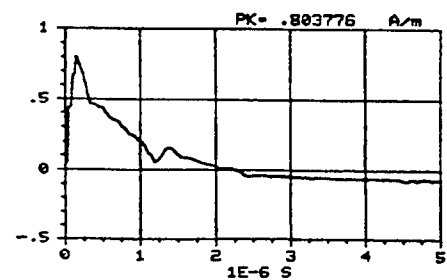
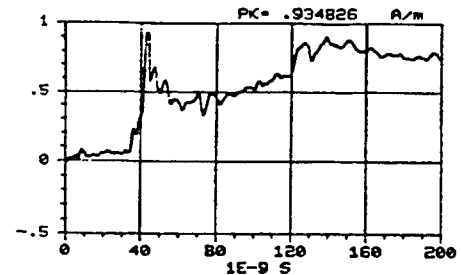


Figure C-102. Z component of the magnetic field measured at location -125/50/1 using sensor H104-C. REPS pulse 213 generating 6.2 kV/m at 50 m.

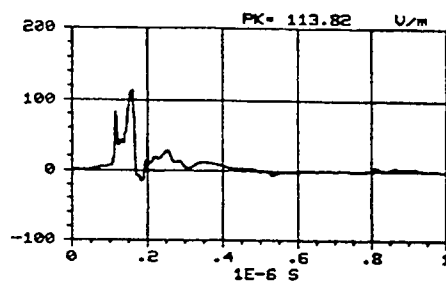
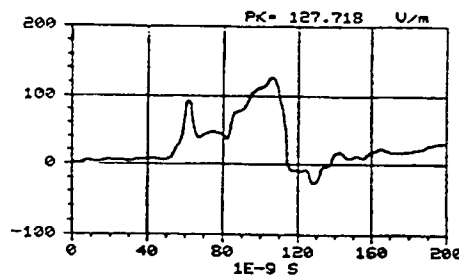


Figure C-103. X component of the electric field measured at location -150/50/1 using sensor E201-C. REPS pulse 340 generating 6.4 kV/m at 50 m.

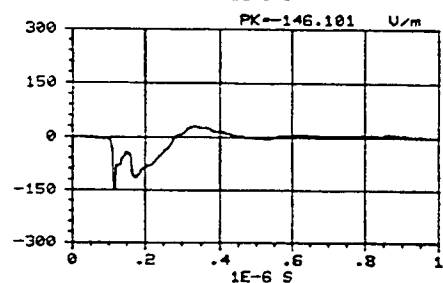
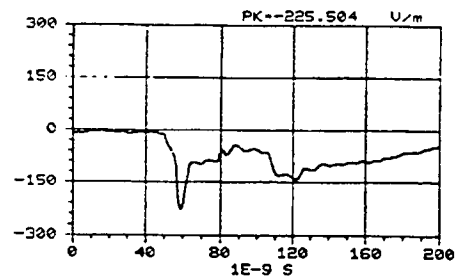


Figure C-104. -Y component of the electric field measured at location -150/50/1 using sensor E201-C. REPS pulse 343 generating 6.2 kV/m at 50 m.

Appendix C, 1-m data

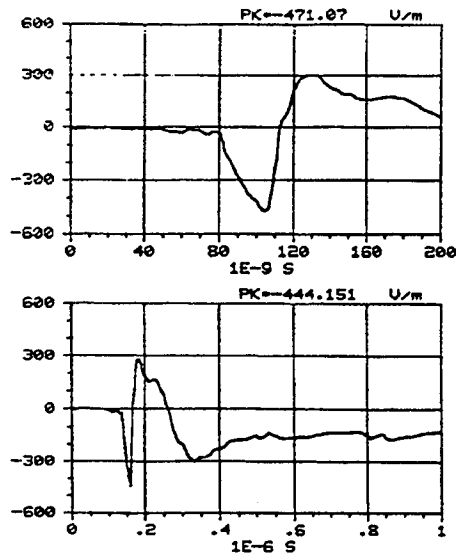


Figure C-105. Z component of the electric field measured at location -150/50/1 using sensor E201-C. REPS pulse 341 generating 6.4 kV/m at 50 m.

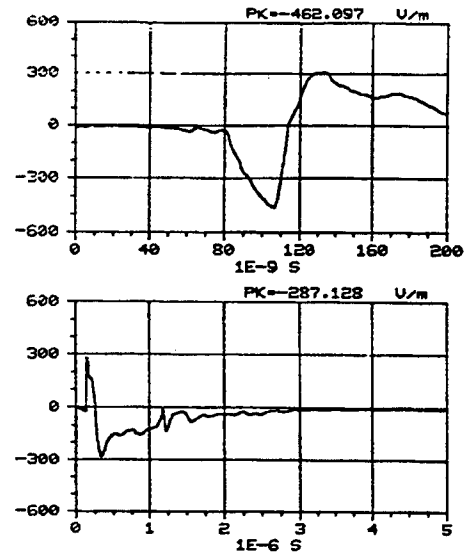


Figure C-106. Z component of the electric field measured at location -150/50/1 using sensor E201-C. REPS pulse 342 generating 6.2 kV/m at 50 m.

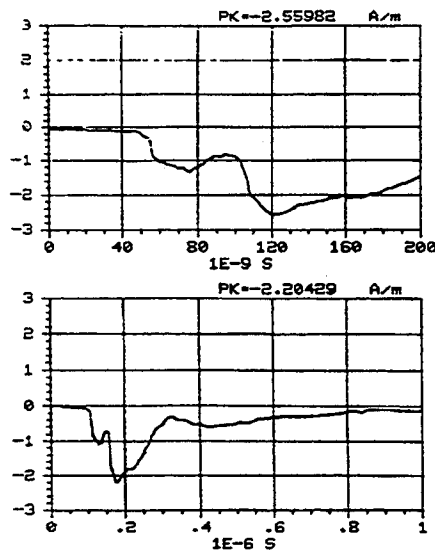


Figure C-107. X component of the magnetic field measured at location -150/50/1 using sensor H104-C. REPS pulse 344 generating 6.3 kV/m at 50 m.

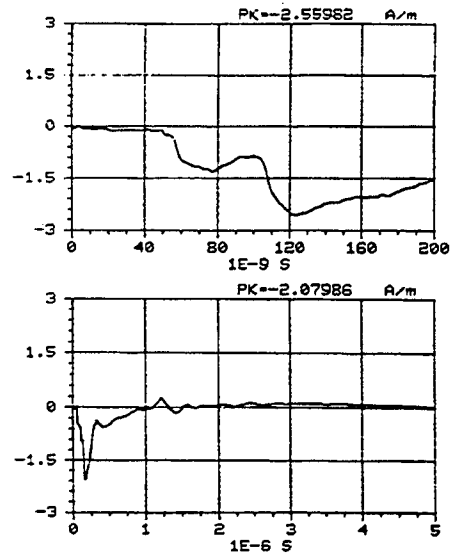


Figure C-108. X component of the magnetic field measured at location -150/50/1 using sensor H104-C. REPS pulse 345 generating 6.1 kV/m at 50 m.

Appendix C, 1-m data

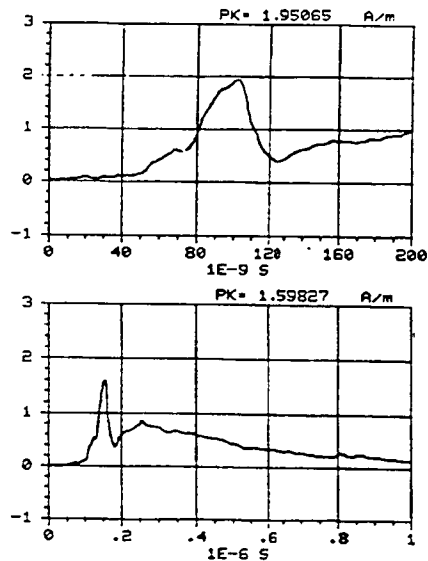


Figure C-109. Y component of the magnetic field measured at location -150/50/1 using sensor H104-C. REPS pulse 346 generating 6.1 kV/m at 50 m.

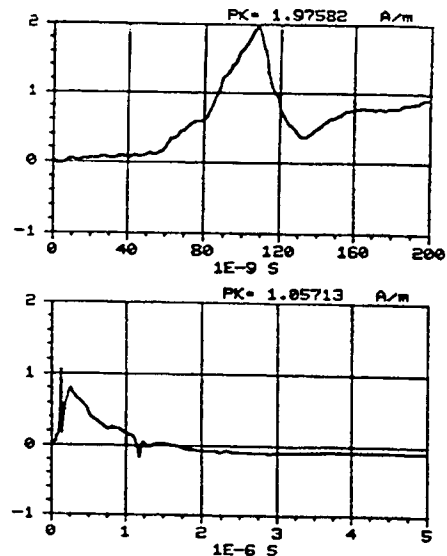


Figure C-110. Y component of the magnetic field measured at location -150/50/1 using sensor H104-C. REPS pulse 347 generating 6.1 kV/m at 50 m.

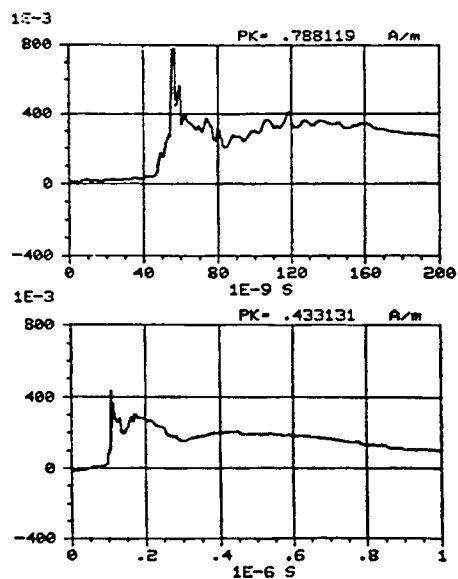


Figure C-111. Z component of the magnetic field measured at location -150/50/1 using sensor H104-C. REPS pulse 350 generating 6.3 kV/m at 50 m.

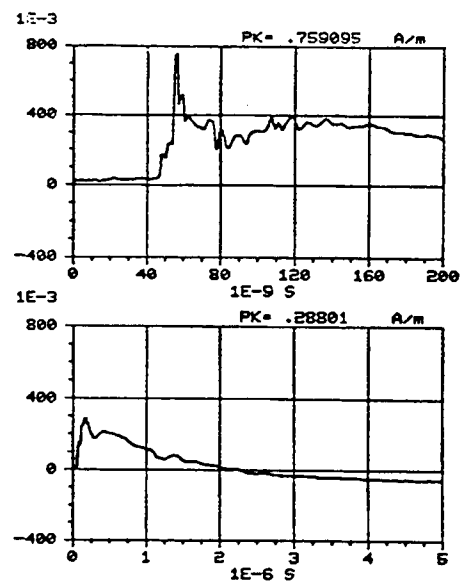


Figure C-112. Z component of the magnetic field measured at location -150/50/1 using sensor H104-C. REPS pulse 351 generating 6.2 kV/m at 50 m.

Appendix C, 1-m data

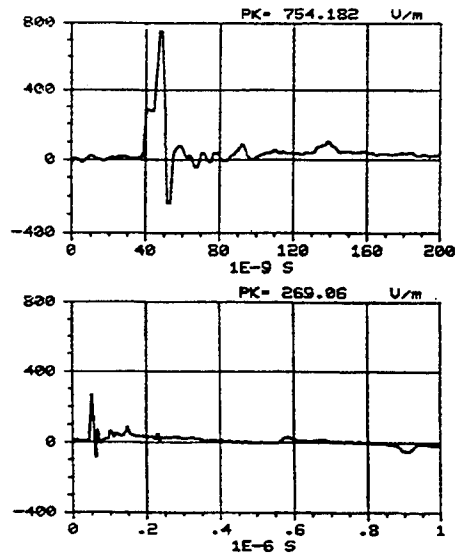


Figure C-113. X component of the electric field measured at location 0/75/1 using sensor E201-C. REPS pulse 141 generating 6.4 kV/m at 50 m.

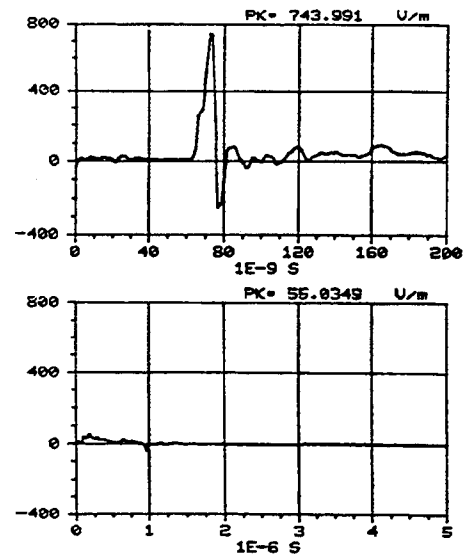


Figure C-114. X component of the electric field measured at location 0/75/1 using sensor E201-C. REPS pulse 142 generating 6.4 kV/m at 50 m.

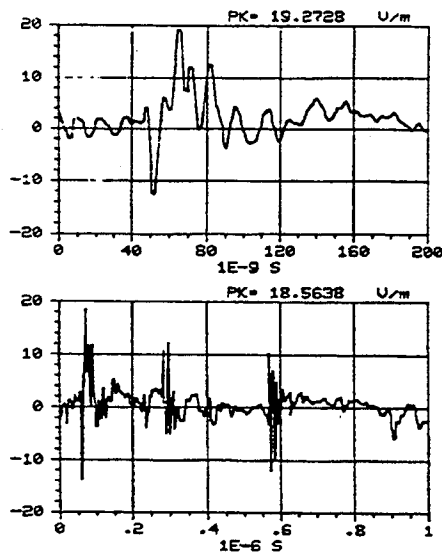


Figure C-115. -Y component of the electric field measured at location 0/75/1 using sensor E201-C. REPS pulse 140 generating 6.3 kV/m at 50 m.

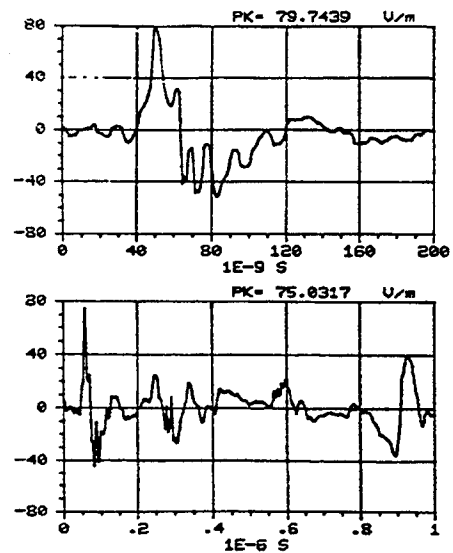


Figure C-116. Z component of the electric field measured at location 0/75/1 using sensor E201-C. REPS pulse 137 generating 6.3 kV/m at 50 m.

Appendix C, 1-m data

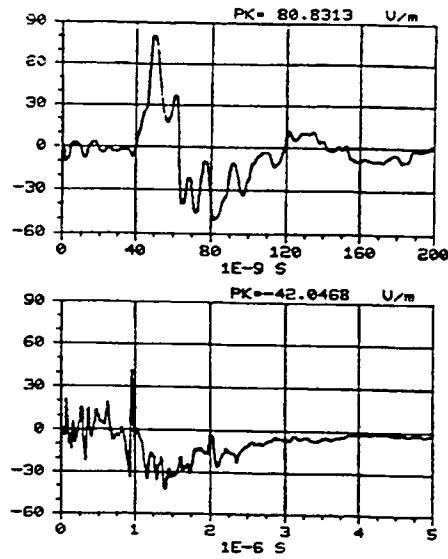


Figure C-117. Z component of the electric field measured at location 0/75/1 using sensor E201-C. REPS pulse 138 generating 6.3 kV/m at 50 m.

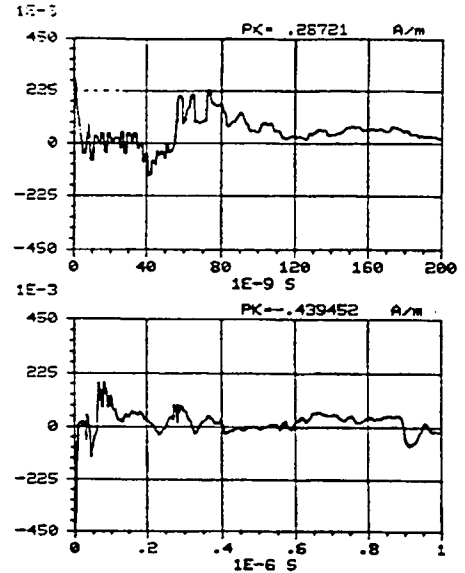


Figure C-118. X component of the magnetic field measured at location 0/75/1 using sensor H104-C. REPS pulse 135 generating 6.2 kV/m at 50 m.

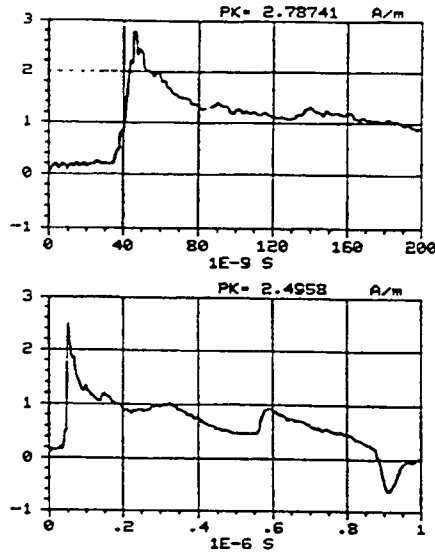


Figure C-119. Y component of the magnetic field measured at location 0/75/1 using sensor H104-C. REPS pulse 131 generating 6.3 kV/m at 50 m.

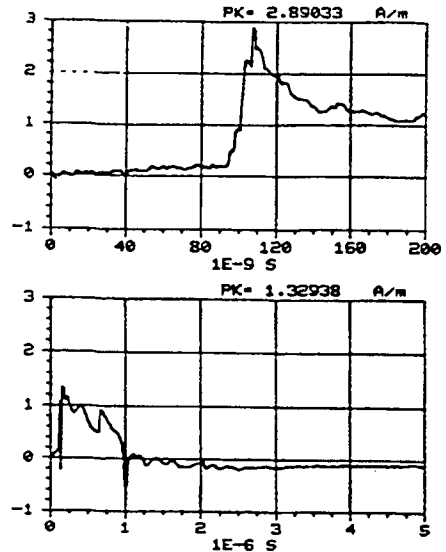


Figure C-120. Y component of the magnetic field measured at location 0/75/1 using sensor H104-C. REPS pulse 133 generating 6.2 kV/m at 50 m.

Appendix C, 1-m data

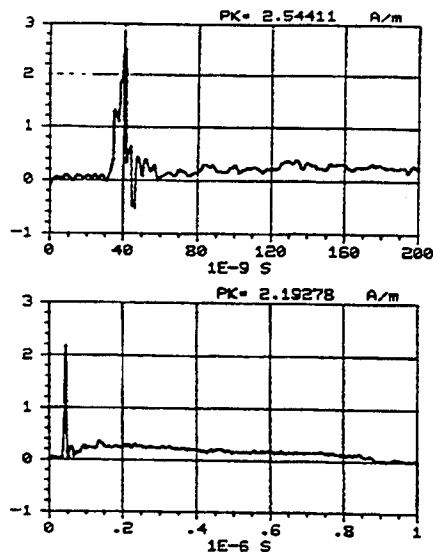


Figure C-121. Z component of the magnetic field measured at location 0/75/1 using sensor H104-C. REPS pulse 136 generating 6.2 kV/m at 50 m.

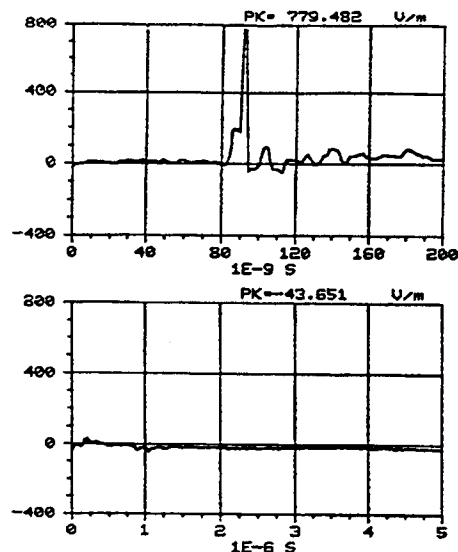


Figure C-122. X component of the electric field measured at location -25/75/1 using sensor E201-C. REPS pulse 124 generating 6.6 kV/m at 50 m.

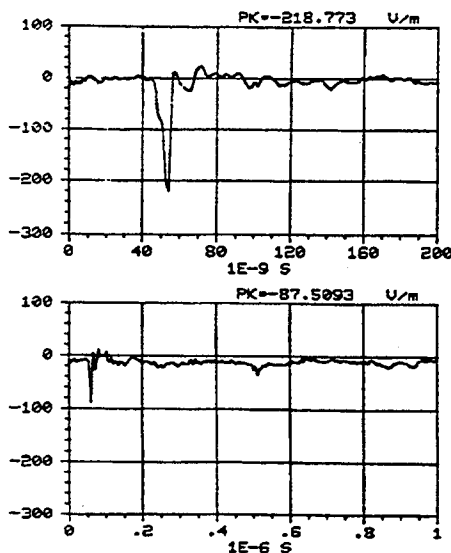


Figure C-123. -Y component of the electric field measured at location -25/75/1 using sensor E201-C. REPS pulse 121 generating 6.3 kV/m at 50 m.

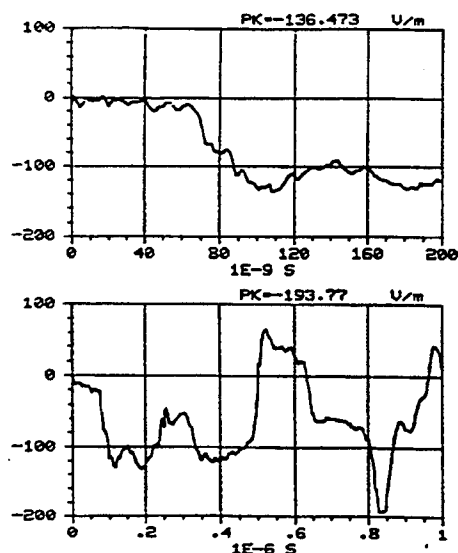


Figure C-124. Z component of the electric field measured at location -25/75/1 using sensor E201-C. REPS pulse 122 generating 6.3 kV/m at 50 m.

Appendix C, 1-m data

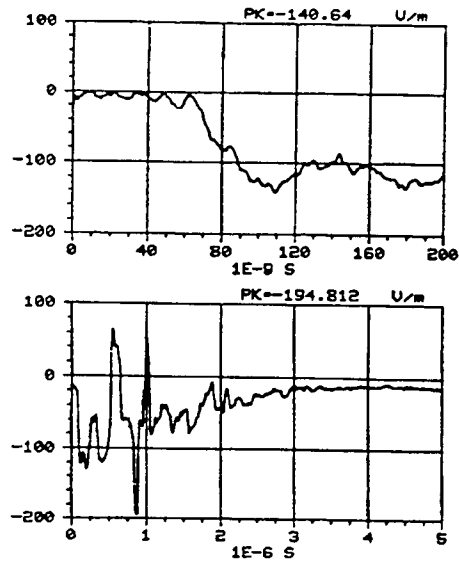


Figure C-125. Z component of the electric field measured at location -25/75/1 using sensor E201-C. REPS pulse 123 generating 6.4 kV/m at 50 m.

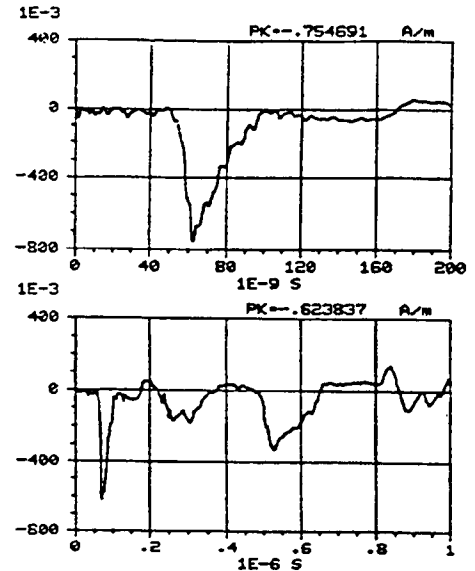


Figure C-126. X component of the magnetic field measured at location -25/75/1 using sensor H104-C. REPS pulse 128 generating 6.3 kV/m at 50 m.

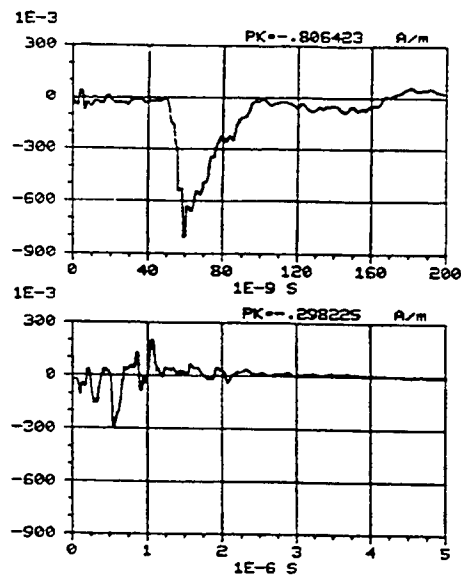


Figure C-127. X component of the magnetic field measured at location -25/75/1 using sensor H104-C. REPS pulse 129 generating 6.4 kV/m at 50 m.

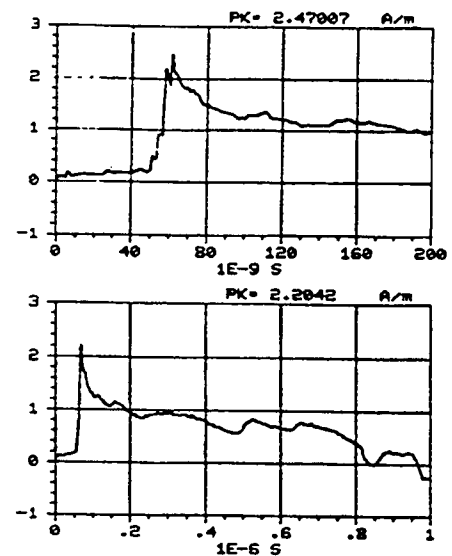


Figure C-128. Y component of the magnetic field measured at location -25/75/1 using sensor H104-C. REPS pulse 126 generating 6.3 kV/m at 50 m.

Appendix C, 1-m data

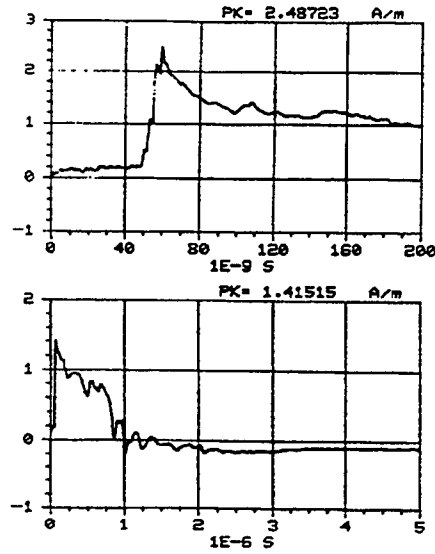


Figure C-129. Y component of the magnetic field measured at location -25/75/1 using sensor H104-C. REPS pulse 127 generating 6.2 kV/m at 50 m.

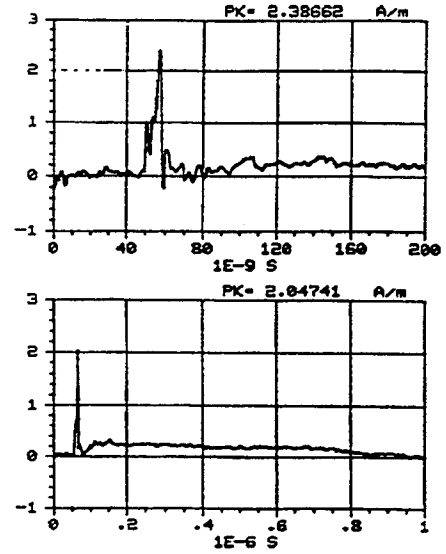


Figure C-130. Z component of the magnetic field measured at location -25/75/1 using sensor H104-C. REPS pulse 130 generating 6 kV/m at 50 m.

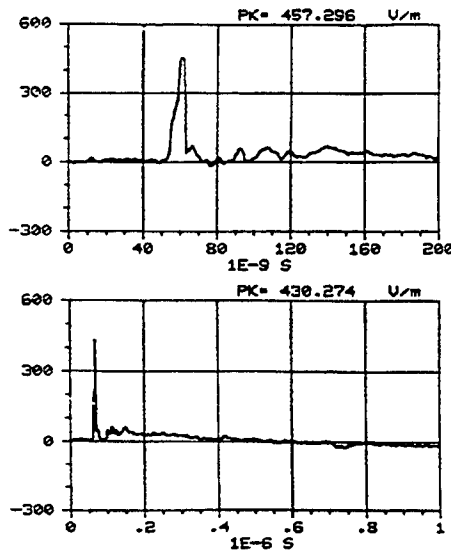


Figure C-131. X component of the electric field measured at location -50/75/1 using sensor E201-C. REPS pulse 117 generating 6.3 kV/m at 50 m.

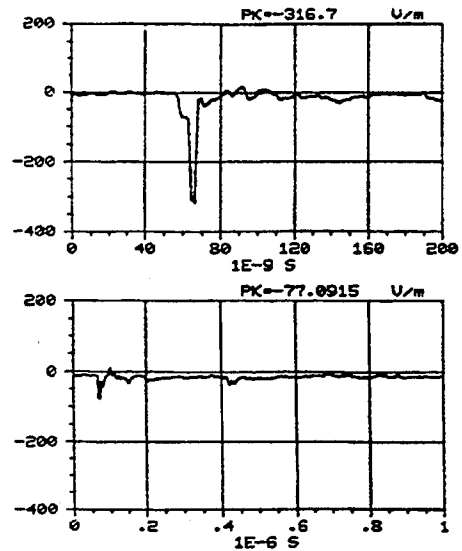


Figure C-132. -Y component of the electric field measured at location -50/75/1 using sensor E201-C. REPS pulse 120 generating 6.5 kV/m at 50 m.

Appendix C, 1-m data

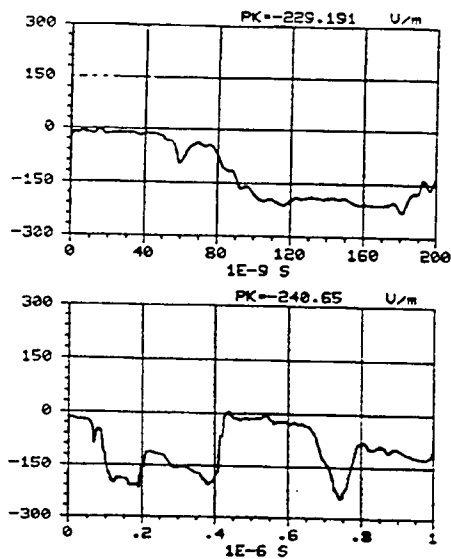


Figure C-133. Z component of the electric field measured at location -50/75/1 using sensor E201-C. REPS pulse 118 generating 6.3 kV/m at 50 m.

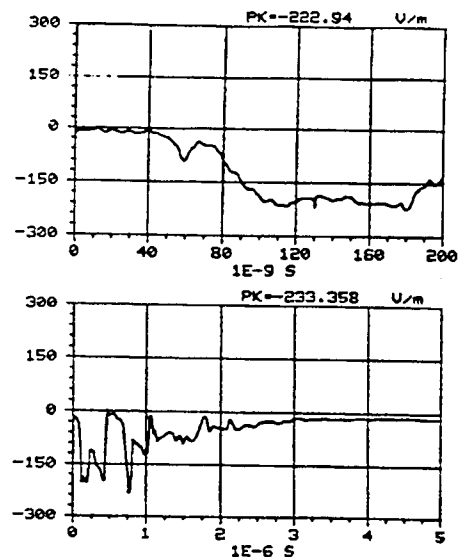


Figure C-134. Z component of the electric field measured at location -50/75/1 using sensor E201-C. REPS pulse 119 generating 6.3 kV/m at 50 m.

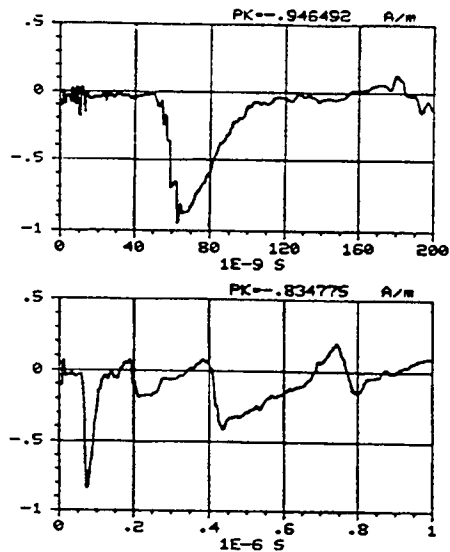


Figure C-135. X component of the magnetic field measured at location -50/75/1 using sensor H104-C. REPS pulse 114 generating 6.2 kV/m at 50 m.

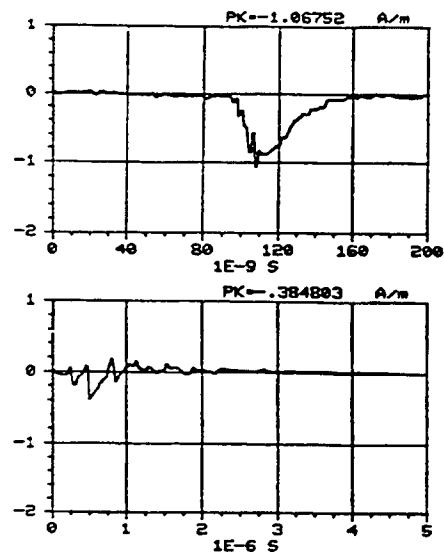


Figure C-136. X component of the magnetic field measured at location -50/75/1 using sensor H104-C. REPS pulse 115 generating 6.5 kV/m at 50 m.

Appendix C, 1-m data

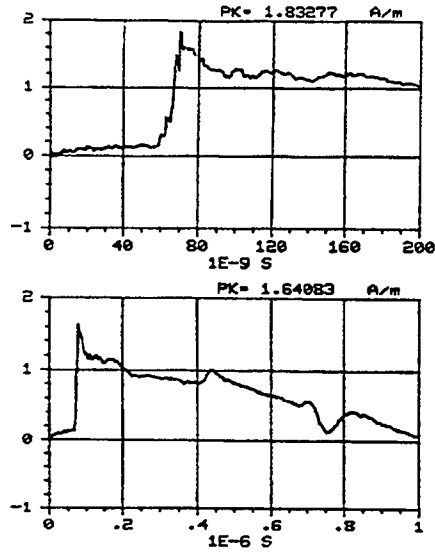


Figure C-137. Y component of the magnetic field measured at location -50/75/1 using sensor H104-C. REPS pulse 112 generating 6.4 kV/m at 50 m.

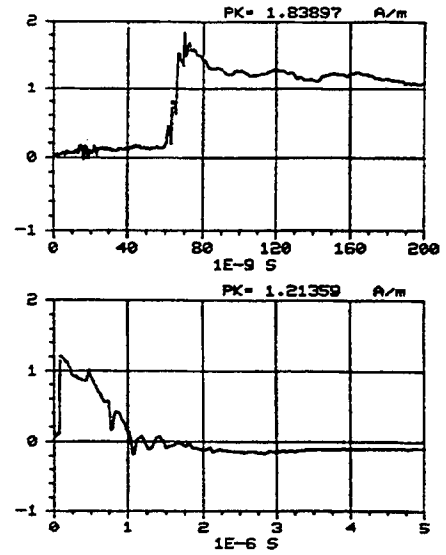


Figure C-138. Y component of the magnetic field measured at location -50/75/1 using sensor H104-C. REPS pulse 113 generating 6.5 kV/m at 50 m.

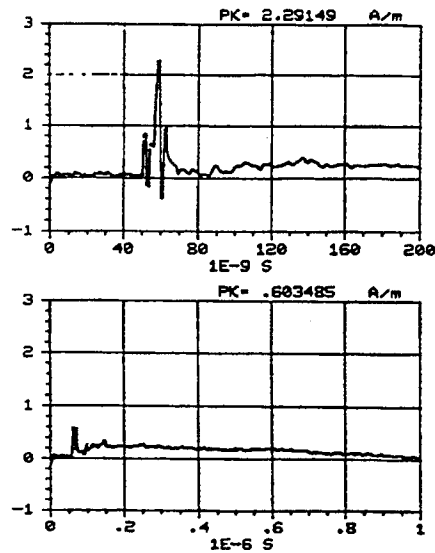


Figure C-139. Z component of the magnetic field measured at location -50/75/1 using sensor H104-C. REPS pulse 116 generating 6.4 kV/m at 50 m.

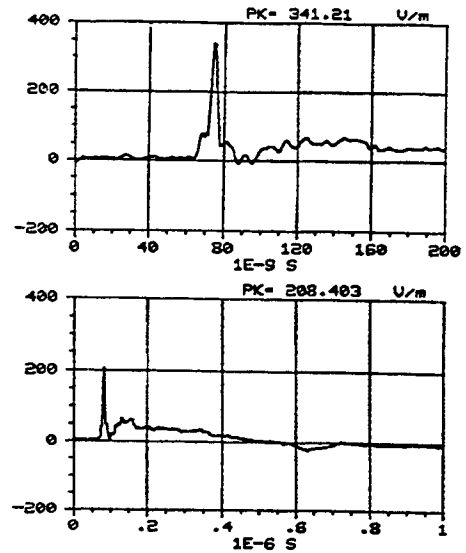


Figure C-140. X component of the electric field measured at location -75/75/1 using sensor E201-C. REPS pulse 143 generating 6.4 kV/m at 50 m.

Appendix C, 1-m data

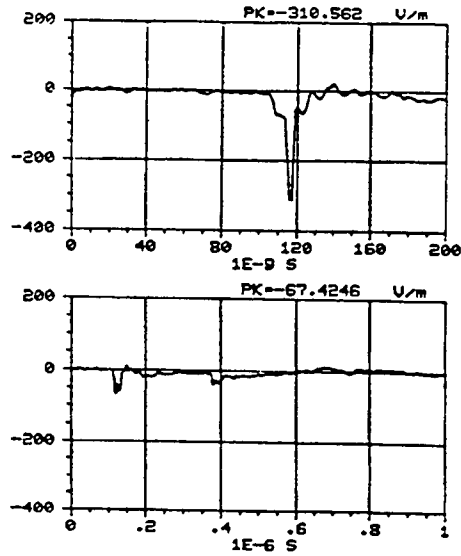


Figure C-141. -Y component of the electric field measured at location -75/75/1 using sensor E201-C. REPS pulse 146 generating 6.5 kV/m at 50 m.

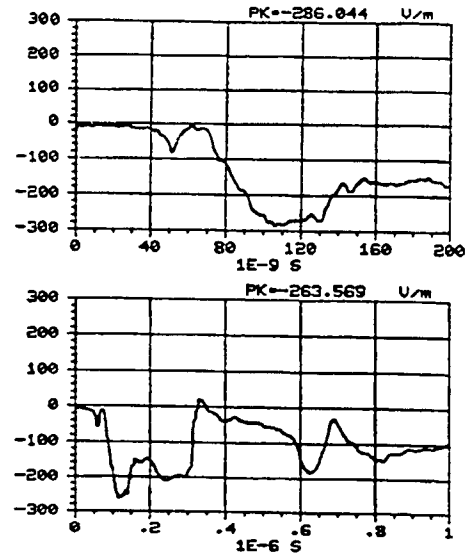


Figure C-142. Z component of the electric field measured at location -75/75/1 using sensor E201-C. REPS pulse 144 generating 6.2 kV/m at 50 m.

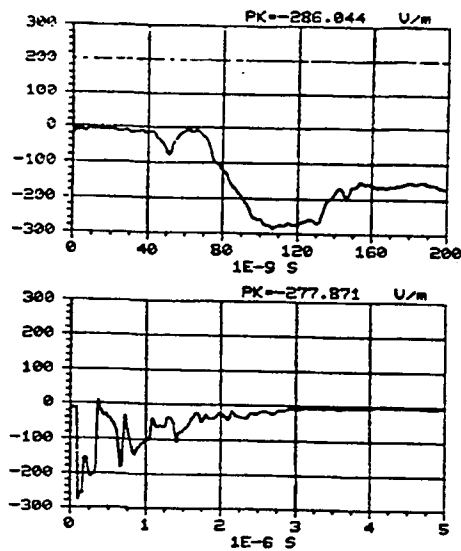


Figure C-143. Z component of the electric field measured at location -75/75/1 using sensor E201-C. REPS pulse 145 generating 6.3 kV/m at 50 m.

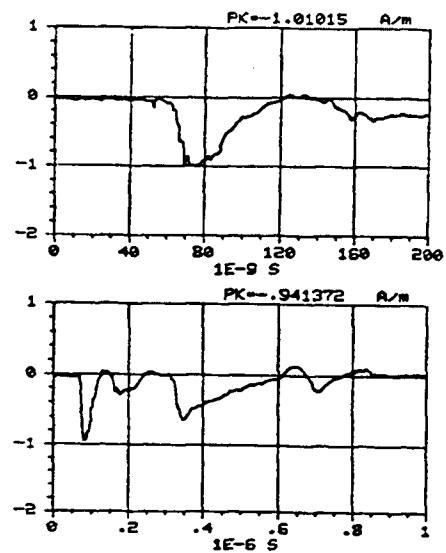


Figure C-144. X component of the magnetic field measured at location -75/75/1 using sensor H104-C. REPS pulse 149 generating 6.3 kV/m at 50 m.

Appendix C, 1-m data

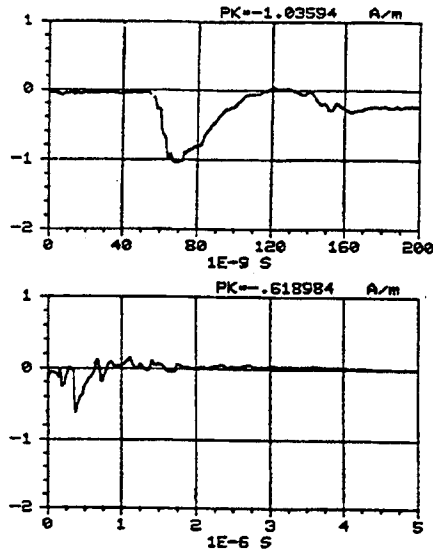


Figure C-145. X component of the magnetic field measured at location -75/75/1 using sensor H104-C. REPS pulse 150 generating 6.3 kV/m at 50 m.

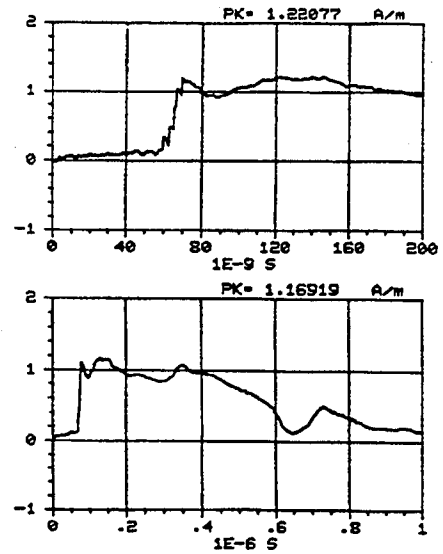


Figure C-146. Y component of the magnetic field measured at location -75/75/1 using sensor H104-C. REPS pulse 147 generating 6.3 kV/m at 50 m.

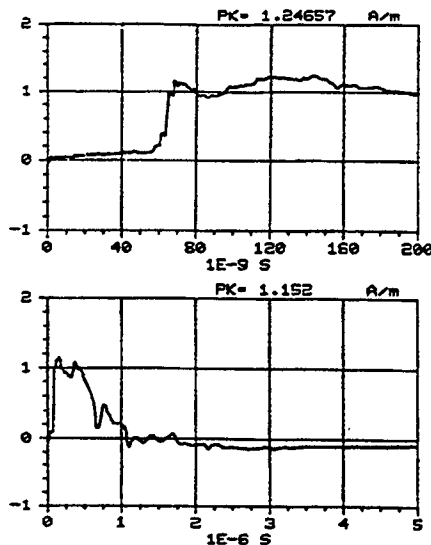


Figure C-147. Y component of the magnetic field measured at location -75/75/1 using sensor H104-C. REPS pulse 148 generating 6.4 kV/m at 50 m.

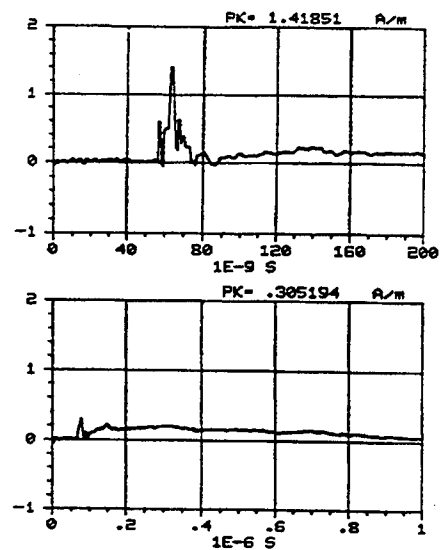


Figure C-148. Z component of the magnetic field measured at location -75/75/1 using sensor H104-C. REPS pulse 151 generating 6.5 kV/m at 50 m.

Appendix C, 1-m data

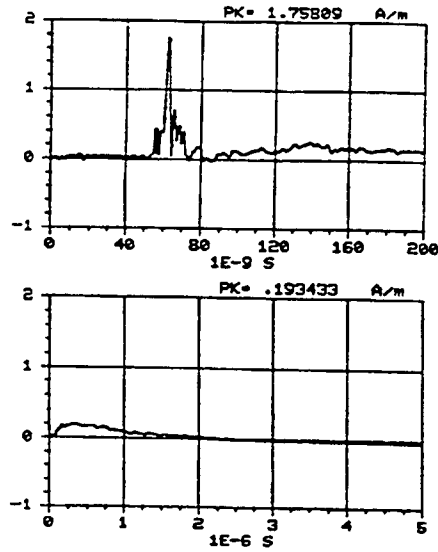


Figure C-149. Z component of the magnetic field measured at location -75/75/1 using sensor H104-C. REPS pulse 152 generating 6.5 kV/m at 50 m.

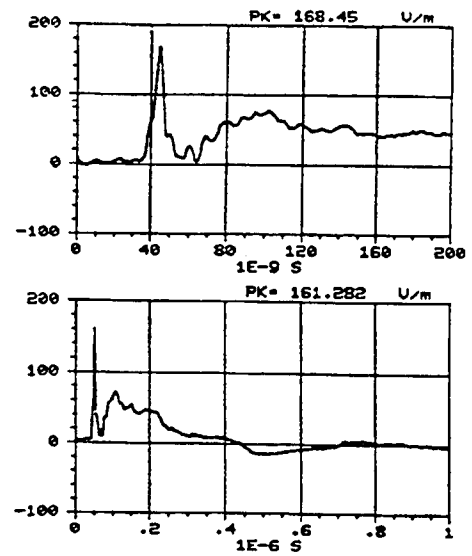


Figure C-150. X component of the electric field measured at location -100/75/1 using sensor E201-C. REPS pulse 165 generating 6.2 kV/m at 50 m.

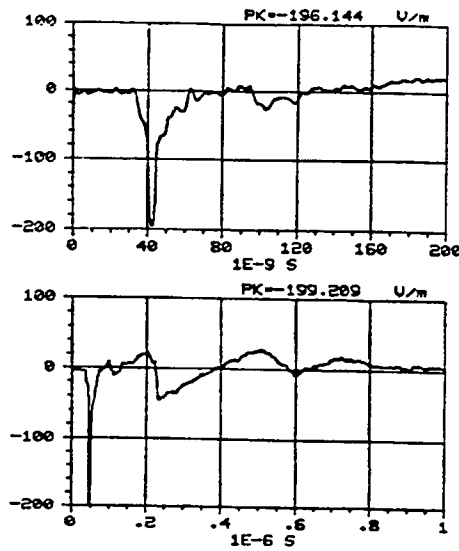


Figure C-151. -Y component of the electric field measured at location -100/75/1 using sensor E201-C. REPS pulse 169 generating 6.2 kV/m at 50 m.

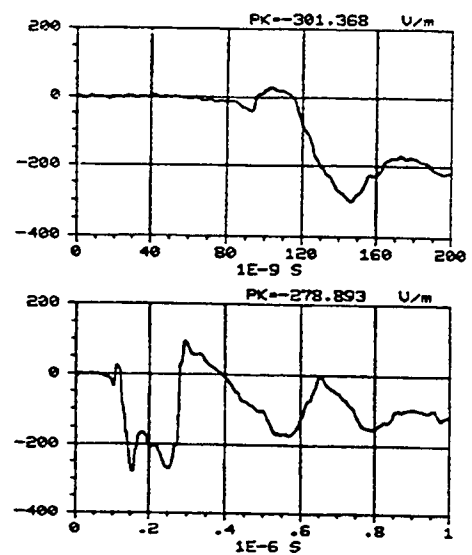


Figure C-152. Z component of the electric field measured at location -100/75/1 using sensor E201-C. REPS pulse 167 generating 6.3 kV/m at 50 m.

Appendix C, 1-m data

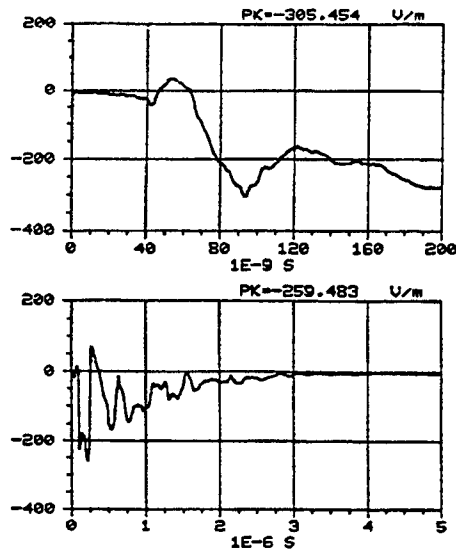


Figure C-153. Z component of the electric field measured at location -100/75/1 using sensor E201-C. REPS pulse 168 generating 6.3 kV/m at 50 m.

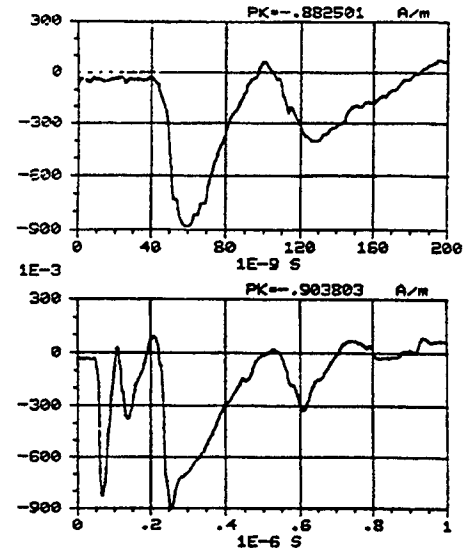


Figure C-154. X component of the magnetic field measured at location -100/75/1 using sensor H104-C. REPS pulse 173 generating 6.1 kV/m at 50 m.

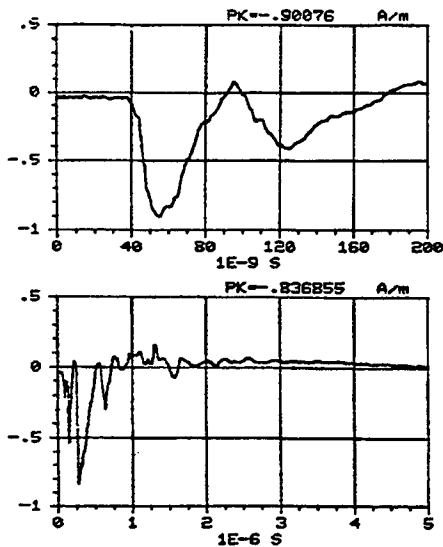


Figure C-155. X component of the magnetic field measured at location -100/75/1 using sensor H104-C. REPS pulse 174 generating 6.3 kV/m at 50 m.

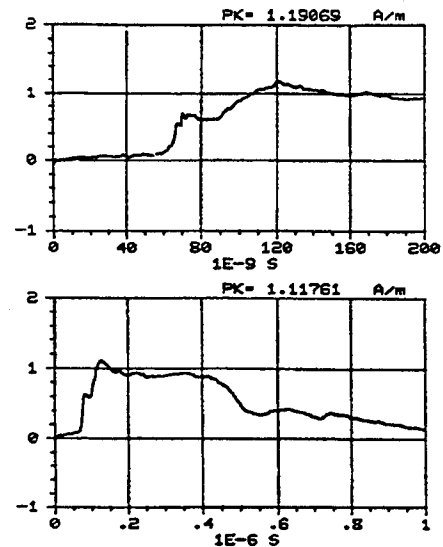


Figure C-156. Y component of the magnetic field measured at location -100/75/1 using sensor H104-C. REPS pulse 171 generating 6.2 kV/m at 50 m.

Appendix C, 1-m data

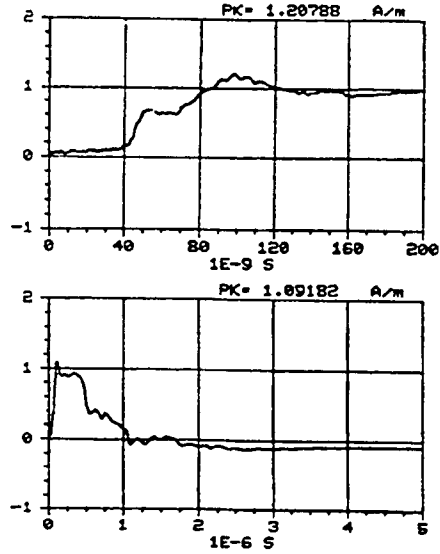


Figure C-157. Y component of the magnetic field measured at location -100/75/1 using sensor H104-C. REPS pulse 175 generating 6.6 kV/m at 50 m.

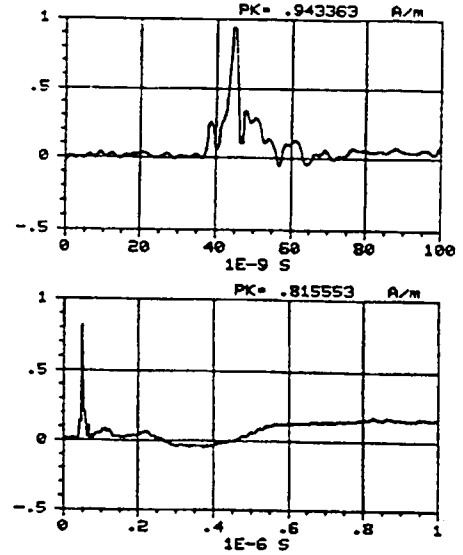


Figure C-158. Z component of the magnetic field measured at location -100/75/1 using sensor H104-C. REPS pulse 178 generating 6.3 kV/m at 50 m.

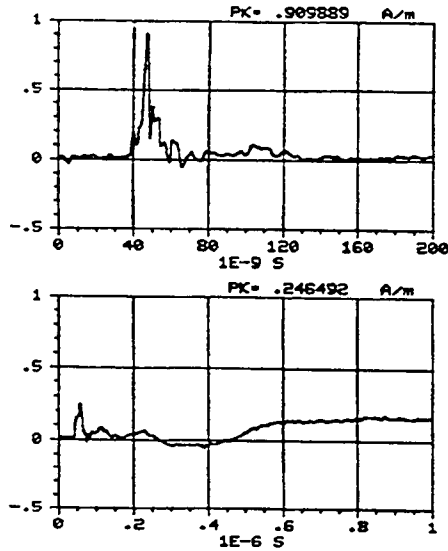


Figure C-159. Z component of the magnetic field measured at location -100/75/1 using sensor H104-C. REPS pulse 176 generating 6.2 kV/m at 50 m.

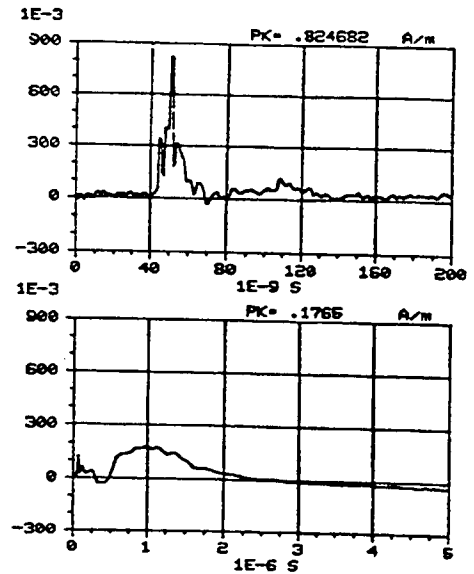


Figure C-160. Z component of the magnetic field measured at location -100/75/1 using sensor H104-C. REPS pulse 177 generating 6.2 kV/m at 50 m.

Appendix C, 1-m data

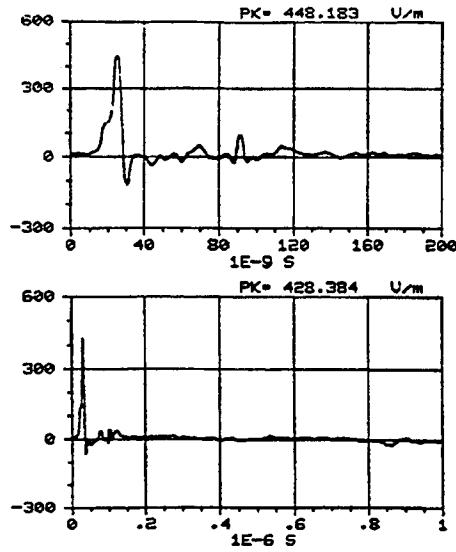


Figure C-161. X component of the electric field measured at location 0/92/1 using sensor E102-C. REPS pulse 281 generating 6.1 kV/m at 50 m.

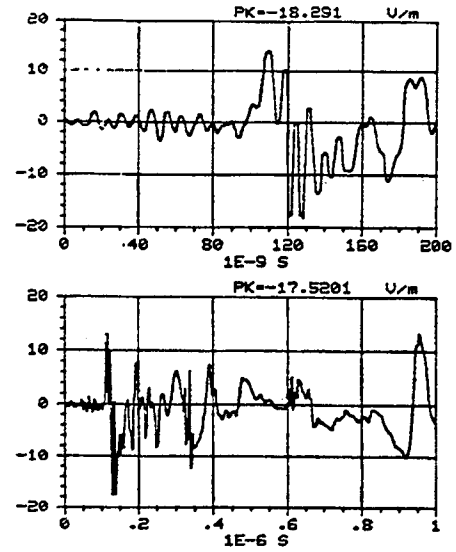


Figure C-162. Z component of the electric field measured at location 0/92/1 using sensor E102-C. REPS pulse 283 generating 6.2 kV/m at 50 m.

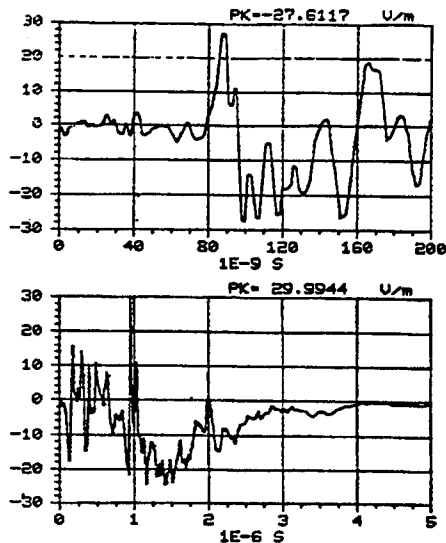


Figure C-163. Z component of the electric field measured at location 0/92/1 using sensor E102-C. REPS pulse 284 generating 6 kV/m at 50 m.

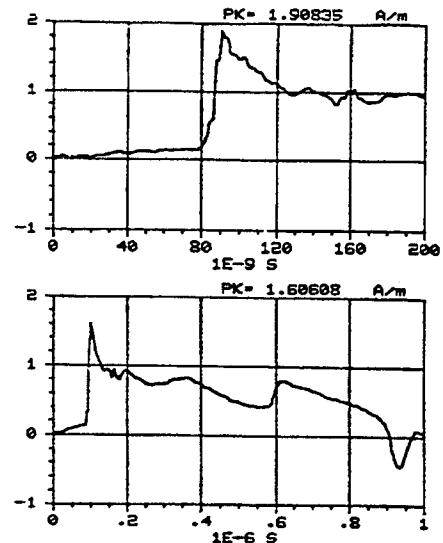


Figure C-164. Y component of the magnetic field measured at location 0/92/1 using sensor H104-C. REPS pulse 279 generating 6.2 kV/m at 50 m.

Appendix C, 2-m data

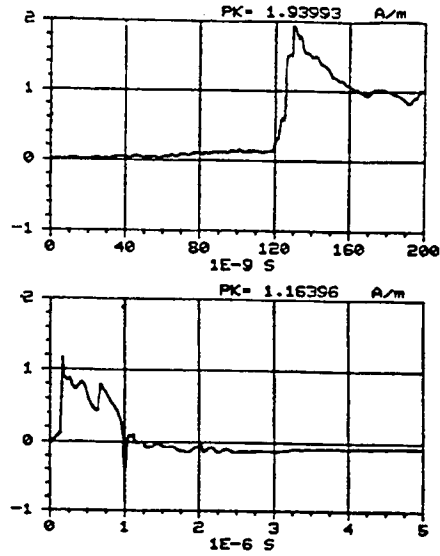


Figure C-165. Y component of the magnetic field measured at location 0/92/1 using sensor H104-C. REPS pulse 280 generating 6.3 kV/m at 50 m.

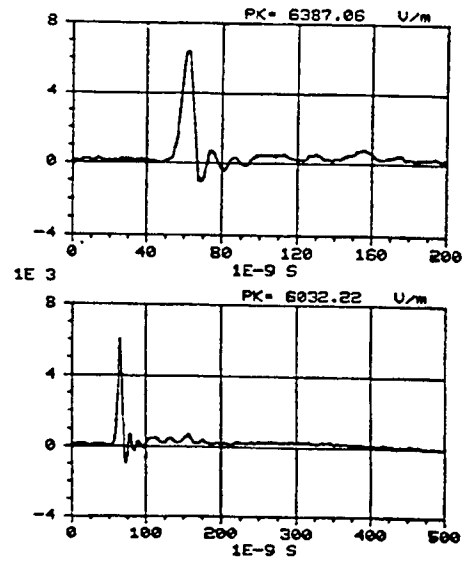


Figure C-166. X component of the electric field measured at location 0/25/2 using sensor E304-C. REPS pulse 46 generating 6.1 kV/m at 50 m.

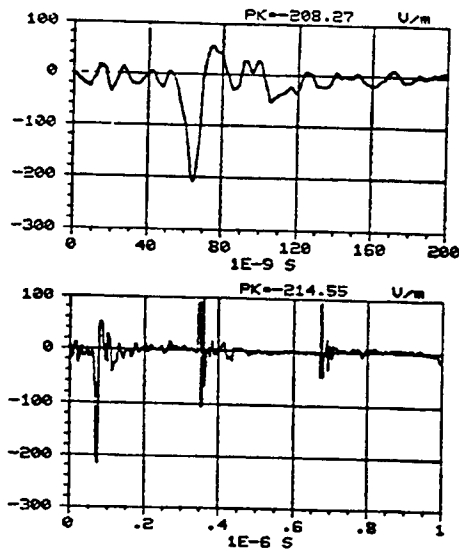


Figure C-167. -Y component of the electric field measured at location 0/25/2 using sensor E201-C. REPS pulse 40 generating 6.1 kV/m at 50 m.

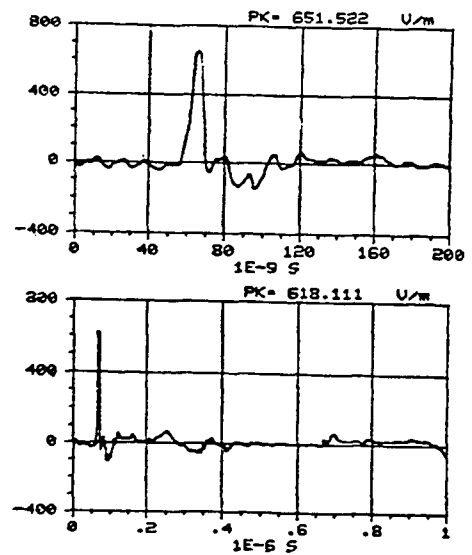


Figure C-168. Z component of the electric field measured at location 0/25/2 using sensor E201-C. REPS pulse 43 generating 6.3 kV/m at 50 m.

Appendix C, 2-m data

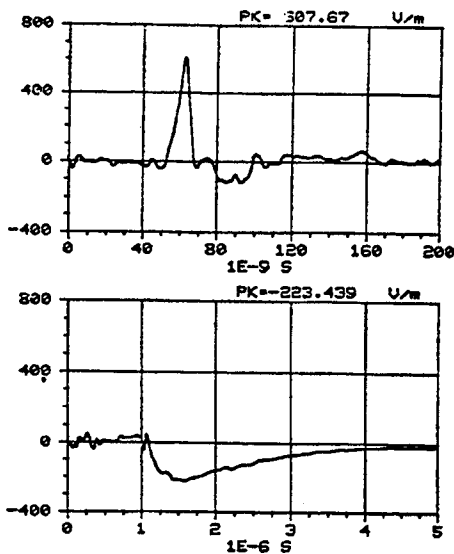


Figure C-169. Z component of the electric field measured at location 0/25/2 using sensor E201-C. REPS pulse 44 generating 6.2 kV/m at 50 m.

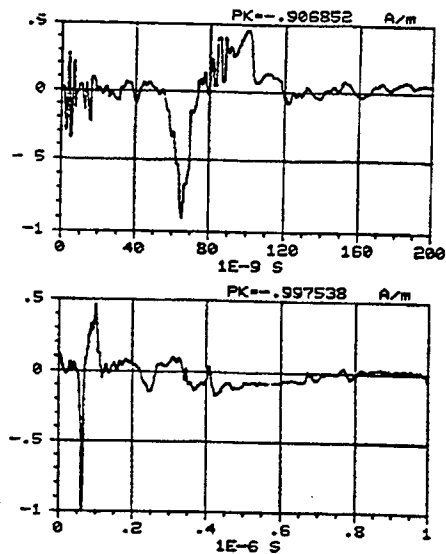


Figure C-170. X component of the magnetic field measured at location 0/25/2 using sensor H104-C. REPS pulse 7 generating 6.5 kV/m at 50 m.

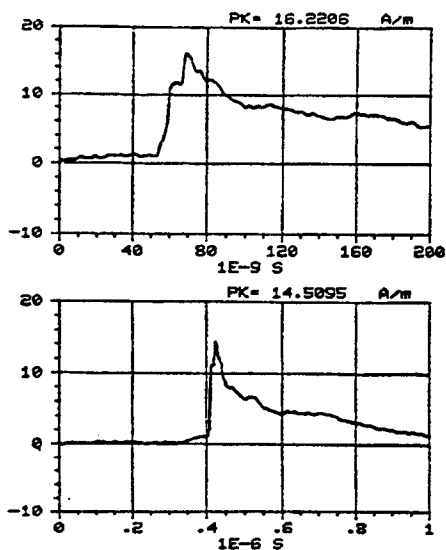


Figure C-171. Y component of the magnetic field measured at location 0/25/2 using sensor H104-C. REPS pulse 8 generating 6.4 kV/m at 50 m.

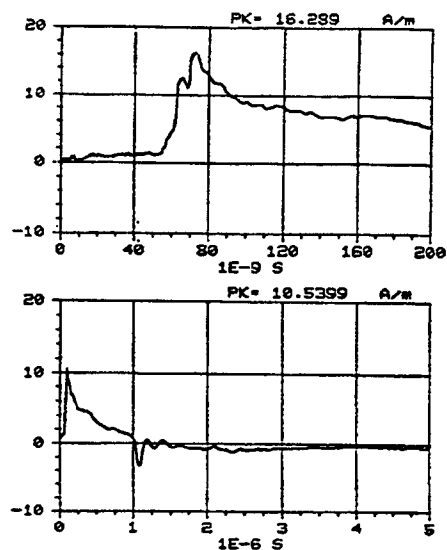


Figure C-172. Y component of the magnetic field measured at location 0/25/2 using sensor H104-C. REPS pulse 9 generating 6.3 kV/m at 50 m.

Appendix C, 2-m data

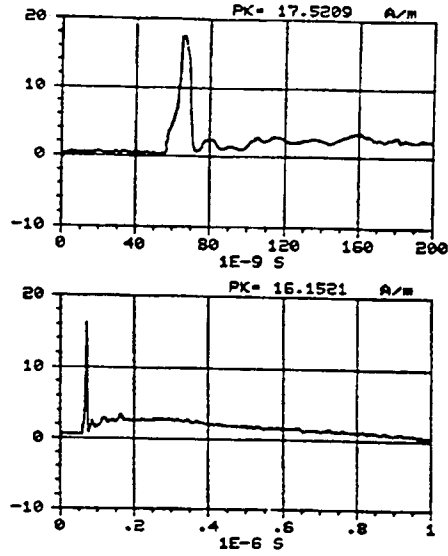


Figure C-173. Z component of the magnetic field measured at location 0/25/2 using sensor H104-C. REPS pulse 10 generating 6.3 kV/m at 50 m.

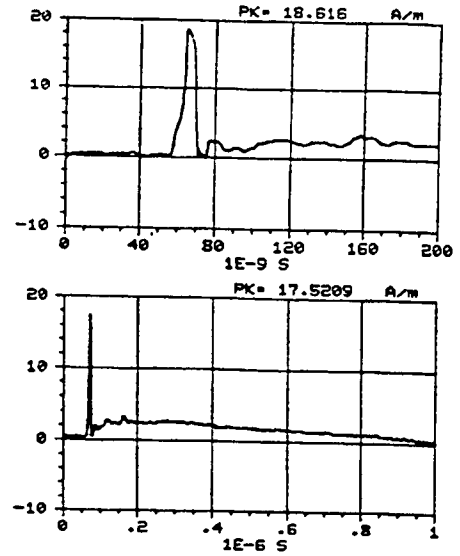


Figure C-174. Z component of the magnetic field measured at location 0/25/2 using sensor H104-C. REPS pulse 11 generating 6.4 kV/m at 50 m.

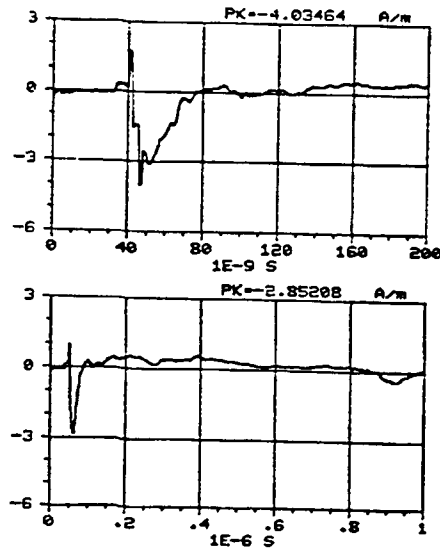


Figure C-175. X component of the magnetic field measured at location -25/25/2 using sensor H104-C. REPS pulse 6 generating 6.9 kV/m at 50 m.

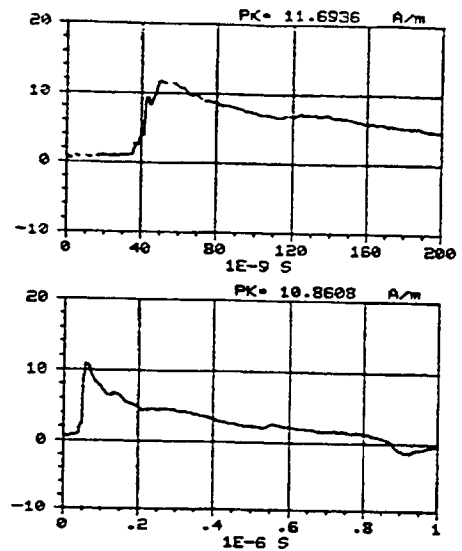


Figure C-176. Y component of the magnetic field measured at location -25/25/2 using sensor H104-C. REPS pulse 2 generating 6.9 kV/m at 50 m.

Appendix C, 2-m data

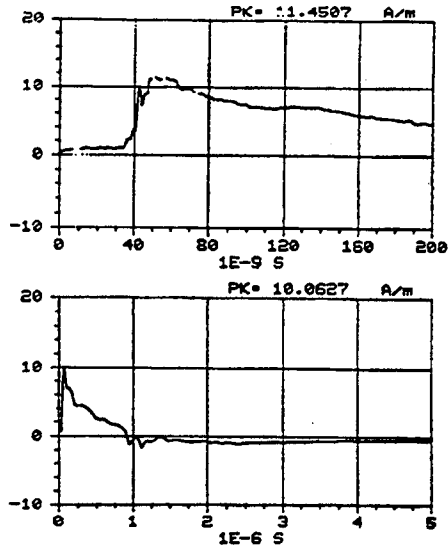


Figure C-177. Y component of the magnetic field measured at location -25/25/2 using sensor H104-C. REPS pulse 3 generating 7 kV/m at 50 m.

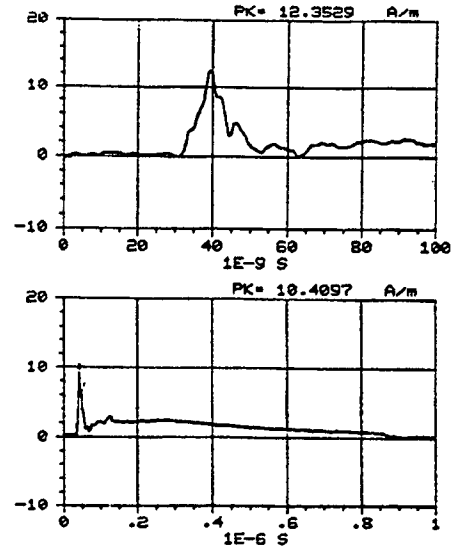


Figure C-178. Z component of the magnetic field measured at location -25/25/2 using sensor H104-C. REPS pulse 45 generating 6.9 kV/m at 50 m.

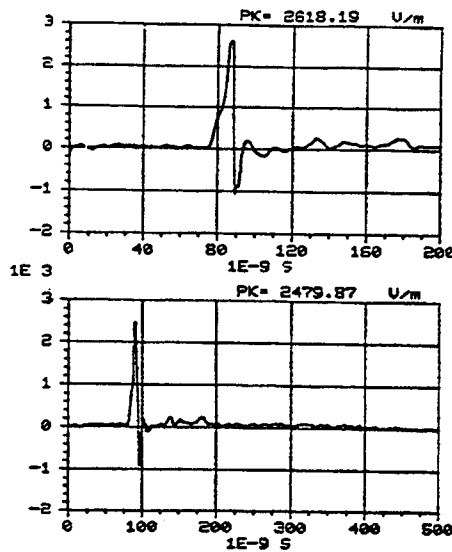


Figure C-179. X component of the electric field measured at location 0/50/2 using sensor E201-C. REPS pulse 39 generating 6.68 kV/m at 50 m.

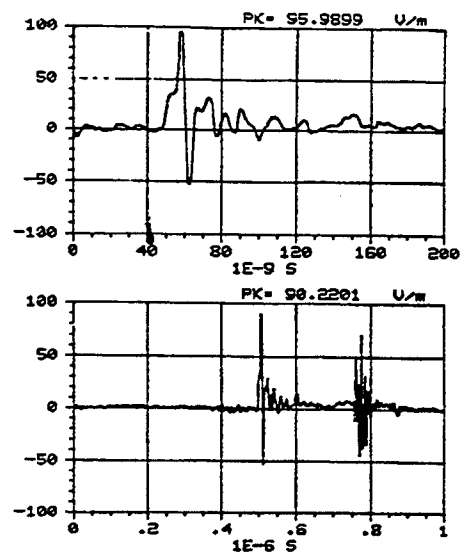


Figure C-180. -Y component of the electric field measured at location 0/50/2 using sensor E201-C. REPS pulse 36 generating 6.65 kV/m at 50 m.

Appendix C, 2-m data

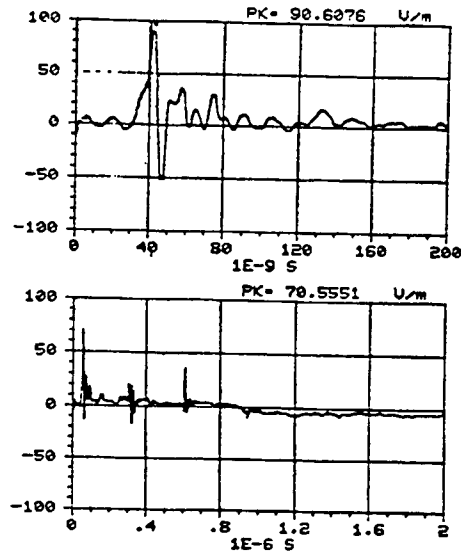


Figure C-181. -Y component of the electric field measured at location 0/50/2 using sensor E201-C. REPS pulse 61 generating 6.1 kV/m at 50 m.

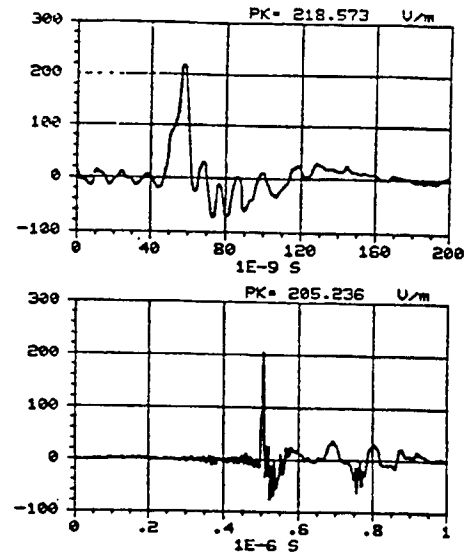


Figure C-182. Z component of the electric field measured at location 0/50/2 using sensor E201-C. REPS pulse 56 generating 6 kV/m at 50 m.

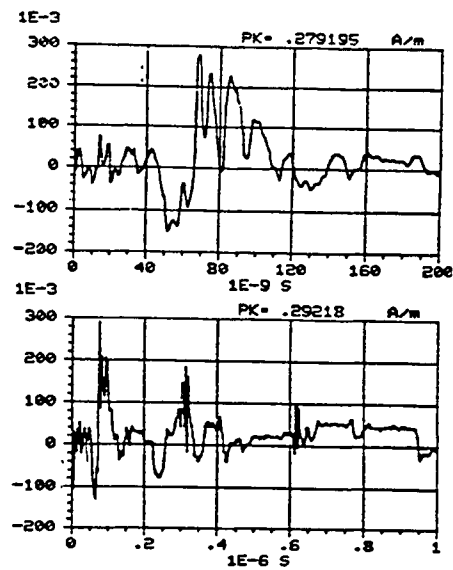


Figure C-183. X component of the magnetic field measured at location 0/50/2 using sensor H104-C. REPS pulse 18 generating 6.4 kV/m at 50 m.

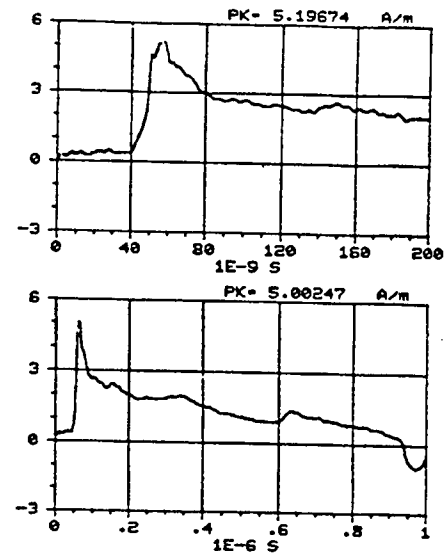


Figure C-184. Y component of the magnetic field measured at location 0/50/2 using sensor H104-C. REPS pulse 19 generating 6.3 kV/m at 50 m.

Appendix C, 2-m data

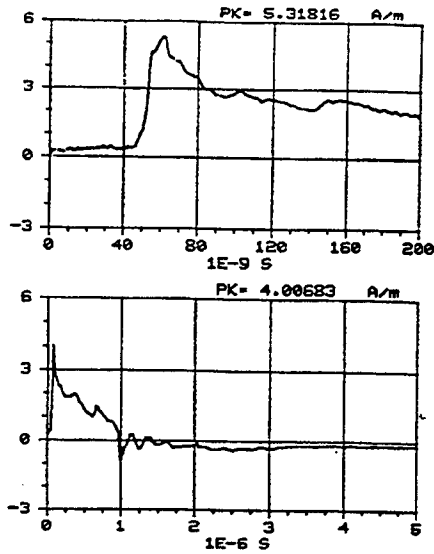


Figure C-185. Y component of the magnetic field measured at location 0/50/2 using sensor H104-C. REPS pulse 20 generating 6.3 kV/m at 50 m.

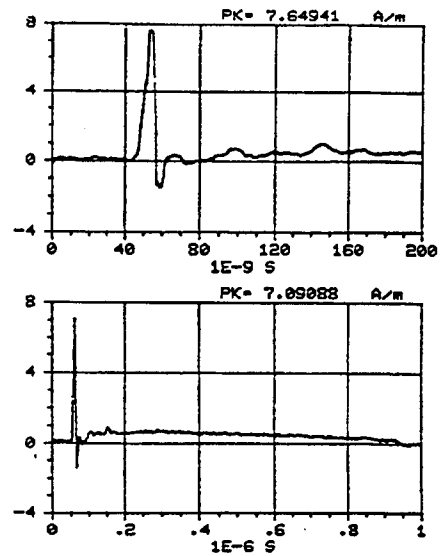


Figure C-186. Z component of the magnetic field measured at location 0/50/2 using sensor H104-C. REPS pulse 21 generating 6.1 kV/m at 50 m.

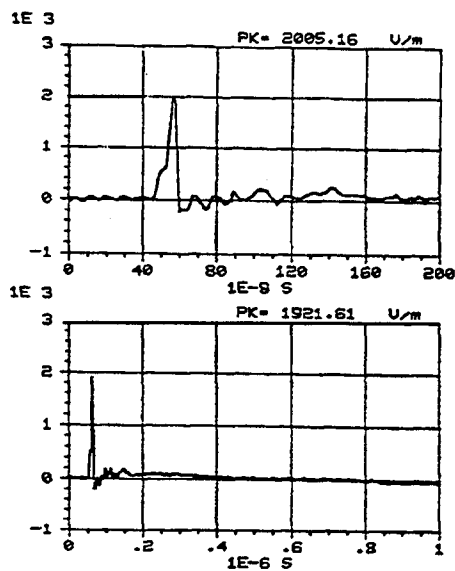


Figure C-187. X component of the electric field measured at location -25/50/2 using sensor E304-C. REPS pulse 91 generating 6.3 kV/m at 50 m.

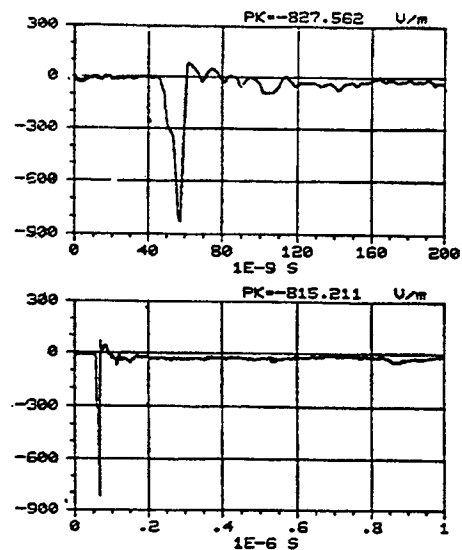


Figure C-188. -Y component of the electric field measured at location -25/50/2 using sensor E304-C. REPS pulse 87 generating 6.3 kV/m at 50 m.

Appendix C, 2-m data

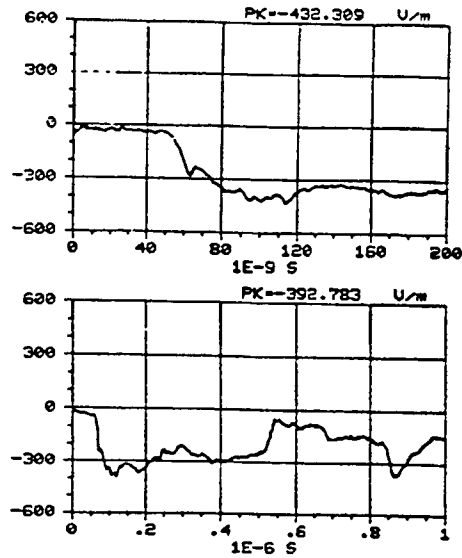


Figure C-189. Z component of the electric field measured at location -25/50/2 using sensor E304-C. REPS pulse 88 generating 6.4 kV/m at 50 m.

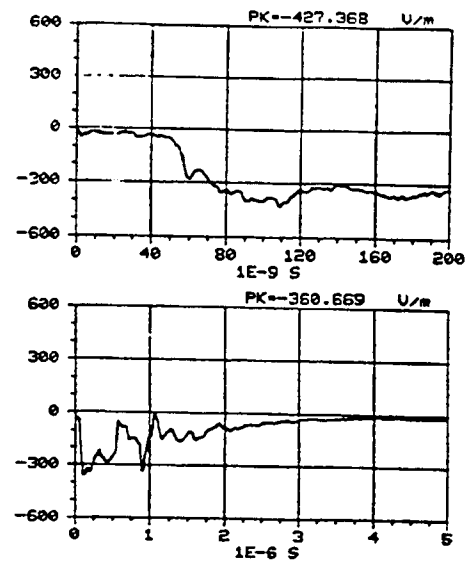


Figure C-190. Z component of the electric field measured at location -25/50/2 using sensor E304-C. REPS pulse 90 generating 6.2 kV/m at 50 m.

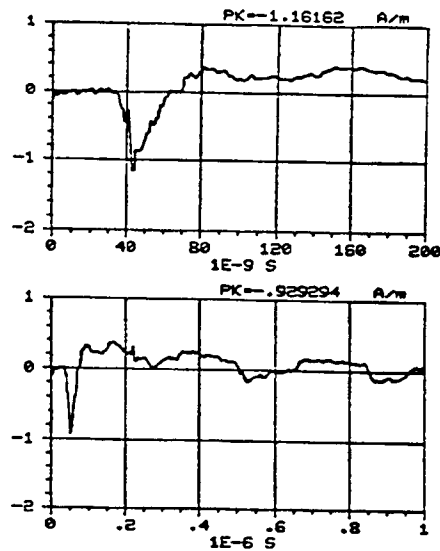


Figure C-191. X component of the magnetic field measured at location -25/50/2 using sensor H104-C. REPS pulse 81 generating 6.3 kV/m at 50 m.

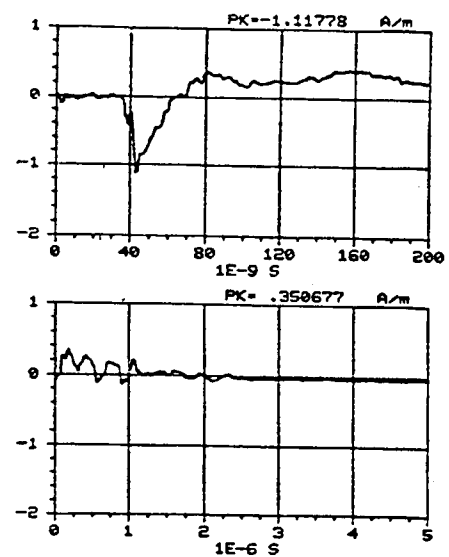


Figure C-192. X component of the magnetic field measured at location -25/50/2 using sensor H104-C. REPS pulse 82 generating 6.5 kV/m at 50 m.

Appendix C, 2-m data

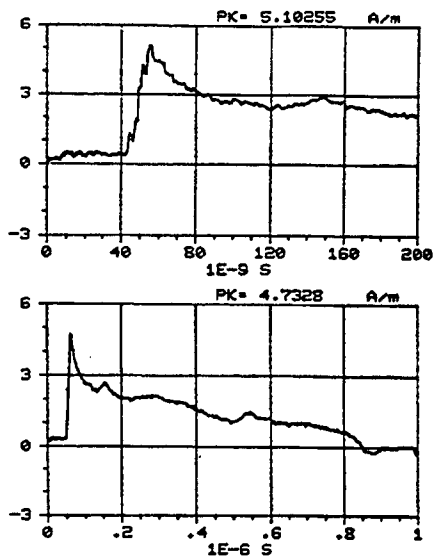


Figure C-193. Y component of the magnetic field measured at location -25/50/2 using sensor H104-C. REPS pulse 79 generating 6.2 kV/m at 50 m.

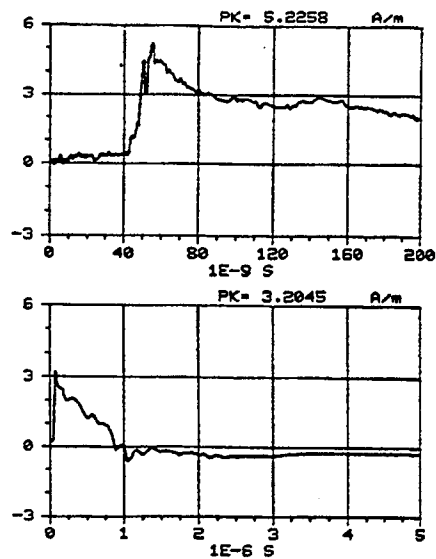


Figure C-194. Y component of the magnetic field measured at location -25/50/2 using sensor H104-C. REPS pulse 80 generating 6.2 kV/m at 50 m.

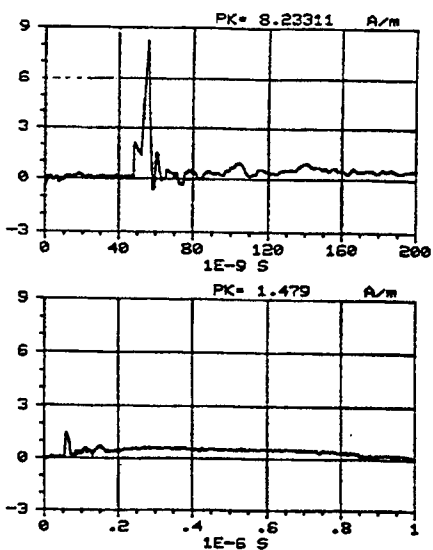


Figure C-195. Z component of the magnetic field measured at location -25/50/2 using sensor H104-C. REPS pulse 78 generating 6.3 kV/m at 50 m.

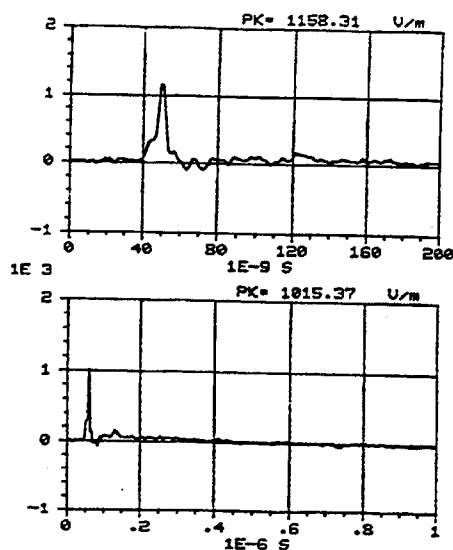


Figure C-196. X component of the electric field measured at location -50/50/2 using sensor E304-C. REPS pulse 99 generating 6.4 kV/m at 50 m.

Appendix C, 2-m data

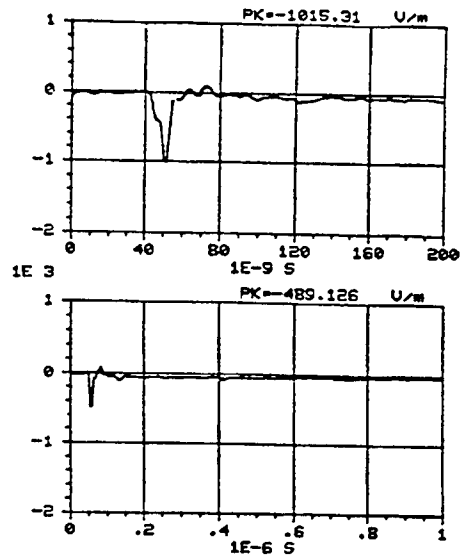


Figure C-197. -Y component of the electric field measured at location -50/50/2 using sensor E304-C. REPS pulse 96 generating 6.3 kV/m at 50 m.

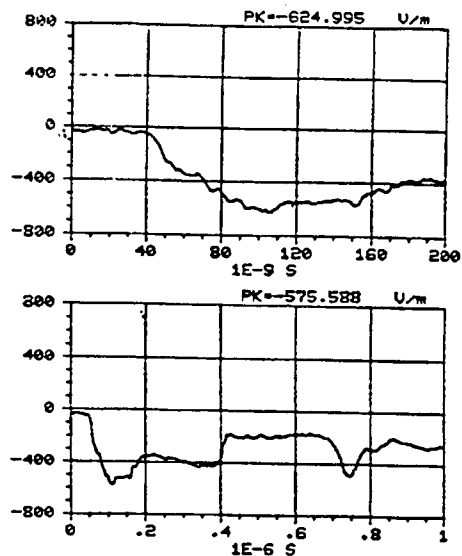


Figure C-198. Z component of the electric field measured at location -50/50/2 using sensor E304-C. REPS pulse 97 generating 6.2 kV/m at 50 m.

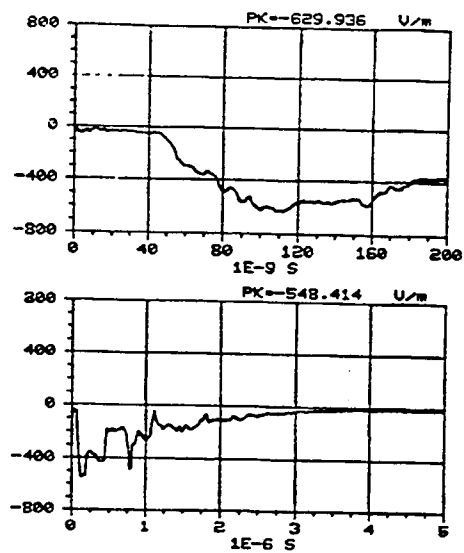


Figure C-199. Z component of the electric field measured at location -50/50/2 using sensor E304-C. REPS pulse 98 generating 6.5 kV/m at 50 m.

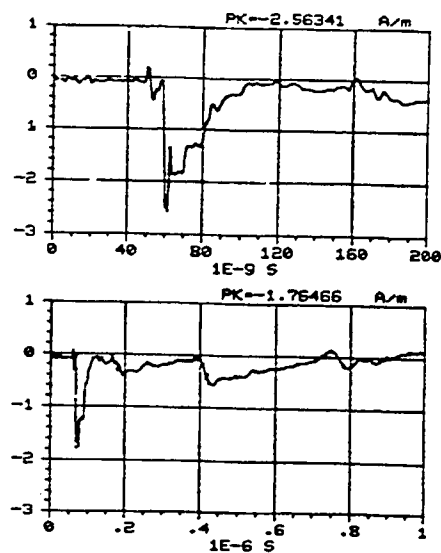


Figure C-200. X component of the magnetic field measured at location -50/50/2 using sensor H104-C. REPS pulse 108 generating 6.2 kV/m at 50 m.

Appendix C, 2-m data

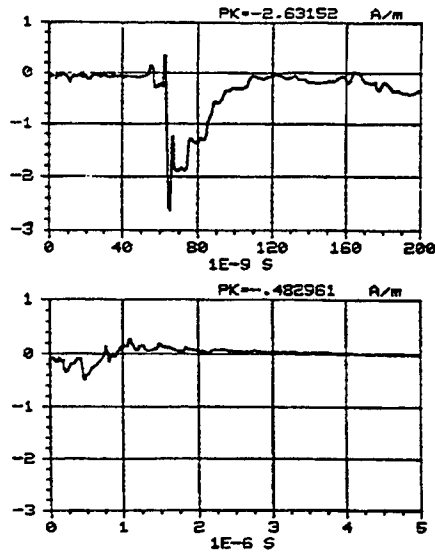


Figure C-201. X component of the magnetic field measured at location -50/50/2 using sensor H104-C. REPS pulse 109 generating 6.3 kV/m at 50 m.

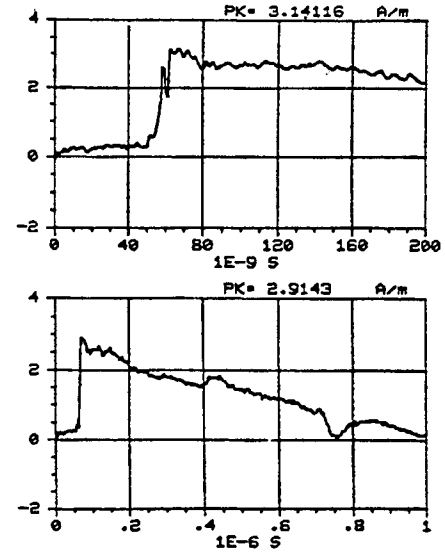


Figure C-202. Y component of the magnetic field measured at location -50/50/2 using sensor H104-C. REPS pulse 110 generating 6.5 kV/m at 50 m.

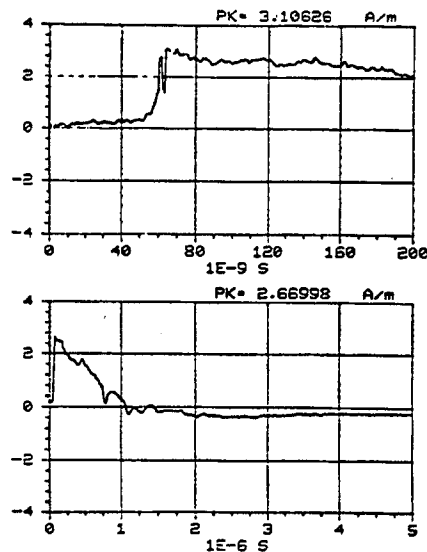


Figure C-203. Y component of the magnetic field measured at location -50/50/2 using sensor H104-C. REPS pulse 111 generating 6.3 kV/m at 50 m.

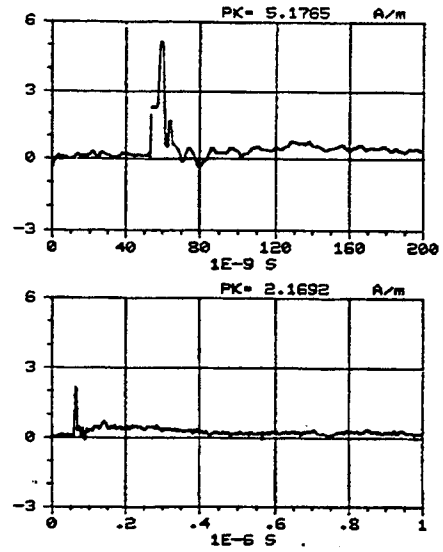


Figure C-204. Z component of the magnetic field measured at location -50/50/2 using sensor H104-C. REPS pulse 107 generating 6.3 kV/m at 50 m.

Appendix C, Symmetry data

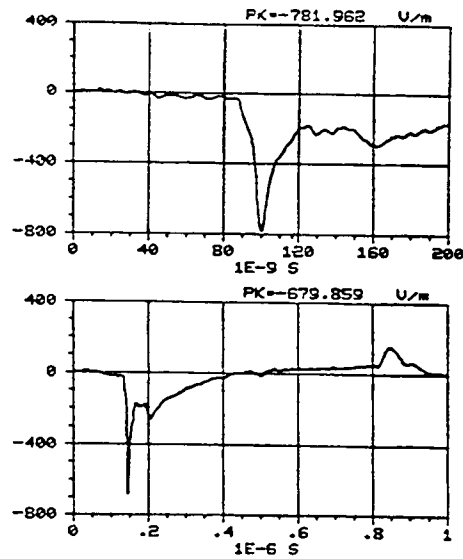


Figure C-205. -X component of the electric field measured at location 50/25/1 using sensor E304-C. REPS pulse 361 generating 6 kV/m at 50 m.

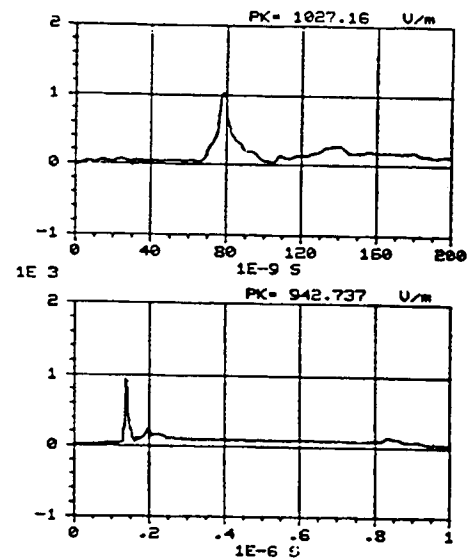


Figure C-206. -Y component of the electric field measured at location 50/25/1 using sensor E304-C. REPS pulse 364 generating 6.1 kV/m at 50 m.

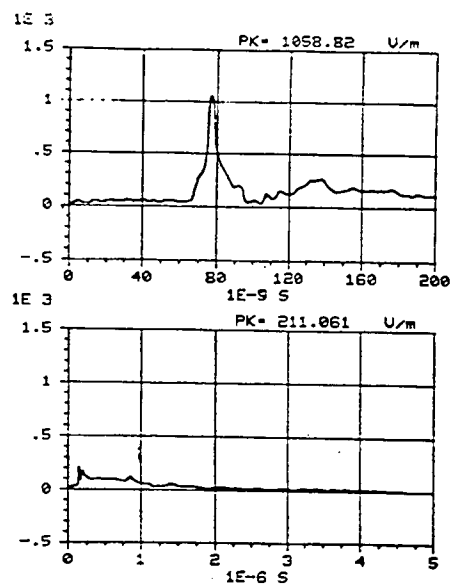


Figure C-207. -Y component of the electric field measured at location 50/25/1 using sensor E304-C. REPS pulse 365 generating 6.2 kV/m at 50 m.

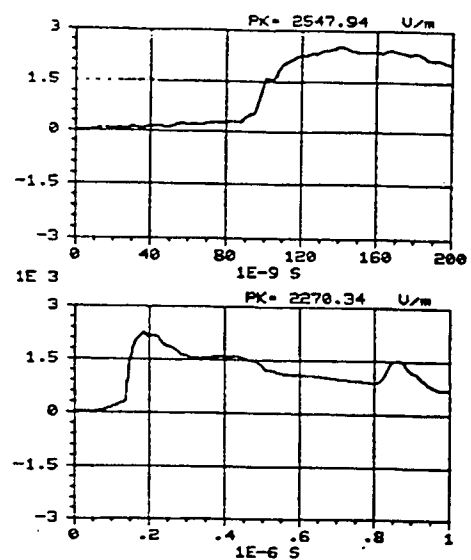


Figure C-208. Z component of the electric field measured at location 50/25/1 using sensor E304-C. REPS pulse 362 generating 6.3 kV/m at 50 m.

Appendix C, Symmetry data

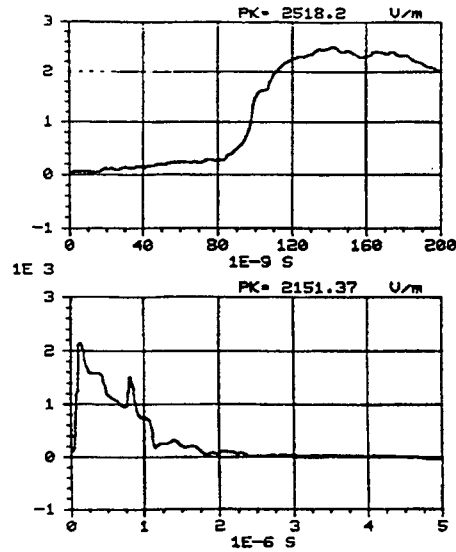


Figure C-209. Z component of the electric field measured at location 50/25/1 using sensor E304-C. REPS pulse 363 generating 5.9 kV/m at 50 m.

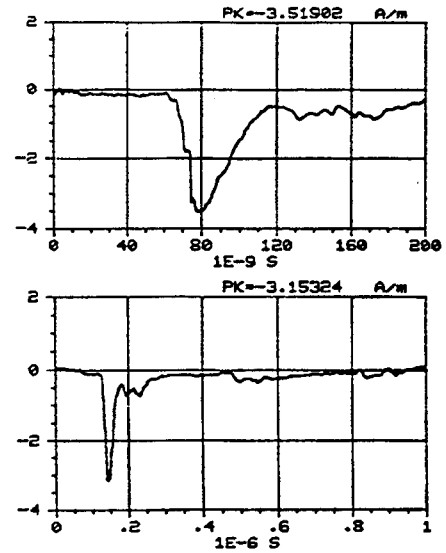


Figure C-210. -X component of the magnetic field measured at location 50/25/1 using sensor H104-C. REPS pulse 366 generating 6.2 kV/m at 50 m.

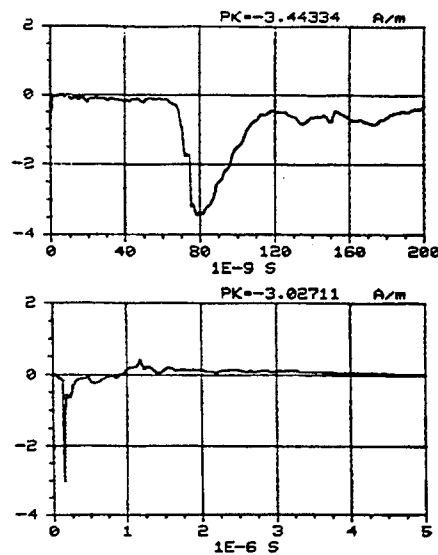


Figure C-211. -X component of the magnetic field measured at location 50/25/1 using sensor H104-C. REPS pulse 367 generating 6.1 kV/m at 50 m.

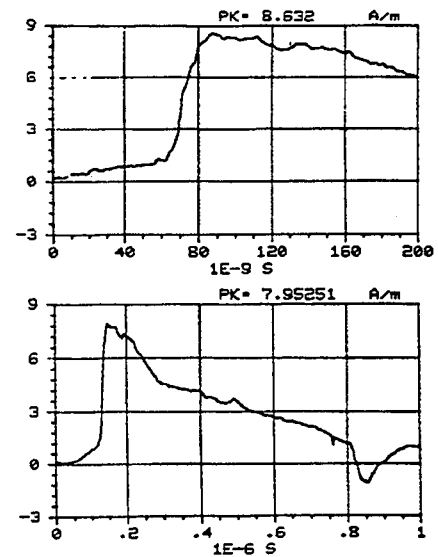


Figure C-212. Y component of the magnetic field measured at location 50/25/1 using sensor H104-C. REPS pulse 370 generating 6.1 kV/m at 50 m.

Appendix C, Symmetry data

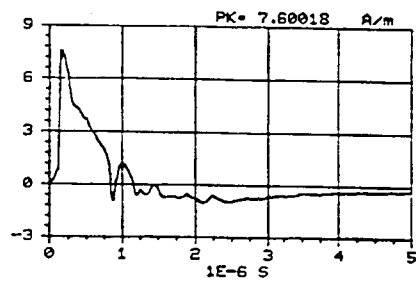
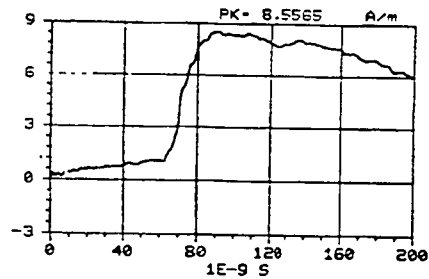


Figure C-213. Y component of the magnetic field measured at location 50/25/1 using sensor H104-C. REPS pulse 371 generating 6.1 kV/m at 50 m.

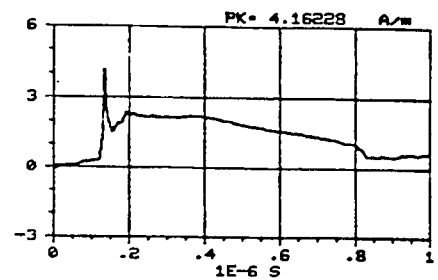
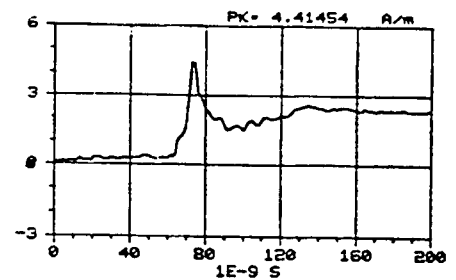


Figure C-214. Z component of the magnetic field measured at location 50/25/1 using sensor H104-C. REPS pulse 368 generating 6.1 kV/m at 50 m.

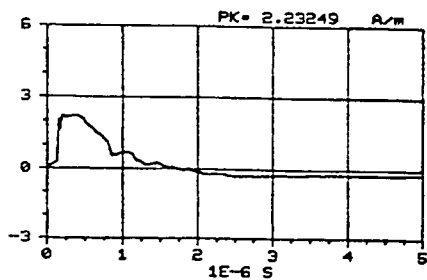
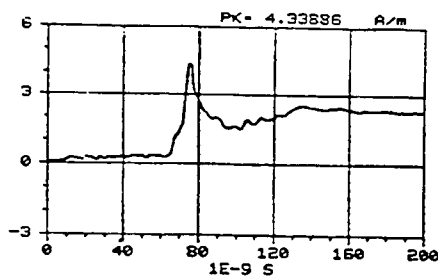


Figure C-215. Z component of the magnetic field measured at location 50/25/1 using sensor H104-C. REPS pulse 369 generating 6 kV/m at 50 m.

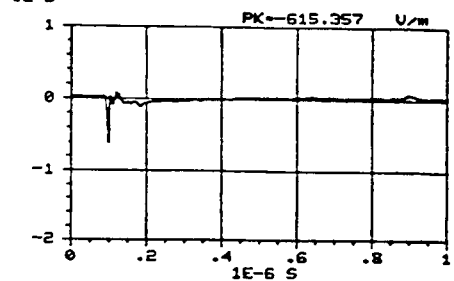
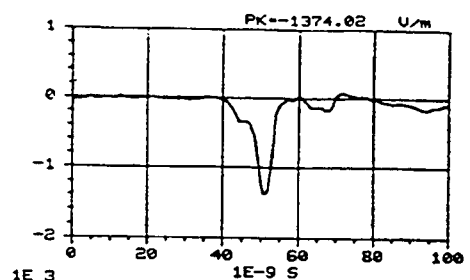


Figure C-216. -X component of the electric field measured at location 25/50/1 using sensor E201-C. REPS pulse 339 generating 6.3 kV/m at 50 m.

Appendix C, Symmetry data

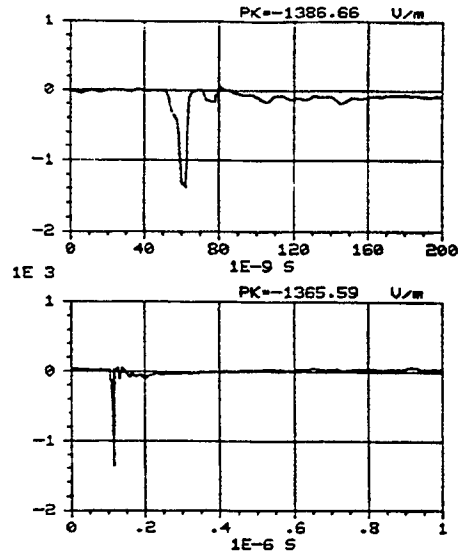


Figure C-217. -X component of the electric field measured at location 25/50/1 using sensor E201-C. REPS pulse 338 generating 6.1 kV/m at 50 m.

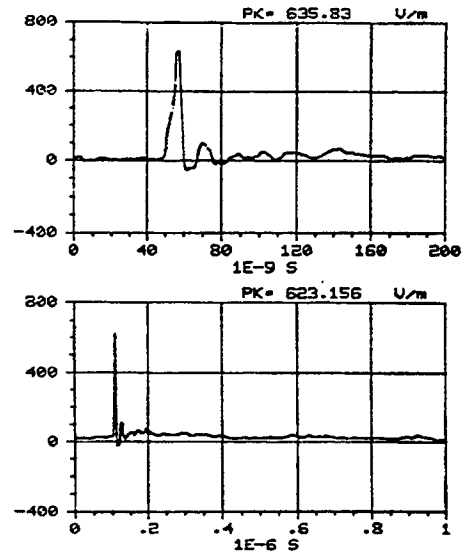


Figure C-218. -Y component of the electric field measured at location 25/50/1 using sensor E201-C. REPS pulse 337 generating 6.4 kV/m at 50 m.

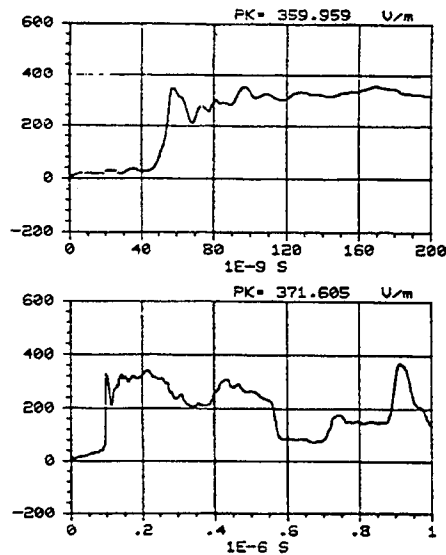


Figure C-219. Z component of the electric field measured at location 25/50/1 using sensor E201-C. REPS pulse 335 generating 6 kV/m at 50 m.

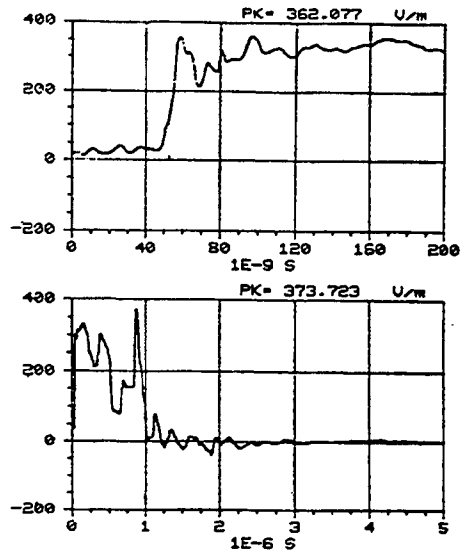


Figure C-220. Z component of the electric field measured at location 25/50/1 using sensor E201-C. REPS pulse 336 generating 6.3 kV/m at 50 m.

Appendix C, Symmetry data

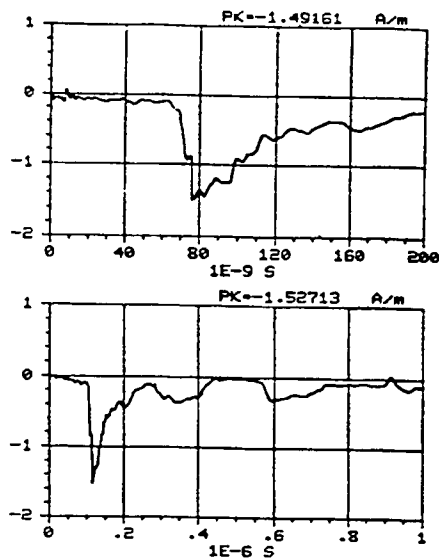


Figure C-221. -X component of the magnetic field measured at location 25/50/1 using sensor H104-C. REPS pulse 331 generating 6.4 kV/m at 50 m.

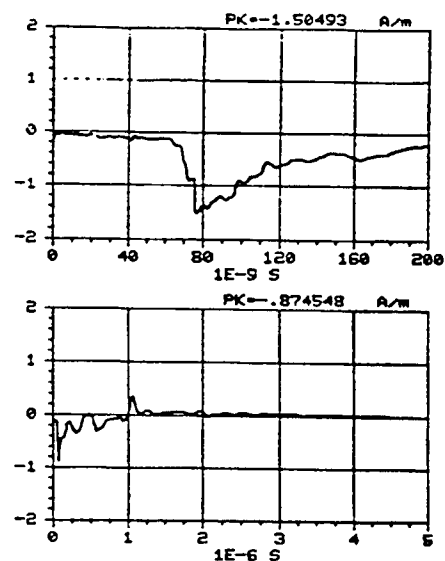


Figure C-222. -X component of the magnetic field measured at location 25/50/1 using sensor H104-C. REPS pulse 332 generating 6.2 kV/m at 50 m.

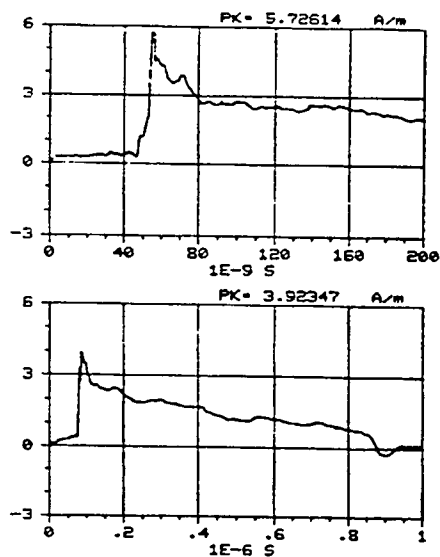


Figure C-223. Y component of the magnetic field measured at location 25/50/1 using sensor H104-C. REPS pulse 329 generating 6.3 kV/m at 50 m.

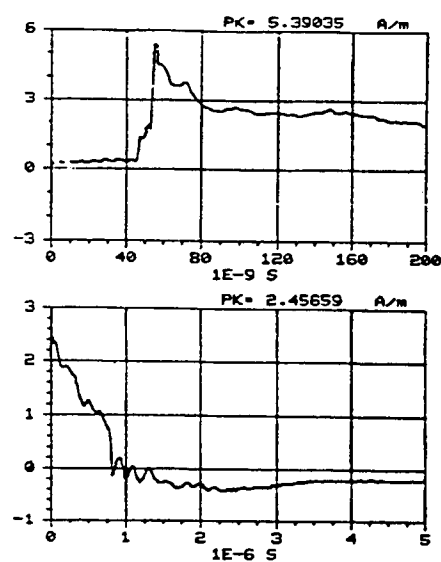


Figure C-224. Y component of the magnetic field measured at location 25/50/1 using sensor H104-C. REPS pulse 330 generating 6.3 kV/m at 50 m.

Appendix C, Symmetry data

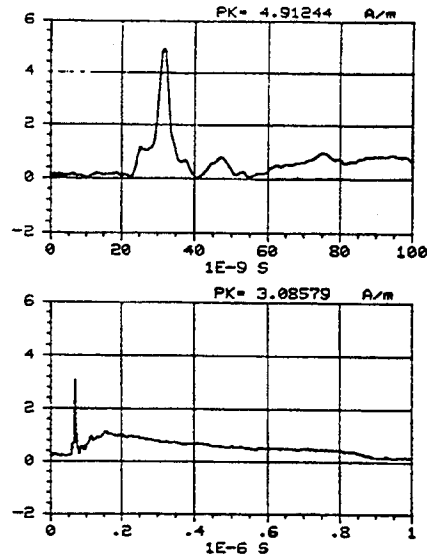


Figure C-225. Z component of the magnetic field measured at location 25/50/1 using sensor H104-C. REPS pulse 334 generating 6.2 kV/m at 50 m.

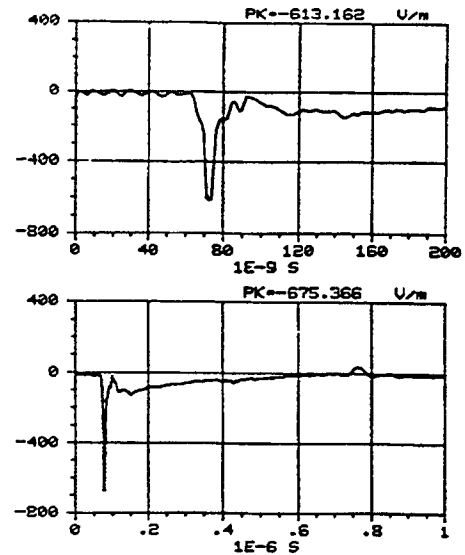


Figure C-226. -X component of the electric field measured at location 50/50/1 using sensor E304-C. REPS pulse 263 generating 6.1 kV/m at 50 m.

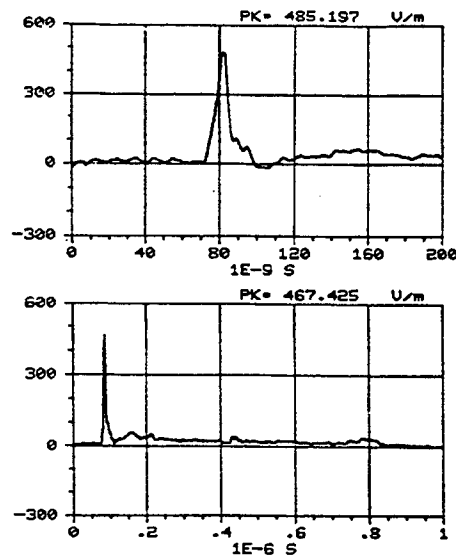


Figure C-227. -Y component of the electric field measured at location 50/50/1 using sensor E304-C. REPS pulse 262 generating 6.1 kV/m at 50 m.

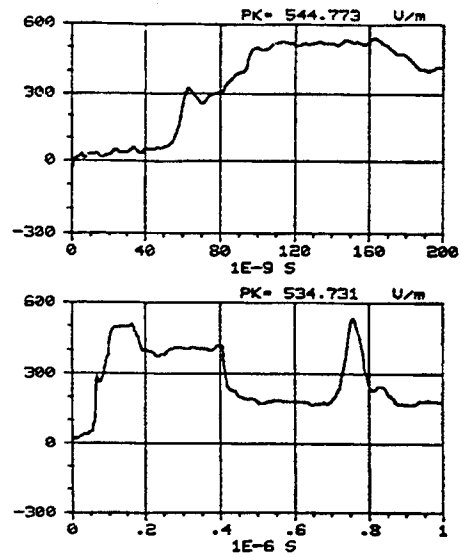


Figure C-228. Z component of the electric field measured at location 50/50/1 using sensor E304-C. REPS pulse 260 generating 6.1 kV/m at 50 m.

Appendix C, Symmetry data

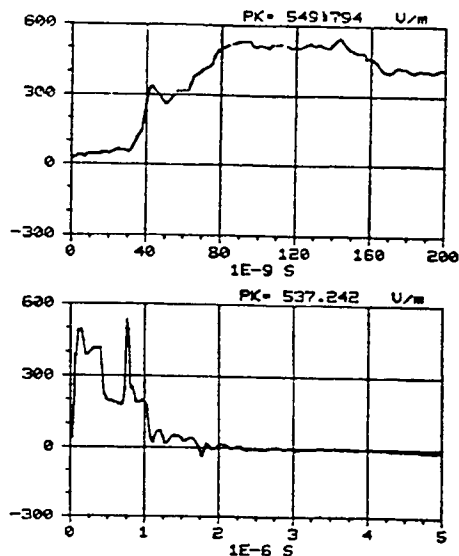


Figure C-229. Z component of the electric field measured at location 50/50/1 using sensor E304-C. REPS pulse 261 generating 6 kV/m at 50 m.

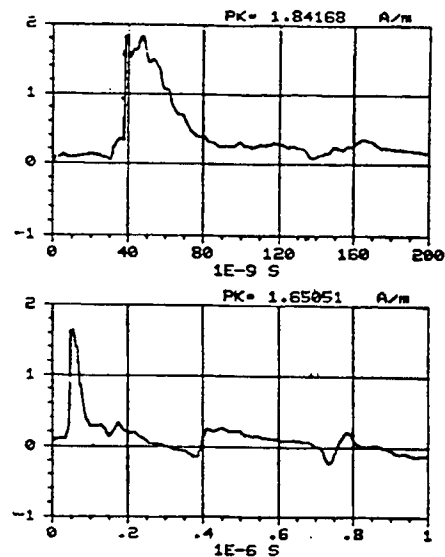


Figure C-230. X component of the magnetic field measured at location 50/50/1 using sensor H104-C. REPS pulse 254 generating 6.1 kV/m at 50 m.

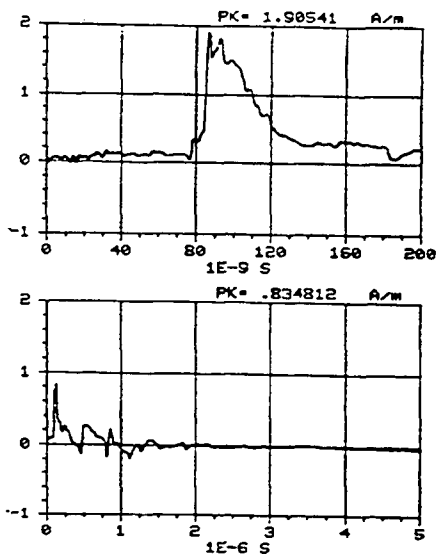


Figure C-231. X component of the magnetic field measured at location 50/50/1 using sensor H104-C. REPS pulse 255 generating 6 kV/m at 50 m.

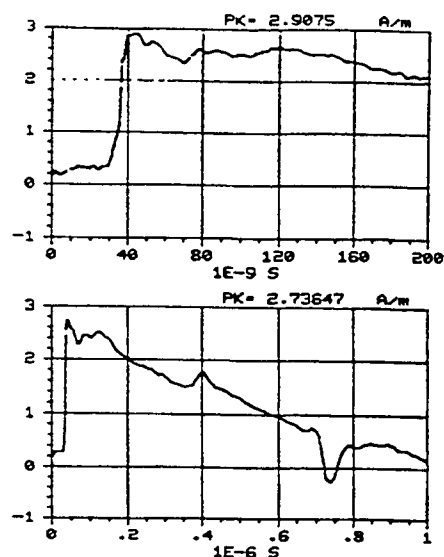


Figure C-232. Y component of the magnetic field measured at location 50/50/1 using sensor H104-C. REPS pulse 256 generating 6.3 kV/m at 50 m.

Appendix C, Symmetry data

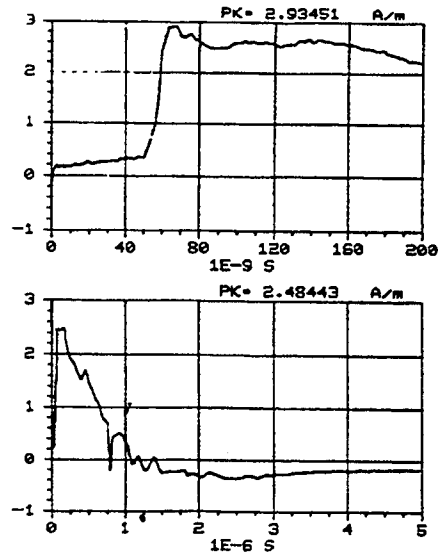


Figure C-233. Y component of the magnetic field measured at location 50/50/1 using sensor H104-C. REPS pulse 257 generating 6 kV/m at 50 m.

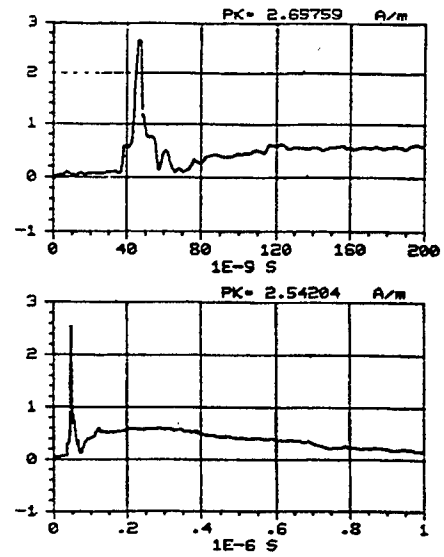


Figure C-234. Z component of the magnetic field measured at location 50/50/1 using sensor H104-C. REPS pulse 259 generating 6.2 kV/m at 50 m.

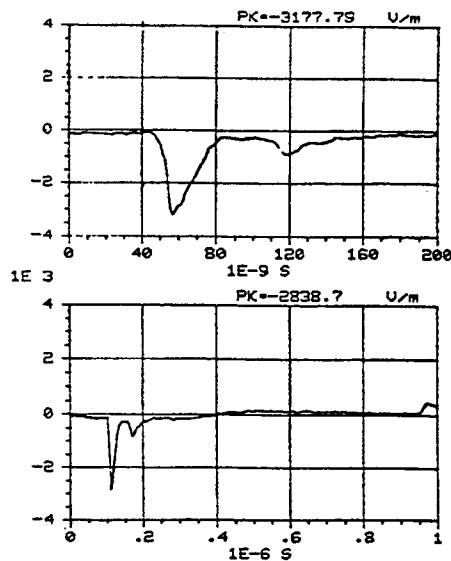


Figure C-235. -X component of the electric field measured at location 25/0/1 using sensor E403-C. REPS pulse 403 generating 6.2 kV/m at 50 m.

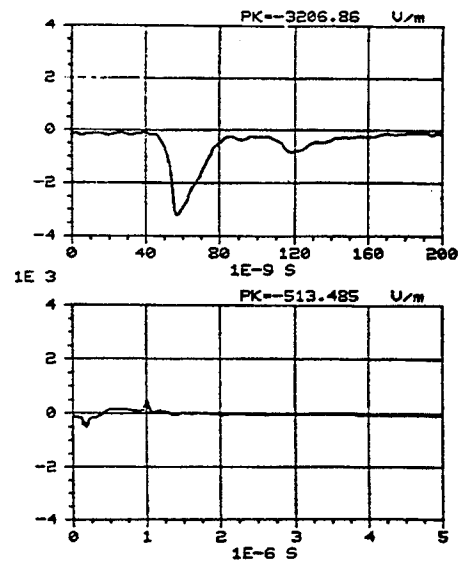


Figure C-236. -X component of the electric field measured at location 25/0/1 using sensor E403-C. REPS pulse 404 generating 6 kV/m at 50 m.

Appendix C, Symmetry data

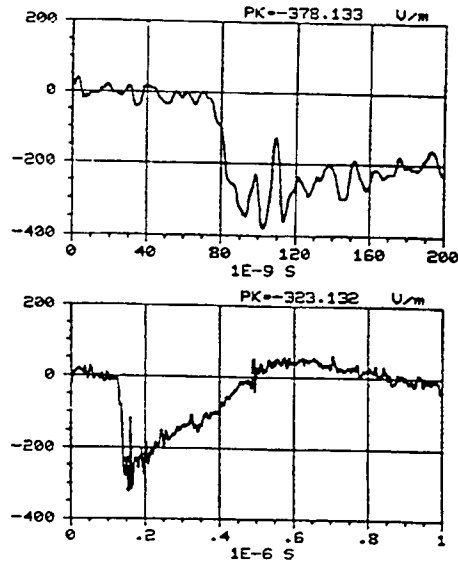


Figure C-237. -Y component of the electric field measured at location 25/0/1 using sensor E403-C. REPS pulse 407 generating 6.2 kV/m at 50 m.

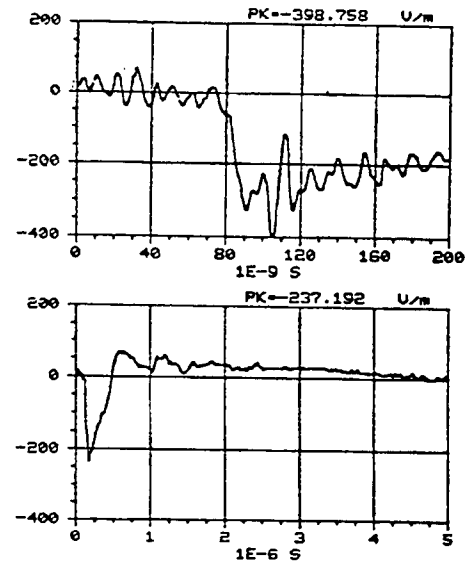


Figure C-238. -Y component of the electric field measured at location 25/0/1 using sensor E403-C. REPS pulse 408 generating 6.3 kV/m at 50 m.

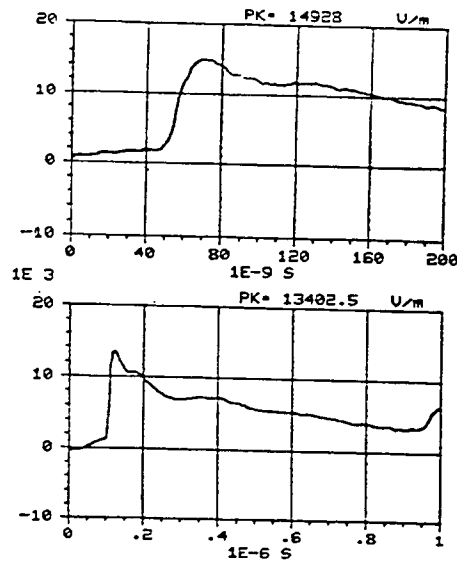


Figure C-239. Z component of the electric field measured at location 25/0/1 using sensor E403-C. REPS pulse 405 generating 6.3 kV/m at 50 m.

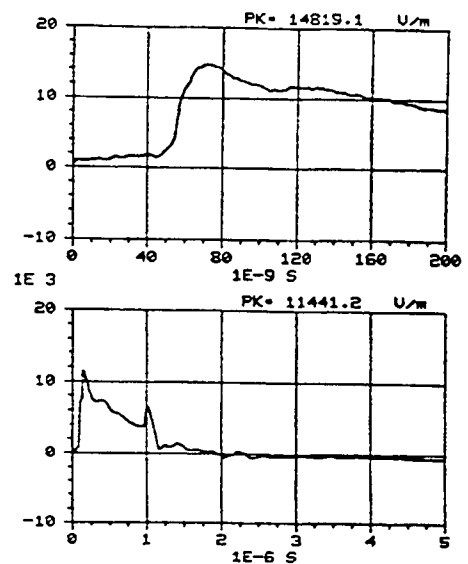


Figure C-240. Z component of the electric field measured at location 25/0/1 using sensor E403-C. REPS pulse 406 generating 6.2 kV/m at 50 m.

Appendix C, Symmetry data

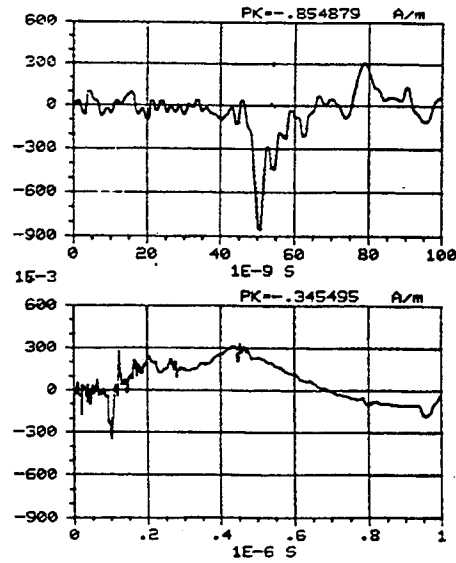


Figure C-241. -X component of the magnetic field measured at location 25/0/1 using sensor H104-C. REPS pulse 398 generating 6.2 kV/m at 50 m.

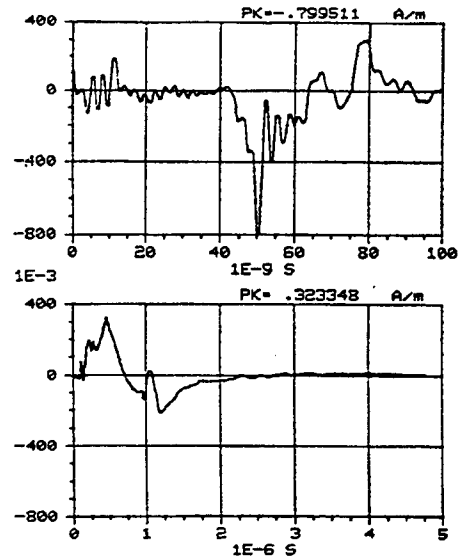


Figure C-242. -X component of the magnetic field measured at location 25/0/1 using sensor H104-C. REPS pulse 399 generating 6.2 kV/m at 50 m.

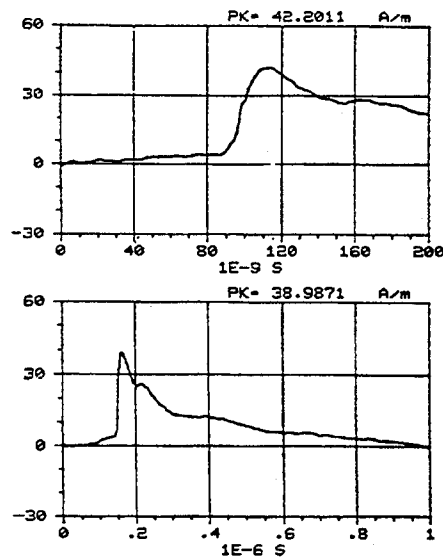


Figure C-243. Y component of the magnetic field measured at location 25/0/1 using sensor H104-C. REPS pulse 401 generating 6.2 kV/m at 50 m.

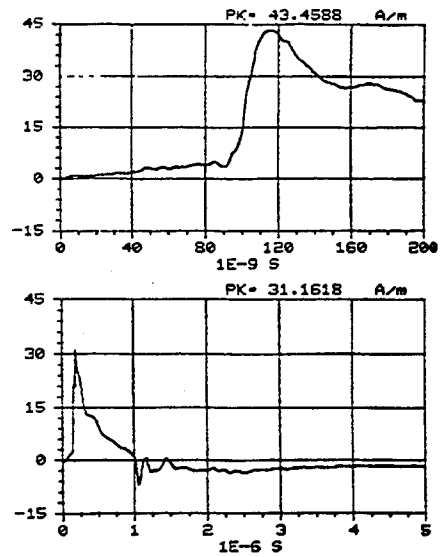


Figure C-244. Y component of the magnetic field measured at location 25/0/1 using sensor H104-C. REPS pulse 402 generating 6.2 kV/m at 50 m.

Appendix C, Symmetry data

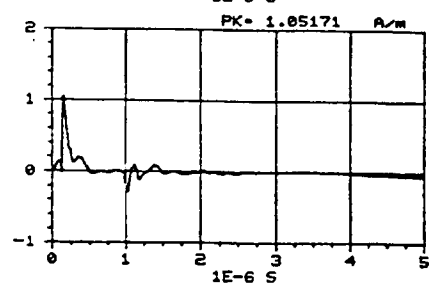
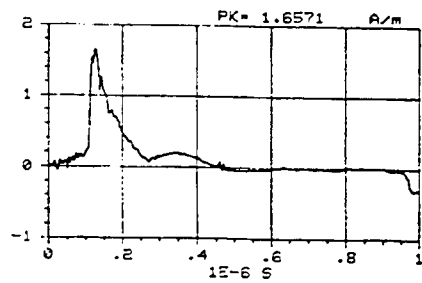
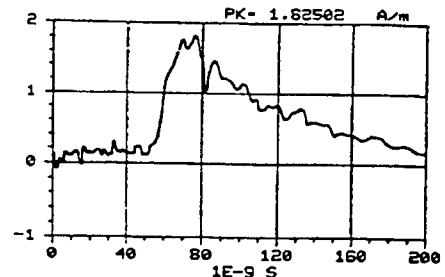
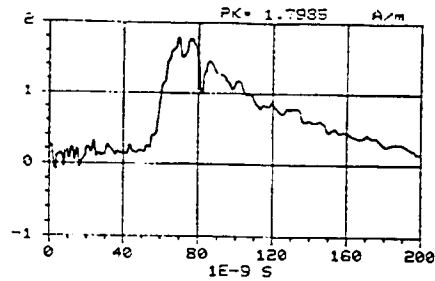


Figure C-245. Z component of the magnetic field measured at location 25/0/1 using sensor H104-C. REPS pulse 396 generating 6.2 kV/m at 50 m.

Figure C-246. Z component of the magnetic field measured at location 25/0/1 using sensor H104-C. REPS pulse 397 generating 6.2 kV/m at 50 m.

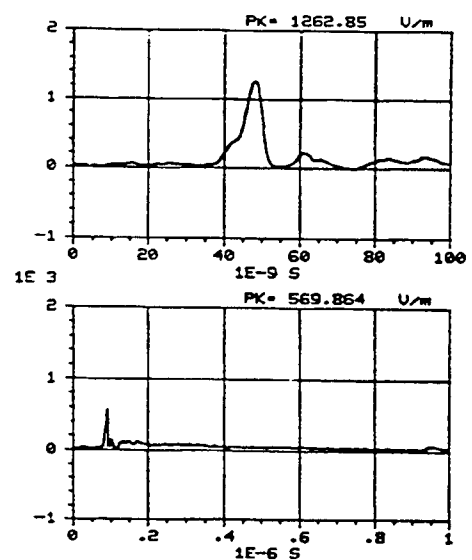
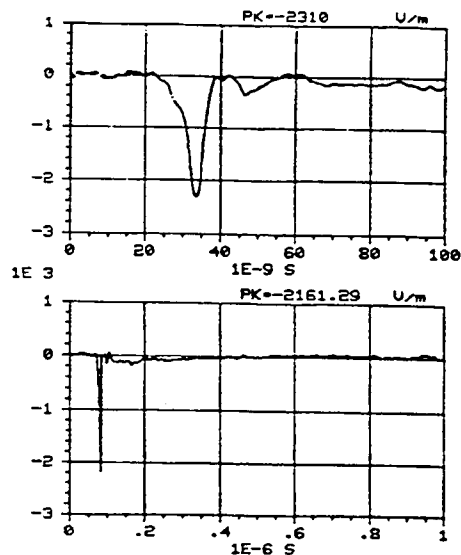


Figure C-247. -X component of the electric field measured at location 18/33/1 using sensor E304-C. REPS pulse 357 generating 6.2 kV/m at 50 m.

Figure C-248. -Y component of the electric field measured at location 18/33/1 using sensor E304-C. REPS pulse 360 generating 6.2 kV/m at 50 m.

Appendix C, Symmetry data

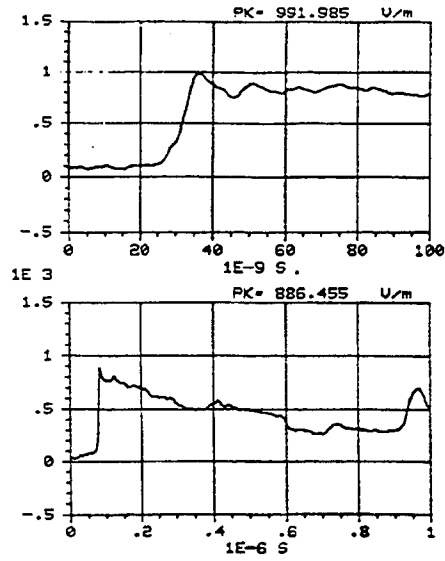


Figure C-249. Z component of the electric field measured at location 18/33/1 using sensor E304-C. REPS pulse 358 generating 6.1 kV/m at 50 m.

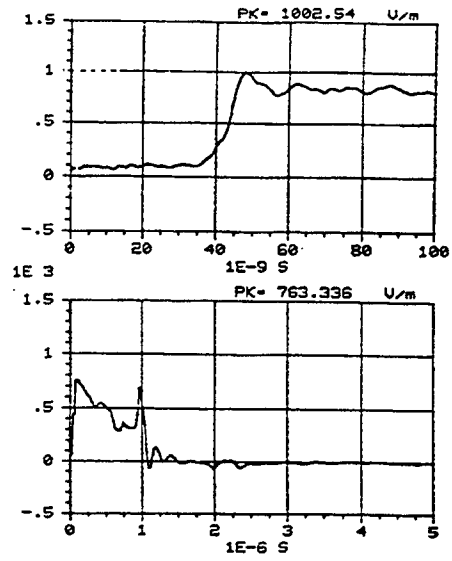


Figure C-250. Z component of the electric field measured at location 18/33/1 using sensor E304-C. REPS pulse 359 generating 6.1 kV/m at 50 m.

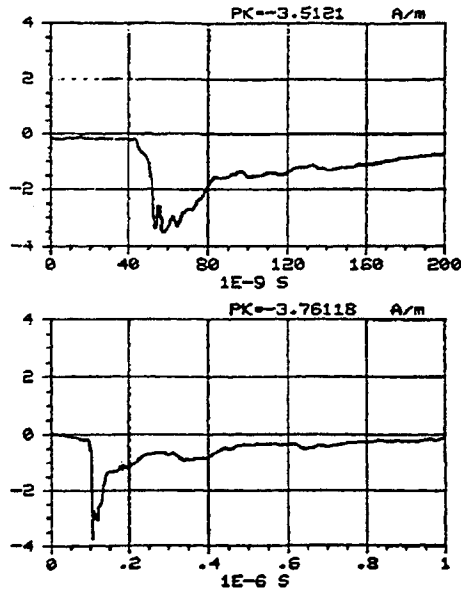


Figure C-251. X component of the magnetic field measured at location 18/33/1 using sensor H104-C. REPS pulse 353 generating 6.2 kV/m at 50 m.

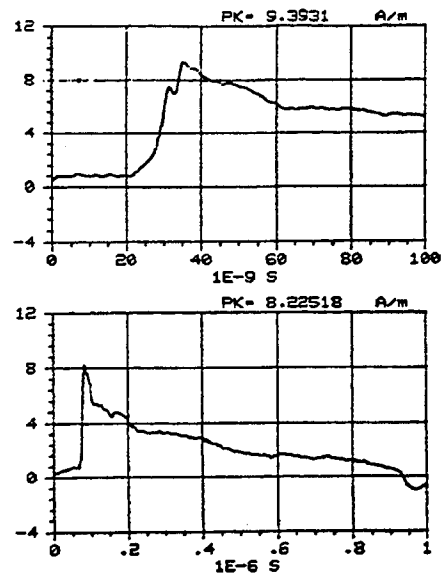


Figure C-252. Y component of the magnetic field measured at location 18/33/1 using sensor H104-C. REPS pulse 355 generating 6.3 kV/m at 50 m.

Appendix C, Symmetry data

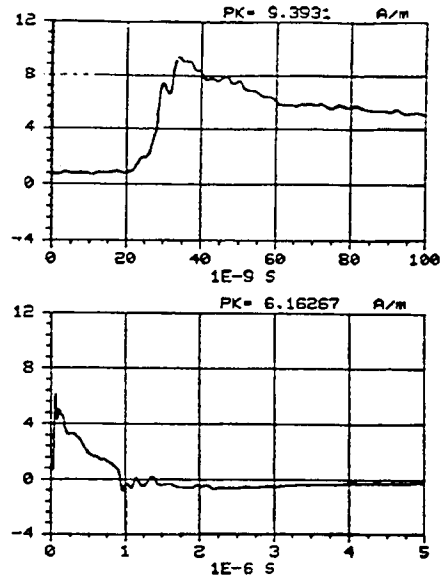


Figure C-253. Y component of the magnetic field measured at location 18/33/1 using sensor H104-C. REPS pulse 356 generating 6.3 kV/m at 50 m.

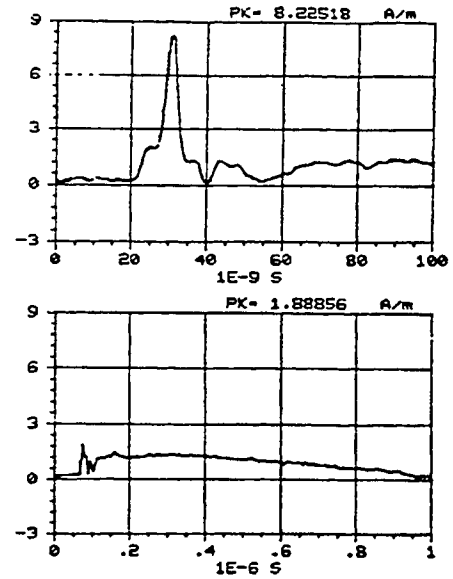


Figure C-254. Z component of the magnetic field measured at location 18/33/1 using sensor H104-C. REPS pulse 354 generating 6.1 kV/m at 50 m.

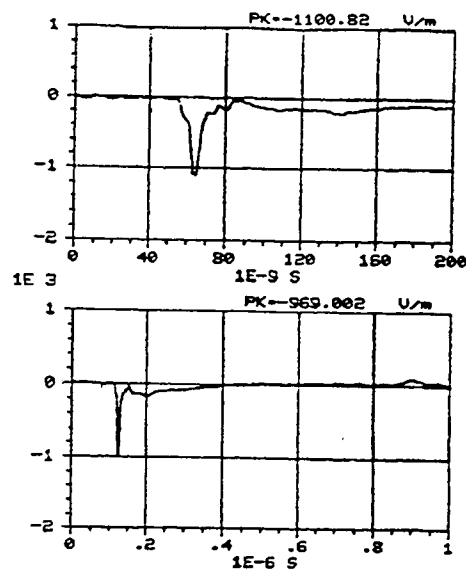


Figure C-255. -X component of the electric field measured at location 35/35/1 using sensor E304-C. REPS pulse 378 generating 6.3 kV/m at 50 m.

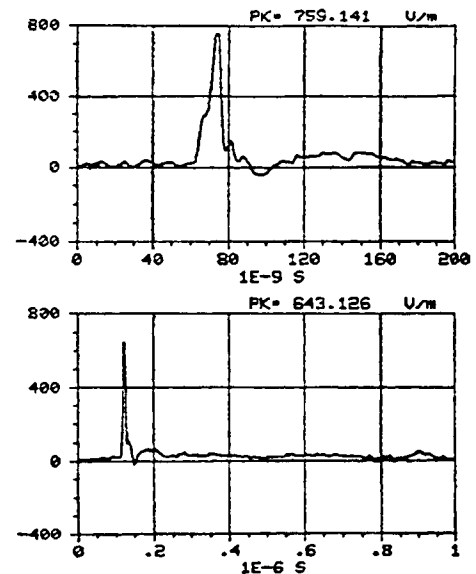


Figure C-256. -Y component of the electric field measured at location 35/35/1 using sensor E304-C. REPS pulse 385 generating 6.1 kV/m at 50 m.

Appendix C, Symmetry data

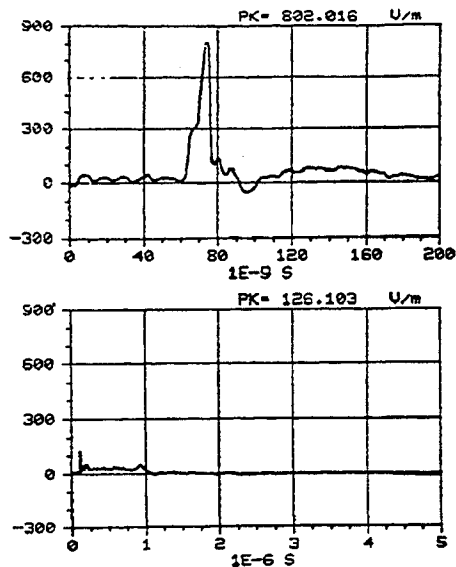


Figure C-257. -Y component of the electric field measured at location 35/35/1 using sensor E304-C. REPS pulse 384 generating 6.2 kV/m at 50 m.

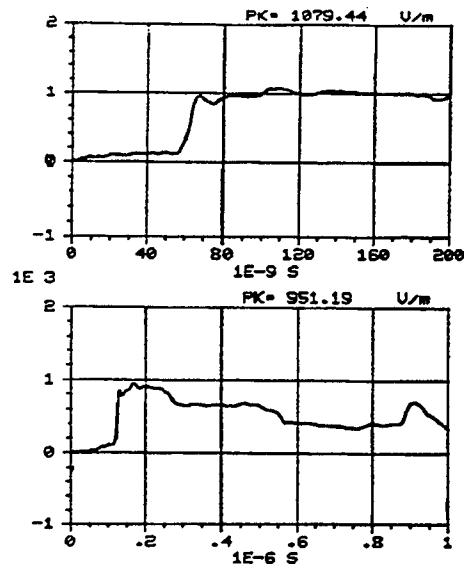


Figure C-258. Z component of the electric field measured at location 35/35/1 using sensor E304-C. REPS pulse 380 generating 6.1 kV/m at 50 m.

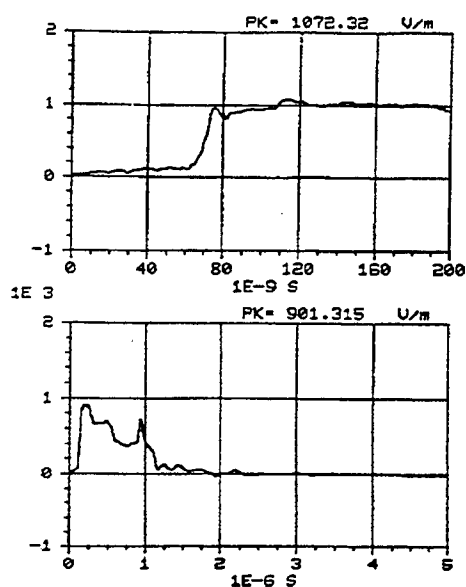


Figure C-259. Z component of the electric field measured at location 35/35/1 using sensor E304-C. REPS pulse 383 generating 6.2 kV/m at 50 m.

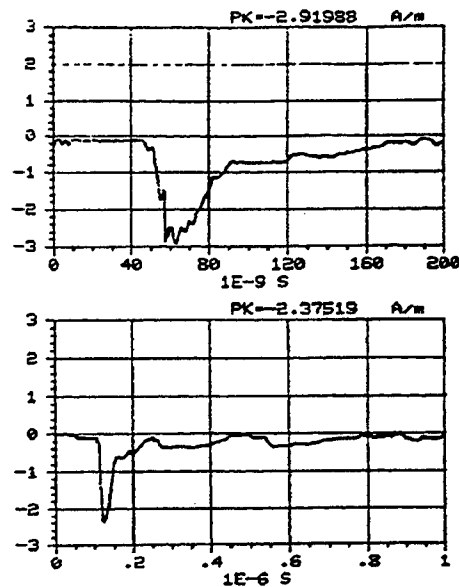


Figure C-260. -X component of the magnetic field measured at location 35/35/1 using sensor H104-C. REPS pulse 372 generating 6.3 kV/m at 50 m.

Appendix C, Symmetry data

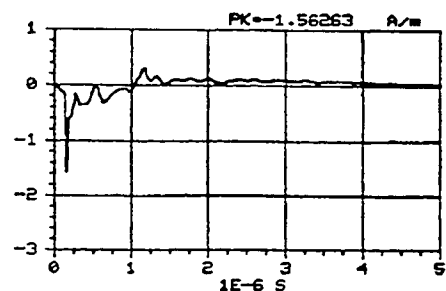
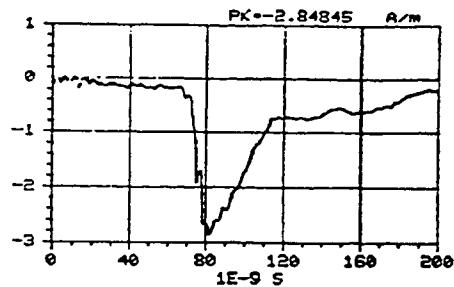


Figure C-261. -X component of the magnetic field measured at location 35/35/1 using sensor H104-C. REPS pulse 373 generating 6.2 kV/m at 50 m.

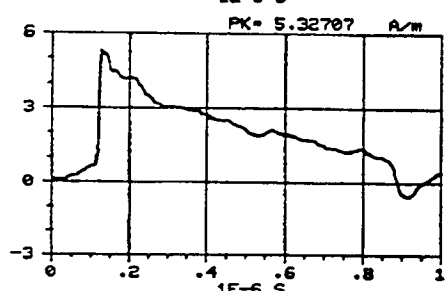
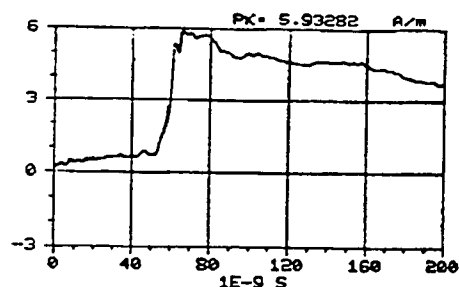


Figure C-262. Y component of the magnetic field measured at location 35/35/1 using sensor H104-C. REPS pulse 276 generating 6.3 kV/m at 50 m.

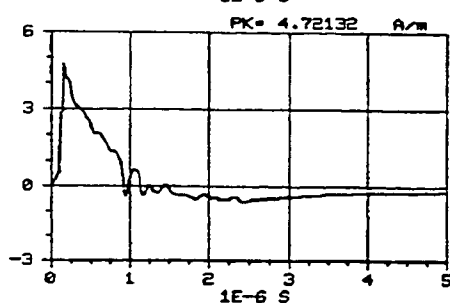
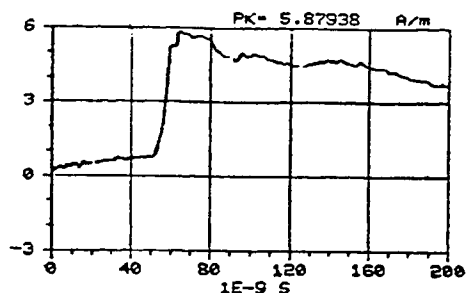


Figure C-263. Y component of the magnetic field measured at location 35/35/1 using sensor H104-C. REPS pulse 377 generating 6.2 kV/m at 50 m.

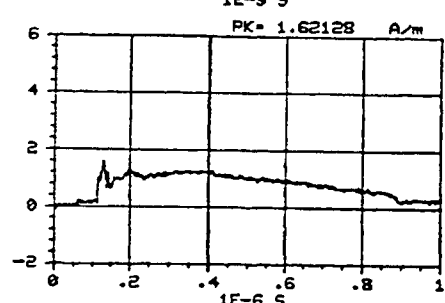
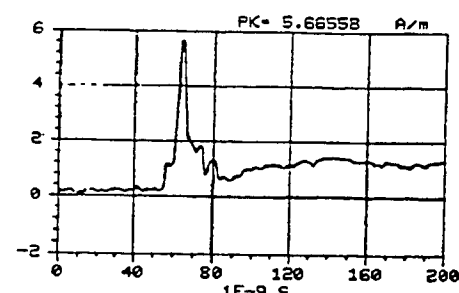


Figure C-264. Z component of the magnetic field measured at location 35/35/1 using sensor H104-C. REPS pulse 374 generating 6.2 kV/m at 50 m.

Appendix C, Symmetry data

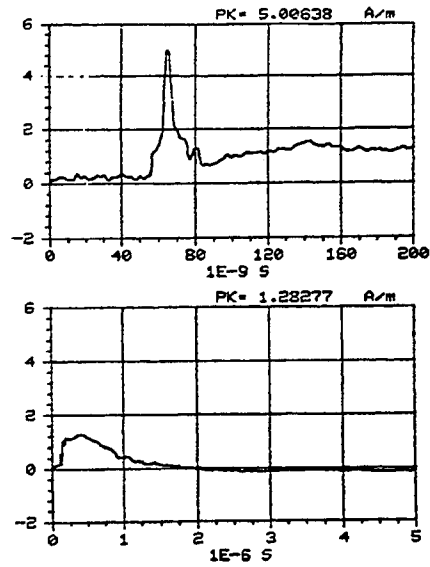


Figure C-265. Z component of the magnetic field measured at location 35/35/1 using sensor H104-C. REPS pulse 375 generating 6 kV/m at 50 m.

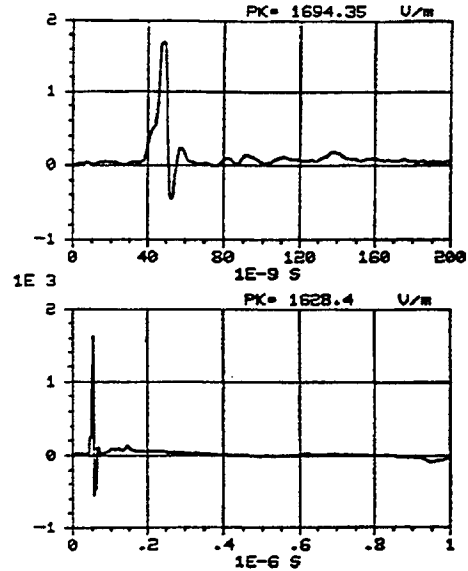


Figure C-266. X component of the electric field measured at location 0/-50/1 using sensor E304-C. REPS pulse 270 generating 6.3 kV/m at 50 m.

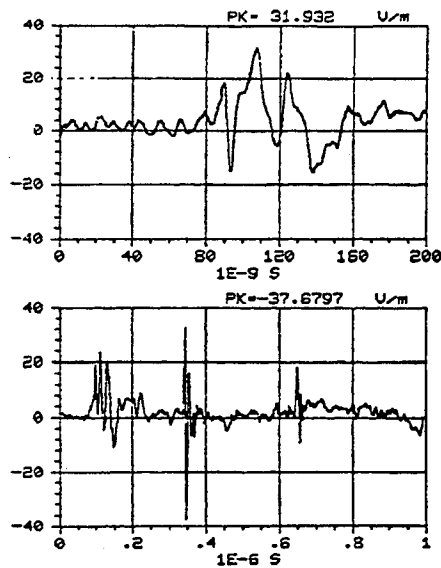


Figure C-267. Y component of the electric field measured at location 0/-50/1 using sensor E304-C. REPS pulse 273 generating 6.2 kV/m at 50 m.

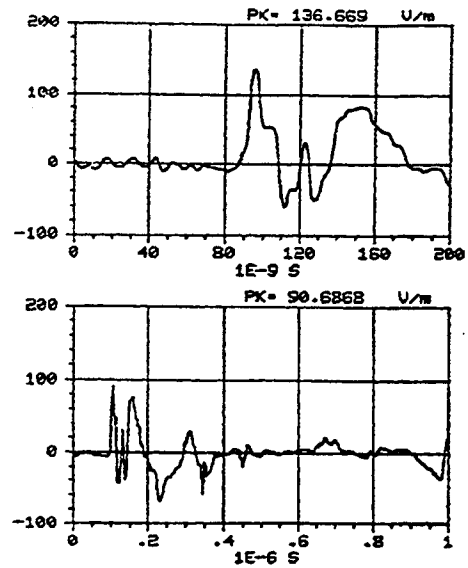


Figure C-268. Z component of the electric field measured at location 0/-50/1 using sensor E304-C. REPS pulse 271 generating 6.3 kV/m at 50 m.

Appendix C, Symmetry data

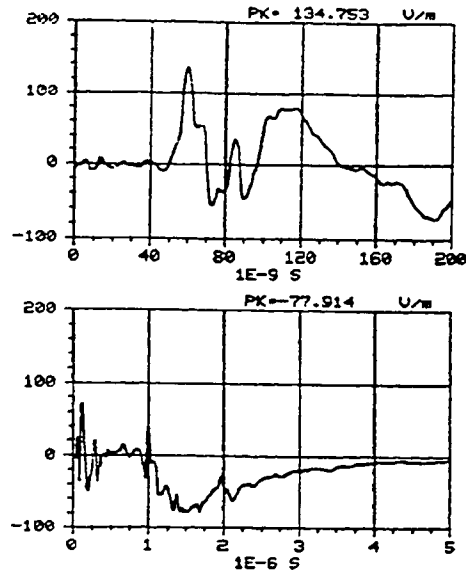


Figure C-269. Z component of the electric field measured at location 0/-50/1 using sensor E304-C. REPS pulse 272 generating 6.2 kV/m at 50 m.

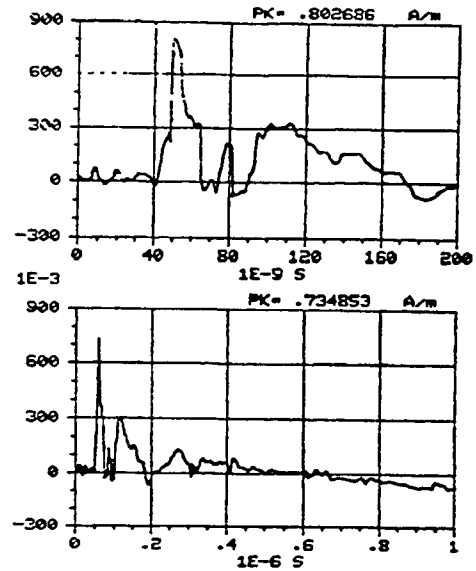


Figure C-270. X component of the magnetic field measured at location 0/-50/1 using sensor H104-C. REPS pulse 274 generating 6.4 kV/m at 50 m.

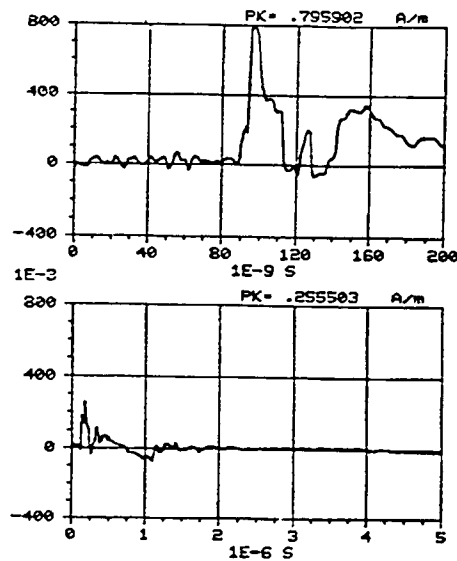


Figure C-271. X component of the magnetic field measured at location 0/-50/1 using sensor H104-C. REPS pulse 275 generating 6.3 kV/m at 50 m.

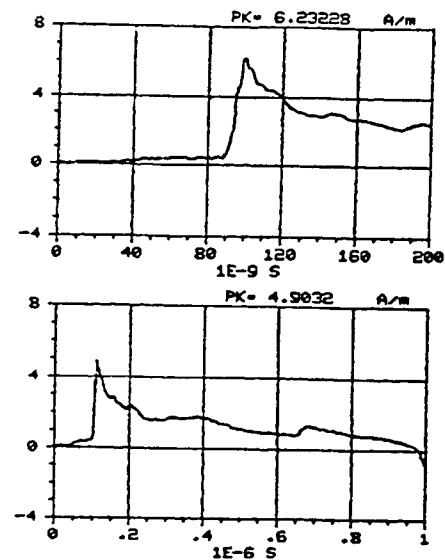


Figure C-272. Y component of the magnetic field measured at location 0/-50/1 using sensor H104-C. REPS pulse 276 generating 6.3 kV/m at 50 m.

Appendix C, Symmetry data

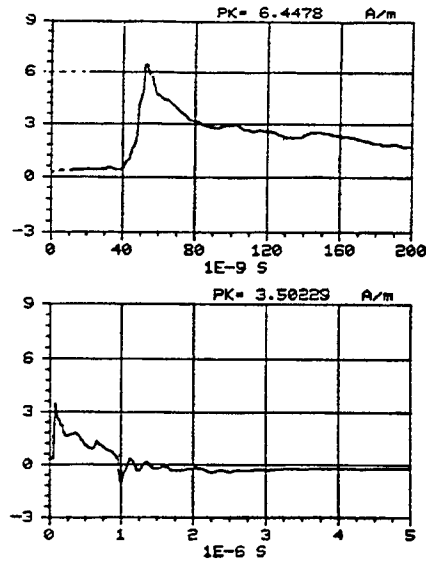


Figure C-273. Y component of the magnetic field measured at location 0/-50/1 using sensor H104-C. REPS pulse 277 generating 6.2 kV/m at 50 m.

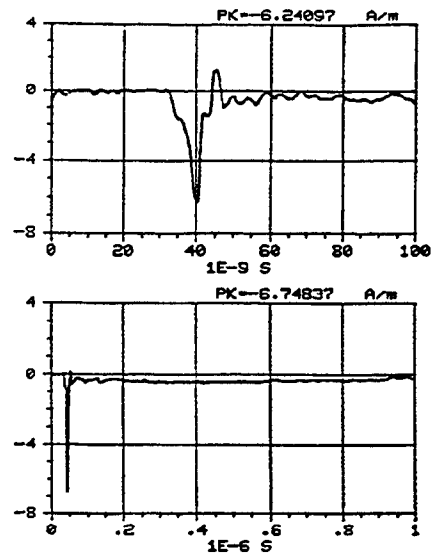


Figure C-274. Z component of the magnetic field measured at location 0/-50/1 using sensor H104-C. REPS pulse 278 generating 6.2 kV/m at 50 m.

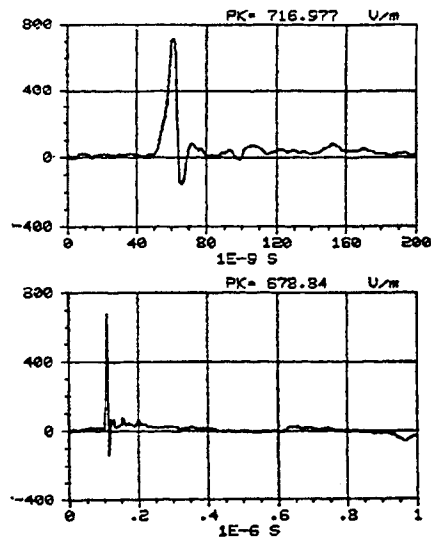


Figure C-275. X component of the electric field measured at location 0/-75/1 using sensor E304-C. REPS pulse 387 generating 6.3 kV/m at 50 m.

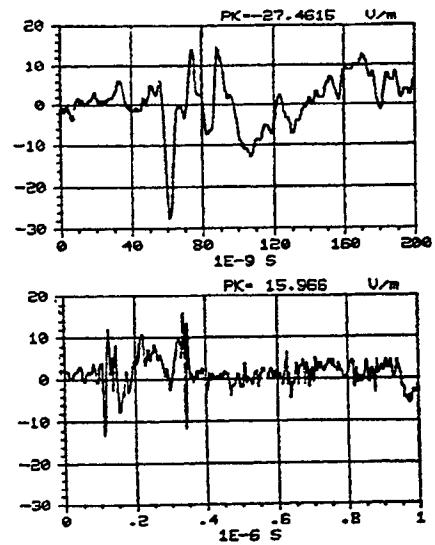


Figure C-276. Y component of the electric field measured at location 0/-75/1 using sensor E304-C. REPS pulse 390 generating 6.2 kV/m at 50 m.

Appendix C, Symmetry data

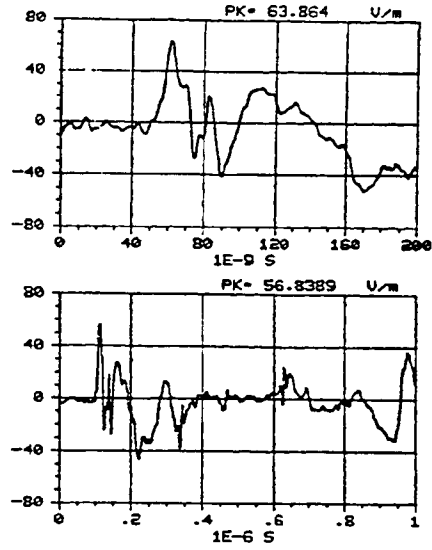


Figure C-277. Z component of the electric field measured at location 0/-75/1 using sensor E304-C. REPS pulse 388 generating 6.4 kV/m at 50 m.

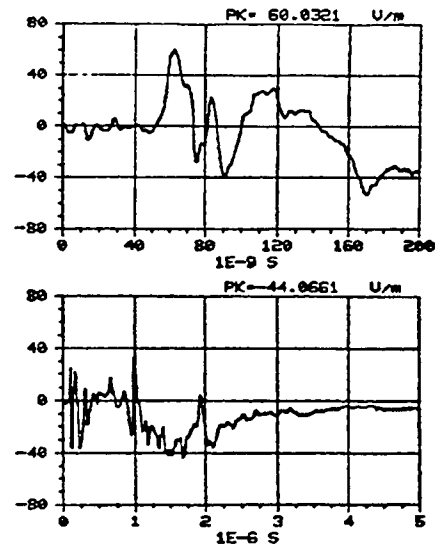


Figure C-278. Z component of the electric field measured at location 0/-75/1 using sensor E304-C. REPS pulse 389 generating 6.3 kV/m at 50 m.

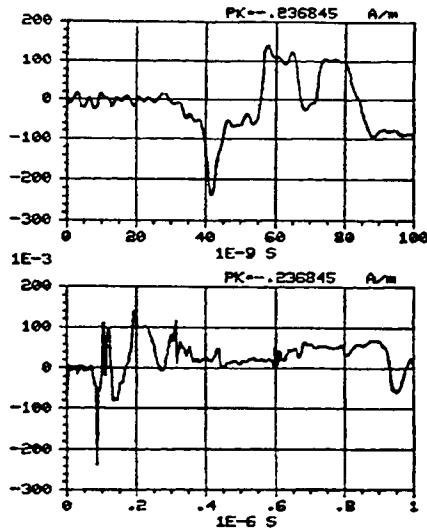


Figure C-279. -X component of the magnetic field measured at location 0/-75/1 using sensor H104-C. REPS pulse 392 generating 6.3 kV/m at 50 m.

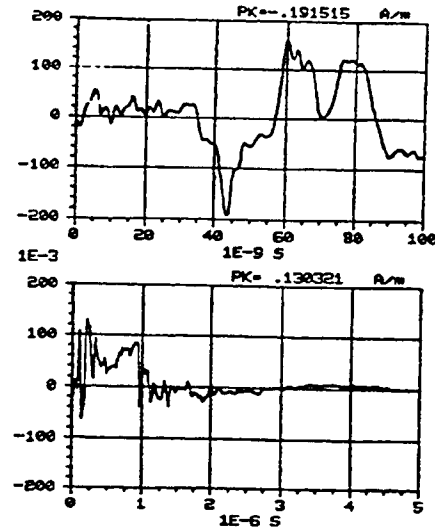


Figure C-280. -X component of the magnetic field measured at location 0/-75/1 using sensor H104-C. REPS pulse 393 generating 6.1 kV/m at 50 m.

Appendix C, Symmetry data

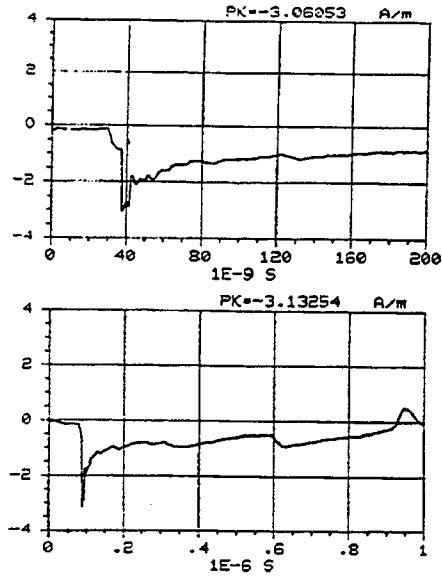


Figure C-281. -Y component of the magnetic field measured at location 0/-75/1 using sensor H104-C. REPS pulse 394 generating 6.3 kV/m at 50 m.

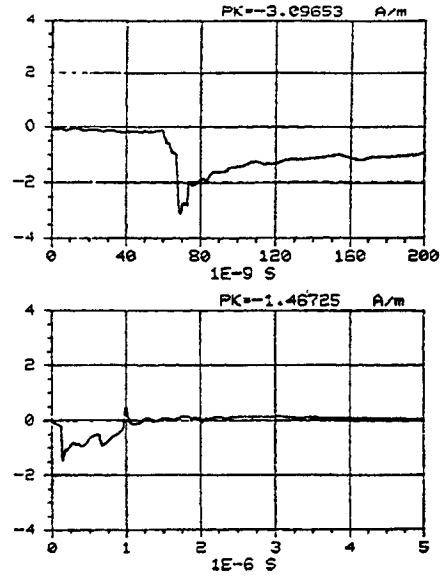


Figure C-282. -Y component of the magnetic field measured at location 0/-75/1 using sensor H104-C. REPS pulse 395 generating 6.2 kV/m at 50 m.

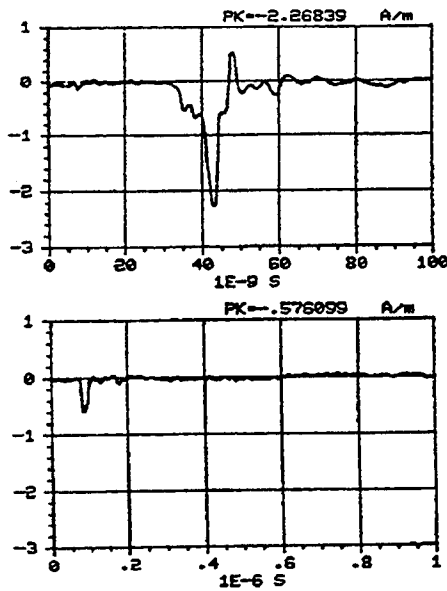


Figure C-283. Z component of the magnetic field measured at location 0/-75/1 using sensor H104-C. REPS pulse 391 generating 6.1 kV/m at 50 m.

Appendix C, Arc data

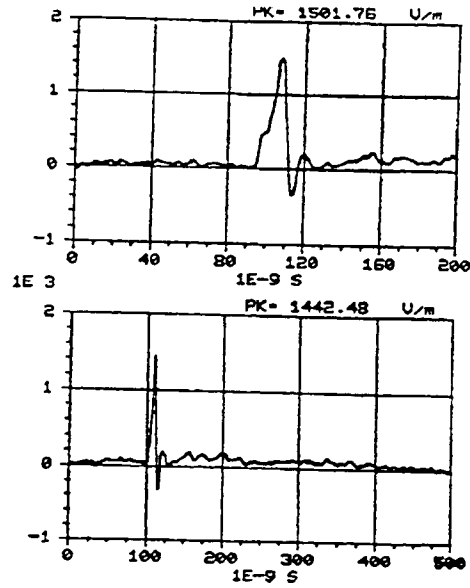


Figure C-284. X component of the electric field measured at location 0/50/1 using sensor E304-C. REPS pulse 47 generating 6.1 kV/m at 50 m.

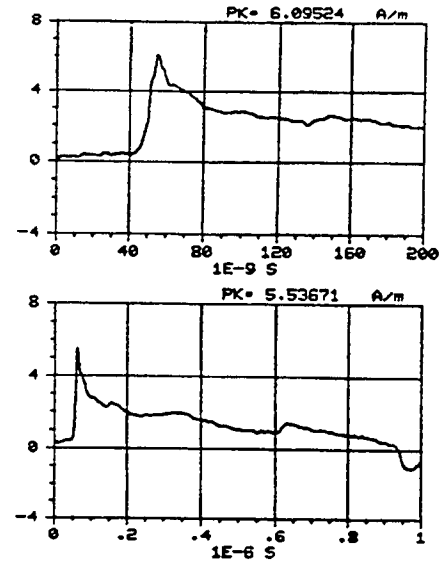


Figure C-285. Y component of the magnetic field measured at location 0/50/1 using sensor H104-C. REPS pulse 13 generating 6.3 kV/m at 50 m.

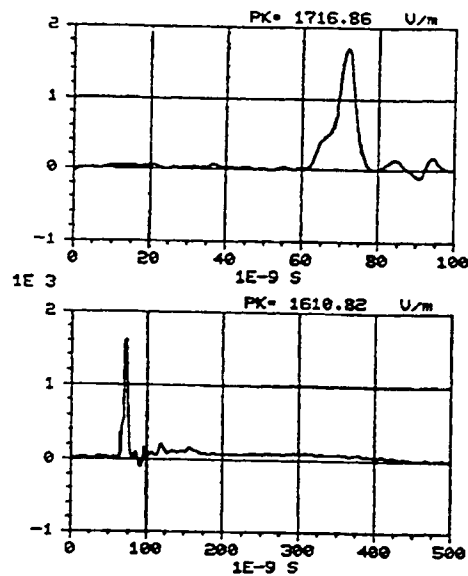


Figure C-286. T component of the electric field measured at location -19/46/1 using sensor E304-C. REPS pulse 309 generating 6.2 kV/m at 50 m.

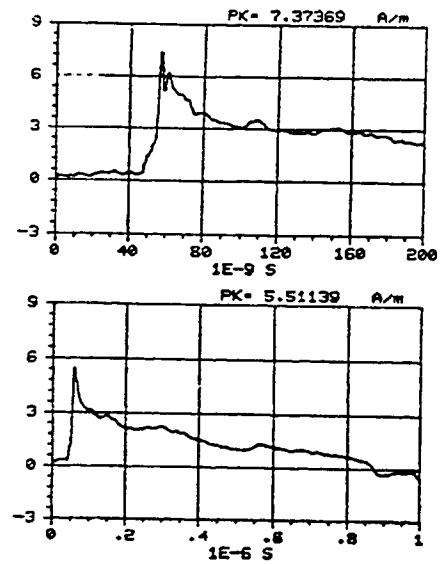


Figure C-287. R component of the magnetic field measured at location -19/46/1 using sensor H104-C. REPS pulse 305 generating 6.1 kV/m at 50 m.

Appendix C, Arc data

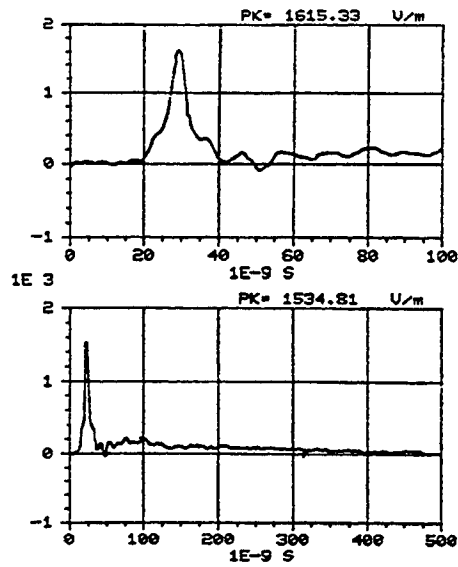


Figure C-288. *T* component of the electric field measured at location -35/35/1 using sensor E304-C. REPS pulse 293 generating 6.2 kV/m at 50 m.

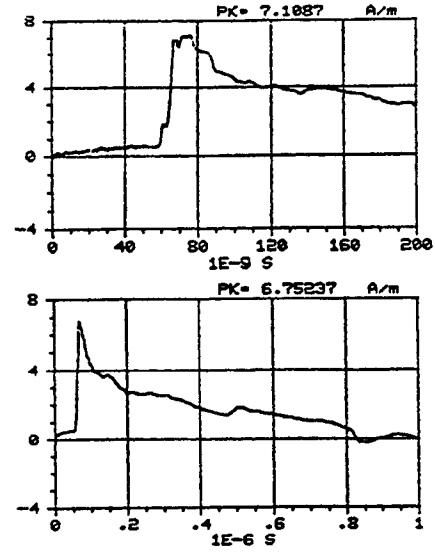


Figure C-289. *R* component of the magnetic field measured at location -35/35/1 using sensor H104-C. REPS pulse 298 generating 6.4 kV/m at 50 m.

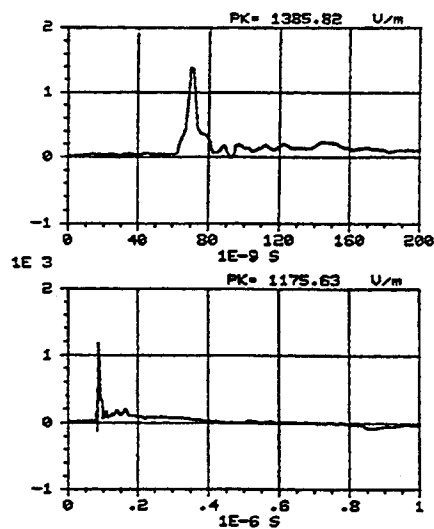


Figure C-290. *X* component of the electric field measured at location -35/35/1 using sensor E304-C. REPS pulse 287 generating 6.3 kV/m at 50 m.

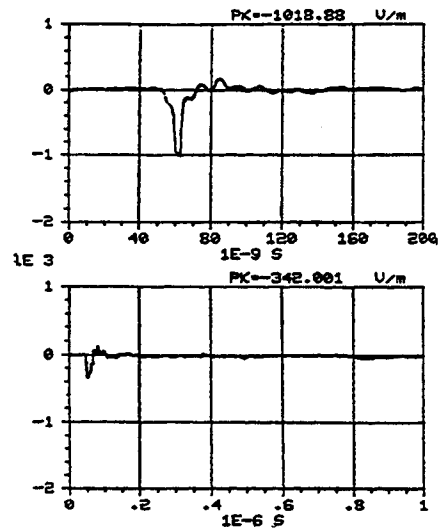


Figure C-291. *-Y* component of the electric field measured at location -35/35/1 using sensor E304-C. REPS pulse 292 generating 6.5 kV/m at 50 m.

Appendix C, Arc data

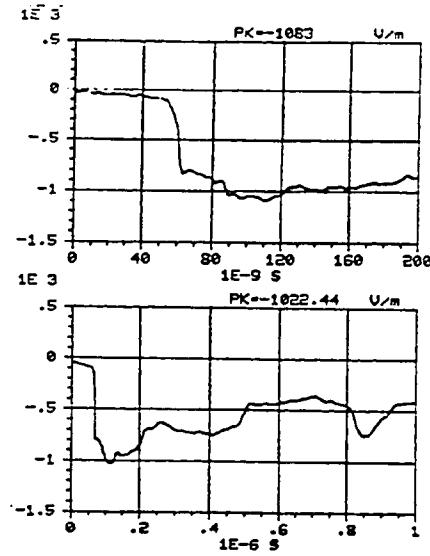


Figure C-292. Z component of the electric field measured at location -35/35/1 using sensor E304-C. REPS pulse 288 generating 6.3 kV/m at 50 m.

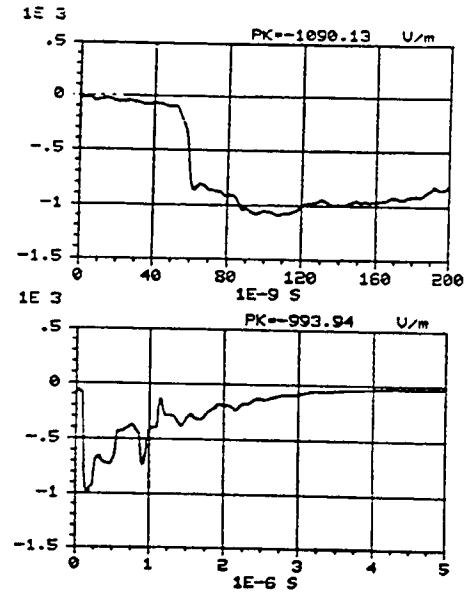


Figure C-293. Z component of the electric field measured at location -35/35/1 using sensor E304-C. REPS pulse 289 generating 6.3 kV/m at 50 m.

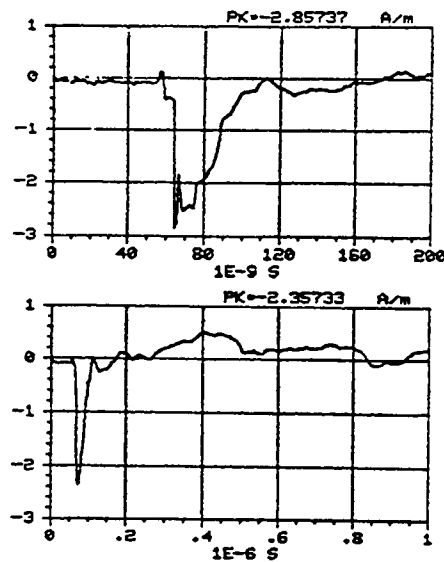


Figure C-294. X component of the magnetic field measured at location -35/35/1 using sensor H104-C. REPS pulse 300 generating 6.2 kV/m at 50 m.

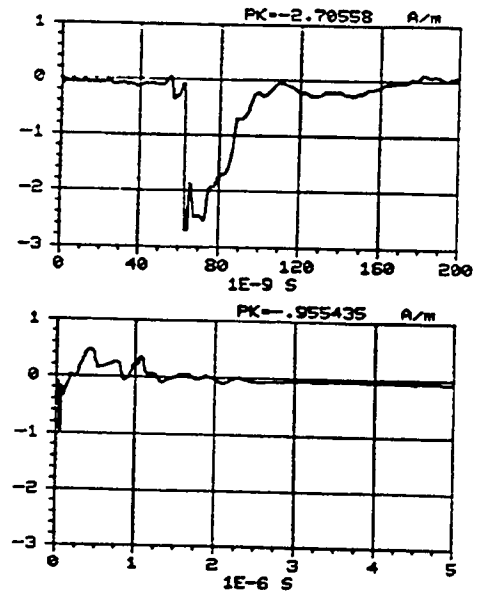


Figure C-295. X component of the magnetic field measured at location -35/35/1 using sensor H104-C. REPS pulse 301 generating 6.2 kV/m at 50 m.

Appendix C, Arc data

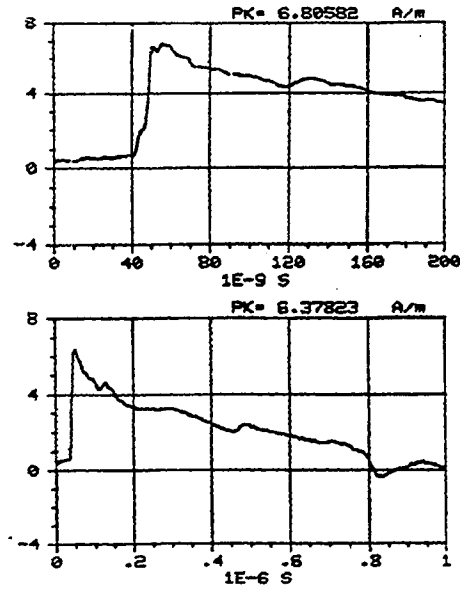


Figure C-296. Y component of the magnetic field measured at location -35/35/1 using sensor H104-C. REPS pulse 303 generating 6.4 kV/m at 50 m.

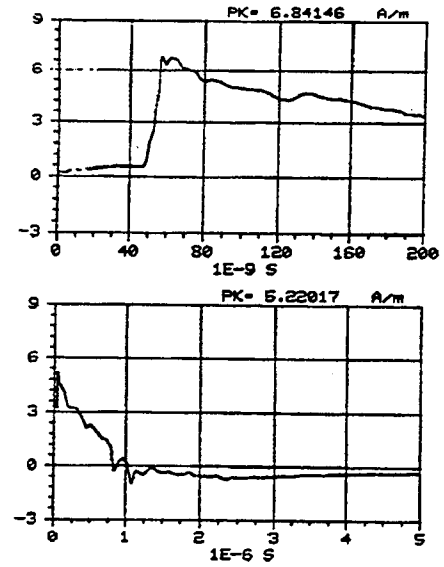


Figure C-297. Y component of the magnetic field measured at location -35/35/1 using sensor H104-C. REPS pulse 304 generating 6.2 kV/m at 50 m.

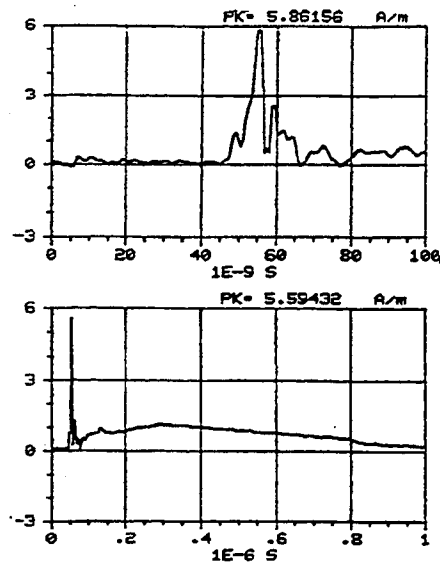


Figure C-298. Z component of the magnetic field measured at location -35/35/1 using sensor H104-C. REPS pulse 302 generating 6.3 kV/m at 50 m.

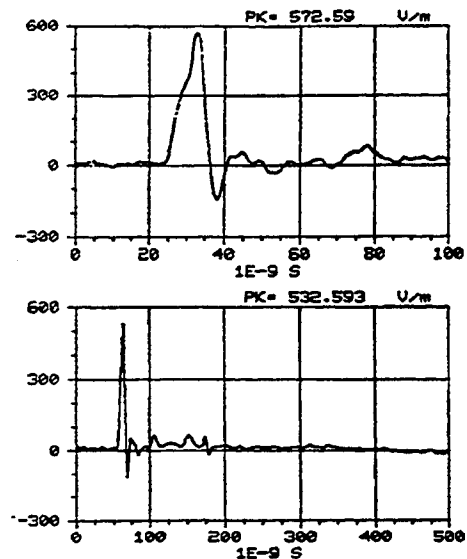


Figure C-299. X component of the electric field measured at location 0/85/1 using sensor E201-C. REPS pulse 324 generating 6.1 kV/m at 50 m.

Appendix C, Arc data

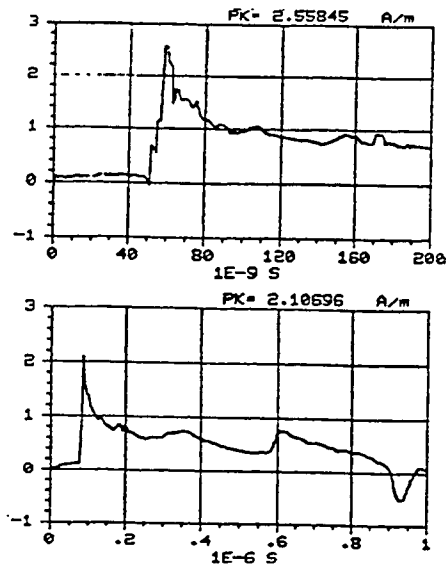


Figure C-300. Y component of the magnetic field measured at location 0/85/1 using sensor H104-C. REPS pulse 326 generating 6.2 kV/m at 50 m.

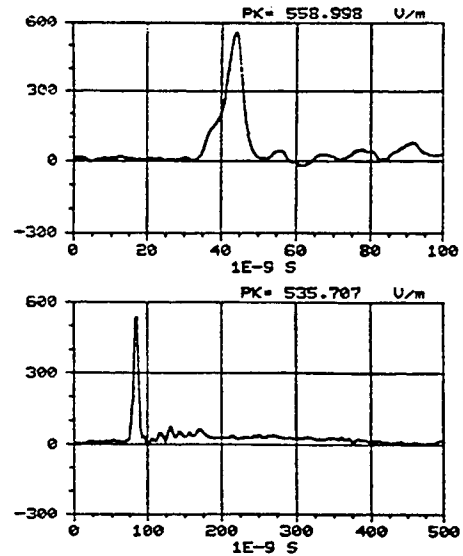


Figure C-301. T component of the electric field measured at location -33/79/1 using sensor E304-C. REPS pulse 314 generating 6.2 kV/m at 50 m.

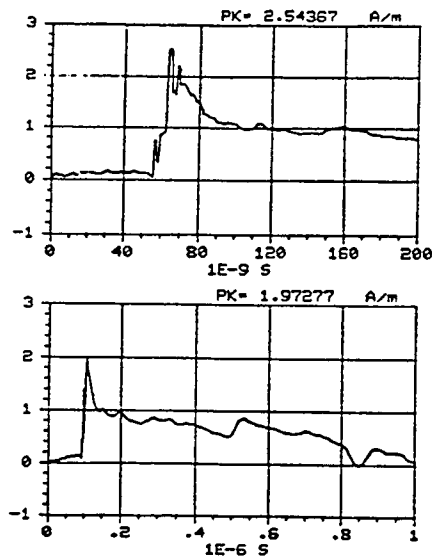


Figure C-302. R component of the magnetic field measured at location -33/79/1 using sensor H104-C. REPS pulse 316 generating 6.1 kV/m at 50 m.

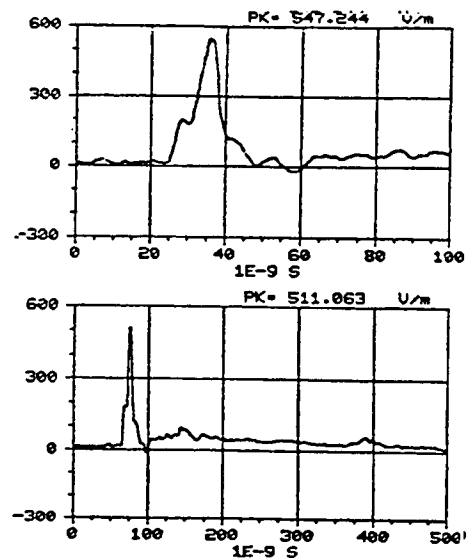


Figure C-303. T component of the electric field measured at location -60/60/1 using sensor E201-C. REPS pulse 320 generating 6 kV/m at 50 m.

Appendix C, Arc data

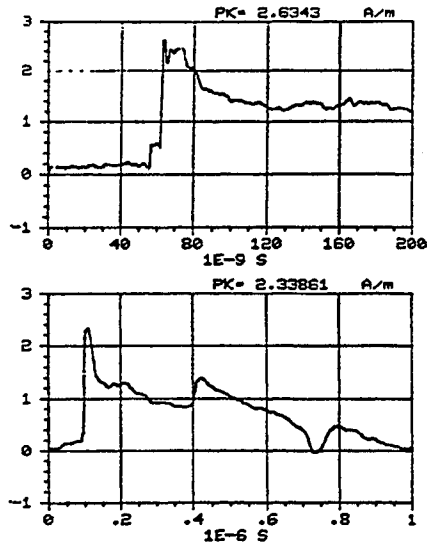


Figure C-304. R component of the magnetic field measured at location -60/60/1 using sensor H104-C. REPS pulse 318 generating 6.3 kV/m at 50 m.

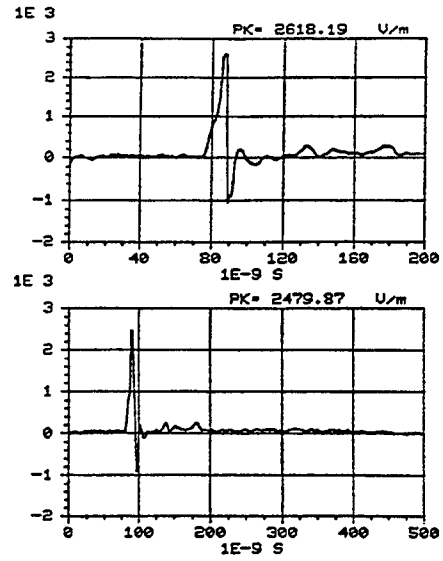


Figure C-305. X component of the electric field measured at location 0/50/2 using sensor E304-C. REPS pulse 48 generating 6.2 kV/m at 50 m.

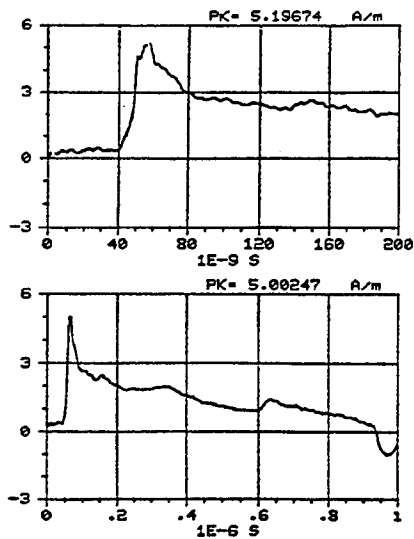


Figure C-306. Y component of the magnetic field measured at location 0/50/2 using sensor H104-C. REPS pulse 19 generating 6.3 kV/m at 50 m.

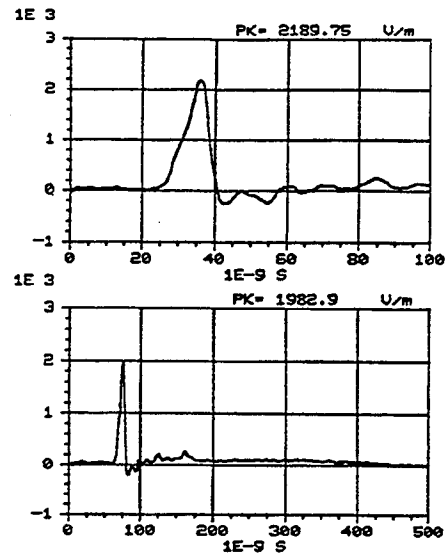


Figure C-307. T component of the electric field measured at location -19/46/2 using sensor E304-C. REPS pulse 313 generating 6.2 kV/m at 50 m.

Appendix C, Arc data

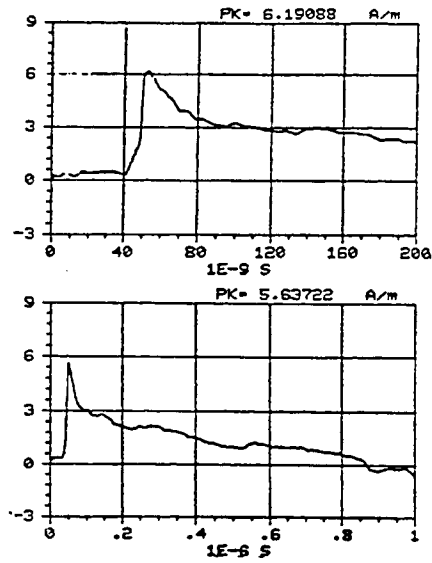


Figure C-308. R component of the magnetic field measured at location -19/46/2 using sensor H104-C. REPS pulse 306 generating 6.2 kV/m at 50 m.

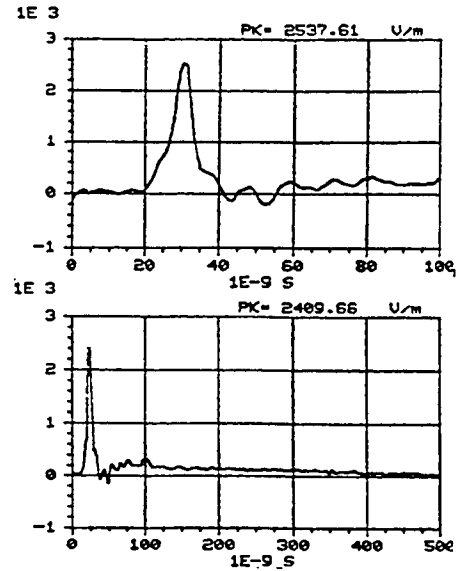


Figure C-309. T component of the electric field measured at location -35/35/1 using sensor E304-C. REPS pulse 295 generating 6.3 kV/m at 50 m.

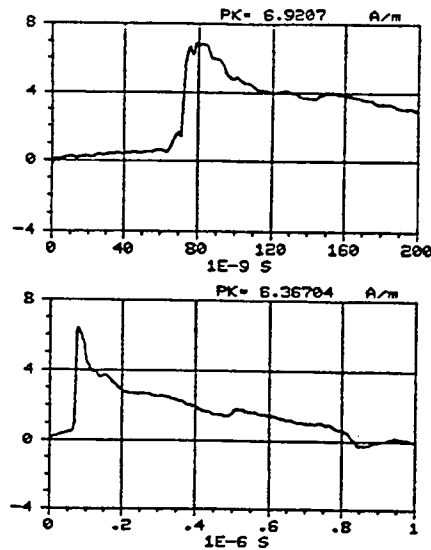


Figure C-310. R component of the magnetic field measured at location -35/35/1 using sensor H104-C. REPS pulse 299 generating 6.3 kV/m at 50 m.

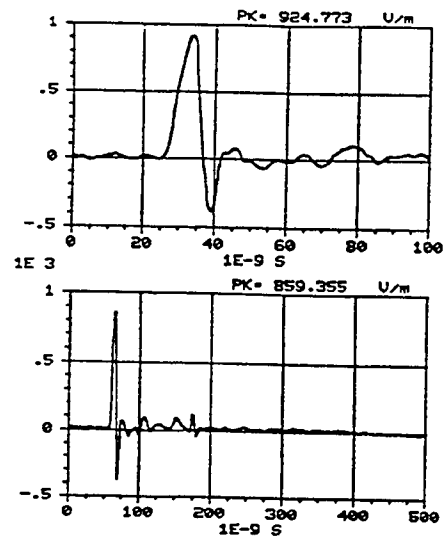


Figure C-311. X component of the electric field measured at location 0/85/2 using sensor E201-C. REPS pulse 325 generating 6.3 kV/m at 50 m.

Appendix C, Arc data

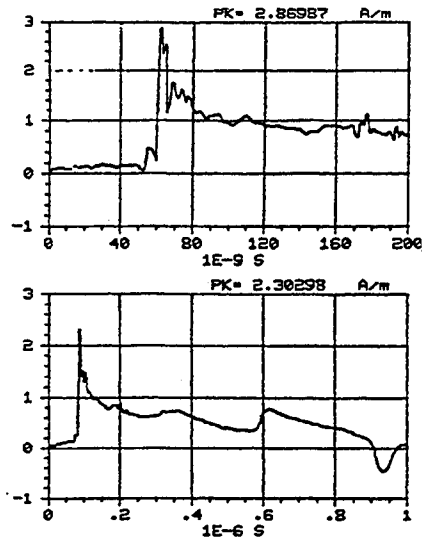


Figure C-312. Y component of the magnetic field measured at location 0/85/2 using sensor H104-C. REPS pulse 328 generating 6.3 kV/m at 50 m.

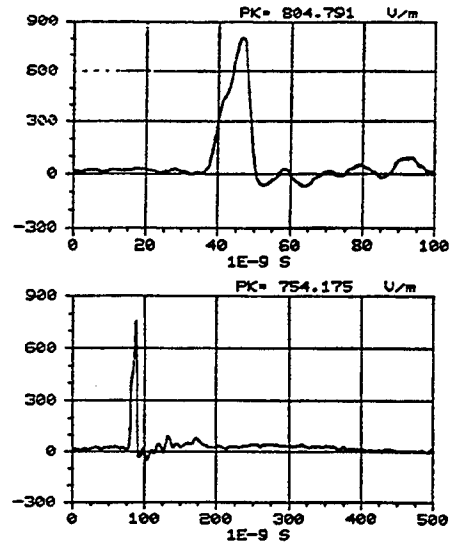


Figure C-313. T component of the electric field measured at location -33/79/2 using sensor E304-C. REPS pulse 315 generating 6.1 kV/m at 50 m.

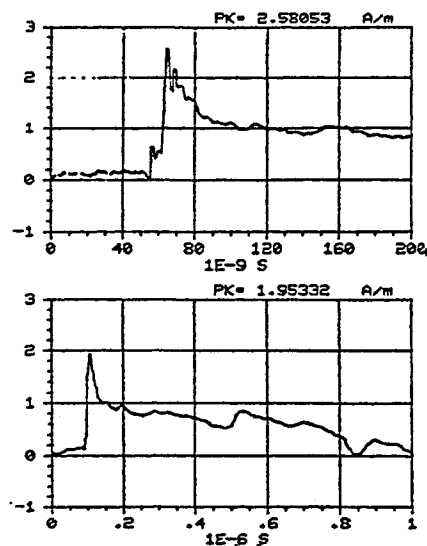


Figure C-314. R component of the magnetic field measured at location -33/79/2 using sensor H104-C. REPS pulse 317 generating 6.2 kV/m at 50 m.

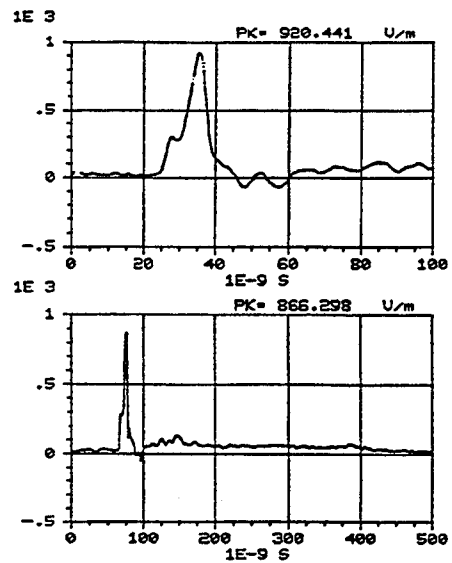


Figure C-315. T component of the electric field measured at location -60/60/2 using sensor E201-C. REPS pulse 322 generating 6.2 kV/m at 50 m.

Appendix C, Arc data

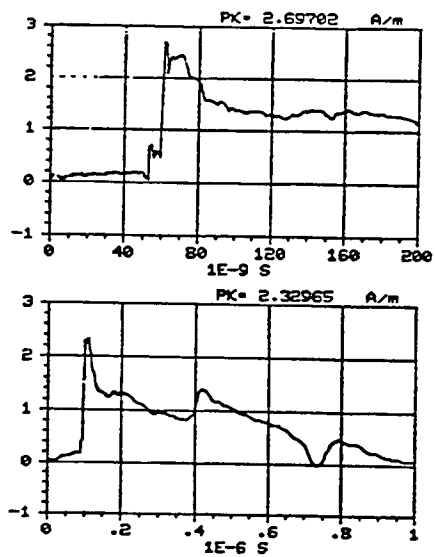


Figure C-316. R component of the magnetic field measured at location -60/60/2 using sensor H104-C. REPS pulse 319 generating 6.2 kV/m at 50 m.

Appendix D.—Pulser Output Waveforms

Contents

Page

Tables

D-1. REPS Operating Parameters	187
--------------------------------------	-----

Figures

D-1. REPS output waveforms for pulses 2, 3, 4, 6	188
D-2. REPS output waveforms for pulses 7, 8, 9, 10	188
D-3. REPS output waveforms for pulses 11, 13, 14, 15	189
D-4. REPS output waveforms for pulses 16, 17, 18, 19	189
D-5. REPS output waveforms for pulses 20, 21, 36, 38	190
D-6. REPS output waveforms for pulses 39, 40, 43, 44	190
D-7. REPS output waveforms for pulses 45, 46, 47, 48	191
D-8. REPS output waveforms for pulses 49, 52, 53, 54	191
D-9. REPS output waveforms for pulses 56, 58, 61, 73	192
D-10. REPS output waveforms for pulses 74, 75, 76, 77	192
D-11. REPS output waveforms for pulses 78, 79, 80, 81	193
D-12. REPS output waveforms for pulses 82, 83, 84, 85	193
D-13. REPS output waveforms for pulses 86, 87, 88, 90	194
D-14. REPS output waveforms for pulses 91, 92, 93, 94	194
D-15. REPS output waveforms for pulses 95, 96, 97, 98	195
D-16. REPS output waveforms for pulses 99, 101, 103, 104	195
D-17. REPS output waveforms for pulses 105, 106, 107, 108	196
D-18. REPS output waveforms for pulses 109, 110, 111, 112	196
D-19. REPS output waveforms for pulses 113, 114, 115, 116	197
D-20. REPS output waveforms for pulses 117, 118, 119, 120	197
D-21. REPS output waveforms for pulses 121, 122, 123, 124	198
D-22. REPS output waveforms for pulses 126, 127, 128, 129	198
D-23. REPS output waveforms for pulses 130, 131, 133, 135	199
D-24. REPS output waveforms for pulses 136, 137, 138, 140	199
D-25. REPS output waveforms for pulses 141, 142, 143, 144	200
D-26. REPS output waveforms for pulses 145, 146, 147, 148	200
D-27. REPS output waveforms for pulses 149, 150, 151, 152	201
D-28. REPS output waveforms for pulses 155, 156, 158, 159	201
D-29. REPS output waveforms for pulses 161, 162, 163, 164	202
D-30. REPS output waveforms for pulses 165, 167, 168, 169	202
D-31. REPS output waveforms for pulses 171, 173, 174, 175	203
D-32. REPS output waveforms for pulses 176, 177, 178, 179	203

Appendix D

D-33. REPS output waveforms for pulses 180, 181, 182, 183	204
D-34. REPS output waveforms for pulses 184, 185, 192, 194	204
D-35. REPS output waveforms for pulses 195, 196, 197, 198	205
D-36. REPS output waveforms for pulses 199, 200, 201, 202	205
D-37. REPS output waveforms for pulses 203, 204, 205, 206	206
D-38. REPS output waveforms for pulses 208, 209, 210, 212	206
D-39. REPS output waveforms for pulses 213, 214, 215, 216	207
D-40. REPS output waveforms for pulses 217, 221, 222, 223	207
D-41. REPS output waveforms for pulses 224, 225, 226, 227	208
D-42. REPS output waveforms for pulses 228, 230, 231, 232	208
D-43. REPS output waveforms for pulses 233, 234, 235, 236	209
D-44. REPS output waveforms for pulses 237, 238, 239, 240	209
D-45. REPS output waveforms for pulses 241, 243, 244, 245	210
D-46. REPS output waveforms for pulses 246, 247, 248, 249	210
D-47. REPS output waveforms for pulses 254, 255, 256, 257	211
D-48. REPS output waveforms for pulses 259, 260, 261, 262	211
D-49. REPS output waveforms for pulses 263, 264, 265, 266	212
D-50. REPS output waveforms for pulses 267, 270, 271, 272	212
D-51. REPS output waveforms for pulses 273, 274, 275, 276	213
D-52. REPS output waveforms for pulses 277, 278, 279, 280	213
D-53. REPS output waveforms for pulses 281, 283, 284, 287	214
D-54. REPS output waveforms for pulses 288, 289, 292, 293	214
D-55. REPS output waveforms for pulses 295, 298, 299, 300	215
D-56. REPS output waveforms for pulses 301, 302, 303, 304	215
D-57. REPS output waveforms for pulses 305, 306, 309, 313	216
D-58. REPS output waveforms for pulses 314, 315, 316, 317	216
D-59. REPS output waveforms for pulses 318, 319, 320, 322	217
D-60. REPS output waveforms for pulses 324, 325, 326, 328	217
D-61. REPS output waveforms for pulses 329, 330, 331, 332	218
D-62. REPS output waveforms for pulses 334, 335, 336, 337	218
D-63. REPS output waveforms for pulses 338, 339, 340, 341	219
D-64. REPS output waveforms for pulses 342, 343, 344, 345	219
D-65. REPS output waveforms for pulses 346, 347, 350, 351	220
D-66. REPS output waveforms for pulses 353, 354, 355, 356	220
D-67. REPS output waveforms for pulses 357, 358, 359, 360	221
D-68. REPS output waveforms for pulses 361, 362, 363, 364	221
D-69. REPS output waveforms for pulses 365, 366, 367, 368	222
D-70. REPS output waveforms for pulses 369, 370, 371, 372	222
D-71. REPS output waveforms for pulses 373, 374, 375, 376	223
D-72. REPS output waveforms for pulses 377, 378, 380, 383	223
D-73. REPS output waveforms for pulses 384, 385, 387, 388	224
D-74. REPS output waveforms for pulses 389, 390, 391, 392	224
D-75. REPS output waveforms for pulses 393, 394, 395, 396	225
D-76. REPS output waveforms for pulses 397, 398, 399, 401	225
D-77. REPS output waveforms for pulses 402, 403, 404, 405	226
D-78. REPS output waveforms for pulses 406, 407, 408	226

Each time REPS is fired, the incident B-dot is recorded to monitor the performance of the simulator, as well as account for any shot-to-shot pulse variations. This appendix contains all of the pulser monitor waveforms (fig. D-1 through D-78) corresponding to the field data listed in appendix C. Table D-1 contains the simulator operating parameters (gas pressures, charge voltages) for each pulse.

The data are organized sequentially by pulse number.

Table D-1. REPS operating parameters.

Pulse number	Charge voltage (kV)	Marx switch (N ₂)	Output switch (SF ₆)	Gas pressure (ppi)		Trigger switch (N ₂)
				Marx vessel (SF ₆)	Peaking capacitor (SF ₆)	
1-69	68	17	30	1.5	38	32
70-159	68	17	30	1.6	38	32
160-284	68	17	30	1.5	38	32
285-306	68	17	30	1.6	38	32
307-408	68	17	30	1.5	38	32

Appendix D

Figure D-1. REPS output waveforms for pulses 2, 3, 4, and 6.

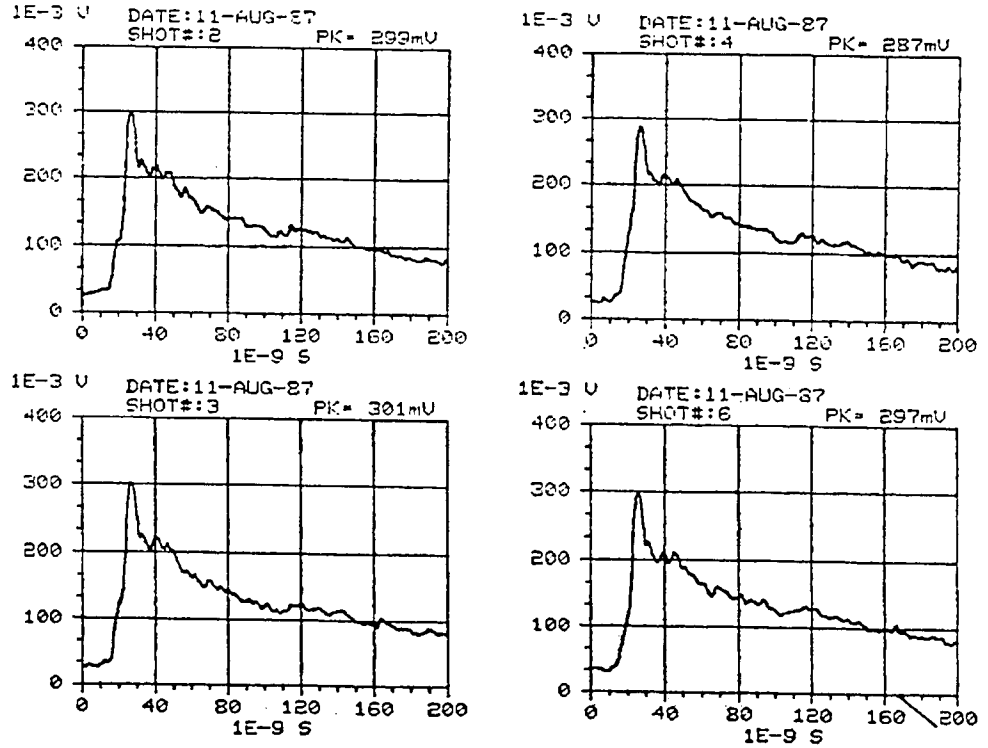


Figure D-2. REPS output waveforms for pulses 7, 8, 9, and 10.

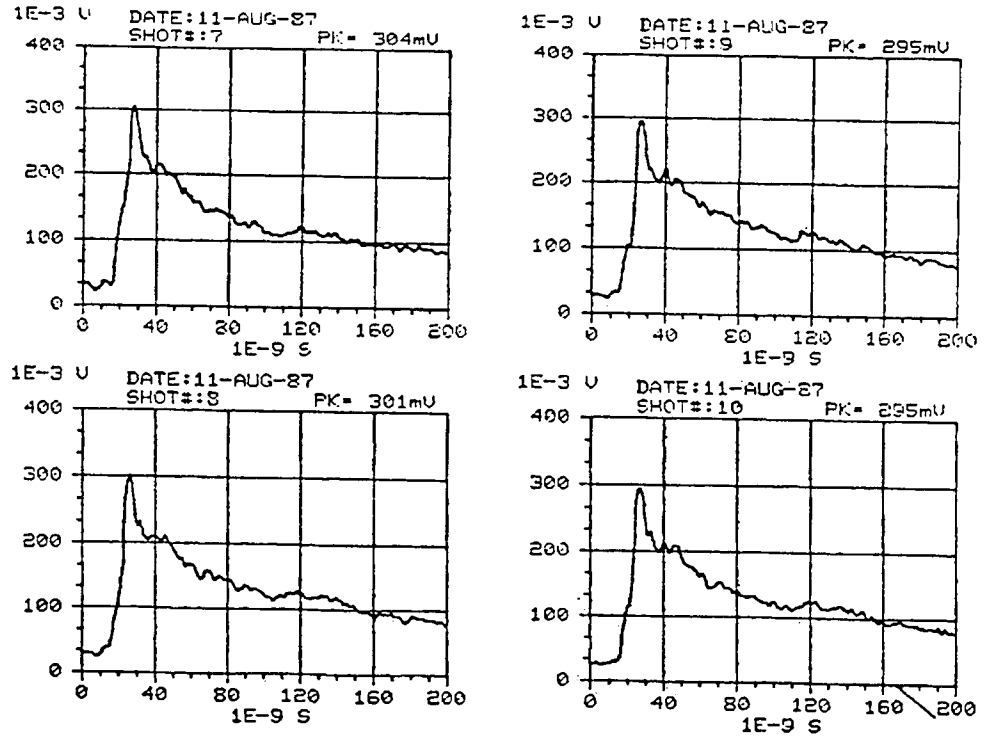


Figure D-3. REPS output waveforms for pulses 11, 13, 14, and 15.

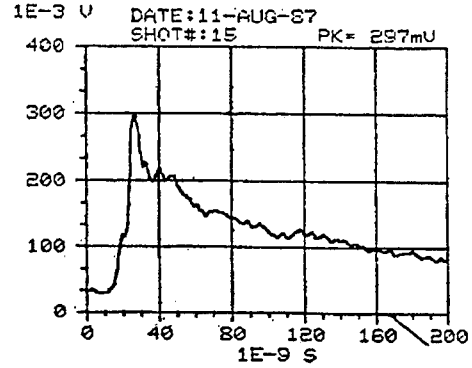
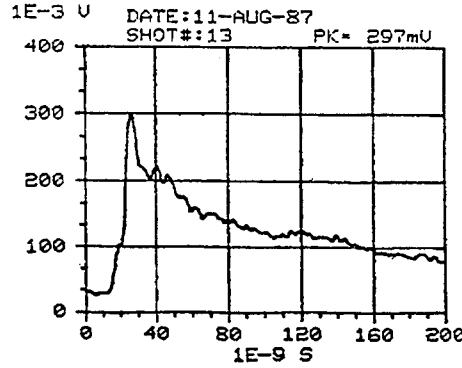
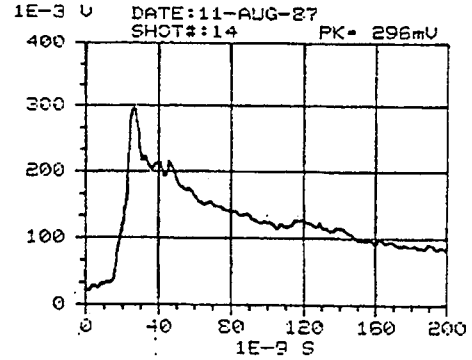
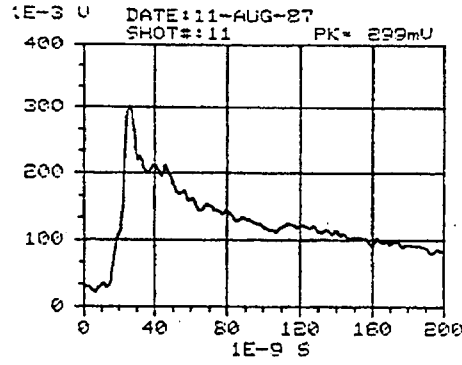
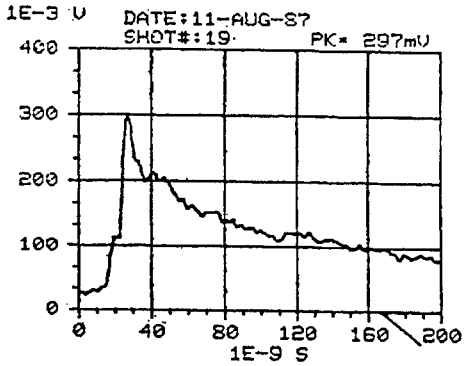
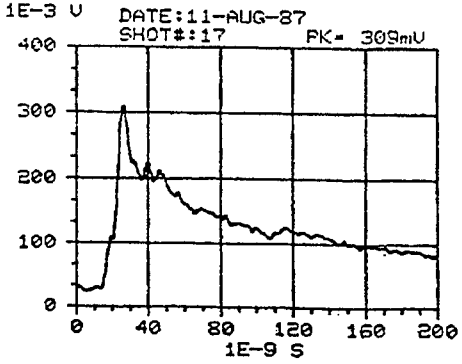
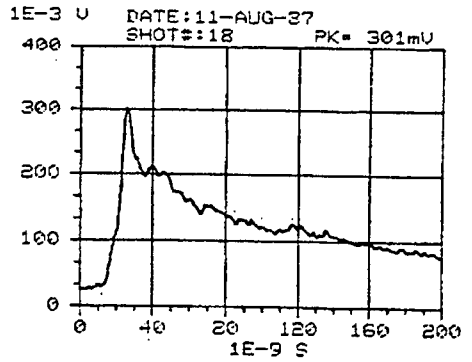
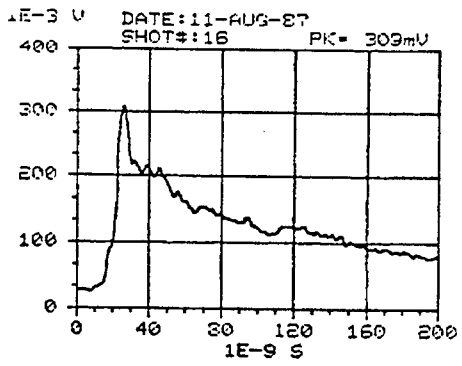


Figure D-4. REPS output waveforms for pulses 16, 17, 18, and 19.



Appendix D

Figure D-5. REPS output waveforms for pulses 20, 21, 36, and 38.

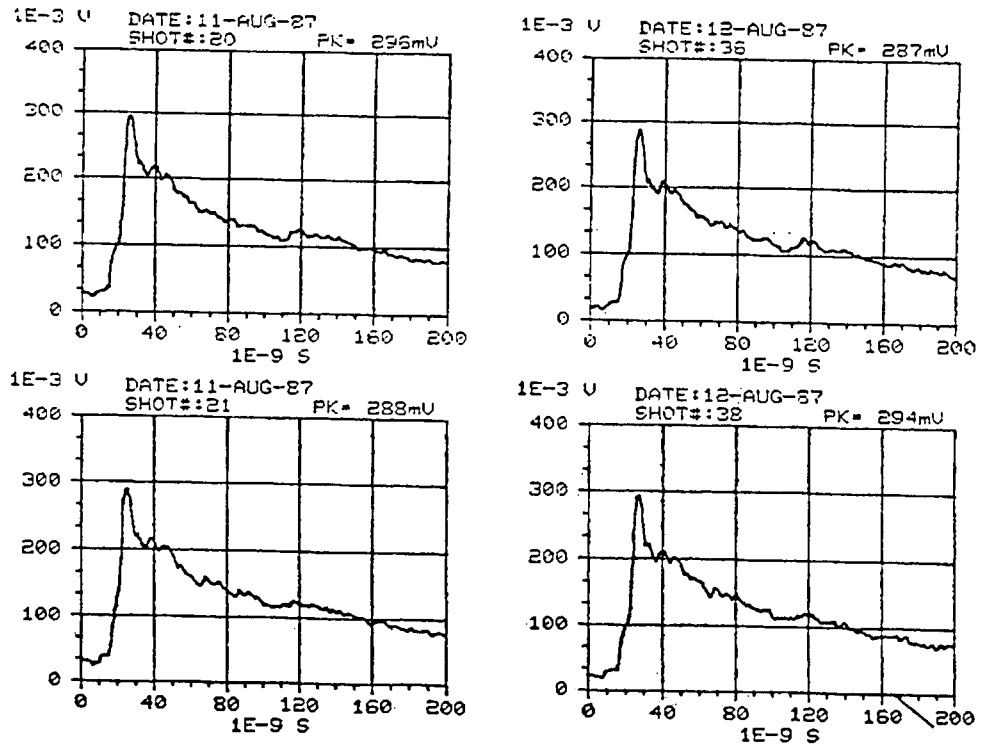


Figure D-6. REPS output waveforms for pulses 39, 40, 43, and 44.

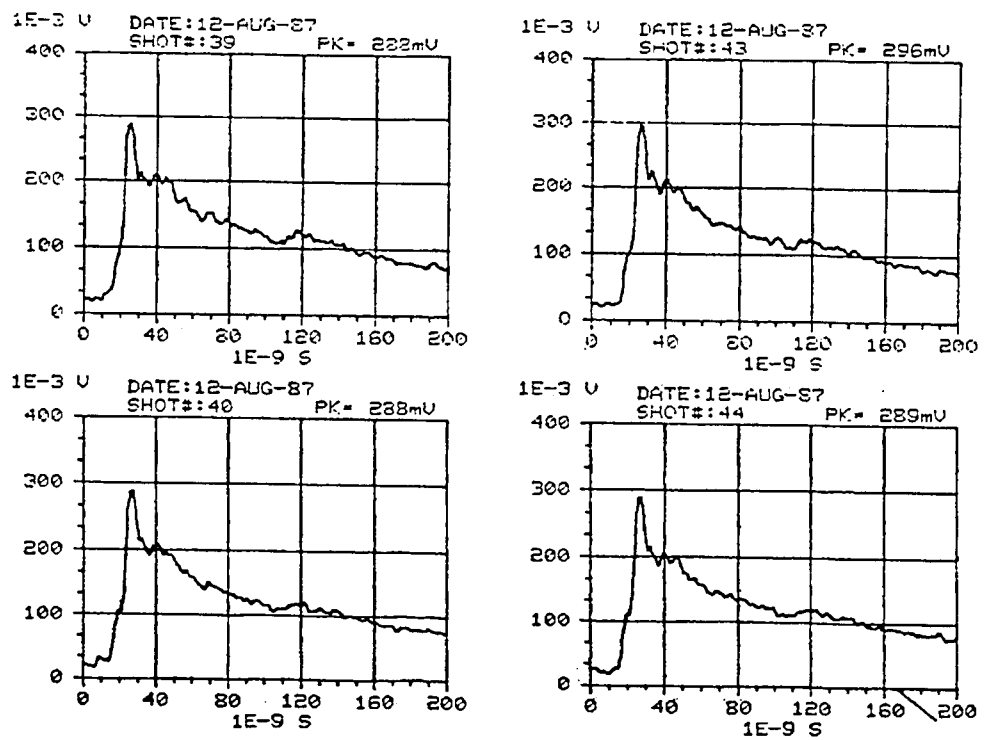


Figure D-7. REPS output waveforms for pulses 45, 46, 47, and 48.

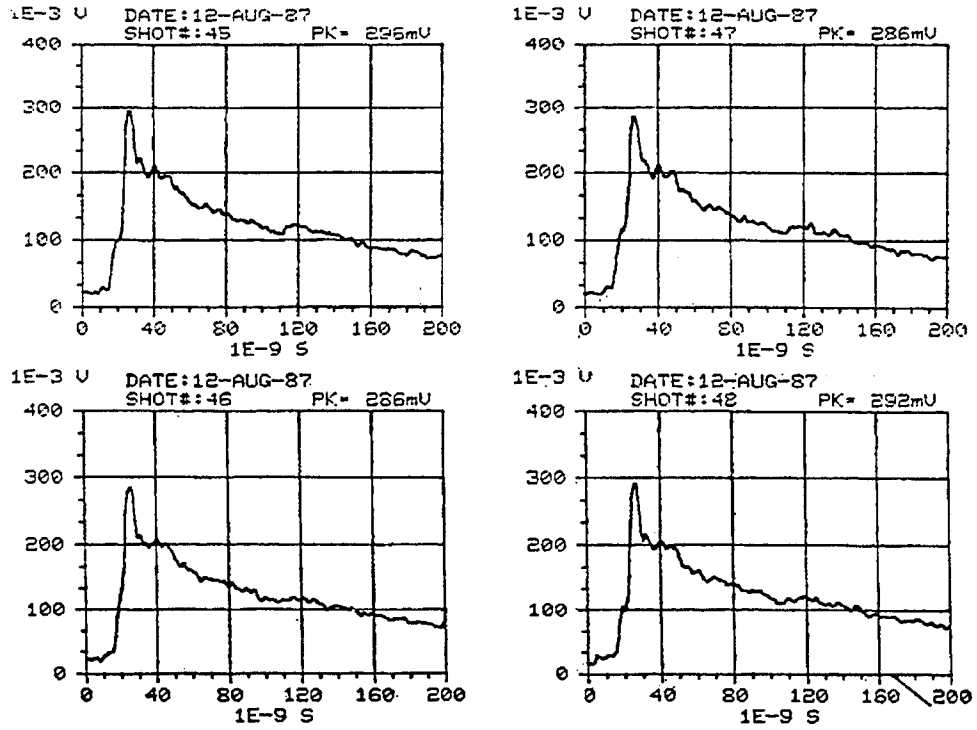
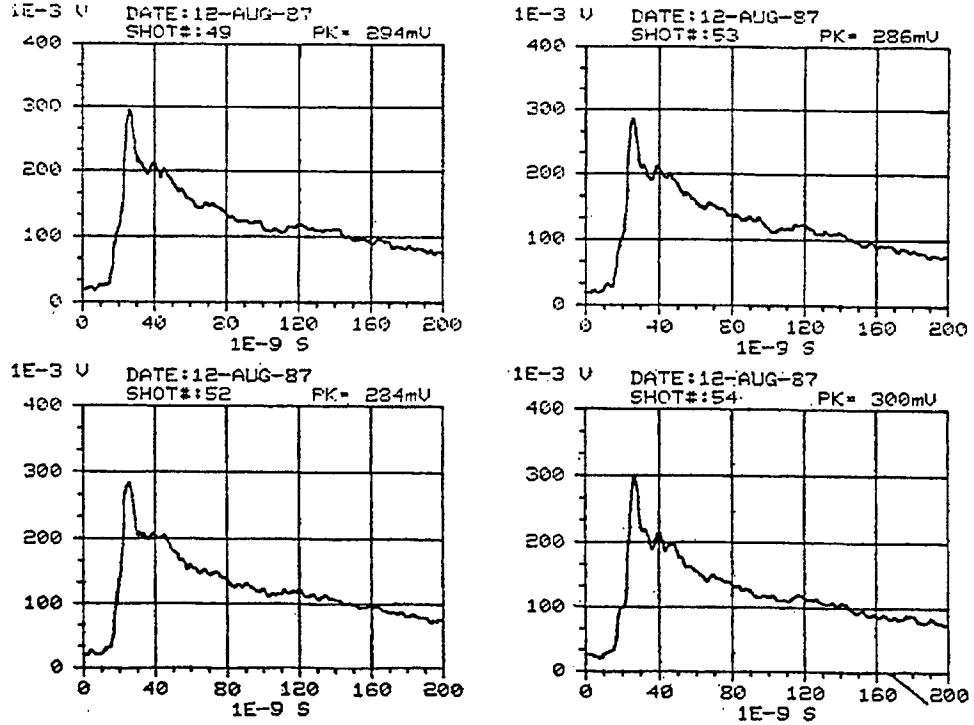


Figure D-8. REPS output waveforms for pulses 49, 52, 53, and 54.



Appendix D

Figure D-9. REPS output waveforms for pulses 56, 58, 61, and 73.

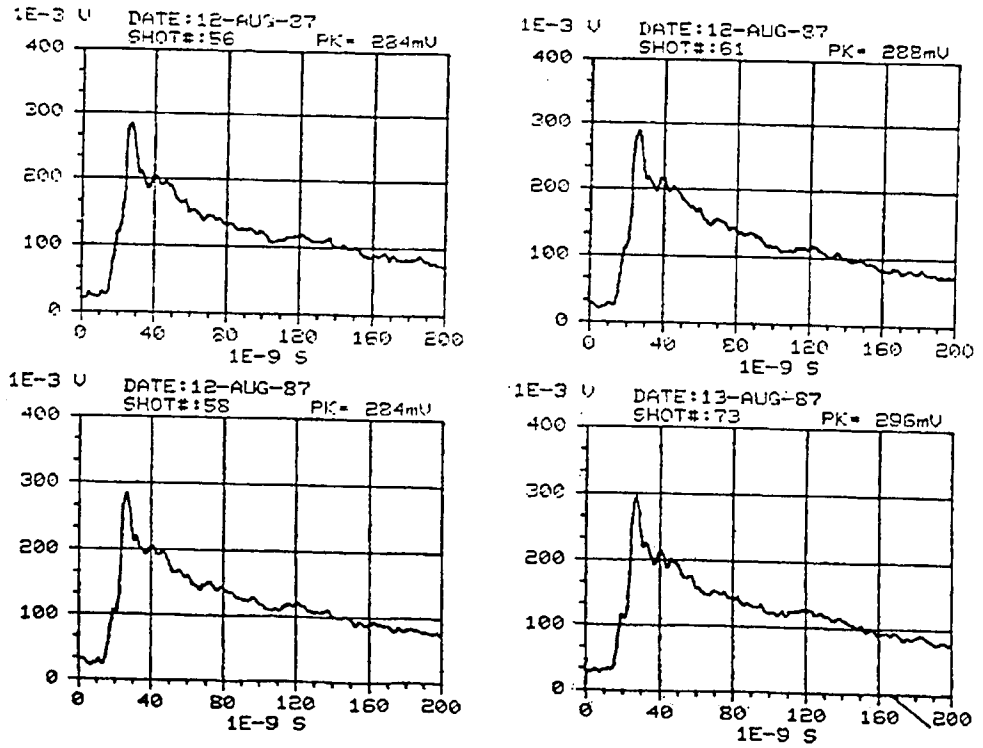


Figure D-10. REPS output waveforms for pulses 74, 75, 76, and 77.

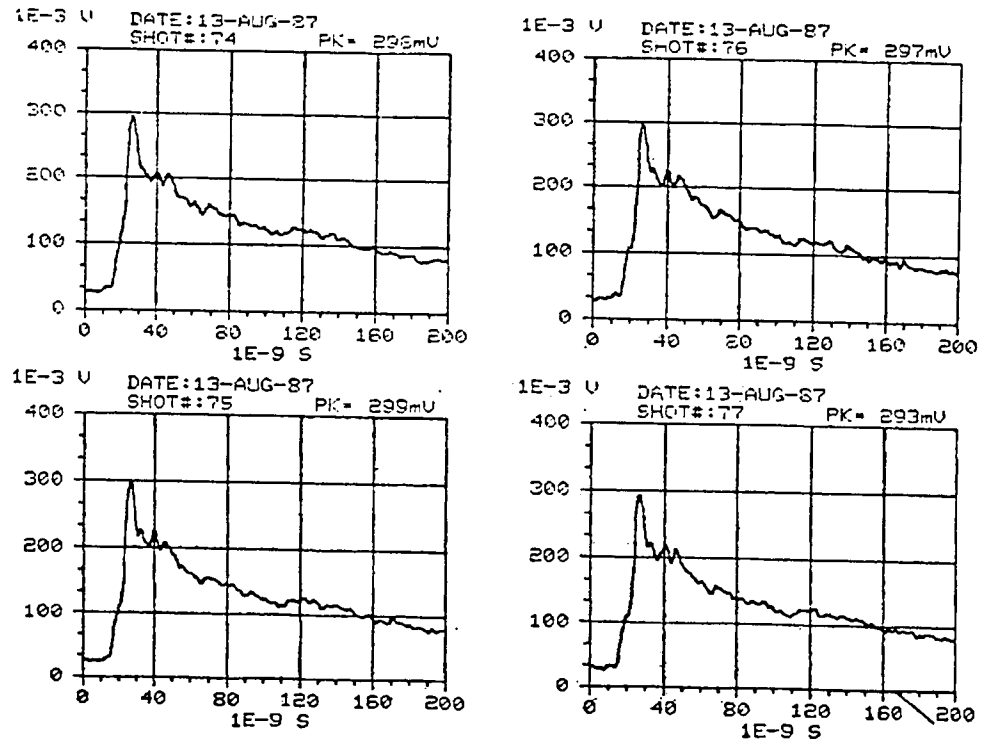


Figure D-11. REPS output waveforms for pulses 78, 79, 80, and 81.

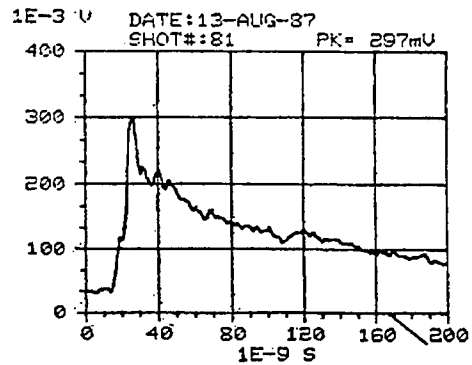
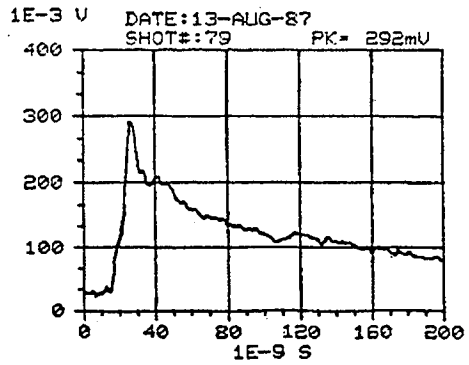
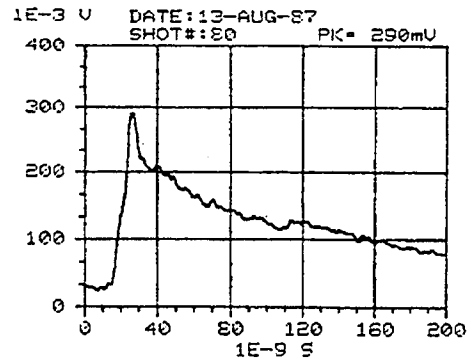
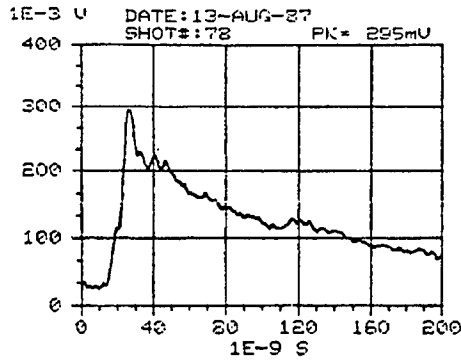
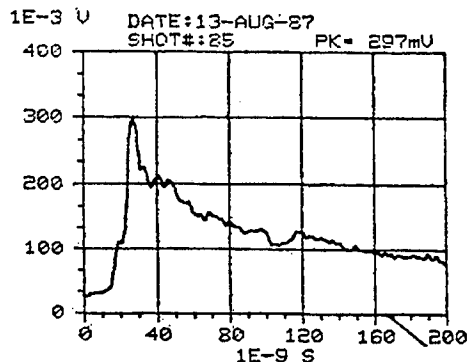
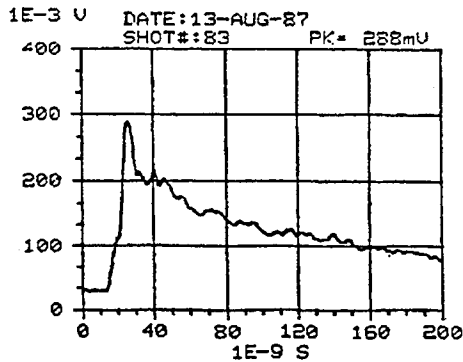
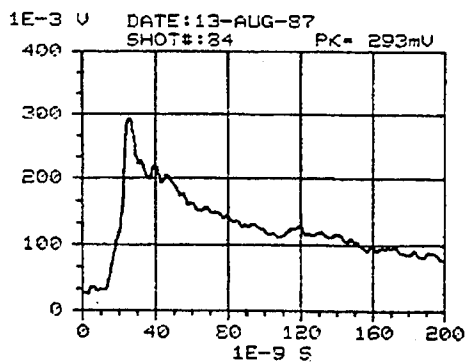
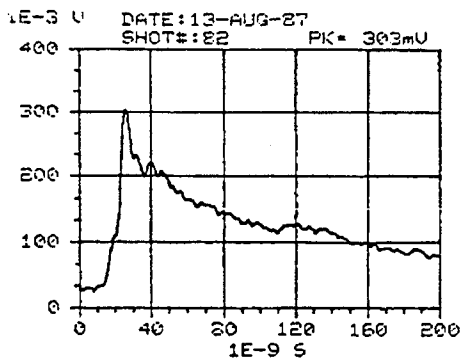


Figure D-12. REPS output waveforms for pulses 82, 83, 84, and 85.



Appendix D

Figure D-13. REPS output waveforms for pulses 86, 87, 88, and 90.

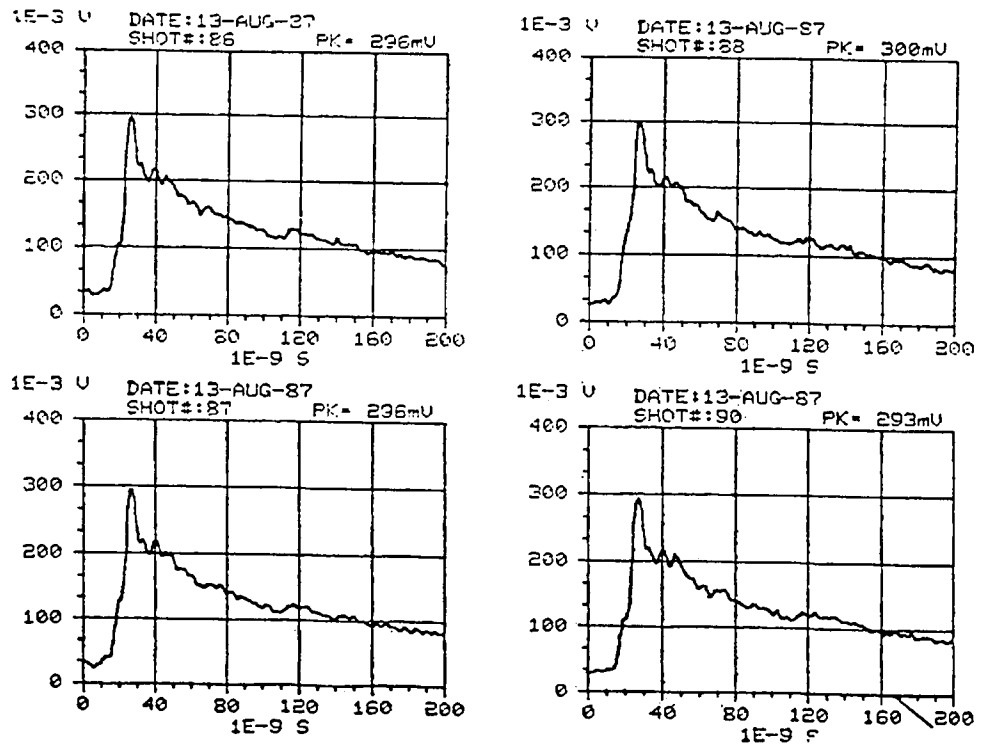


Figure D-14. REPS output waveforms for pulses 91, 92, 93, and 94.

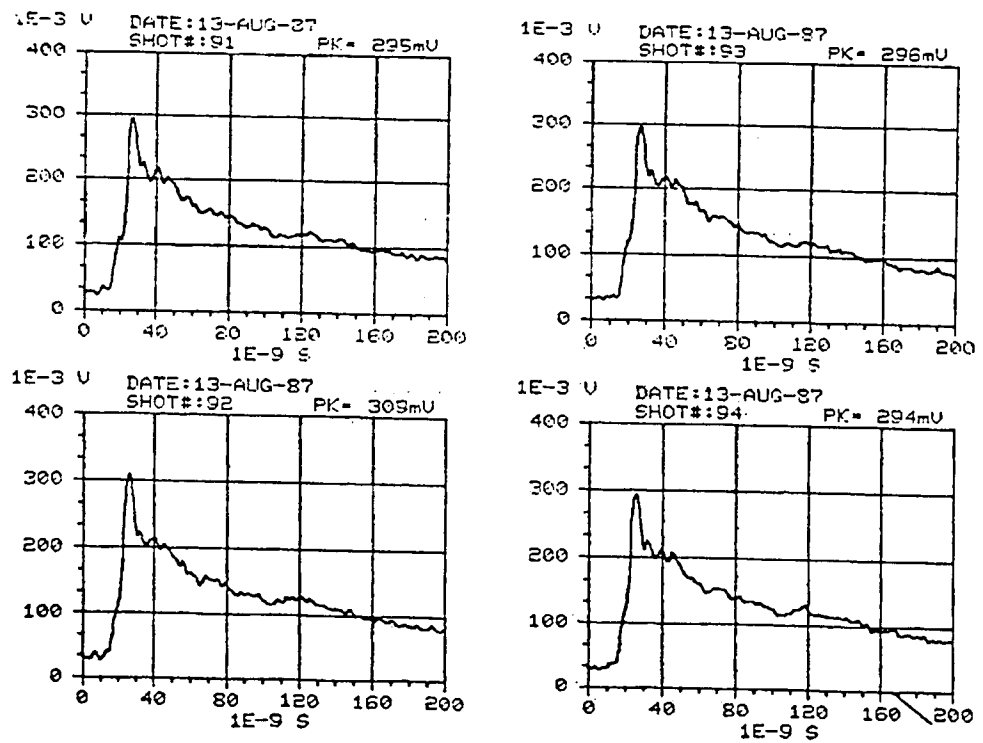


Figure D-15. REPS output waveforms for pulses 95, 96, 97, and 98.

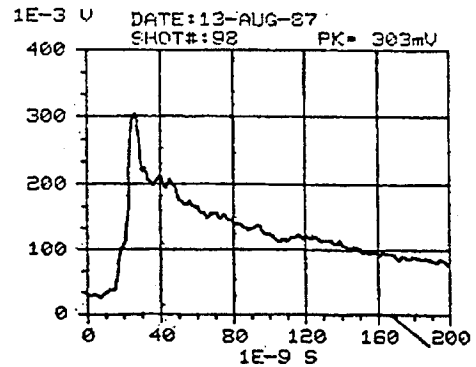
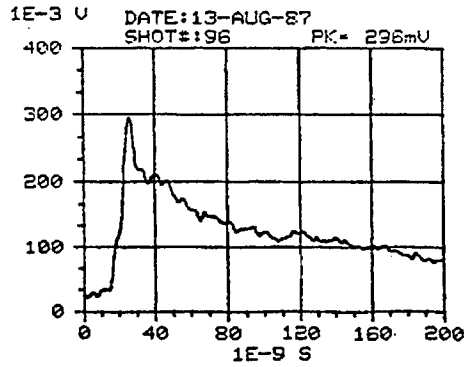
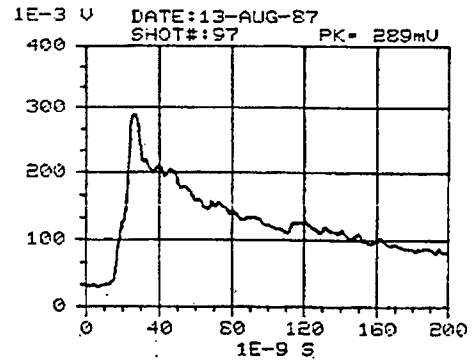
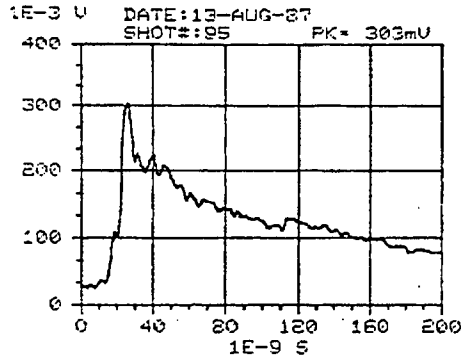
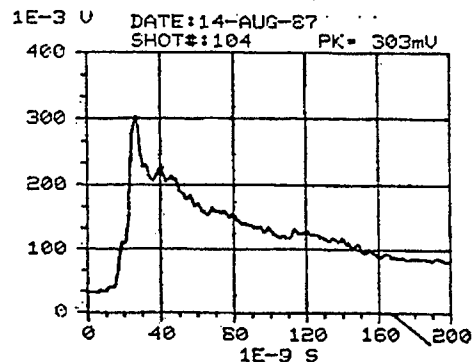
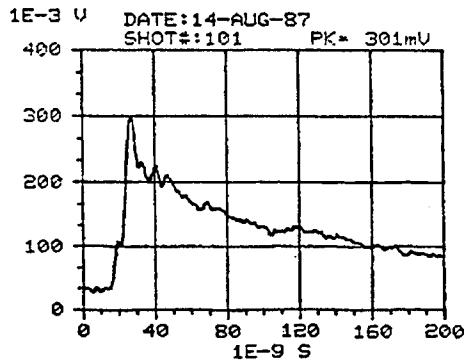
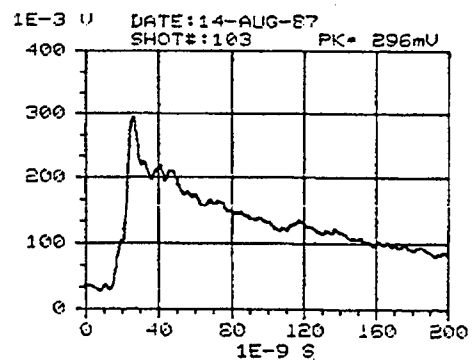
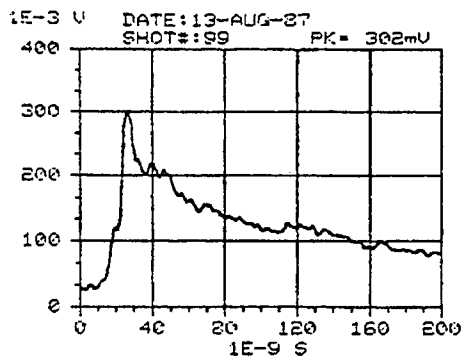


Figure D-16. REPS output waveforms for pulses 99, 101, 103, and 104.



Appendix D

Figure D-17. REPS output waveforms for pulses 105, 106, 107, and 108.

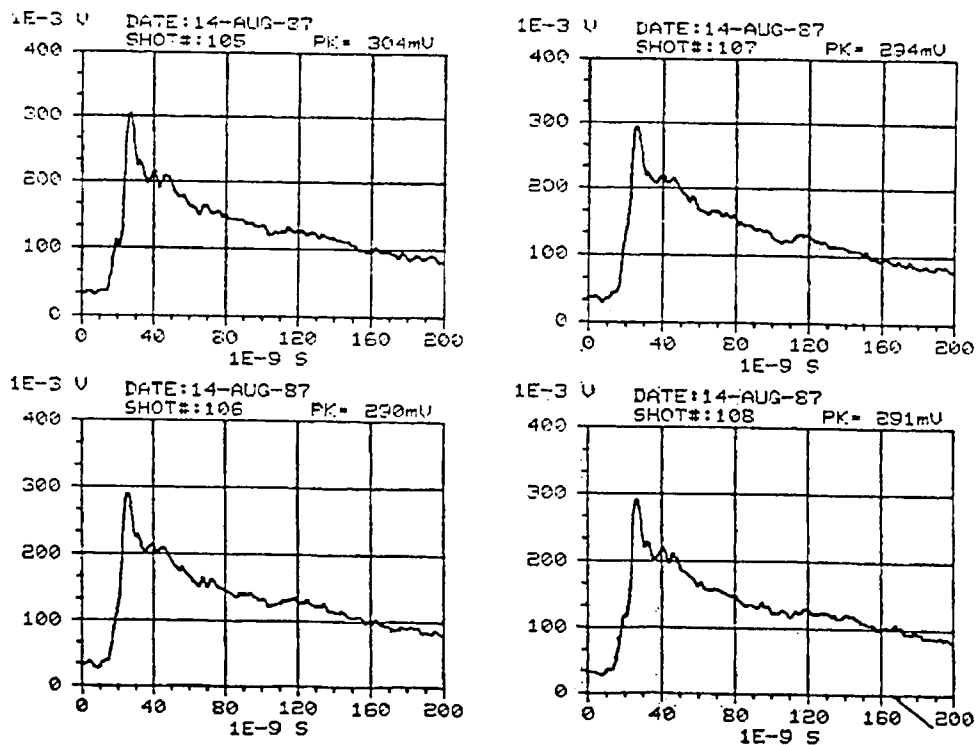


Figure D-18. REPS output waveforms for pulses 109, 110, 111, and 112.

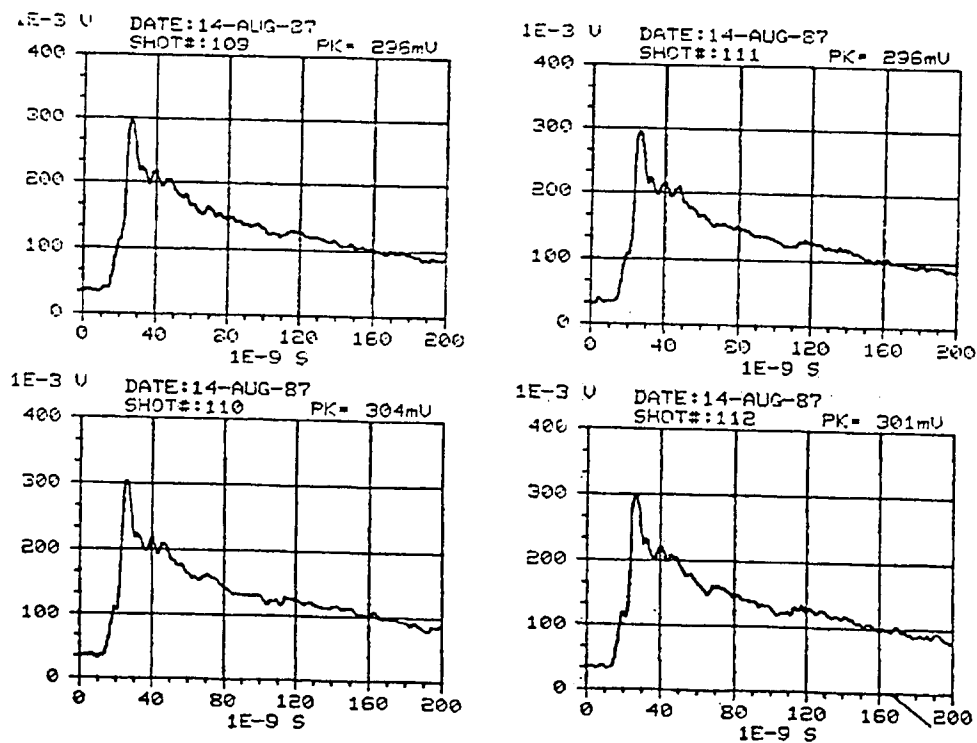


Figure D-19. REPS output waveforms for pulses 113, 114, 115, and 116.

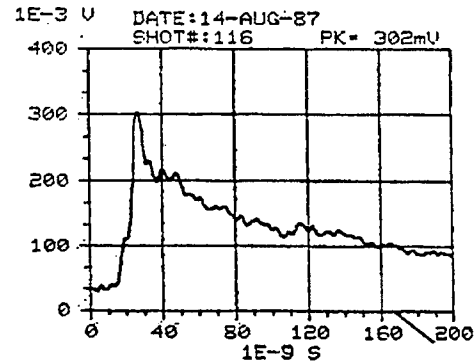
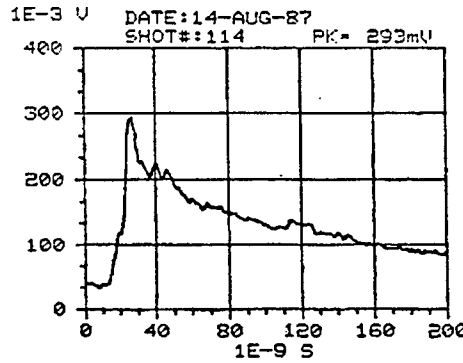
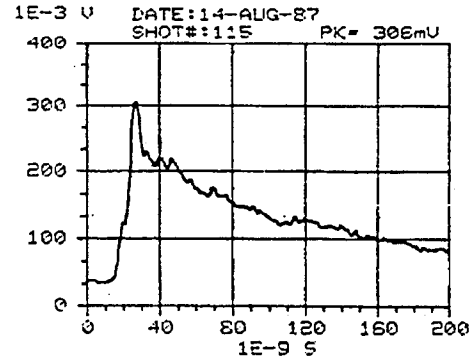
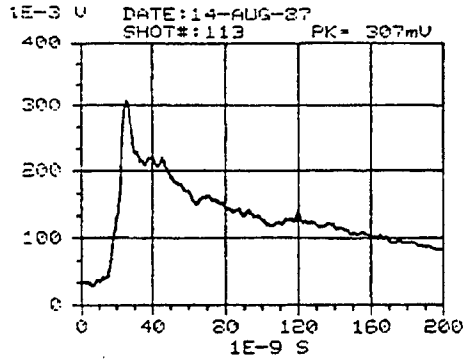
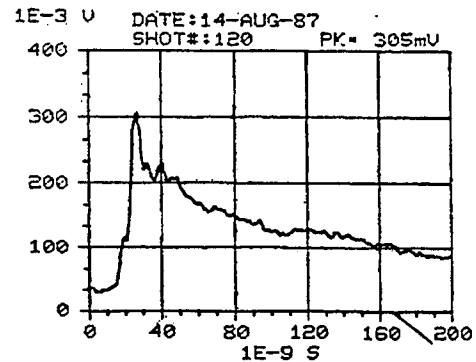
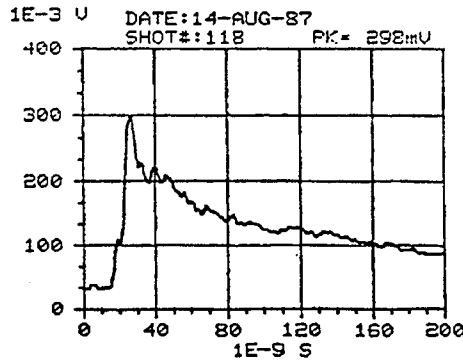
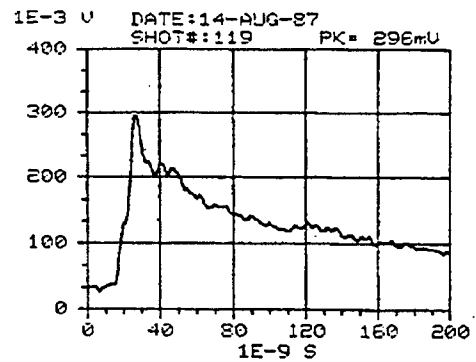
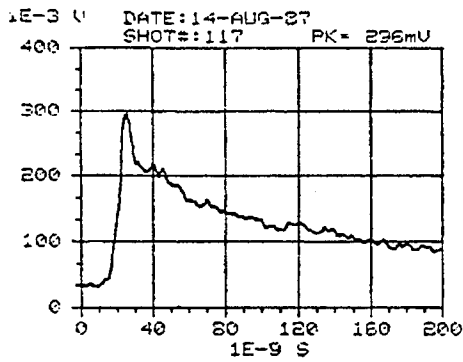


Figure D-20. REPS output waveforms for pulses 117, 118, 119, and 120.



Appendix D

Figure D-21. REPS output waveforms for pulses 121, 122, 123, and 124.

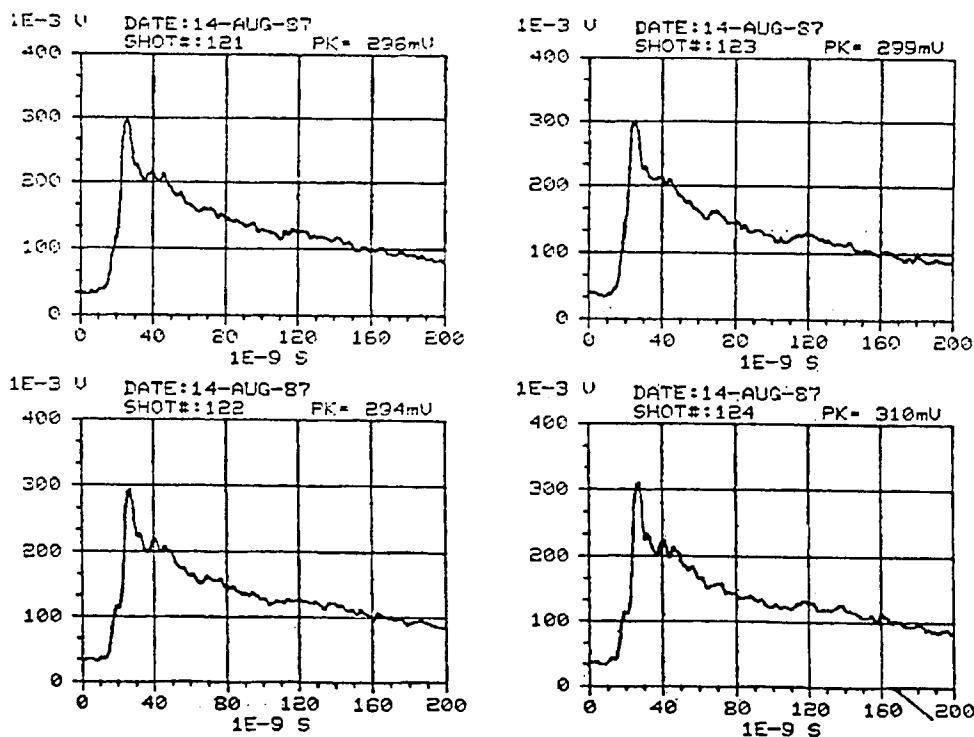


Figure D-22. REPS output waveforms for pulses 126, 127, 128, and 129.

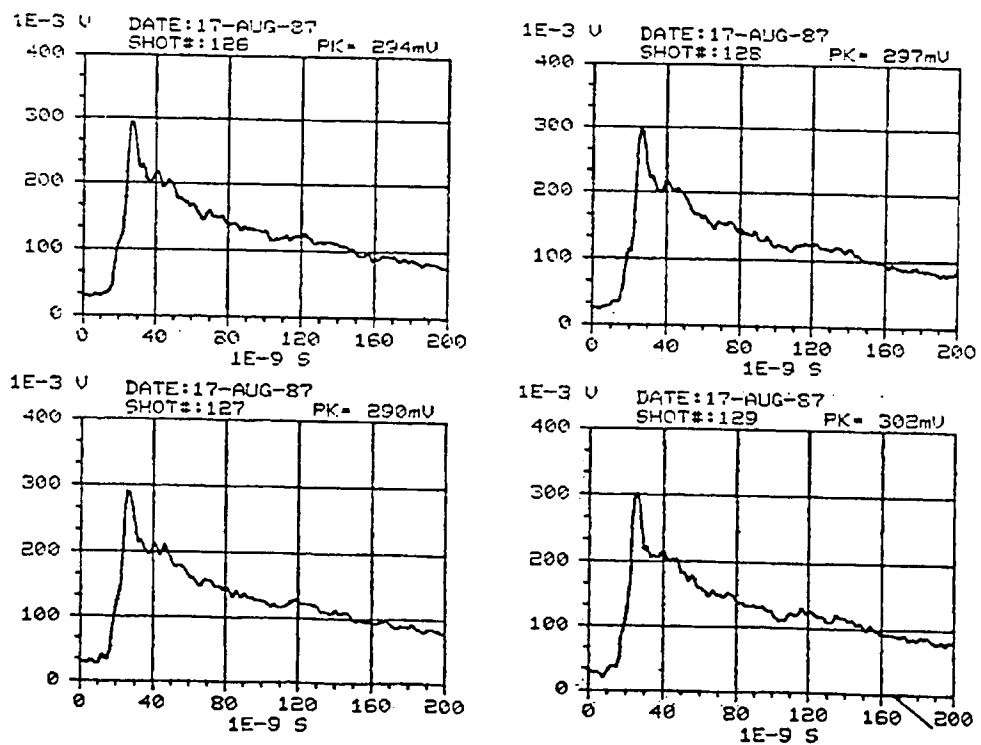


Figure D-23. REPS output waveforms for pulses 130, 131, 133, and 135.

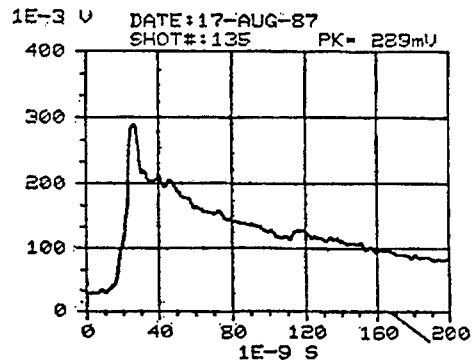
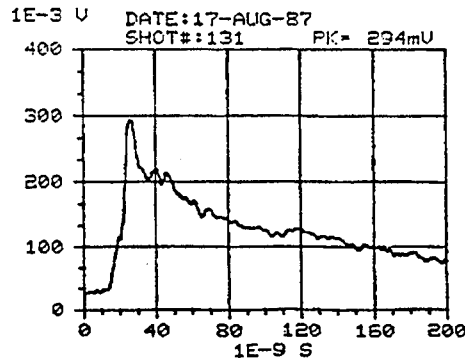
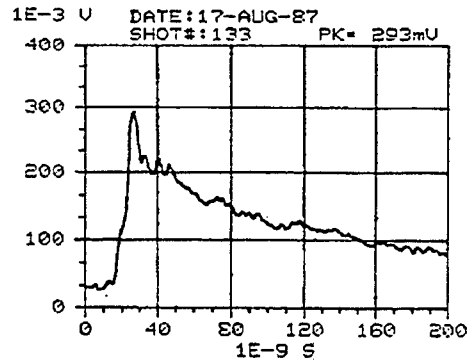
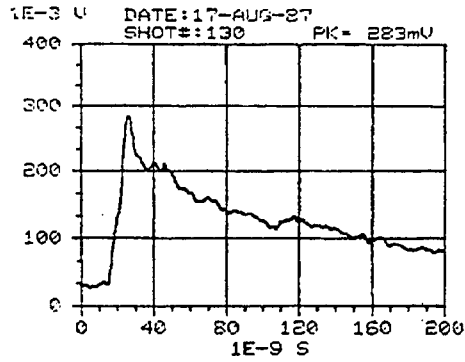
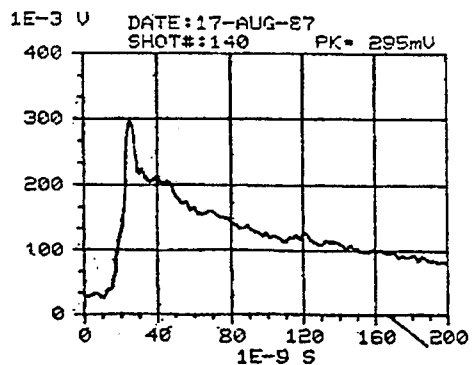
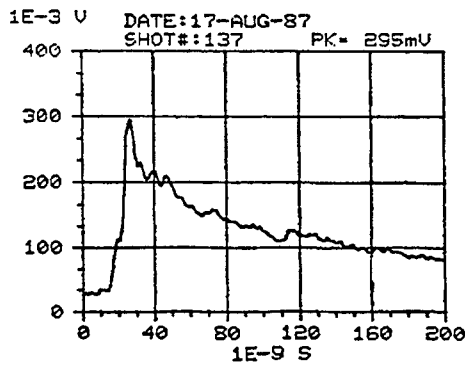
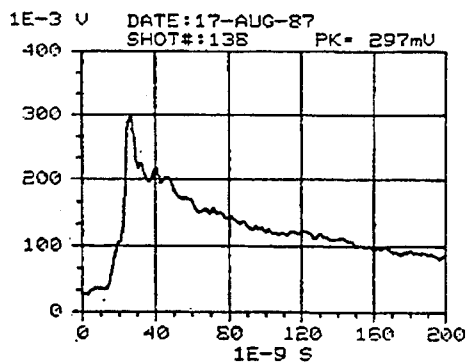
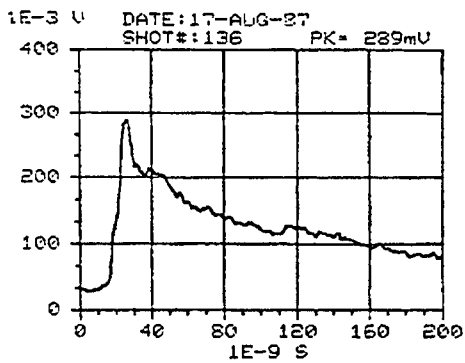


Figure D-24. REPS output waveforms for pulses 136, 137, 138, and 140.



Appendix D

Figure D-25. REPS output waveforms for pulses 141, 142, 143, and 144.

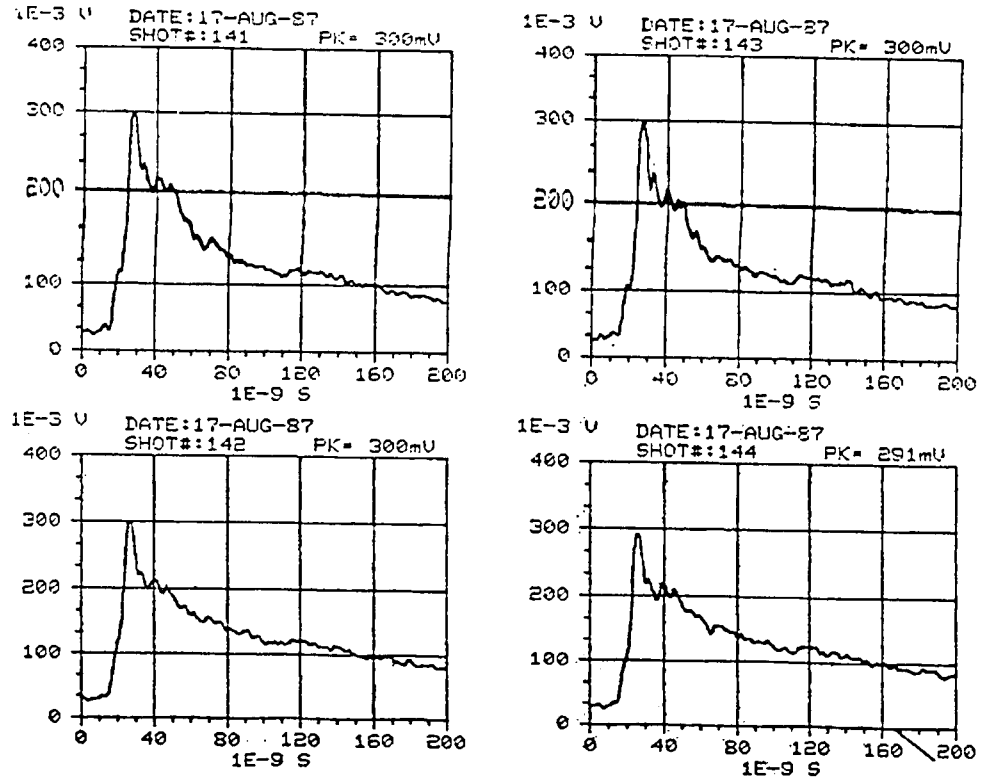


Figure D-26. REPS output waveforms for pulses 145, 146, 147, and 148.

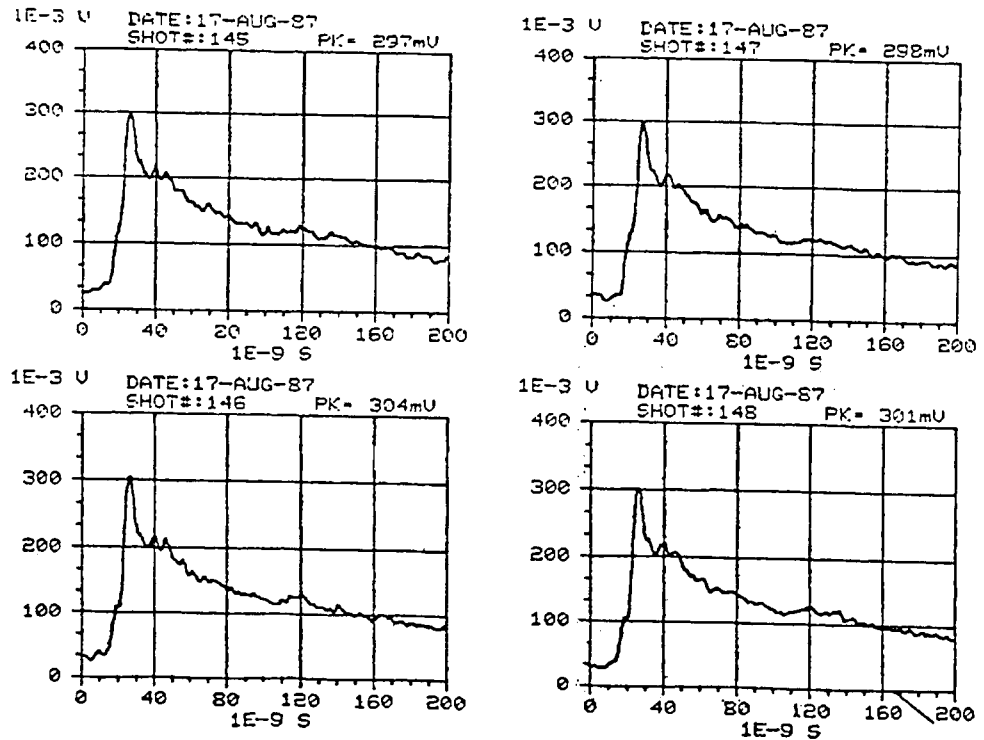


Figure D-27. REPS output waveforms for pulses 149, 150, 151, and 152.

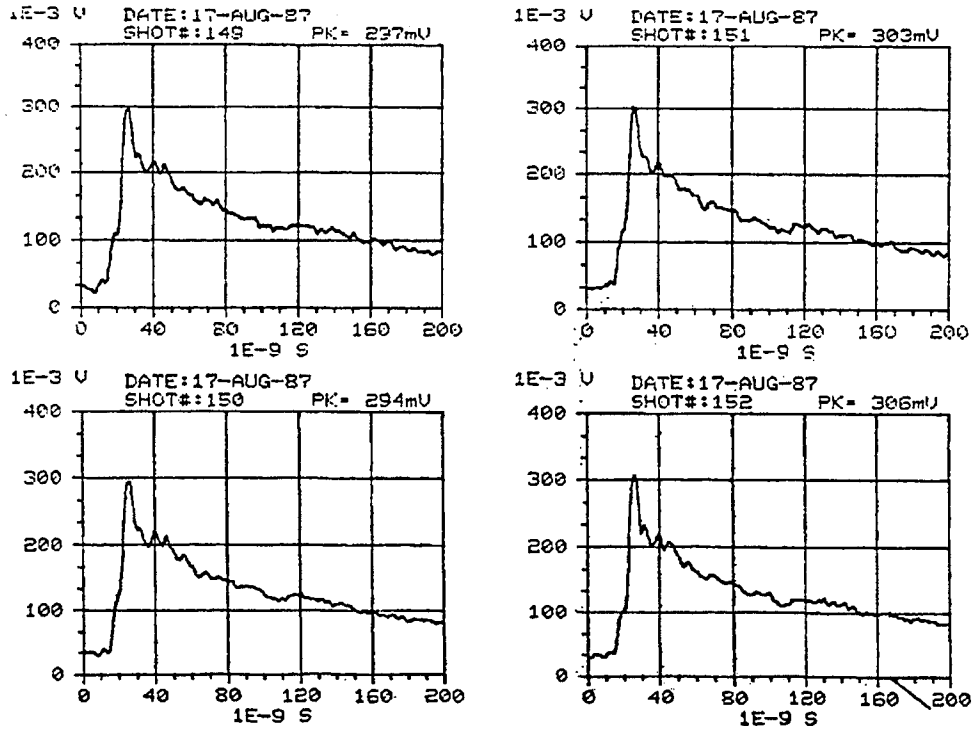
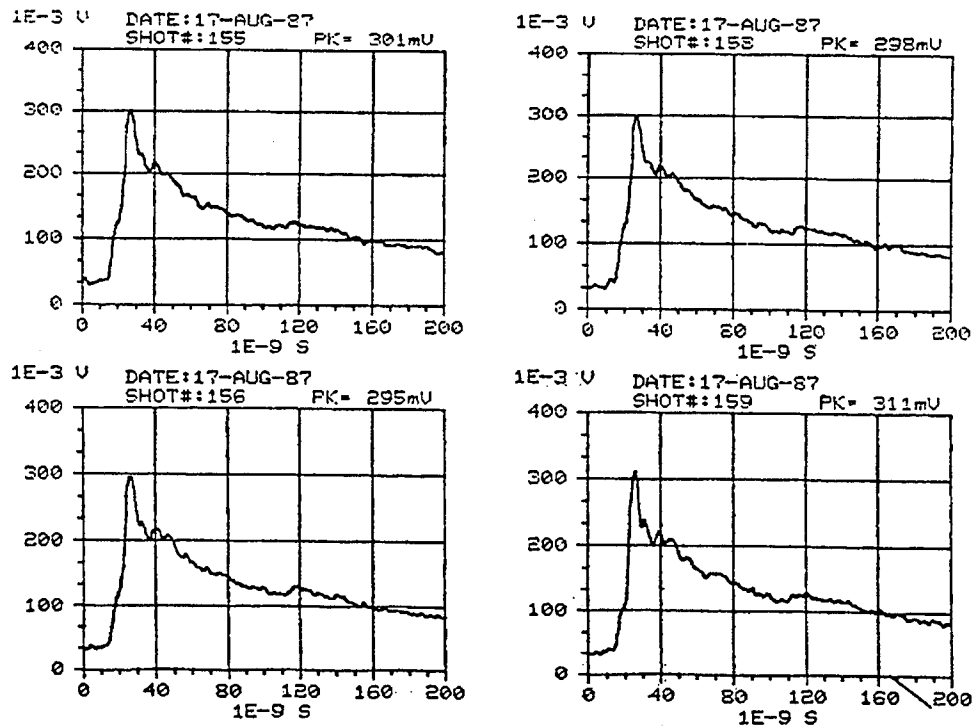


Figure D-28. REPS output waveforms for pulses 155, 156, 158, and 159.



Appendix D

Figure D-29. REPS output waveforms for pulses 161, 162, 163, and 164.

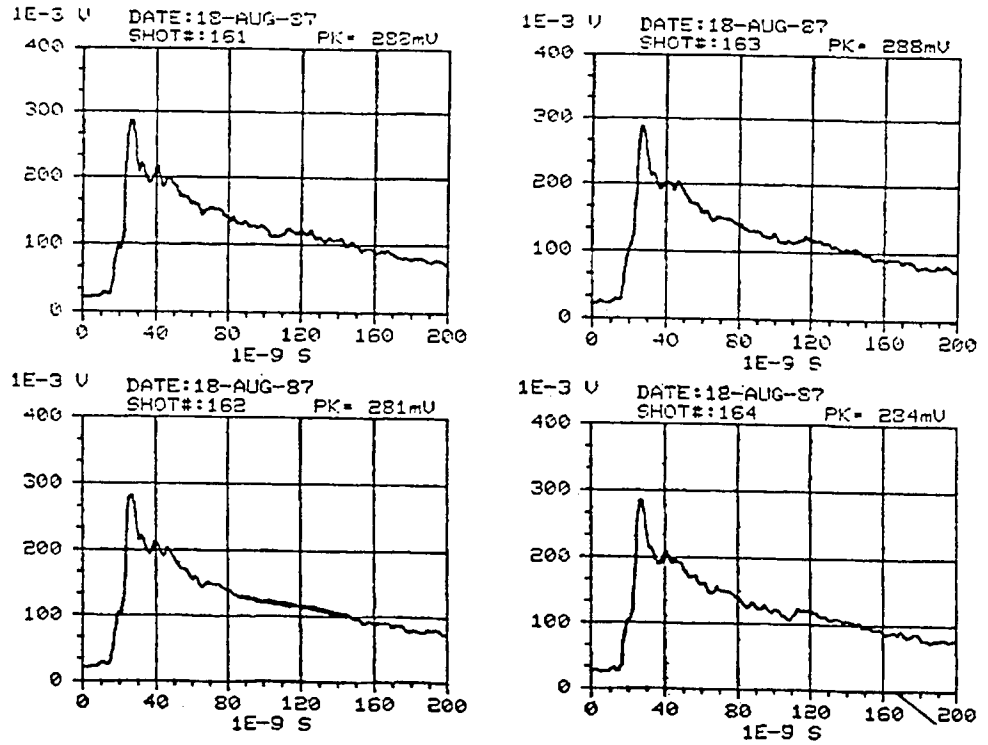


Figure D-30. REPS output waveforms for pulses 165, 167, 168, and 169.

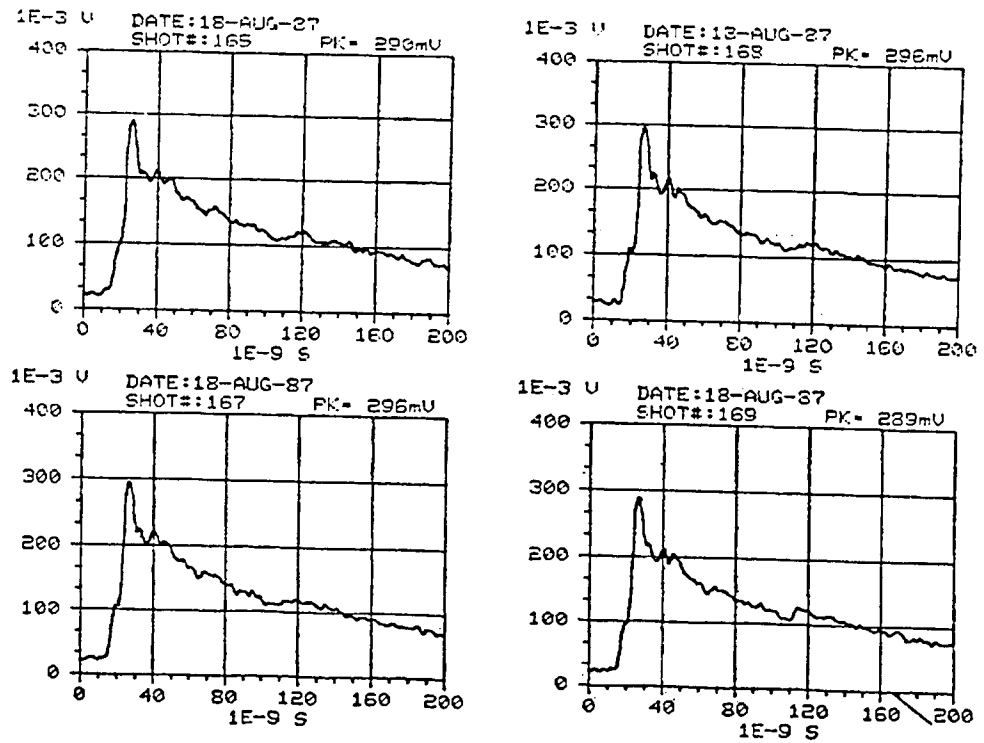


Figure D-31. REPS output waveforms for pulses 171, 173, 174, and 175.

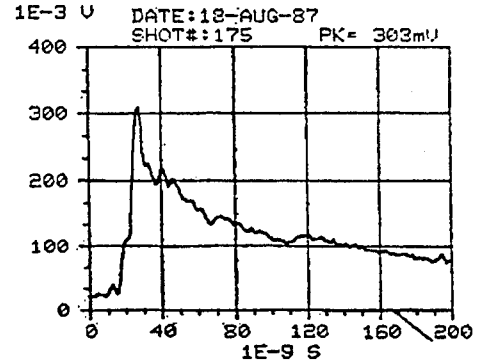
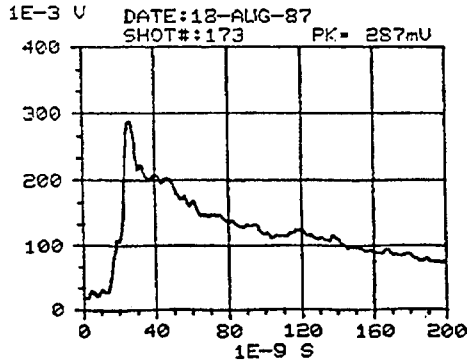
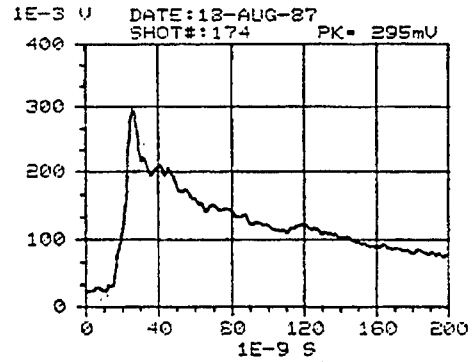
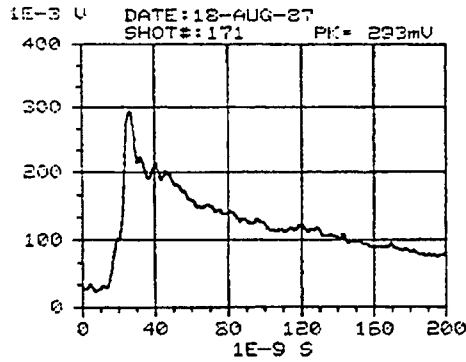
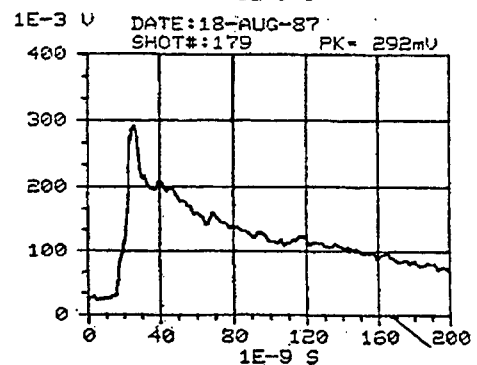
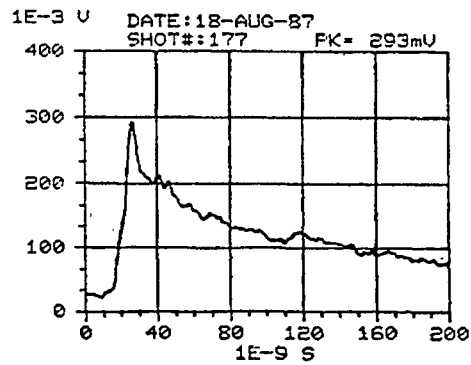
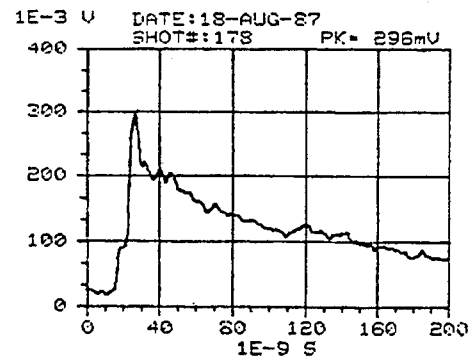
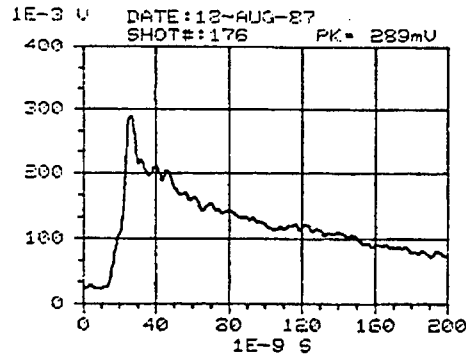


Figure D-32. REPS output waveforms for pulses 176, 177, 178, and 179.



Appendix D

Figure D-33. REPS output waveforms for pulses 180, 181, 182, and 183.

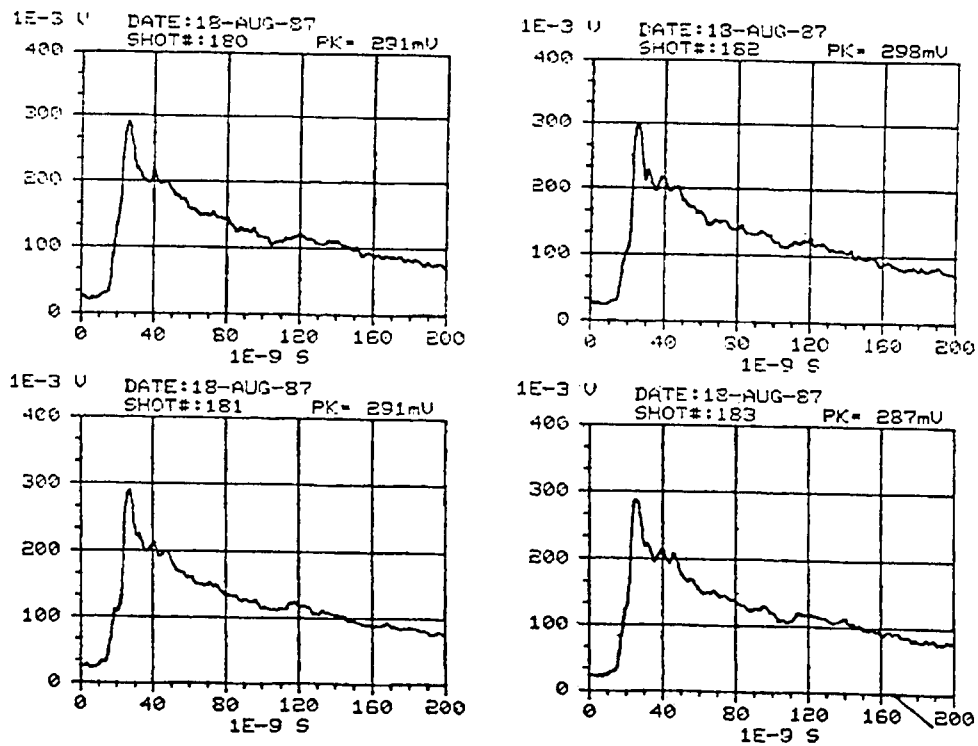


Figure D-34. REPS output waveforms for pulses 184, 185, 192, and 194.

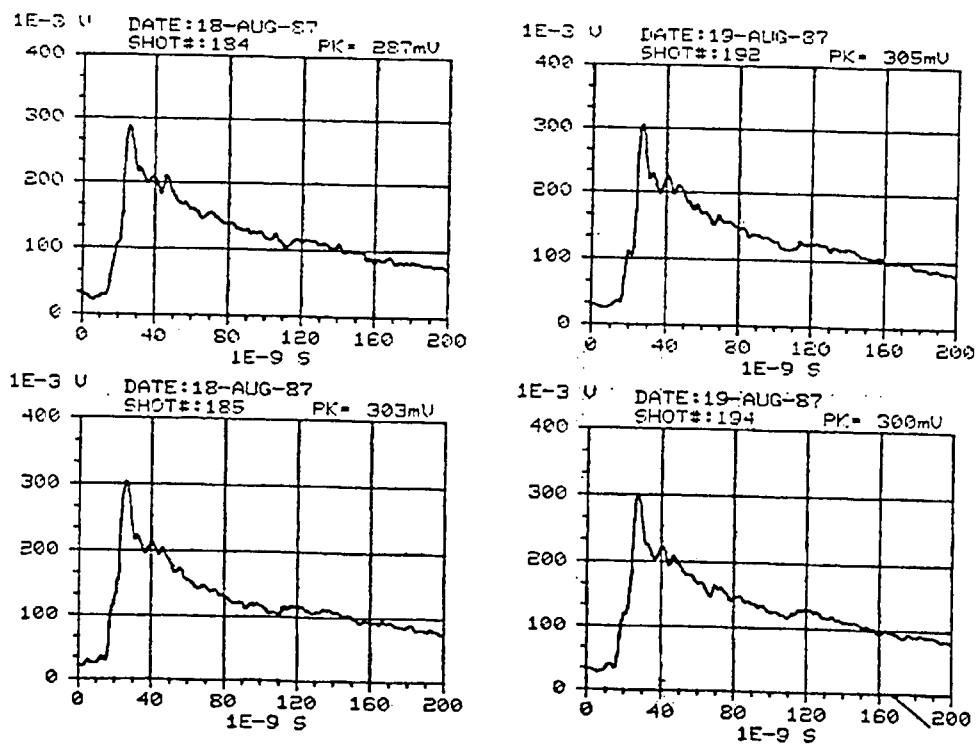


Figure D-35. REPS output waveforms for pulses 195, 196, 197, and 198.

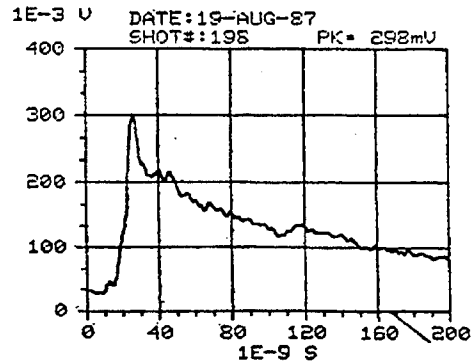
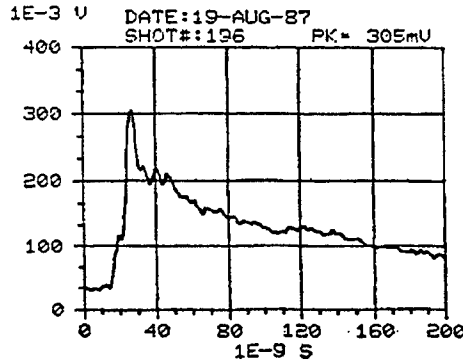
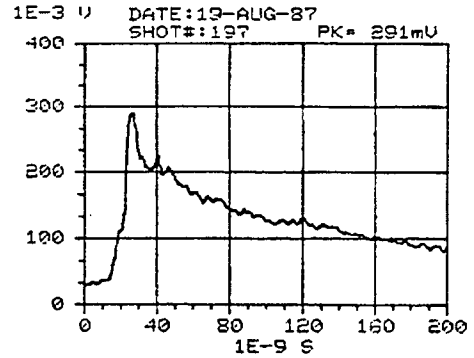
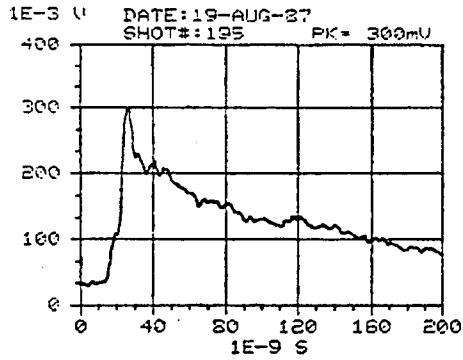
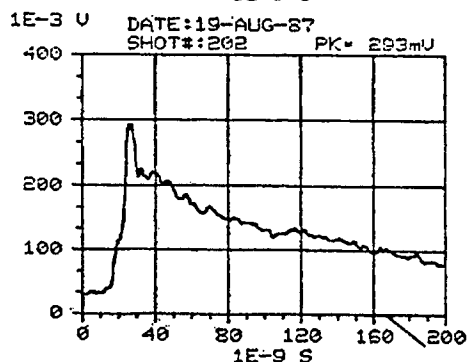
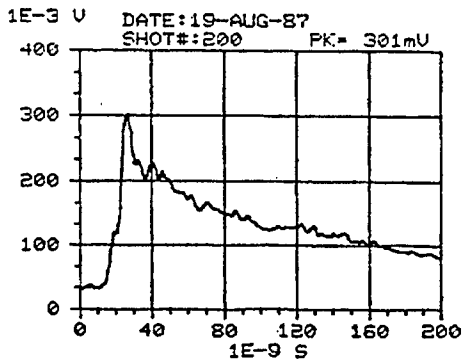
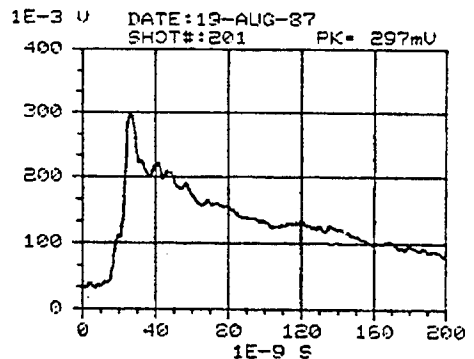
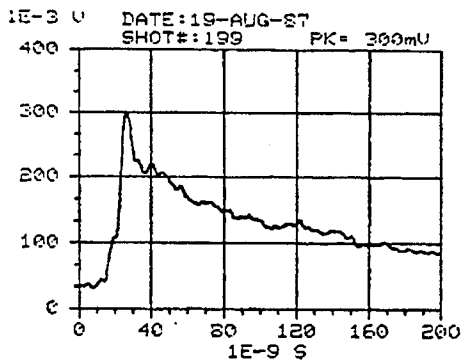


Figure D-36. REPS output waveforms for pulses 199, 200, 201, and 202.



Appendix D

Figure D-37. REPS output waveforms for pulses 203, 204, 205, and 206.

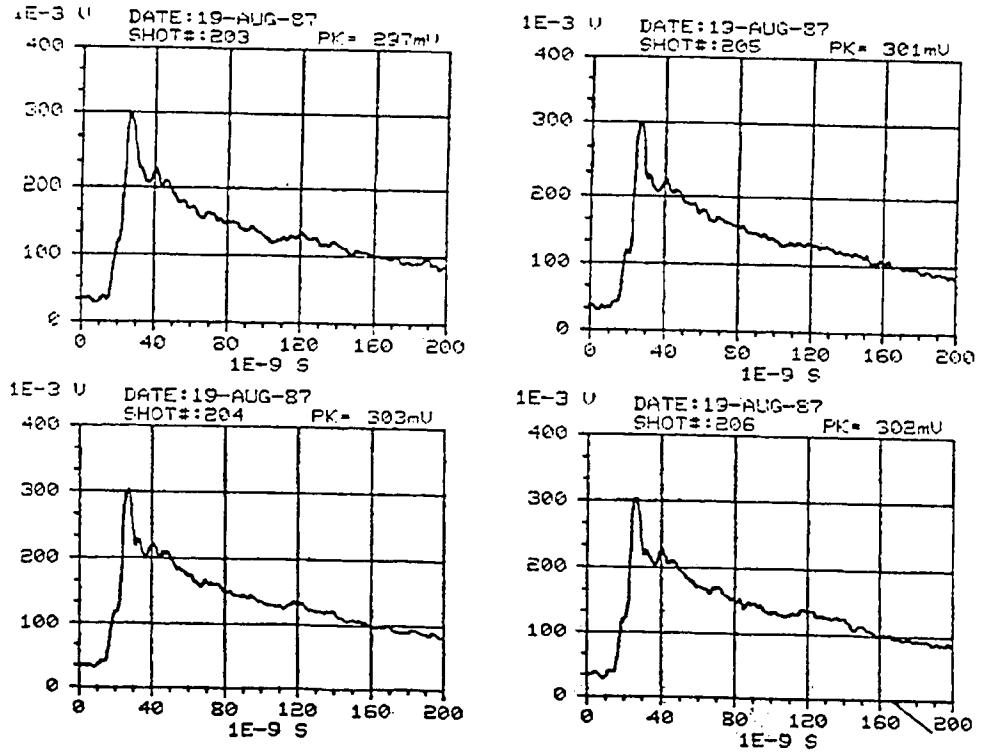


Figure D-38. REPS output waveforms for pulses 208, 209, 210, and 212.

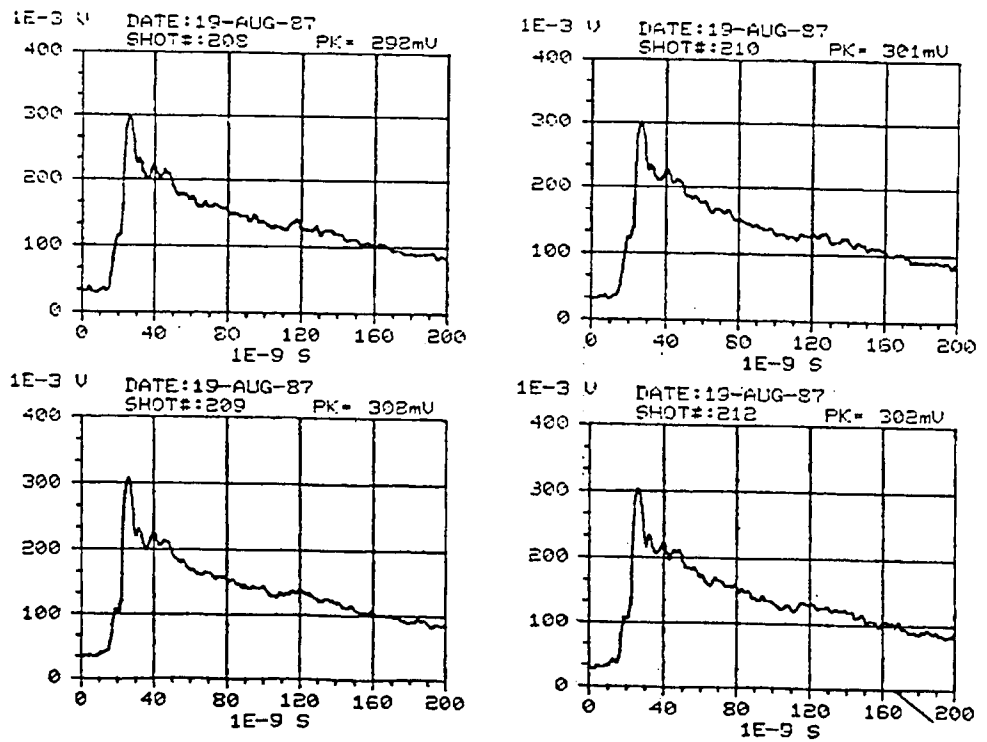


Figure D-39. REPS output waveforms for pulses 213, 214, 215, and 216.

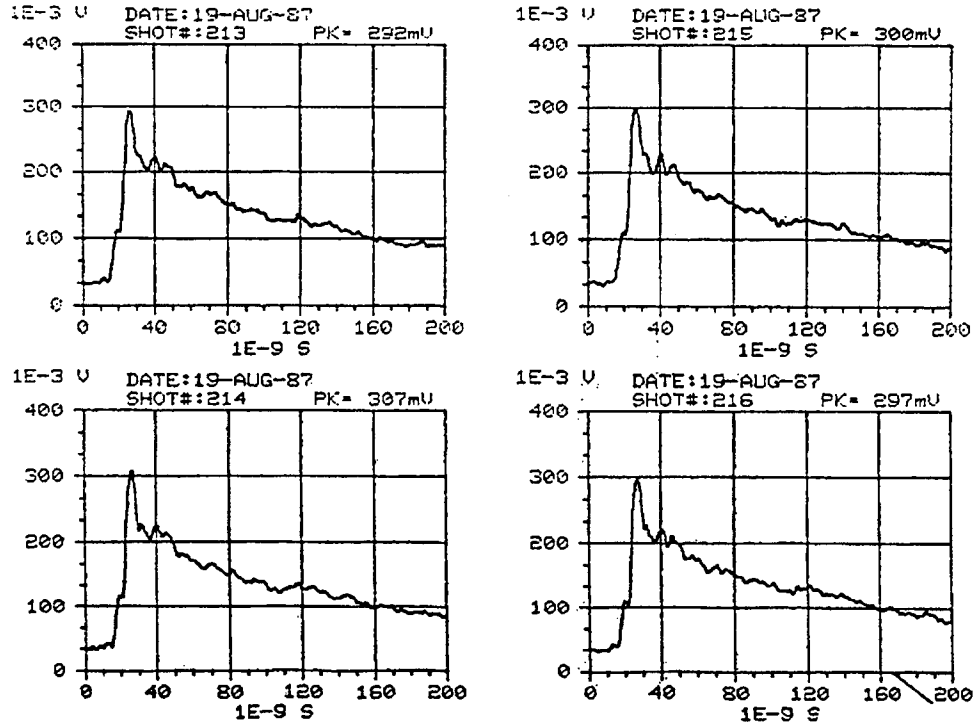
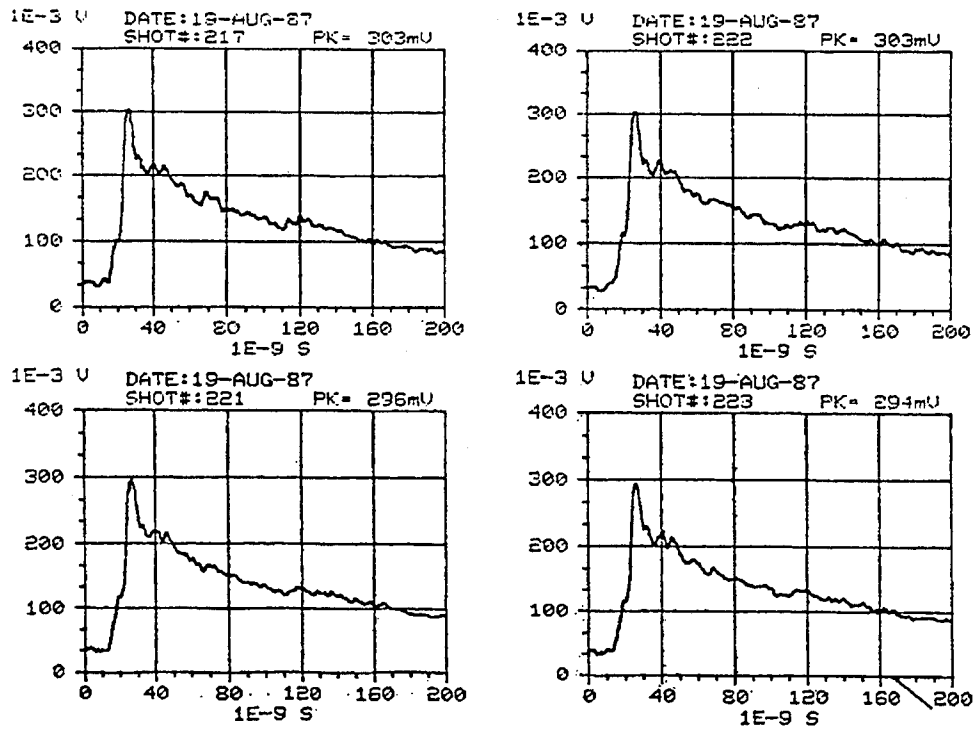


Figure D-40. REPS output waveforms for pulses 217, 221, 222, and 223.



Appendix D

Figure D-41. REPS output waveforms for pulses 224, 225, 226, and 227.

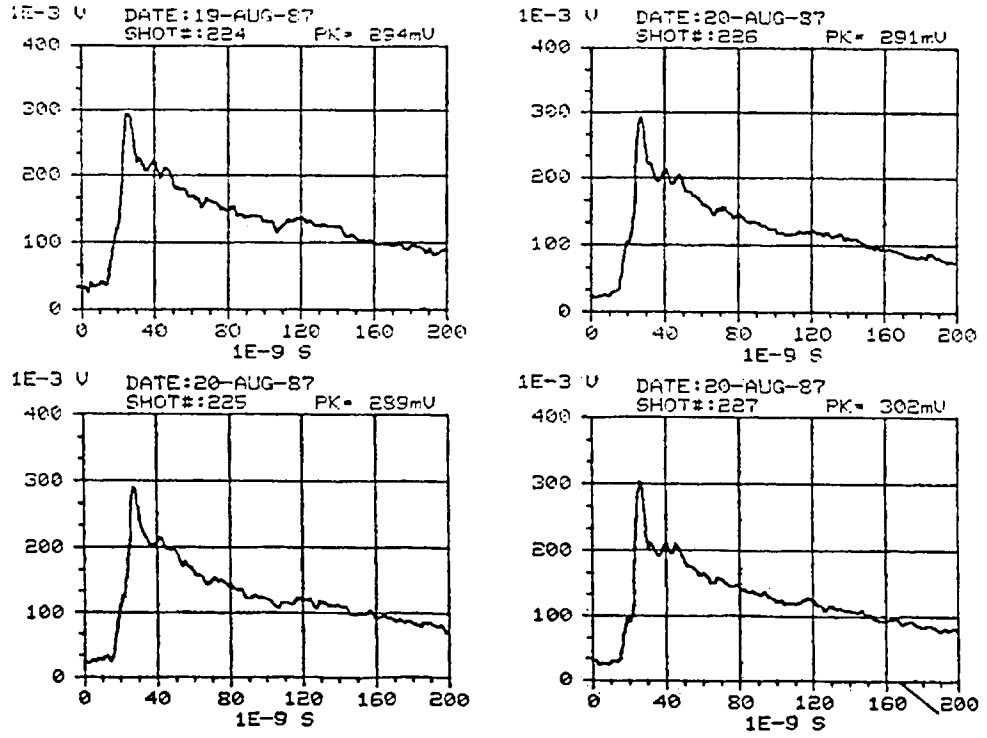


Figure D-42. REPS output waveforms for pulses 228, 230, 231, and 232.

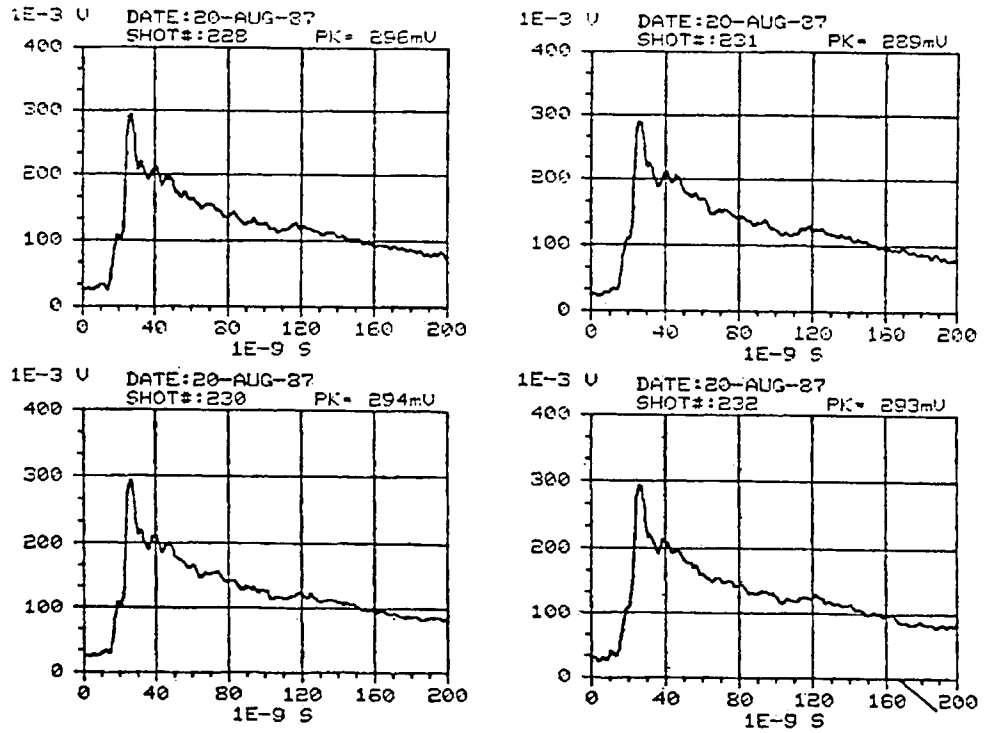


Figure D-43. REPS output waveforms for pulses 233, 234, 235, and 236.

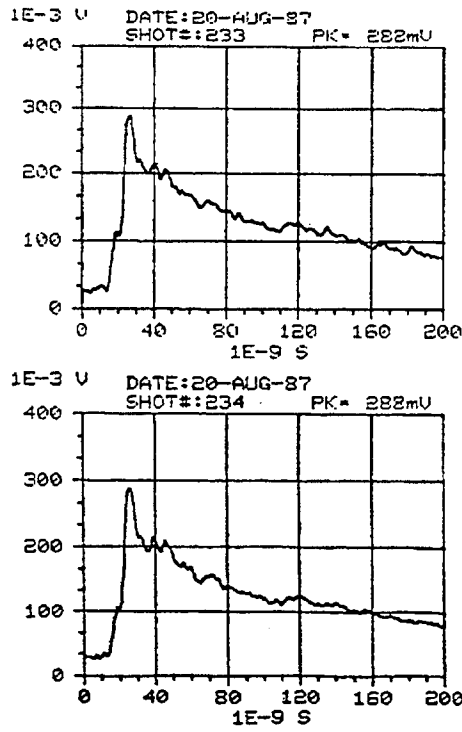
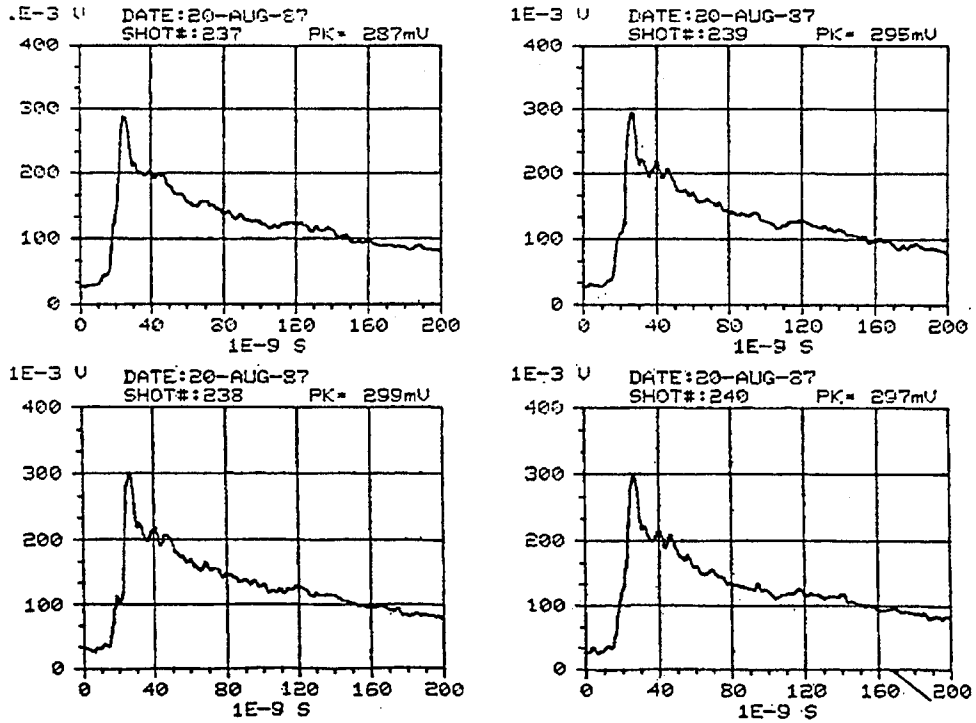


Figure D-44. REPS output waveforms for pulses 237, 238, 239, and 240.



Appendix D

Figure D-45. REPS output waveforms for pulses 241, 243, 244, and 245.

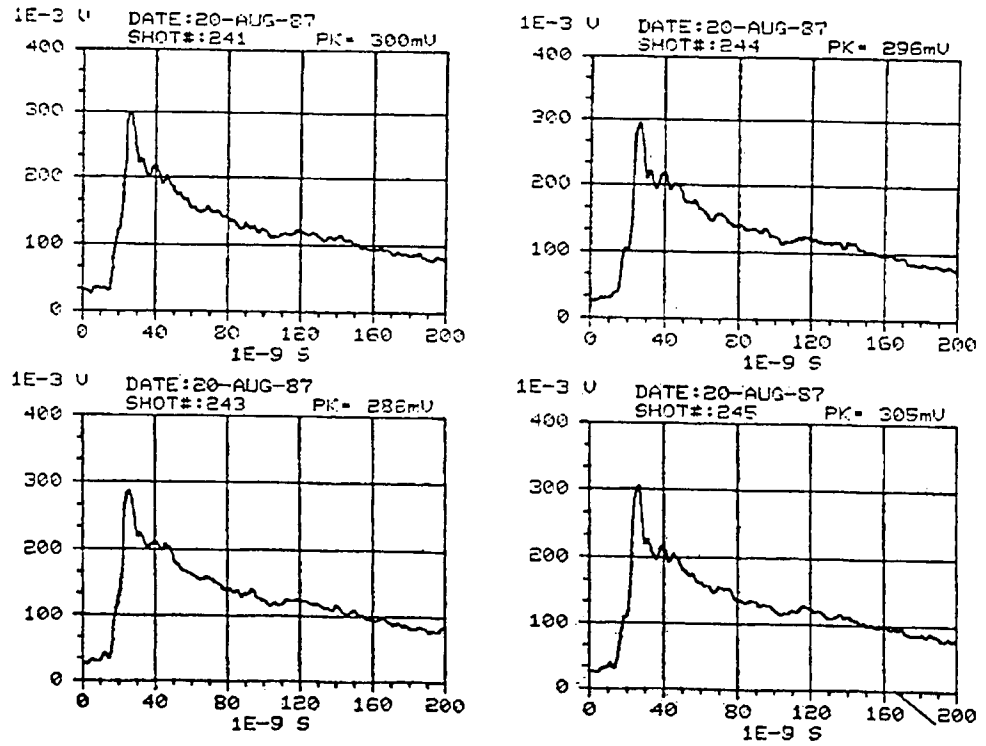


Figure D-46. REPS output waveforms for pulses 246, 247, 248, and 249.

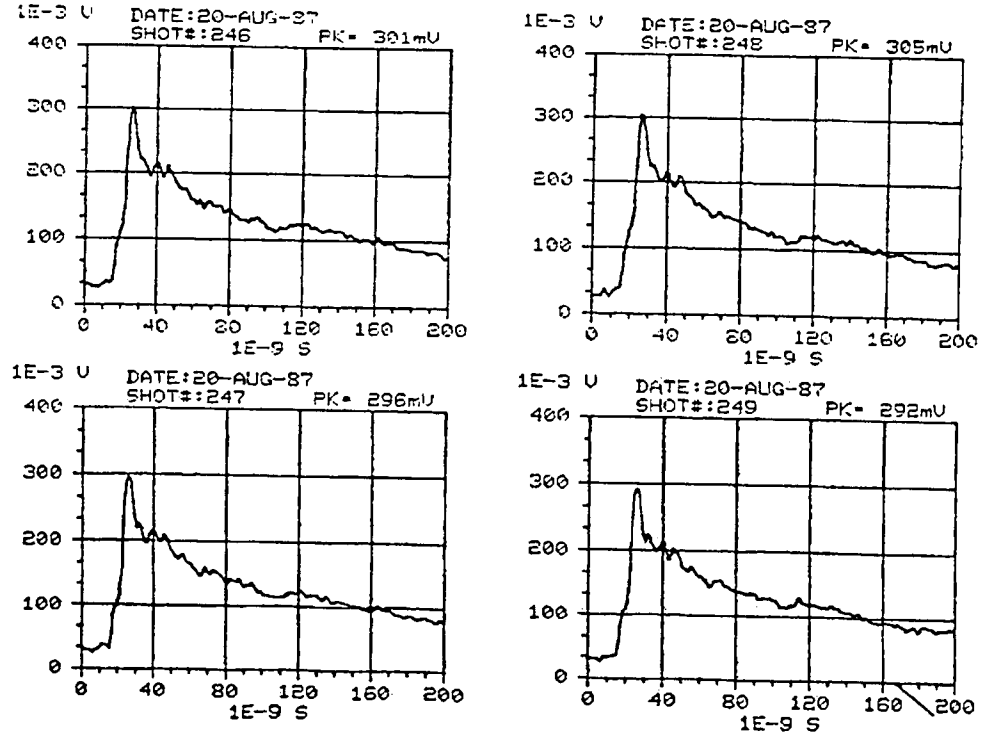


Figure D-47. REPS output waveforms for pulses 254, 255, 256, and 257.

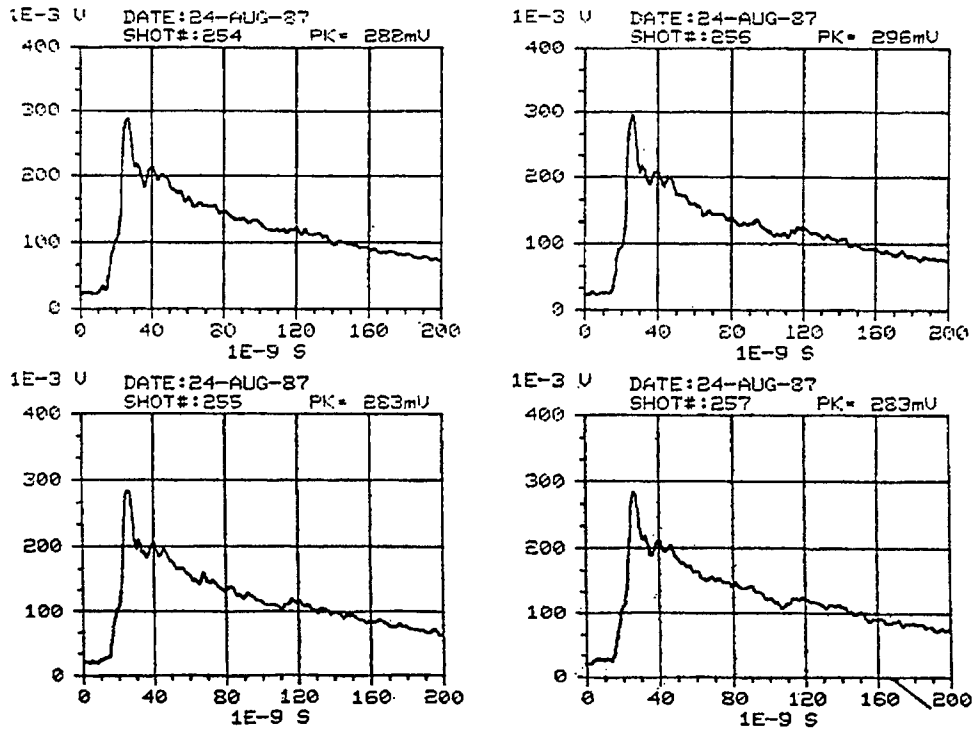
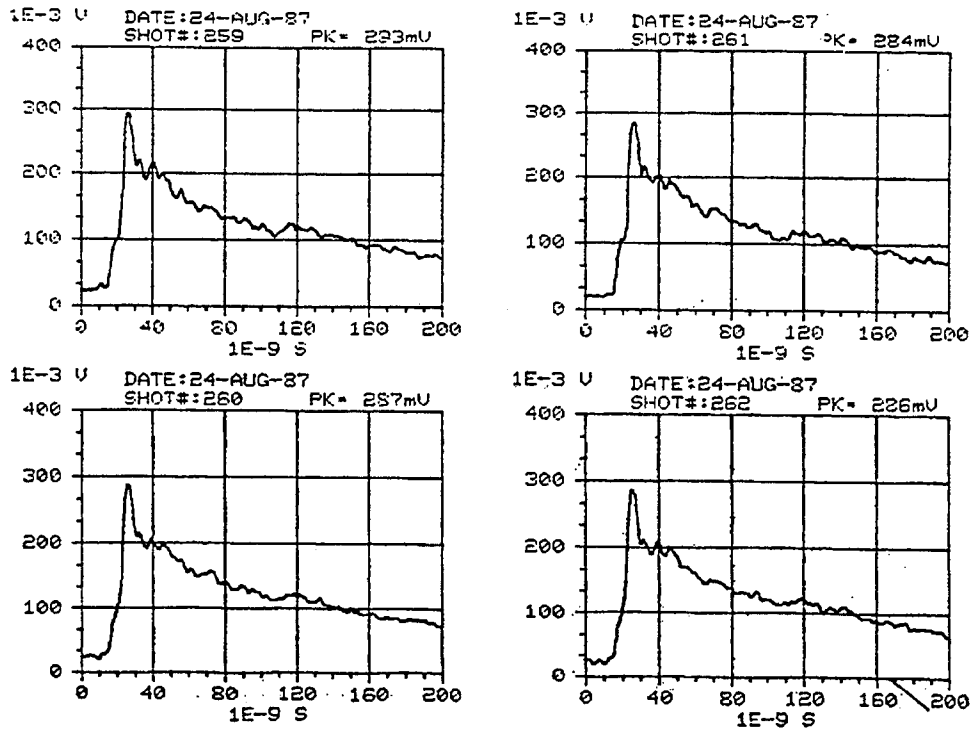


Figure D-48. REPS output waveforms for pulses 259, 260, 261, and 262.



Appendix D

Figure D-49. REPS output waveforms for pulses 263, 264, 265, and 266.

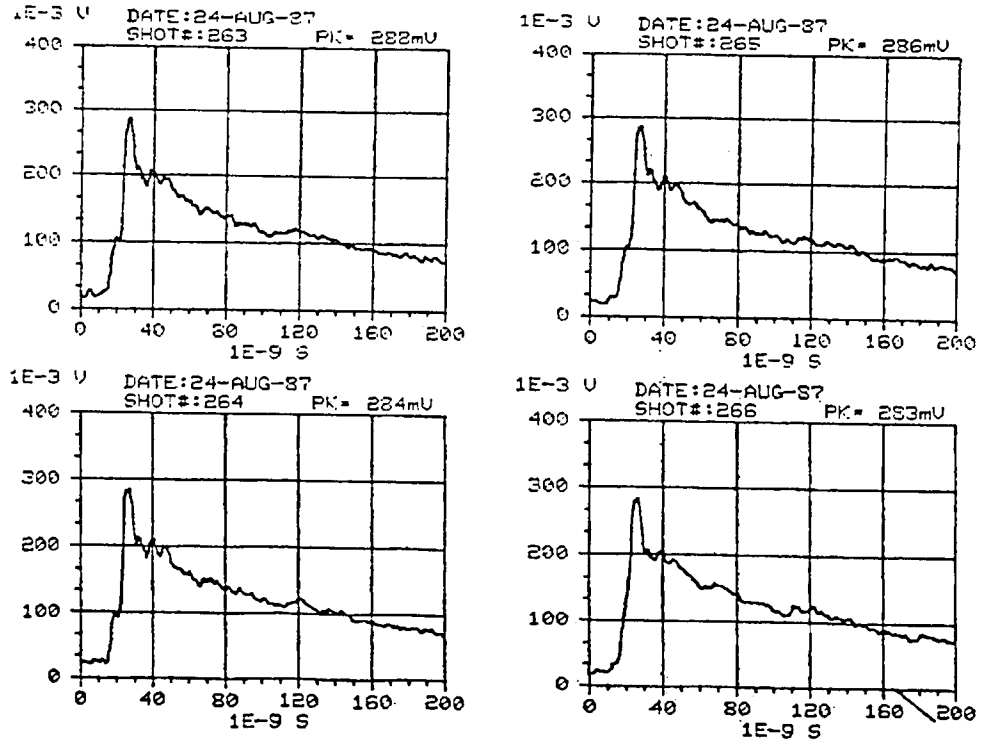


Figure D-50. REPS output waveforms for pulses 267, 270, 271, and 272.

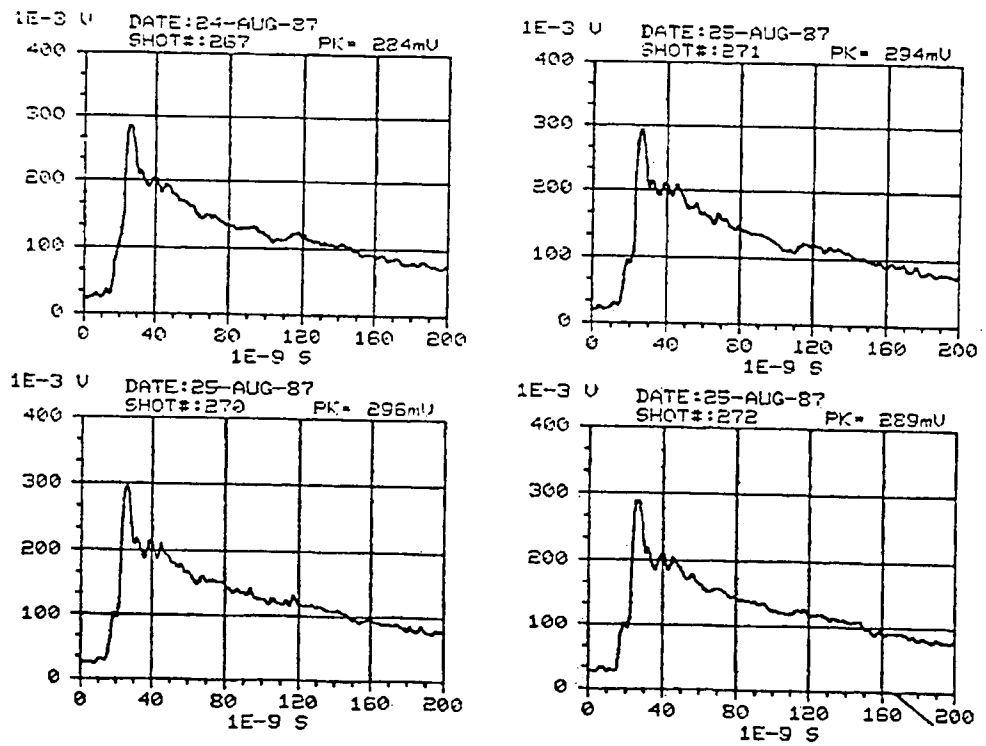


Figure D-51. REPS output waveforms for pulses 273, 274, 275, and 276.

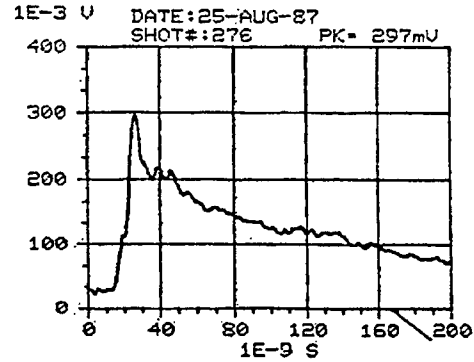
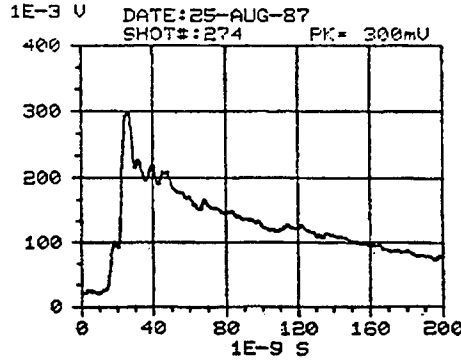
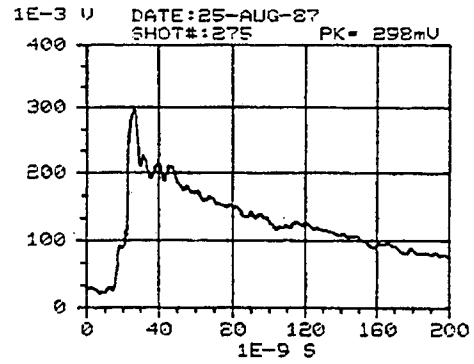
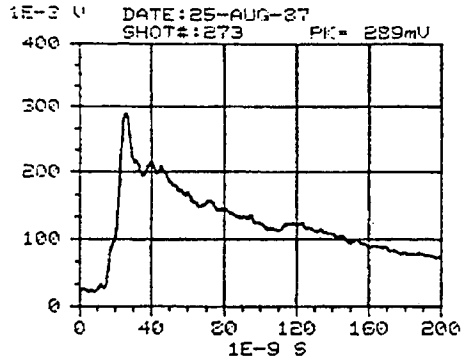
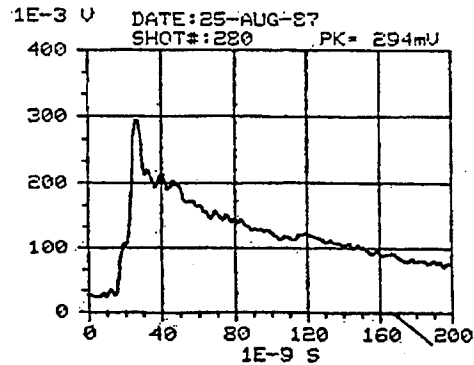
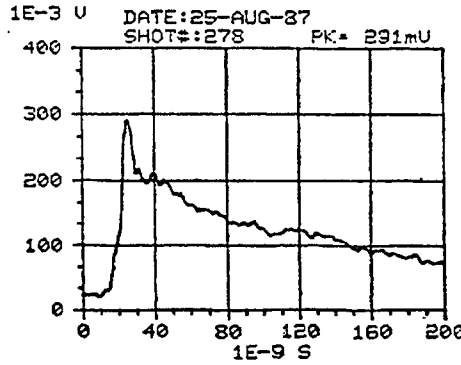
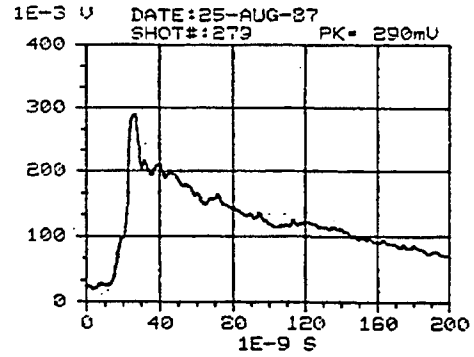
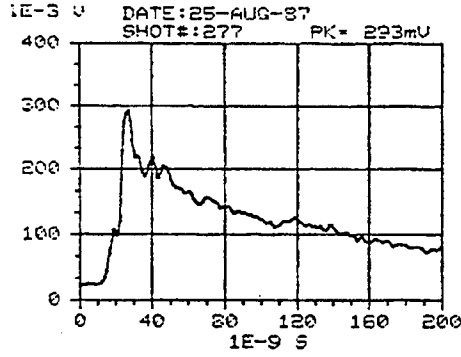


Figure D-52. REPS output waveforms for pulses 277, 278, 279, and 280.



Appendix D

Figure D-53. REPS output waveforms for pulses 281, 283, 284, and 287.

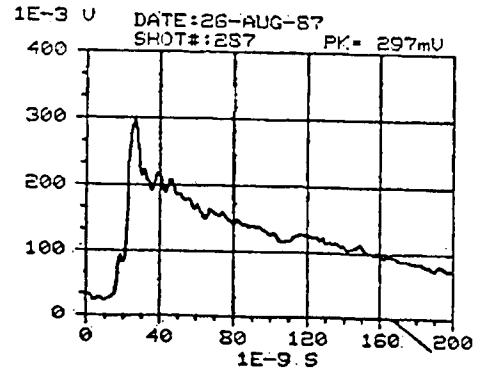
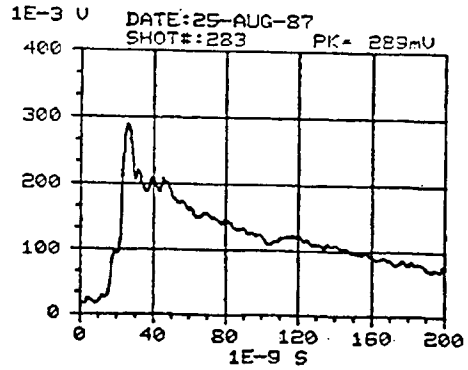
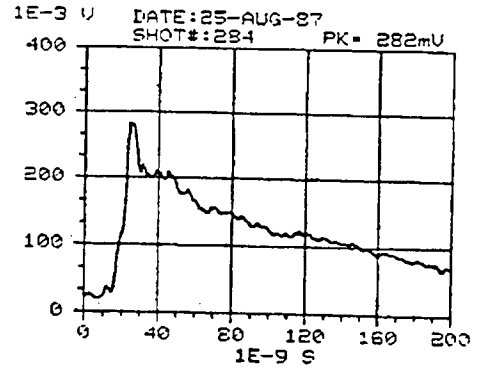
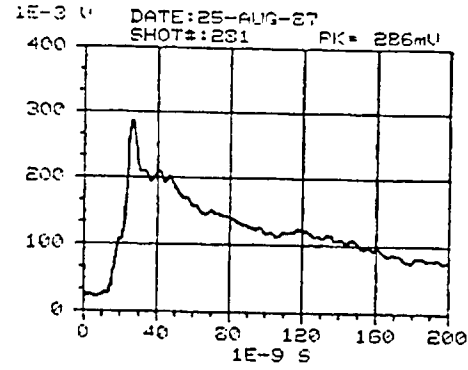


Figure D-54. REPS output waveforms for pulses 288, 289, 292, and 293.

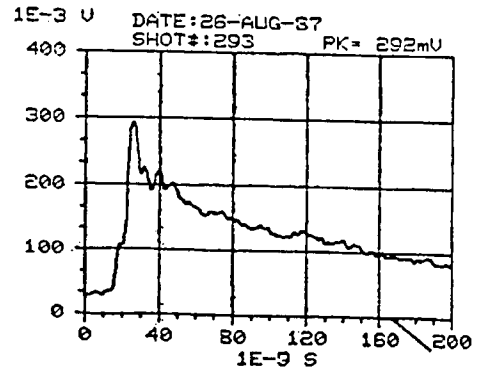
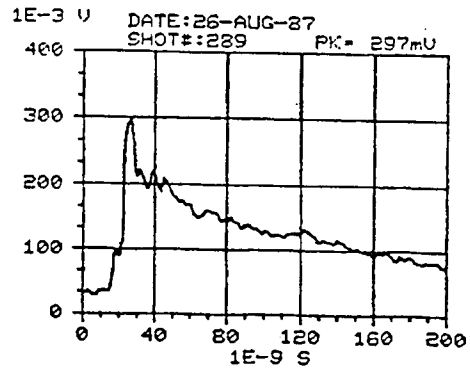
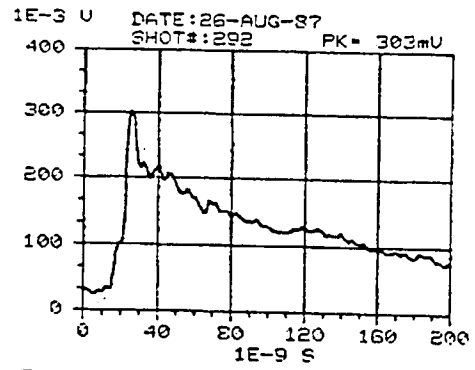
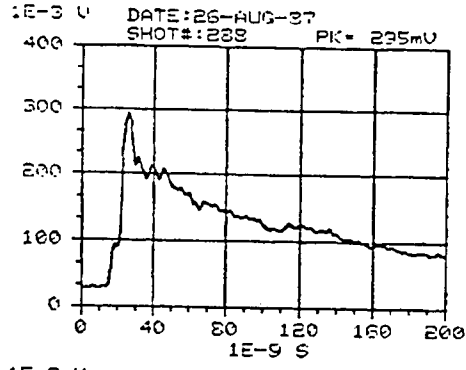


Figure D-55. REPS output waveforms for pulses 295, 298, 299, and 300.

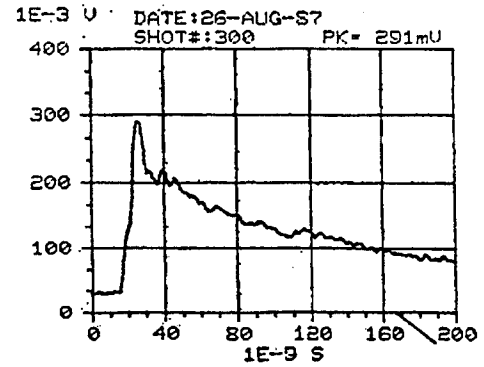
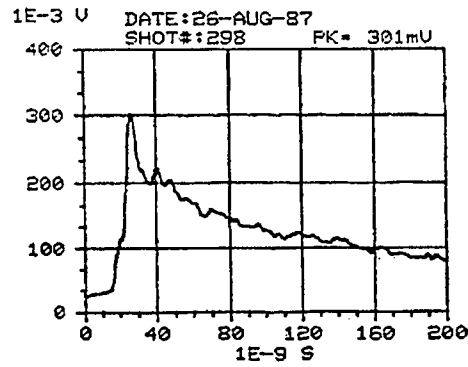
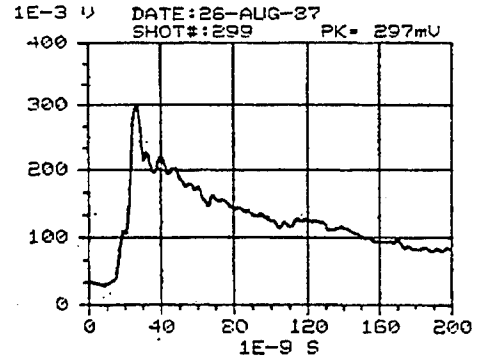
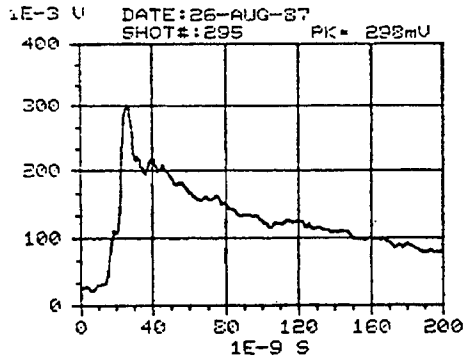
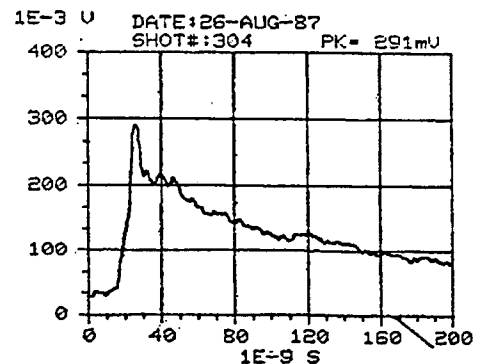
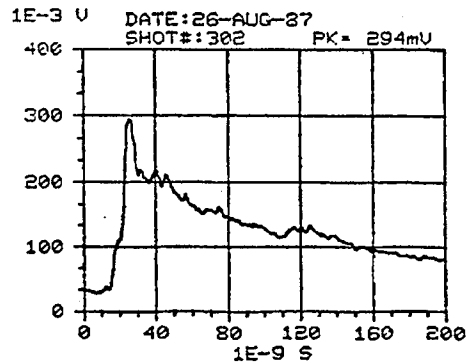
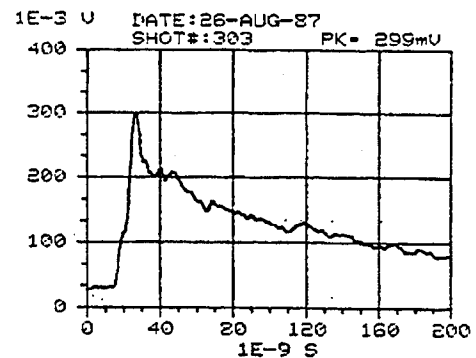
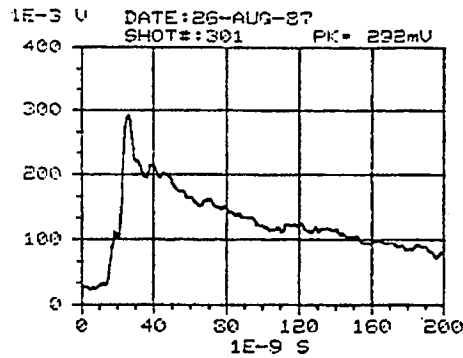


Figure D-56. REPS output waveforms for pulses 301, 302, 303, and 304.



Appendix D

Figure D-57. REPS output waveforms for pulses 305, 306, 309, and 313.

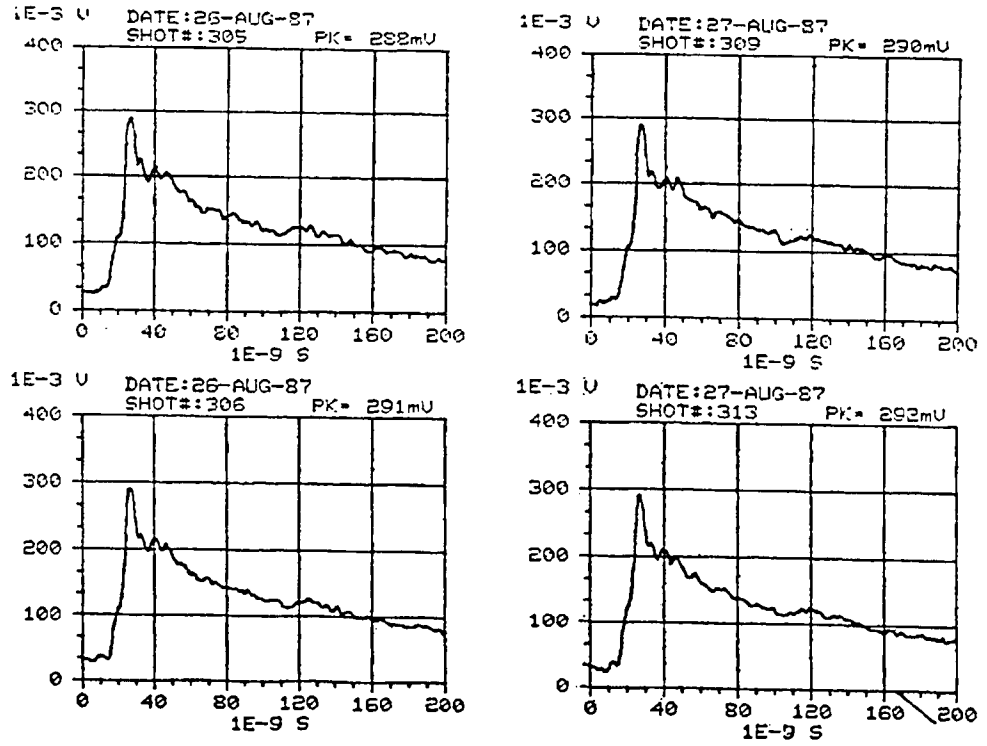


Figure D-58. REPS output waveforms for pulses 314, 315, 316, and 317.

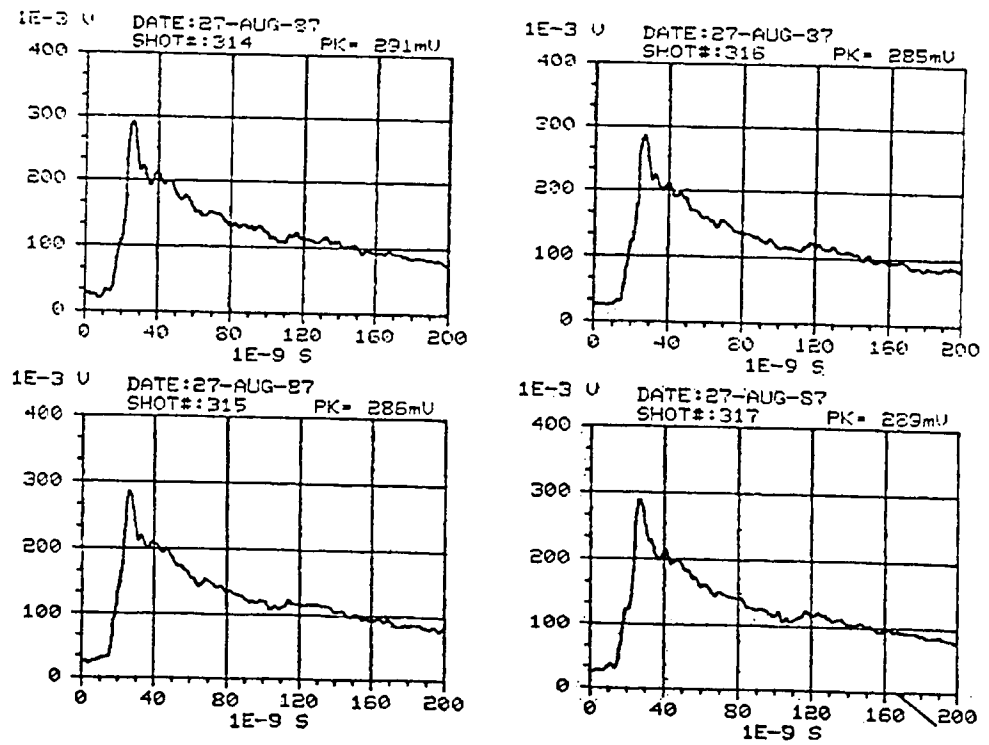


Figure D-59. REPS output waveforms for pulses 318, 319, 320, and 322.

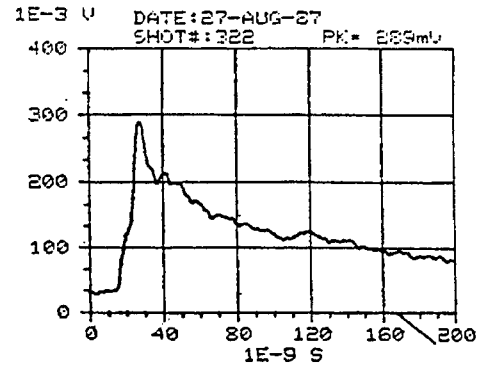
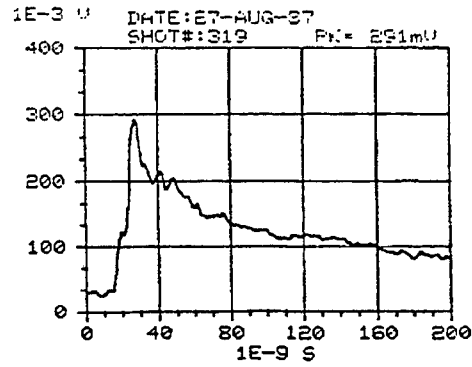
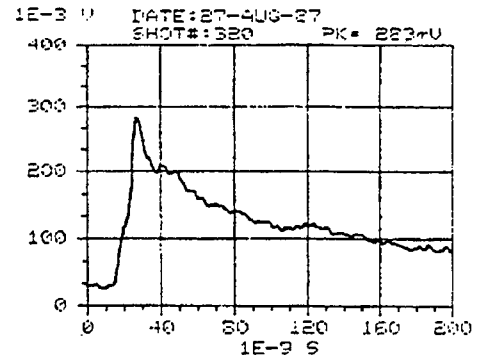
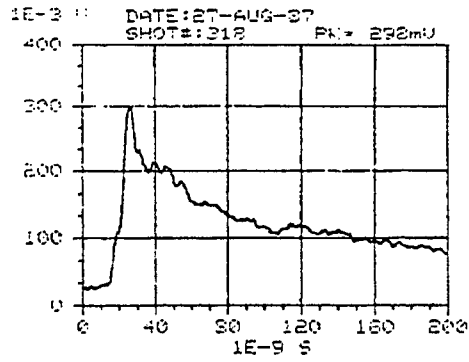
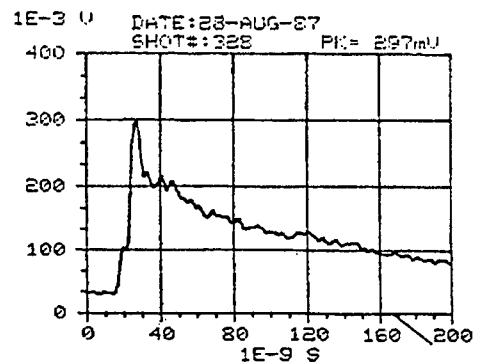
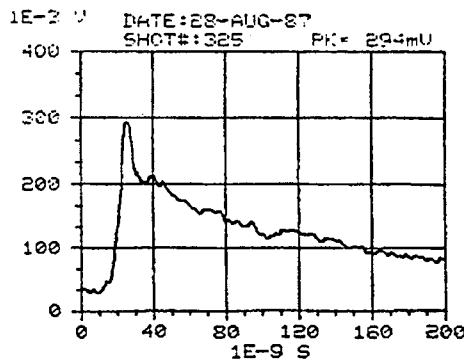
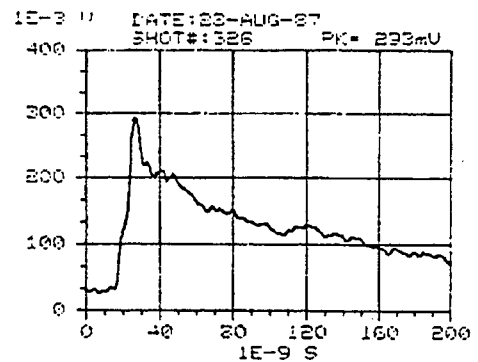
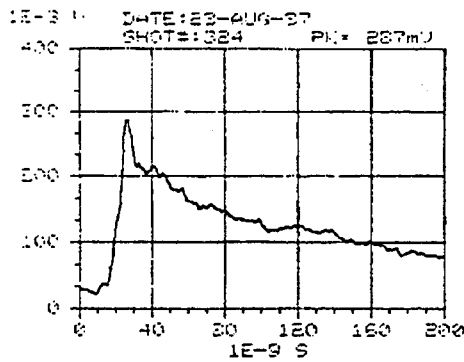


Figure D-60. REPS output waveforms for pulses 324, 325, 326, and 328.



Appendix D

Figure D-61. REPS output waveforms for pulses 329, 330, 331, and 332.

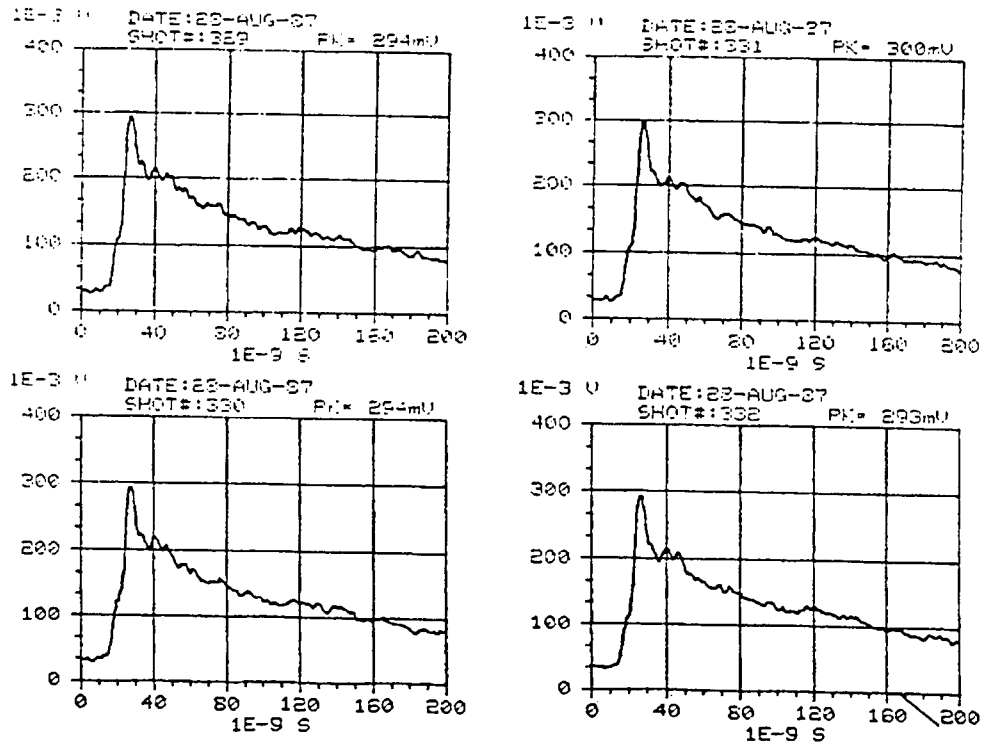


Figure D-62. REPS output waveforms for pulses 334, 335, 336, and 337.

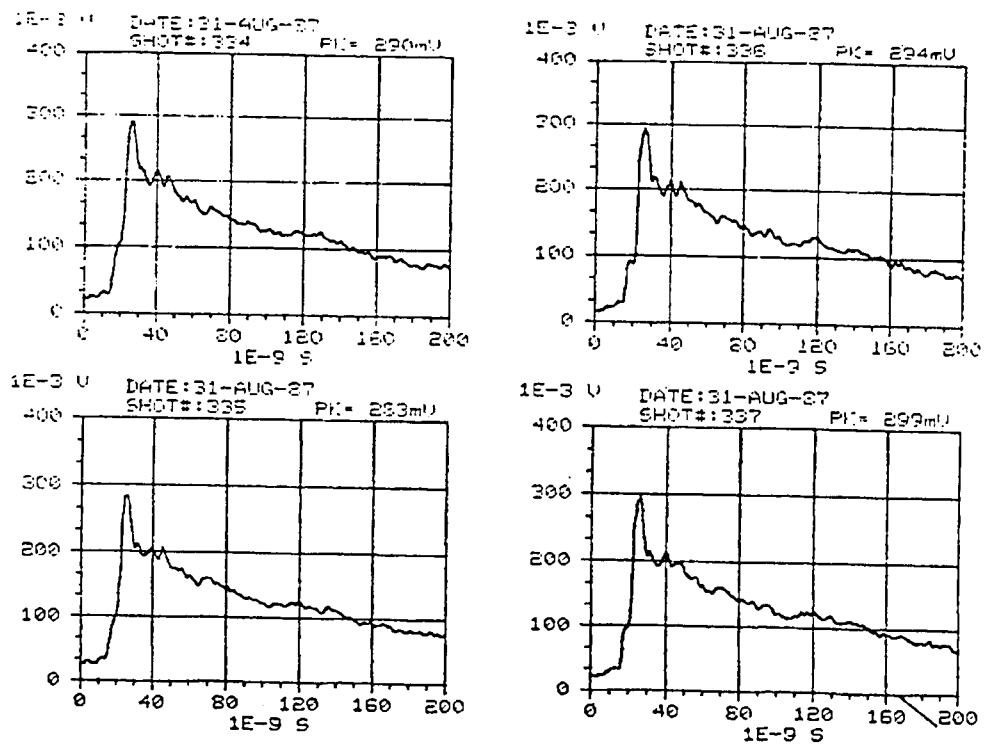


Figure D-63. REPS output waveforms for pulses 338, 339, 340, and 341.

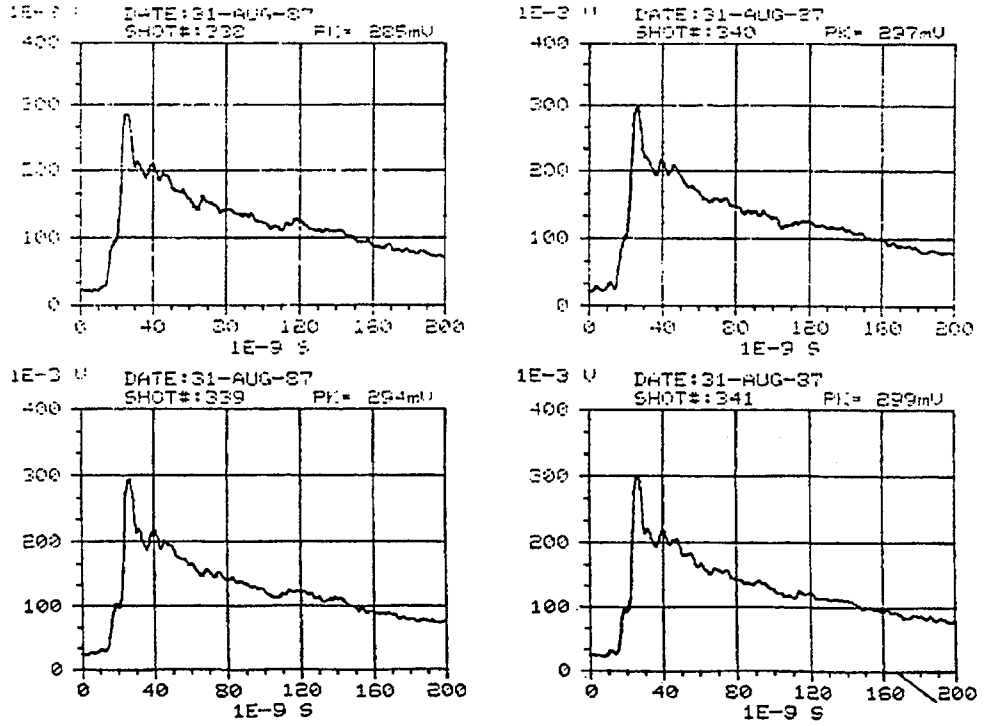
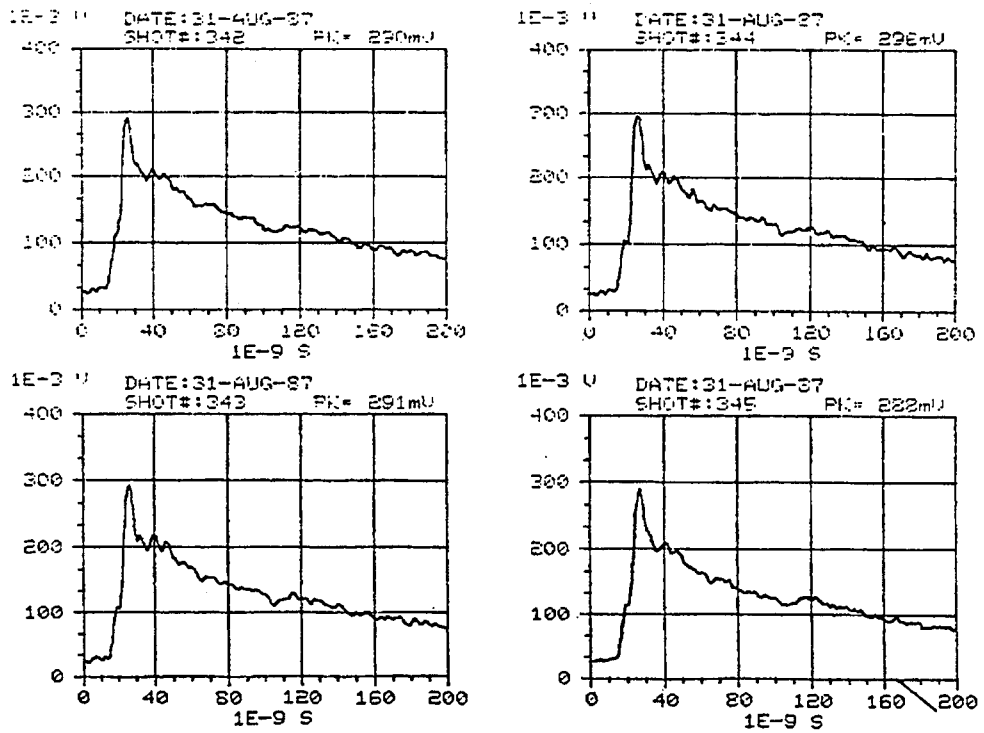


Figure D-64. REPS output waveforms for pulses 342, 343, 344, and 345.



Appendix D

Figure D-65. REPS output waveforms for pulses 346, 347, 350, and 351.

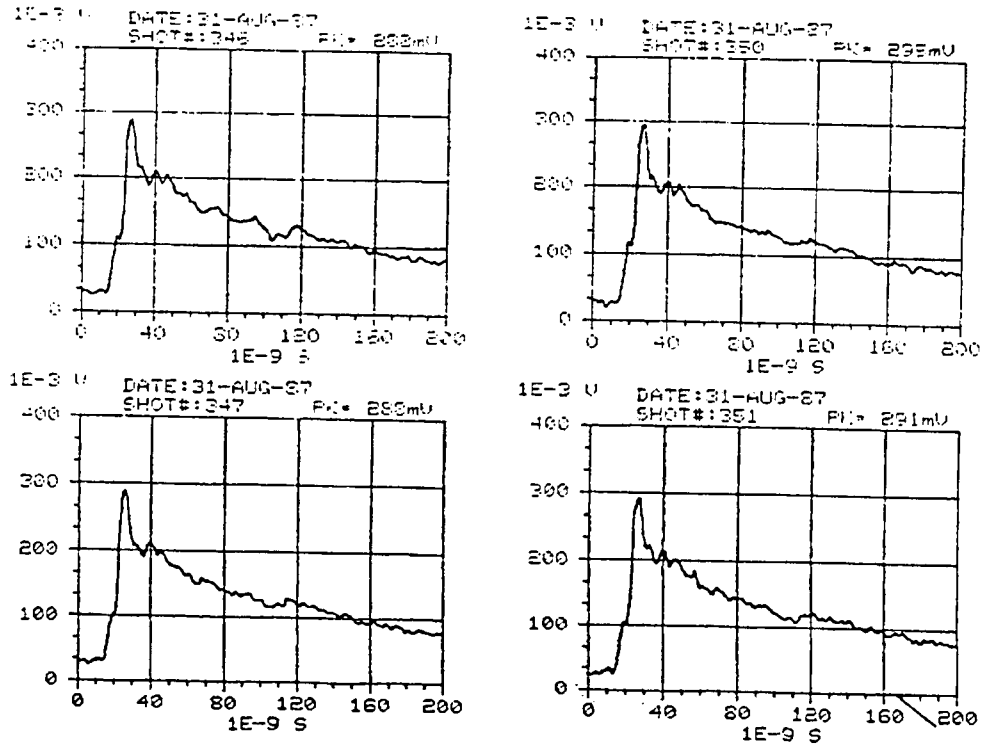


Figure D-66. REPS output waveforms for pulses 353, 354, 355, and 356.

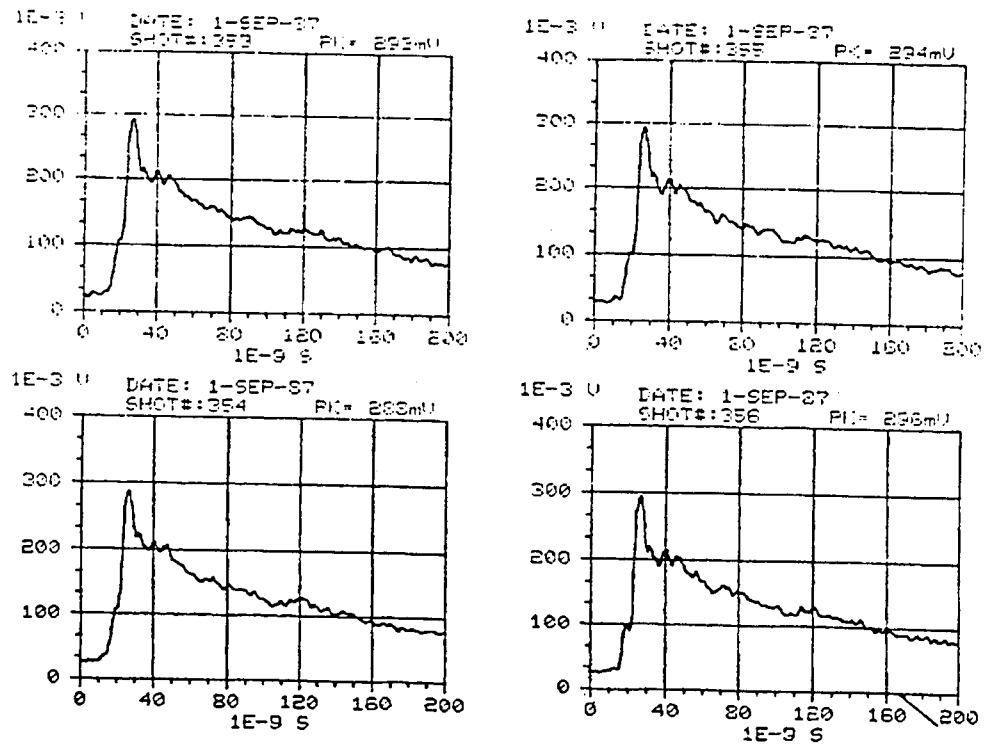


Figure D-67. REPS output waveforms for pulses 357, 358, 359, and 360.

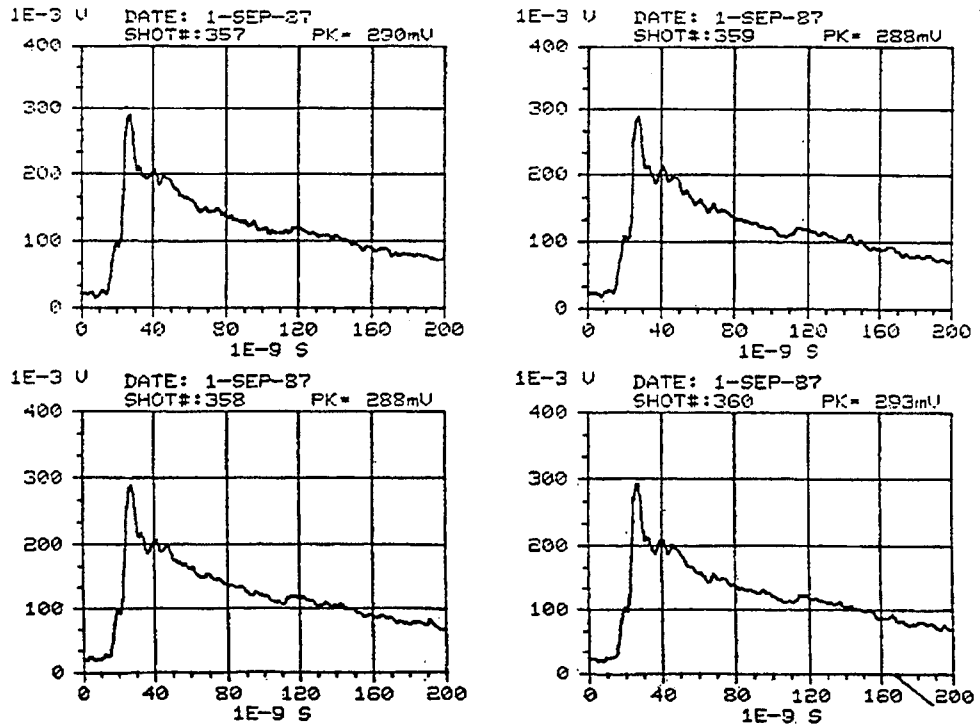
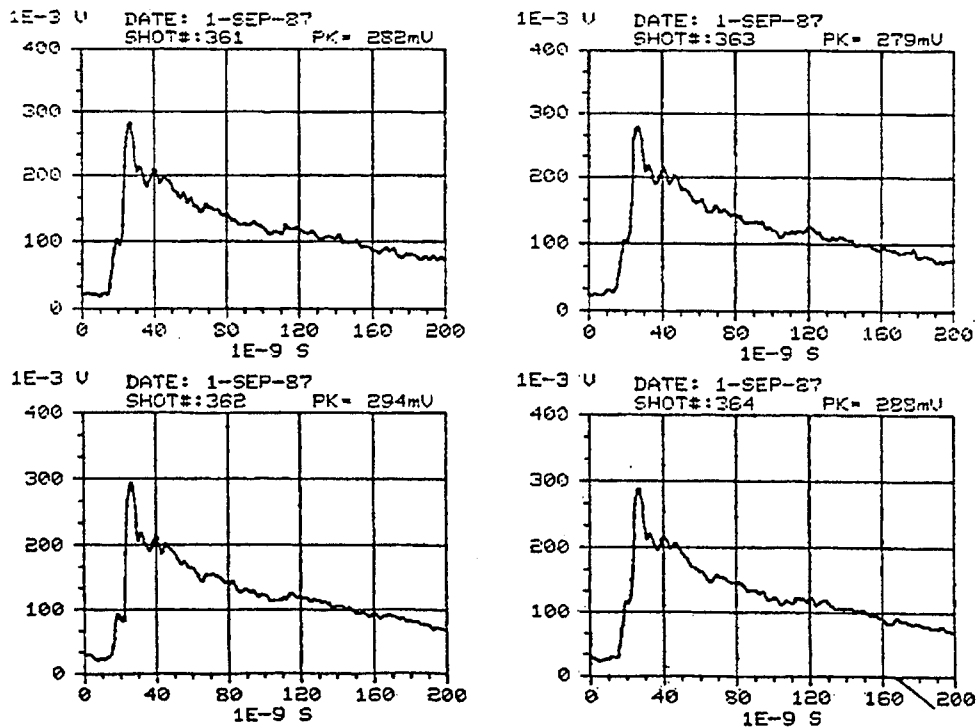


Figure D-68. REPS output waveforms for pulses 361, 362, 363, and 364.



Appendix D

Figure D-69. REPS output waveforms for pulses 365, 366, 367, and 368.

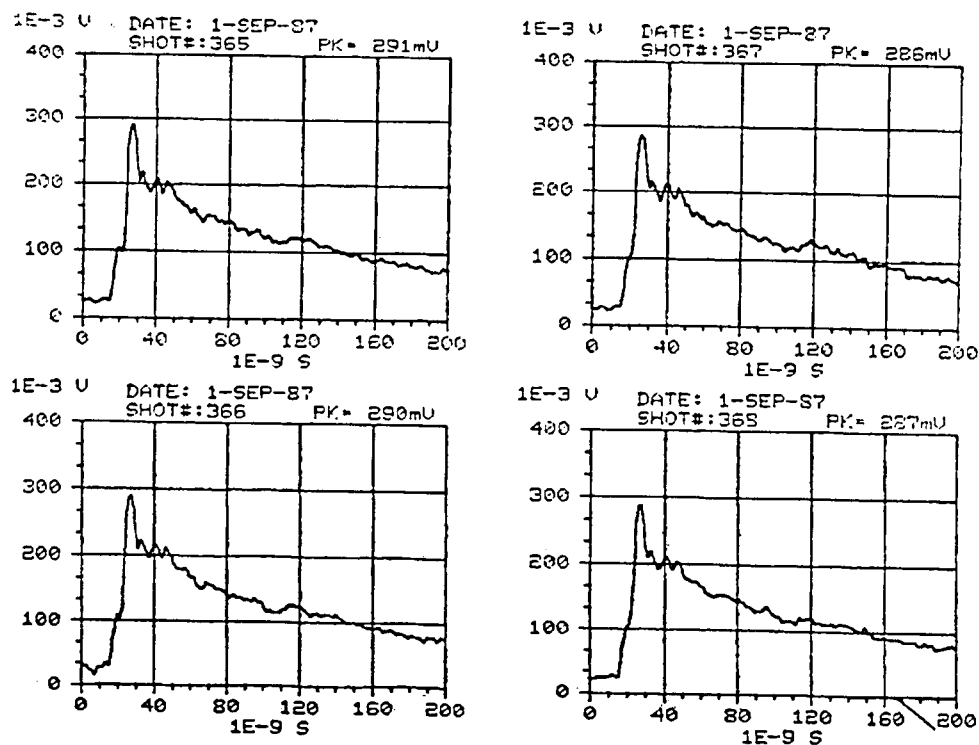


Figure D-70. REPS output waveforms for pulses 369, 370, 371, and 372.

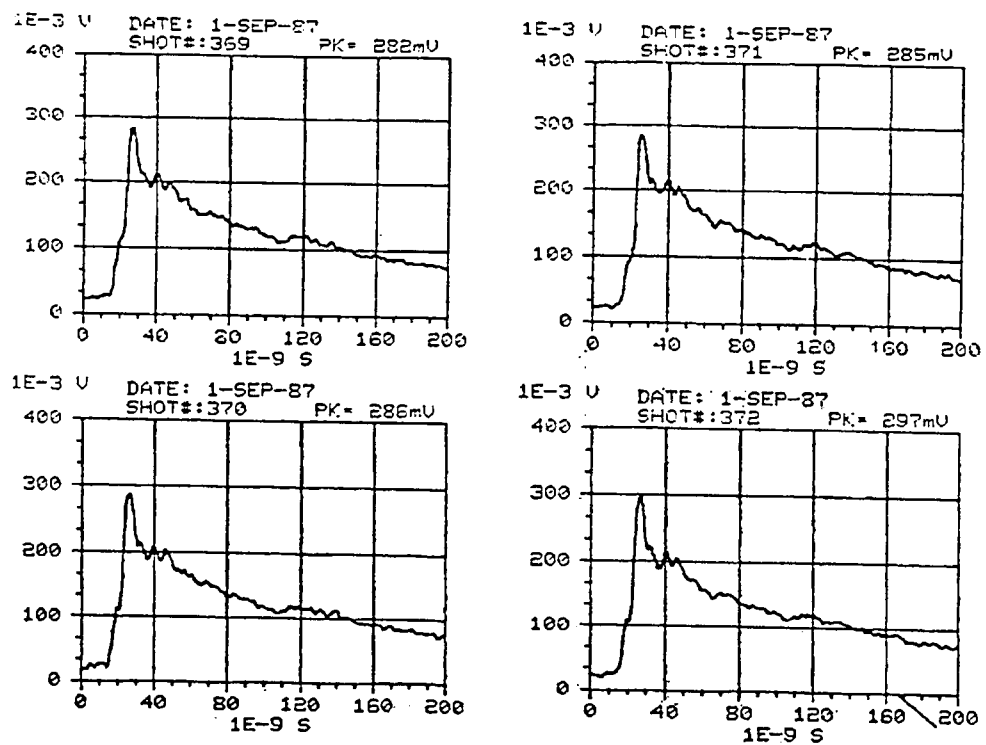


Figure D-71. REPS output waveforms for pulses 373, 374, 375, and 376.

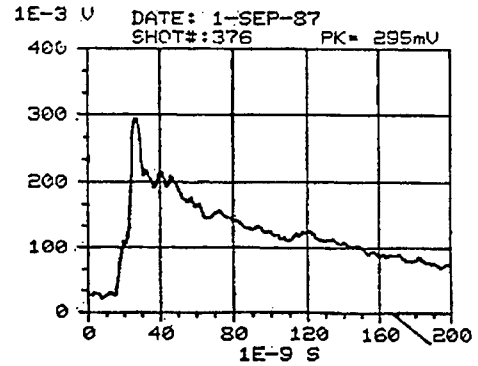
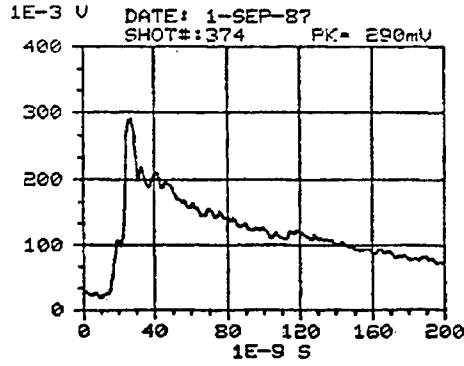
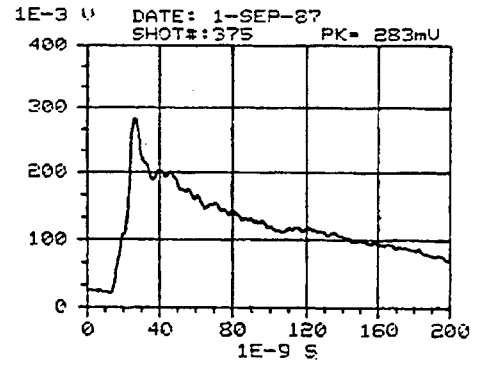
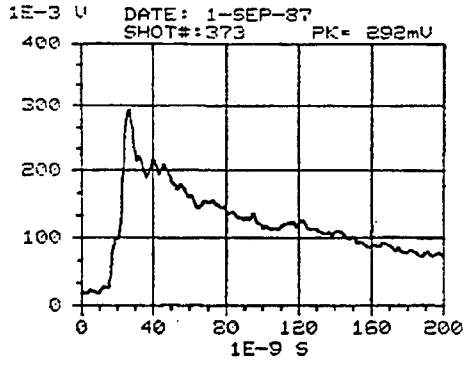
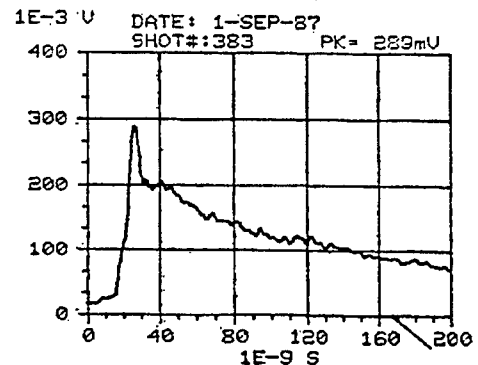
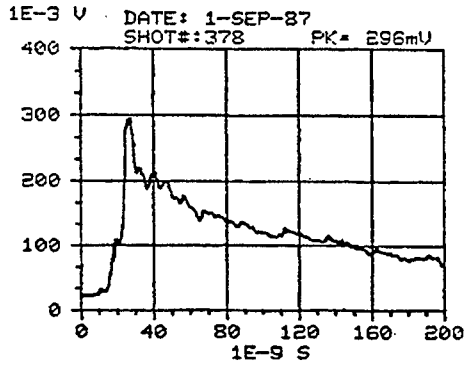
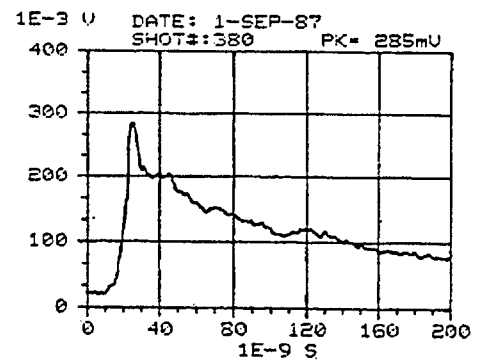
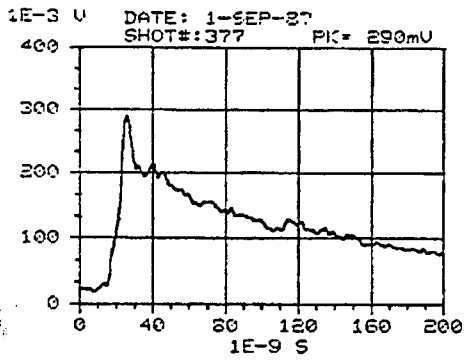


Figure D-72. REPS output waveforms for pulses 377, 378, 380, and 383.



Appendix D

Figure D-73. REPS output waveforms for pulses 384, 385, 387, and 388.

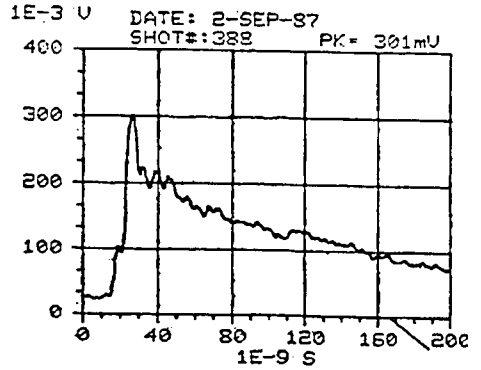
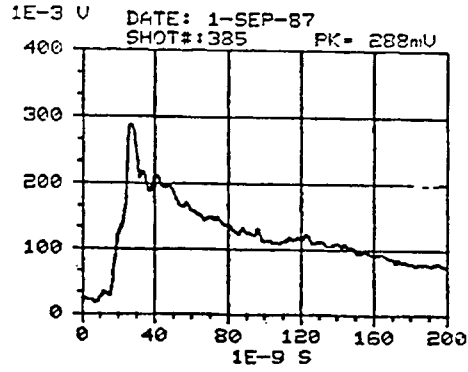
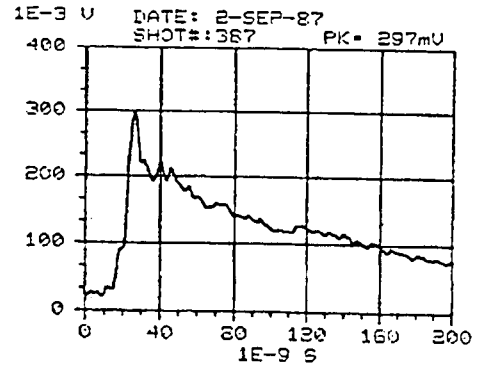
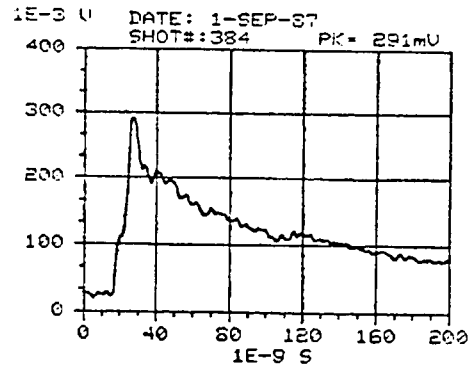


Figure D-74. REPS output waveforms for pulses 389, 390, 391, and 392.

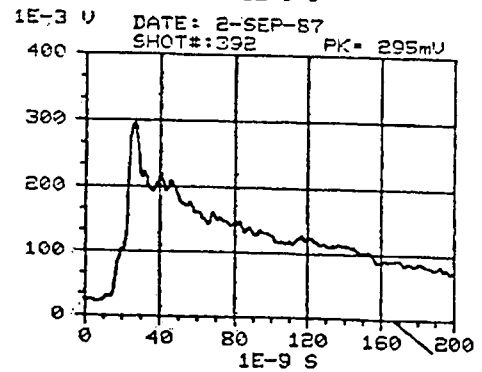
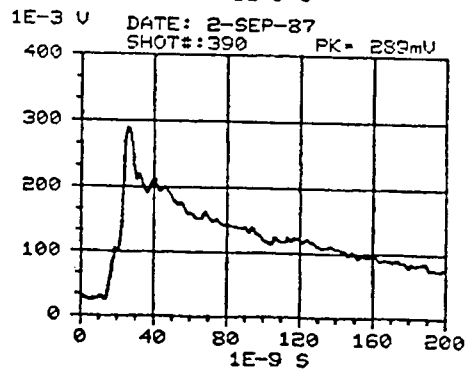
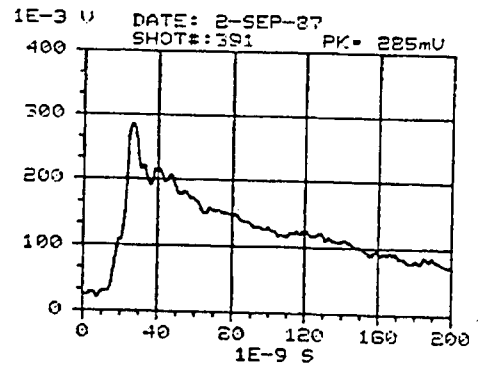
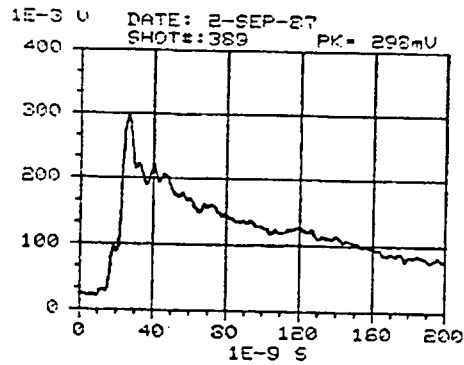


Figure D-75. REPS output waveforms for pulses 393, 394, 395, and 396.

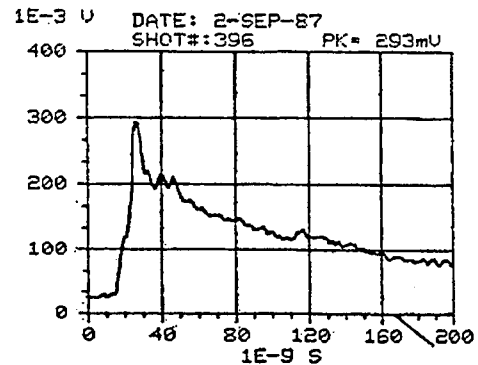
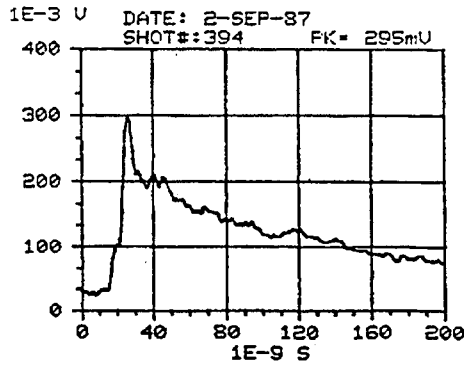
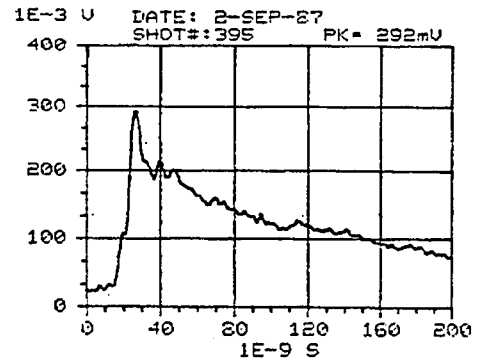
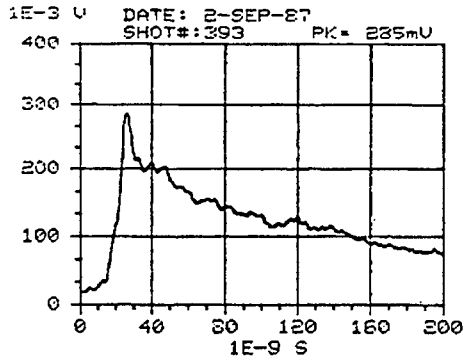
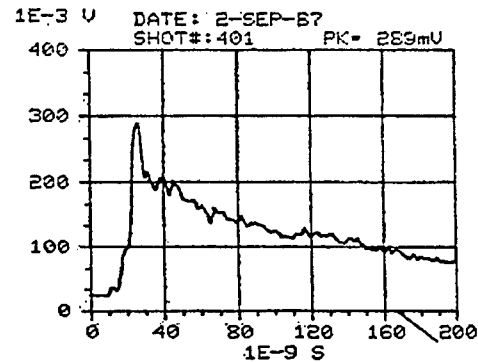
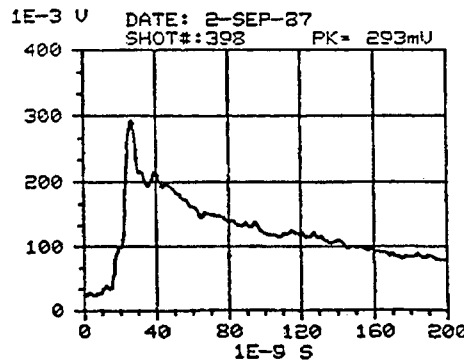
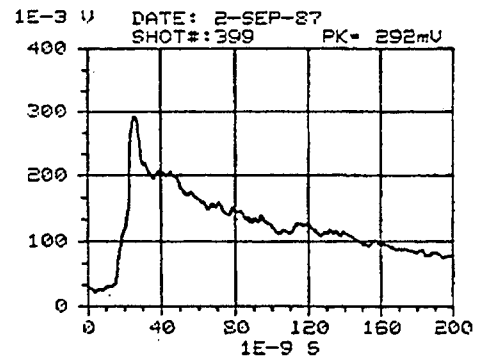
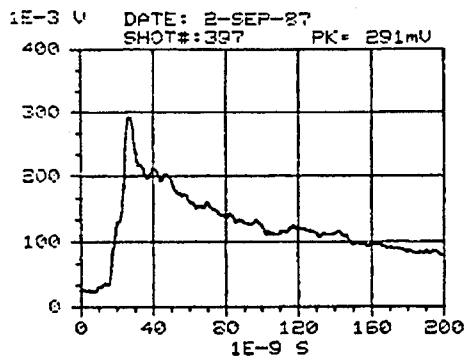


Figure D-76. REPS output waveforms for pulses 397, 398, 399, and 401.



Appendix D

Figure D-77. REPS output waveforms for pulses 402, 403, 404, and 405.

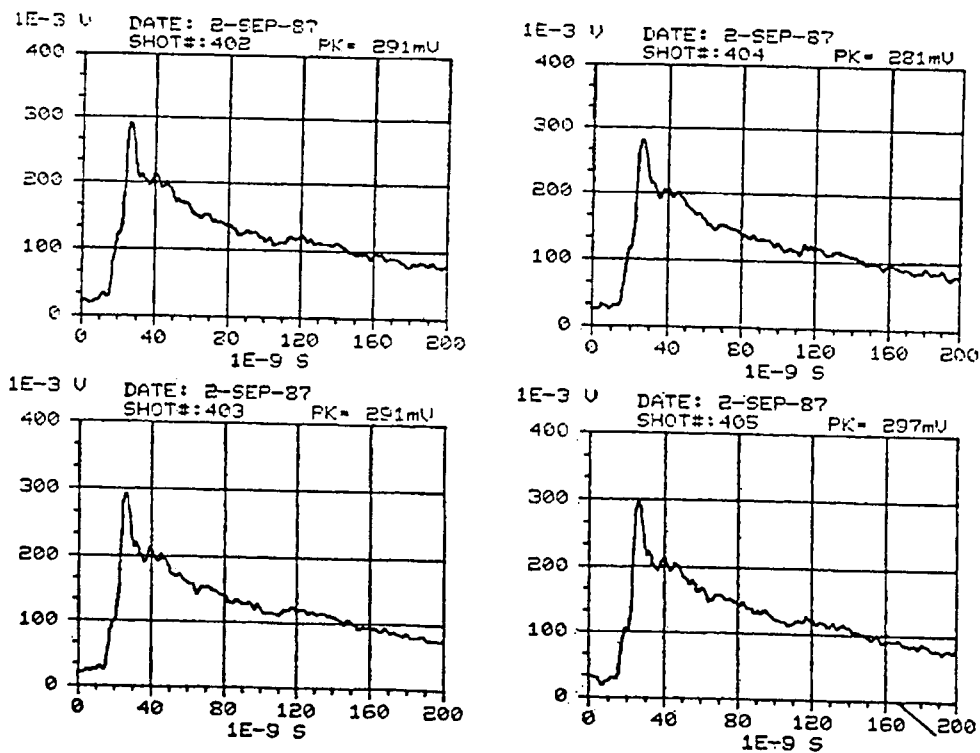
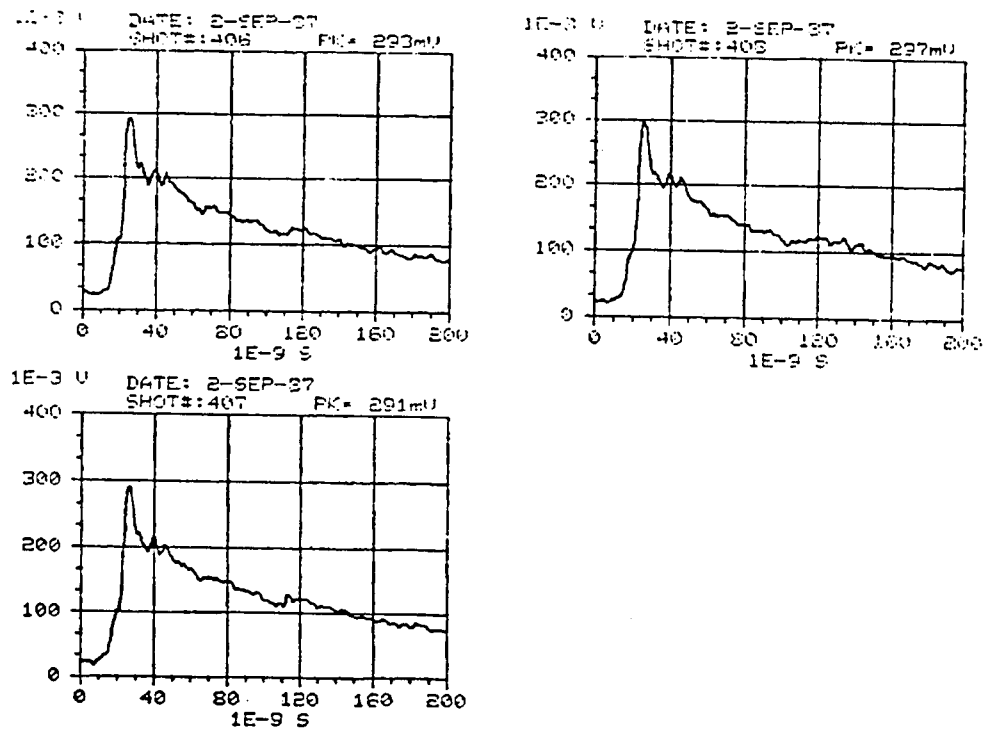


Figure D-78. REPS output waveforms for pulses 406, 407, and 408.



Distribution

Administrator
Defns Techl Info Ctr
Attn DTIC-DDA (2 copies)
Cameron Station Building 5
Alexandria VA 22304-6145

Commander
U.S. Army White Sands Mis Range
Attn STEWS-N Dr. Meason
WSMR NM 88022

Nvl Air Warfare Ctr
Aircraft Division
Attn S. Frazier SY84
Patuxent River MD 20670-5304

Nvl Surfc Warfare Ctr
Dahlgren Div
Attn Code E231 Techl Lbry
Dahlgren VA 22448-5020

Director
Defns Nuc Agcy
Attn RAEE EMP Effects Div
Attn TISI Scntfc Info Div
6801 Telegraph Rd
Alexandria VA 22301-3398

Ensco Inc
5400 Port Royal Rd
Springfield VA 22151

SOL Telecommunications
Attn S. Clark
PO Box 4070
Woodbridge VA 22194-4070

Electro Magnetic Applications Inc
Attn R. Perela
PO Box 26263
Denver CO 80226

U.S. Army Rsrch Lab
Attn AMSRL-SL-CO W. Sowers
Attn AMSRL-SL-CS J. Beilfuss
APG MD 21010-5423

U.S. Army Rsrch Lab
Attn AMSRL-OP-SD-TA
Admin Ser
Attn AMSRL-OP-SD-TP
Techl Pblshng
Attn Techl Lbry (3 copies)
Attn AMSRL-SI Chief Scientist
Attn AMSRL-OP-SD-WB

T. Waltemyer
Attn AMSRL-SS-F Director
Attn AMSRL-SS-SG Director
Attn AMSRL-WT-N Chief
Attn AMSRL-WT-NW
Deputy Chief
Attn AMSRL-WT-ND Chief
Attn AMSRL-WT-NE Chief
Attn AMSRL-WT-NB Chief
Attn AMSRL-WT-NF Chief
Attn AMSRL-WT-NG Chief
Attn AMSRL-WT-NH Chief
Attn AMSRL-WT-NI Chief
Attn AMSRL-WT-NA Chief
Attn AMSRL-WT-NF B. Benwell
(5 copies)
Attn AMSRL-WT-ND E. Patrick
Attn AMSRL-WT-ND J. Stewart
Attn AMSRL-WT-NE J. Daly